The development of computational methods for cracked bodies subjected to cyclic variable loads and temperatures

Thesis submitted for the degree of
Doctor of Philosophy
at the University of Leicester

by

Mohamed Salahuddin
Mohamed Mohidin Habibullah

Department of Engineering
University of Leicester

July 2003

Dedicated to my family

Acknowledgements

First and foremost, I would like to express my sincere gratitude and appreciation to my supervisor, Professor A.R.S. Ponter, for his continued guidance, support and supervision throughout the course of the work presented in this thesis.

I would also like to acknowledge the assistance received from the following individuals, who have contributed in one way or another towards the successful completion of this work: -

Professor A.C.F. Cocks and Dr Bob Ainsworth, for providing useful comments and suggestions, from their vast knowledge and expertise in this field, at the various stages of the work. These were found to be extremely valuable in the pursuit of insights into the analyses conducted.

Dr Chen Haofeng, for his time and assistance in the development of the computational procedures employed in this thesis.

Dr Phil Brown, for his prompt actions in rectifying any problems associated with the workstations used.

Dr Mustapha Boulbibane, for his help in providing useful explanations in the early stages of the research work.

Mr Mohamed Mohidin Habibullah and Mrs Meherunisha Beevi, for their continued support and prayers throughout the length of this work.

Relatives and friends, especially those at Joo Chiat Place in Singapore, for their constant support and blessings.

Finally, the author is eternally grateful of the financial support received from British Energy and the Overseas Research Scholarship (ORS) as well as the essential computing and accommodating facilities provided by University of Leicester.

Abstract

The development of computational methods for cracked bodies subjected to cyclic variable loads and temperatures

This thesis is concerned with the development of computational procedures in the assessment of the structural integrity and lifetime of cracked bodies subjected to cyclic variable loads and temperatures.

The foundation of these techniques is the Linear Matching Method (LMM), related to the methods of elastic compensation and Gloss r-node, used in design calculations for a number of years. It involves matching the behaviours of a non-linear material to that of a linear material, whereby sequences of linear solutions with spatially varying linear moduli are produced. The developed iterative programming algorithms, implemented within the finite element scheme, ABAQUS, would then generate a monotonically reducing sequence of upper bounds, ultimately converging to the least upper bound loads.

In their applications, the significance of these programming methods is two-fold. The first is the investigations into the overall behaviour of cracked structures under the combined actions of mechanical and thermal loads. The numerical limit loads and ratchet limits so identified, which describe the onset of plastic collapse and the unlimited accumulation of plastic strains respectively, were found to be stable, with good converged solutions achieved within 40-60 iterations. The analyses also revealed the insensitivity of the ratchet boundaries to cyclic hardening, as the perfectly plastic and complete cyclic hardening limits yielded almost identical results.

The other is the examination into the relationship between the near crack tip fields and the cyclic loading histories, in creep and plasticity conditions. It was established that the HRR field criterion is an appropriate representation of the behaviour of the mechanically and thermally induced crack tip fields. This enabled the crack tip fracture criterion to be evaluated in all conditions, with the observed phenomenon described by two distinct behaviours; strongly influenced by the effect of the elastic stress intensity factor and the reference stress respectively.

The analyses conducted demonstrated the capability of the adopted numerical procedures in appraising the behaviour of cracked structures under cyclic loading histories, with the conservativeness of current solution procedures in R5 clearly evident in the results enclosed.

Mohamed Salahuddin
Mohamed Mohidin Habibullah

Contents

Chapter 1: Introduction

1.1. General Introduction

In recent years, there has been a surge towards the increasing use of structural components operating at elevated temperatures. This economically driven trend has caused current operational power-generating plants, petrochemical reactors, steam and gas turbines, *etc*, to function at much higher temperatures than previously envisaged. This continued quest in improving the efficiency of existing equipment, often experiencing complex cyclic loading histories, called for the development of effective and reliable life assessment methods. The utilization of such techniques would ensure that these structures remains in operation within their design life, whilst satisfying the stringent safety requirements often imposed on them.

In general, the lifetimes of structures operating at elevated temperatures are dependent upon accounting for the deformation and fracture failures experienced in these components. The former is mainly concerned with the excessive plastic deformations associated with the phenomenon of plastic collapse, shakedown and ratchetting, whilst the latter probed into the world of crack growth, among others, due to creep, fatigue and creep-fatigue interaction. The ability in addressing these failures, in structures subjected to steady, cyclic and variable loading conditions, would then provide a means of assessing the remaining life of these structural components. At present, the assessment of structures operating at elevated temperatures is based upon R5 [1], the design life and assessment procedure used by British Energy in the UK. The main objective of this document is to provide a comprehensive

assessment procedure to be easily used by both designers and practitioners. The capability of these procedures is to such an extent that they are now used in conjunction with simulation techniques based upon advanced constitutive equations, in cases where it exceeds the range of the traditional rules-based approach or where greater accuracy is needed.

In recent times, an alternative approach has been developed. It involves the application of numerical methods [2-9], for evaluating sequences of performance indicators in structures subjected to both severe mechanical and thermal loads, operating below and within the creep range. These new methods have the potential of providing assessments, with the results generated combining the accuracy of simulation methods [10,11] and the efficiency of rules-based methods [12,13]. The methods are based upon a new programming technique called the Linear Matching Method (LMM), which generates cyclic loading solutions that correspond to a particular mode of material behaviour. Belonging to the family of related methods such as the Elastic Compensation Method (ECM) [14] and the Gloss r-node Method [15], the LMM essentially involves matching of a materially non-linear problem to a sequence of increasingly accurate linear problems. The developed programming method would then pose the problem as the search for the minimisation of a functional, which is then solved as a sequence of linear problems that converge to the minimum consistent with finite element approximations. Thus, the method contains the characteristics of the above-mentioned ECM and Gloss r-node methods, with the programming power and generality of the classical programming methods of Maier [16], Corradi [17], Weichert [18] and others.

The utilization of the LMM has been successfully investigated on several design-related issues. This includes the identification of limit loads [2,4], in structures subjected to

constant loading conditions, and in the presence of cyclic loads and temperatures, the evaluation of shakedown [3,5,8] and ratchetting limits [6,7]. In addition, recent extensions have resulted in their applications to high temperature creep behaviour including the effect of elastic follow-up [9], *i.e.* the evaluation of local creep damage due to the relaxation of stress during creep dwell times. In all these cases, the methods rely upon the standard set of material data used in rules-based methods, *i.e.* elastic moduli, yield stress, steady state creep deformation and rupture times, simple descriptions of creep strains during relaxation, fatigue and creep/fatigue data. Furthermore, its employment within current simulation techniques, allows it to enjoy the expertise and accuracy of such methods, but with the advantage of the solutions being produced at a fraction of time and cost.

This thesis is concerned with the development of the LMM in the contexts of its application in cracked structures. In the field of deformation failure, the focus is on the identification of limits loads, shakedown limits and ratchetting limits in cracked structures subjected to cyclic histories of loads and temperatures. In fracture failure, the interest is in the development of an understanding into the behaviour of crack tip fields, in mechanically and thermally induced cracked structures, under creep, fatigue and creep-fatigue conditions. The implication of these specific problems, in design and life assessment, is investigated, with particular emphasis on solutions produced in current R5 [1] procedures. This thesis is also aimed at generating standard solutions to typical problems, whereby the interaction diagrams developed would provide assistance in making intelligent assessment on the operational safety of the structure in consideration. Finally, it is hoped that the availability of such techniques would ultimately enhance its applicability within current design and life assessment

procedures [1,12,13], as an additional tool in the verification of the accuracy of current solutions or in some cases, perhaps, act as a replacement to current ones.

In this chapter, the problems associated with the deformation and fracture failures, considered in this thesis, are discussed in great detail. The significance of the outlined structural failures in current R5 [1] procedures as well as the possible account of any other known available solutions is also described. This is then followed by a review of the current inelastic analysis methods used in overcoming these specific problems. On the basis of such appraisals, the justification behind the employment of the LMM in this thesis is then provided. An overview of the thesis is also included, at the end, stating precisely the investigations conducted in each chapter.

1.2. Definition of the Problems

1.2.1. Deformation failures

One of the most critical areas in deformation failures, which have been of interest in industry for many years, is the limit load. This is the maximum load that a structure manufactured from a perfectly plastic material can sustain. The implication of this phenomenon in a structure lies in the fact that the application of proportional loads beyond the limit loads, would lead to the failure of the structure from plastic collapse. The accurate identification of these limit loads, for real uncracked and cracked structures, is, thus, an essential pre-cursor to the design and life assessment of these structures. In the context of the R5 [1] procedures, the significance of the limit loads is that it is one of the essential input

parameters required, in methods for assessing creep, fatigue and fatigue-creep interactions over the lifetime of a structure. Primarily, these loads are used for identifying the reference stress [1,19], with the application of the associated method allowing the quantities of interest in a complex structure to be represented in terms of the reference stress and the corresponding fatigue/creep data at the reference stress level. The utilization of these so-called reference stress methods [1,19] is justified on the basis of their ability to compromise between the pessimism of using purely elastic stress analysis and the cost and complexity associated with the full cyclic inelastic computation.

At the present time, the limit loads, employed in the current procedures, are obtained from the works of Miller [20]. In his investigations, he compiled a compendium for estimating the limit loads of structures containing defects, under the various possible conditions. These include variations in structural geometries, loading conditions, crack lengths under constrained and unconstrained rotation conditions, *etc.* Some of his well-known examples are the single-edged notched tension (SENT), single-edged notched bending (SENB) and compact tension (CT) solutions. The availability of limit load solutions, for the most commonly worked on structural problems, has made his work an almost indispensable reference in most structural integrity evaluation procedures. However, in situations where the limit loads to a specific problem does not exist, costly full step-by-step inelastic analysis [10,11] calculations are generally performed. As an alternative to such analyses, the existence of an inelastic limit analysis method, whereby limit loads are computed by a series of simple elastic calculations, is advantageous. The ability of the chosen methodology, in initially reproducing some of Miller's [20] solutions, would also provide the necessary verification of the accuracy and validity of the solutions generated.

In circumstances whereby structures are subjected to cyclic histories of loads and temperatures, the relative variations of the induced mechanical and thermal stresses has serious implications on the life span of the structural components. For certain structural configurations and combinations of loading cycles, large fluctuating stresses may be tolerated without causing any progressive strain growth (reverse-plasticity). In other situations, stresses operating in excess of the initial elastic limit produce very quick accumulation of plastic strains (ratchetting). On the other hand, there are conditions that if some plastic strains are accommodated during the initial loading cycles, the subsequent behaviour of the structure is elastic (shakedown). Whereas ratchetting must be avoided at all cost since it leads to intolerable deformation, reverse-plasticity can be endured provided low cycle fatigue is taken into consideration. Hence, in the design and life assessment of structures, it must be ensured that any inelastic strains/deformation accumulated must be avoided altogether or restricted to the number of cycles within its designed limit so that they will not make the component unserviceable.

In addressing the effect of shakedown, the current R5 [1] procedures adopted Melan's [21] classical shakedown theorem. Fundamentally, this theorem requires the identification of a constant residual stress field, such that the sum of the applied linear elastic stress fields and the constant residual stresses, are kept within yield at all points in the body under all possible loading combinations. Thus, the satisfaction of the equilibrium condition in the body leads to the shakedown limits, identified within the R5 [1] procedures, as lower bound shakedown limits [22].

In the identification of the corresponding reverse-plasticity and ratchetting limits, however, to the best of the author's knowledge, no such procedures exist within R5 [1]. In such situations, an extension of the classical theorem, capable of identifying a time-varying residual stress field, is required, such that the sum of the linear elastic, constant residual and the time-varying residual stress fields, are kept within yield only over some volume of the body. The subsequent cyclic behaviour is, thus, no longer entirely elastic, as there are restricted increments of plastic strains forming a reverse-plasticity mechanism over some part of the body, whilst persisting in the shakedown state in the remaining part. In closing this gap, an early attempt was made by Ponter *et al* [23,24], whereby the behaviour of a two-bar structure subjected to severe thermal loadings, was investigated. Using the simplified assumption of a fully cyclically hardening material, a means of distinguishing shakedown, reverse-plasticity and ratchetting limits was successfully developed. Nonetheless, the availability of a generalized theorem, capable of differentiating these limits with respect to changes in the cyclic properties of the material, implemented within an efficient inelastic analysis method, would be an asset in the current climate of operating structures at elevated temperatures.

In the investigations into the behaviour of cracked structures subjected to cyclic histories of loads and temperatures, however, not much work has been undertaken in the identification of these limits. This is mainly due to the inability of the presently available methods in dealing with the elastic singularity at the crack tip. In overcoming this deficiency, the common practise was to generate solutions using the classical shakedown theorems [21,25], but with the cracks replaced with notches. Examples of such publications include the works of Huang & Stein [26], Feng & Gross [27] and Carpinteri [28]. Practically, however,

the accuracy of these solutions is generally viewed with suspicion, since they do not model the realistic crack conditions experienced in the structure. In this respect, it is, therefore, desirable for an inelastic analysis method to be developed, capable of efficiently identifying the shakedown, reverse-plasticity and ratchetting limits, in both cracked and uncracked conditions. The capability of the chosen methodology, in accurately classifying the three regions, would also be of great assistance to designers and practitioners in making intelligent judgement on the structure's safe operating region. Finally, it is also hoped that the ability of the method to deal with the issues raised, would, perhaps, ultimately lead to the adoption of such methods within current R5 [1] procedures.

1.2.2. Fracture failures

Within the framework of fracture failures, this thesis is concerned in addressing two important crack growth issues. The first is in the development of an understanding into the behaviour of the crack tip fields under cyclic creep loading conditions, in cracked structures subjected to cyclic histories of loads and temperatures. This is one of the most critical failures experienced in many industrial types of equipment, operating at elevated temperatures for extended periods of time. In conducting such investigations, methodologies capable of generating cyclic creep solutions in cracked structures is essential. The availability of such procedures would then enable the characteristics of the near crack tip fields, under the prescribed loading conditions, and their influence on cycle times and material behaviour, to be examined. This would then lead to the possible definition of a crack tip fracture criterion to be identified, which in essence is a representation of the safe operation of the whole structure.

The conventional attitude to this problem is to develop constitutive laws for the material behaviour and to conduct detailed finite element studies of the response of the cracked structures. Although such a procedure is sound and valid, there are, however, a number of problems associated with their employment. Firstly, the constitutive equations used in modelling the material behaviour under the complex loading histories, are often too elaborate and contain a large number of variables, making them very difficult to implement. In addition, their general applications, in all situations, are often questioned, since these laws were identified from extensive experimental studies conducted on a particular batch of material. In circumstances where these constitutive relationships holds true, the complexity and specialised programming knowledge required in computationally implementing these laws, makes such an approach rather unappealing in the current financially conscious environment.

In overcoming the above difficulties, an alternative approach was proposed. This involves examining the behaviour of the cyclically loaded cracked structures, by considering only the extremes of the loading conditions and used in conjunction with simple constitutive material models. A preliminary investigation into this procedure was conducted by Le Mat-Hamata *et al* [29,30], who successfully showed that, in cracked structures subjected to cyclic variable loads, it was possible to develop an understanding into the relationship between the near crack tip fields and the different features of the material response. Their encouraging results formed the basis of the investigations carried out here, whereby an understanding into the behaviour of cracked structures, subjected to both cyclic histories of loads and temperatures, is demanded. The conduction of such examinations, thus, requires the development of a cyclic creep analysis method, capable of implementing within them, simple

constitutive material models. In addition, the availability of such procedures would also enable the appropriateness of current R5 [1] procedures, which treats the effect of thermal stress as an equivalent bending moment, to be validated.

The other area of crack growth, of interest here, is in the development of an understanding into the behaviour of the mechanically and thermally induced crack tip fields, under reverse-plasticity and reverse-plasticity/creep loading conditions, in cracked structures subjected to cyclic variable loads and temperatures. This is, perhaps, one of the most likely behaviour observed in many processes of engineering design and life assessment of structures subjected to cyclic loading histories. Although intensive studies have been undertaken in the past [31,32], the majority of the results obtained were only concerned with the behaviour of cracked structures, under purely variable loads. In the current climate of structures operating at elevated temperatures, a similar investigation into the behaviour of cracked structures, under both variables loads and temperatures, needs to be studied. The existence of analysis methods, capable of generating such solutions, would help in this cause. This would then lead to the relationships between the crack tip fields and the cyclic loading histories to be identified, enabling the corresponding fatigue crack growth and fatigue-creep interaction criteria to be evaluated.

The importance of such investigations was also outlined in the joint report by EPRI/CRIEPI/NE [33], for the liquid metal fast breeder reactor program. Although the collaboration concluded that current flaw assessment procedures, such as R5 [1], are safe, the over-conservatism of the solutions produced is a concern. In describing the behaviour of cracked structures under the prescribed loading conditions, the current procedures entail the

application of two formulations. The first is the small-scale yielding formulation [34], indicating the domination of the elastic stress intensity factor and generally used in describing the behaviour of the cracked structures at low variable loads. The corresponding formulation at high variable loads is the application of the reference stress method [1,19]. Thus, within the current procedures, the summing up of these two formulations, is the criteria often used in describing the overall crack tip behaviour of cracked structures. Therefore, in addressing the effect of over-conservatism in the above conjecture, the numerical solutions generated from the proposed investigations, needs to be compared with solutions obtained from the current procedures. The results of such comparisons would then enable judgement on the validity of the concerns, in these solutions, to be made.

This thesis has, so far, described the areas of deformation and fracture failures, experienced in cracked structures subjected to cyclic histories of loads and temperatures, which needs to be investigated. For each specific structural-related problem discussed, their implication, to the design and life assessment procedures of R5 [1] were also presented. In all these situations, the investigations called for the development of analysis methods, capable of describing the behaviour of cracked structures under the prescribed loading conditions. As a general rule, these analysis methods have to satisfy the following conditions. It needs to be efficient and effective in resolving the issues raised, particularly in the examinations into the performance of the cracked structure at the crack tip. The programming methods developed must also be capable of generating accurate results, possibly requiring as little specialist programming knowledge as possible. Adequate care must also be taken to ensure that the elected analysis methods were capable of monitoring the solution's sensitivity, as well as, securing a reasonable realization in convergence. Last, but not least, the ability of these

methods to be implemented, within existing commercially available software rather than specialist codes, would also be an added advantage.

1.3. Inelastic Analysis Methods

In analysing the behaviour of structures subjected to cyclic histories of loads and temperatures, there are a number of different methods available at the present time. The majority of these methods have been successfully applied to uncracked components, yielding useful explanations to the structural-related problems faced. In cracked conditions, however, an understanding into the behaviour of these mechanically and thermally induced structures, still poses a major difficulty. This, despite, the commendable progress that has been made in recent years, resulting in the emergence of a number of design and life assessment methods.

In the pursuit of answers to the deformation and fracture failure questions declared in the previous section, the strategy employed in this thesis involves examining the capability of the presently available methods applied to uncracked structures. The pros and cons of these methods were then investigated, with the eventual identification of the method with the best potential of being adapted to cracked problems. A review of some of these methods, broadly classified into four main categories, is presented below.

1.3.1. Accumulation of experimental results

This procedure involves investigating the response of a real structure subjected to a combination of real loading (mechanical and thermal) or alternatively looking at a scaled

model and its corresponding scaled loading, through experimental techniques. Proposed by workers at CEA/DEMT [35], the ensuing results obtained are then collated and analysed, by plotting non-dimensionalised graphs, with axes corresponding to the two loads. On these plots, known as Efficiency Diagrams, boundaries indicating the critical limits in creep and plasticity were then identified. Comparisons were then made with solutions obtained from other known numerical methods.

Such examinations have been performed for the problems experienced in the Liquid Metal cooled Fast Breeder Reactors (LMFBR) [36]. It was observed that, in certain circumstances, the CEA/DEMT solutions (shakedown and ratchetting limits) compare favourably, while in other situations, it does not. This implies the necessity in conducting experiments for various ranges of structural problems, under different combinations of loading histories and/or structural geometries. The practicality of performing different arrays of experiments is debatable as these incur excessive cost, which needs to be justified in comparison with other inexpensive available methods. The ability in conducting these experiments is also dependent upon the technological advances made in the field in question. This is the reason behind the exploitation of such an approach is generally restricted to only uncracked structural components, making it rather unattractive in the proposed investigations into the deformation and fracture failure problems experienced in cracked structures. Although, the continued utilization of this method, by the aforementioned institution, is based upon the argument that new data can be constantly updated when acquired, the quantities and restrictions of these data to only specific problems have caused this method not to be highly thought of.

1.3.2. Particular solution methods

These are solutions to idealised structural problems solved using various simplifying assumptions. The common features of these methods entail making a number of simplifications in describing the geometric properties as well as the mechanical behaviour of the materials. Generally, it involves reducing the number of spatial dimensions considered, from a three-dimensional problem to a one or two-dimensional model, and restricting the magnitudes of the deformations to infinitesimal strains. In simplifying the material properties, these solution methods vary by making sensible assumptions on factors such as temperature dependence of properties, hardening rules, cyclic properties, *etc*.

Essentially, these methods involve generating material models, representative of real problems, and investigating their behaviour, under plasticity and creep loading conditions. The results obtained are then analysed and wherever possible, analytical solutions are outlined. An example is the classical Bree [37] solution, for the fuel can problem. Under the combined effects of internal gas pressure and intermittent heat fluxes, there was a concern that the design of the fast-nuclear reactor fuel can was unsafe. This was due to the high thermal stresses experienced in the can wall during start-up and shutdown situations, which may cause structural failures due to excessive straining. In answering these questions, a model of a plane stress nuclear reactor fuel can, subjected to relatively high thermal stresses in the presence of an internal pressure, was examined. The results obtained were then represented in the form of interaction diagrams, or otherwise known as Bree diagrams, clearly distinguishing the various possible modes of structural behaviour, *i.e.* shakedown, ratchetting and reverse-plasticity. The safety of the fuel can was then judged on the basis of such diagrams.

Later, using a different approach, O'Donnell & Porowski [38] conducted a similar investigation for the same fuel can problem. Their examination proved the correctness of the Bree solutions, as the method yielded similar analytical equations, representing the different behavioural modes in the diagrams. Additional studies into the behaviour of the can under creep conditions were also conducted [39], and when presented on these diagrams, provided a means of assessing the operational safety of structures against failure due to creep and plasticity. Another example of a particular solution is the analysis on the three-bar assembly structure by Miller [40]. He examined the possibility of correlating the behaviour of this simple structure to that experienced by pressure vessels subjected to combinations of cyclic thermal and pressure stresses. On the basis of this conjecture, design criteria were then derived, allowing limits to reverse-plasticity and ratchetting to be prescribed. Other workers, belonging to this group of solution methods, are Parkes [41], for the problem of incremental collapse of an aircraft wing as a result of fluctuating thermal stresses superimposed on the normal wing loading, and Gokfeld & Cherniavsky [42], for methods of identifying shakedown limits in shell and plate problems.

The significance of these particular solution methods in engineering design is the ability to conduct repeated simulations on these specific problems, for differing loading conditions and/or structural geometries. For the Bree problem, compendiums of interaction diagrams have been compiled [43], providing designers with instant access to essential information required in structural analysis. These could then be used in design rules or as a comparison with solutions generated using other inelastic analysis methods. Although successful in certain circumstances, question marks still hang over the solution's accuracy and

their relevance in design problems. This is mainly due to the assumptions the above investigators make on the behaviour of structures, under the combined actions of mechanical and thermal loads. There is a concern that the particular views adopted by these researchers, might be based upon an incomplete understanding of the material's behaviour. This would lead to the application of such solution methods, in cracked structures under cyclic loading histories, to be questionable. Furthermore, most of these investigations were only concerned with the deformation failures observed in uncracked structures. To the best of the author's knowledge, no such solutions have been attempted in the field of fracture failures.

1.3.3. Computer solution methods

The use of computers in structural analysis lately, has enabled many complex structures, not analysable before, to be studied and investigated. Using such solution methods, an accurate description of the behaviour of high temperature components is now possible, by following changes in the stress, strain, deformation and material properties in a non-linear analysis process. In recent times, a big leap in interest for these methods was observed. This is mainly due to the extensive developments made within the finite element analysis (FEA) codes, the foundation behind these computer solution methods. The flexibility and reliability of these FEA codes, implemented within very high capacity computers, in conjunction with the comprehensive deformation and material data obtained from the classical constitutive plasticity/creep equations, has enabled a complete inelastic analysis to be performed, even for the most complex design shapes often containing many of the features of practical components.

Today, in engineering industries, there is a wide variety of commercial software, which is based upon FEA. One of them is ANSYS [10], a simulation program that can solve problems ranging from the relatively simple linear elastic analyses to the most challenging non-linear simulations. Another general-purpose finite element modelling package is ABAQUS [11], a tool capable of numerically solving, among others, mechanically and thermally induced structural problems. There are also other examples of purpose-built FEA methods, but only used within the industries it is originally designed for. The CASTEM 2000, developed by the Mechanical Department and Technology (DMT) of the French police, is an example of one of them. BERSAFE, an in-house code used by Nuclear Electric plc, was another one. Although each of these methods is specifically different, the overall organization of the solution process is found to be, by and large, the same.

The advantage of computer solution methods lies in the fact that they are able to solve almost any structural problem, irrespective of the structural geometries and/or loading conditions. Its ability to handle the deformation and fracture failure problems, in both uncracked and cracked structures, has made this method an essential tool in many processes of engineering design and life assessment. Although useful in evaluating structural behaviour, this step-by-step inelastic analysis calculation generally require very large computational effort, for structures subjected to very complex loading histories. There is also the matter of high cost and long analysis time required in performing such tasks, especially in three-dimensional structures. In the analysis of cracked structures subjected to cyclic histories of load and temperatures, the literature behind these methods indicates the unavoidable problems of stability and convergence, which requires considerable expertise to rectify. Thus, in most practical situations, the employment of these methods is generally limited to validating the

result of a designed structural component, rather than performing the full step-by-step inelastic analysis.

1.3.4. Direct solution methods

These are methods that do not follow the evolution of the structural system along a given history of external loading actions. They directly evaluate critical, ultimate states of that evolution and provide only essential information concerning them, without following the step-by-step inelastic structural responses to the assigned loading history. The capability of these methods in answering issues related to design and life assessment of structures has enabled them to withstand the test of time. This, despite the extensive progress made in the above-mentioned computer solution methods, producing inelastic analysis solutions.

The motivation behind the continued development of these methods is as follows. Firstly, in many structural engineering situations, the crucial element is the assessment of the "safety factor" of the "live loads", with respect to the ultimate limit states specified. The utilization of direct methods leads precisely to that assessment, often accompanied by useful information on the kinematics of the structural crisis and the expected stress states under the critical loading conditions. The potentially useful information, which can be gained with bounding theorems, is another notable factor. As the name suggests, these theorems bound the exact solution, producing either conservative or non-conservative results. Thus, the use of these direct methods, based upon such bounding theorems, would allow checks to be performed, with respect to possible local failures and/or un-serviceability. Finally, the most significant reason of them all is the substantial computational savings that could be achieved,

in comparison with solutions produced from computer solution methods. The implementation and commercialisation of software for these direct methods would enable solutions to be generated at a fraction of the time and cost expected of other inelastic analysis methods.

The majority of the direct solution methods developed are concerned with the ultimate limit states associated with plastic collapse, *i.e.* the exhaustion of the load carrying capacity in ductile structures. In structures subjected to variable repeated and cyclic external actions, the corresponding limit states are the safety region (shakedown) and the eventual failures either by incremental collapse (ratchetting) or alternating plastic flow (low cycle fatigue). Under the general heading of limit and shakedown analyses, various methods have been suggested. Some of these techniques are described below.

The use of direct methods as bounding techniques is a major subject of interest. This is in response to the frequent discrepancies existing between the traditional plasticity hypothesis of unlimited ductility and the actual behaviour of the materials with possible local failure. If economically computed, the implementation of these upper/lower bounds methods, within the finite element-modelling scheme, would provide a means of eliminating undesirable thresholds in structural design and life assessment. A variety of bounding theorems and relevant numerical procedures has been proposed, with the works of Maier *et al* [44], Polizzotto *et al* [45] and Ponter [46] leading the way.

In recent times, a special limit and shakedown analyses strategy, exhibiting interesting novel features, has been proposed and developed for versatile engineering use. The methodology basically amounts to a convergent iterative sequence of linear elastic analyses, at

each iteration of which the local (material or sectional) elastic stiffness is suitably modified on the basis of the preceding iterations [2-8,14,15,47,48]. Belonging to the family of the ECM, the success of these methods is based upon their ability to produce solutions within finite iterations as well as practically coping efficiently in their implementations within the current commercial FEA codes.

Thus far, the reviews in the solution methods, described in Sections 1.3.1. to 1.3.4., showed a wide variety of available procedures, potentially capable of analysing the behaviour of cracked structures subjected to cyclic histories of loads and temperatures. Each of these methods approaches the problems differently, with some more capable in implementation, while others having the advantage of being cost and time effective. In most practical situations, however, compromises are usually made, taking into account the various factors involved. Upon careful consideration into each of the method's features, the methodology with the best potential, for further exploration, was identified as the LMM [2-9].

1.3.5. Linear matching method

This method forms the foundation of the analyses conducted in this thesis. It is a non-linear programming technique, developed out of the Elastic Compensation Method (ECM), implemented within the commercial FEA code, ABAQUS. It basically involves sequentially matching the behaviour of a linear rate problem to that of a linear problem. Numerically, sequences of linear solutions with spatially varying moduli are produced, generating upper bounds which monotonically reduce to converge to a least upper bound, associated with the class of displacement fields considered by the finite element approximations. The primary

application of these methods is in the evaluation of the limit loads and shakedown limits for complex structural components [49]. The workers involved in the development of these techniques include, among others, Ponter & Carter [2,3], who presented the initial implementation as well as the formal proofs for the monotonic reduction of these upper bounds and later, Ponter & Engelhardt [5,49], who successfully simplified and generalised the methodology, existing in the present form.

The choice of using the LMM, as the apparatus in addressing the identified deformation and fracture failure problems experienced in cracked structures subjected to cyclic histories of loads and temperatures, is based on its satisfying the following conditions. First and foremost, the methodology combines the flexibility of the computer solution methods as well as the simplicity associated with the direct methods. This implies the possibility of performing structural analysis, with the accuracy but at a fraction of time and cost of the full step-by-step inelastic analysis calculations. Their capability to be implemented within the commercial software, ABAQUS, is another advantage, which unlike other techniques does allow the development and utilization of specialist programming codes. Another feature of this method is its ability to achieve rapid convergence. Past investigations into the identification of limit loads and shakedown limits of uncracked structures have revealed that good converged solutions are generally attained within 30-100 iterations [5]. Although not much work has been undertaken in the field of cracked structures, promising recent results in the capability of the method in identifying the limit loads of cracked structures [4], further justifies the selection of this method. These limit load solutions generated also provided the confidence that an investigation into the behaviour of the crack tip fields under creep and reverse-plasticity conditions is possible. Thus, it is believed that the

application of the LMM, to cracked structures subjected to cyclic loading histories, would be capable of answering the deformation and fracture failure questions posed in the earlier sections.

1.4. Overview of the Thesis

This thesis is broadly divided into seven main chapters, with each chapter focusing on one particular aspect of the problems identified in Section 1.2. The exception is in this chapter (Chapter 1) whereby the subjects of interest were introduced. This was then followed by declarations into the associated deformation and fracture failure problems, experienced in cracked structures subjected to cyclic histories of loads and temperatures, causing an assessment into the various currently available solution techniques to be conducted. From which, the methodology with the best prospect for investigating the behaviour of cracked structures under the prescribed loading histories was then identified as the Linear Matching Method (LMM).

In Chapter 2, the application of the LMM in limit analysis is discussed. It begins with brief statements on the lower and upper bound limit load theorems for the von-Mises yield condition. This is then followed by the discussion into the foundation of the LMM, as an iterative upper bound limit analysis method. Its implementation within ABAQUS is then described, for two cracked numerical problems subjected to constant mechanical loads. Using two different implementation approaches, Procedure A and Procedure B, solutions to the two problems are then compared, enabling the subsequent identification of the superior procedure for further analysis.

In Chapter 3, the theory behind the LMM for shakedown analysis is discussed in great depth. Beginning with an introduction into the fundamental shakedown theorems for a general problem, its implementation for the upper bound shakedown theorem is then presented. For structures loaded in excess of shakedown, extended theorems for the identification of ratchetting limits are also explained. These numerical methods are then applied to the Bree problem [37], in uncracked and cracked conditions, enabling distinctions between the regions of shakedown, reverse-plasticity and ratchetting to be identified. Further examinations are then conducted for an additional industrial problem, considered in R5 [1], allowing comparisons between the numerical solutions and those used in current design and life procedures to be made.

In Chapter 4, the essential concept behind the rapid cycle creep solution is discussed. Using an extension of the LMM, its implementation is then described for two constitutive creep models, Norton's law and the Bailey-Orowan model. For these two creep models considered, the characteristics of the near crack tip fields, subjected to cyclic histories of loads and temperatures, are then investigated on the cracked axisymmetric Bree problem, using the HRR field criterion as the foundation. Calculations are then repeated, for variations in structural geometries, loading histories and material properties, with the ultimate aim of demonstrating the capability of the numerical methods to be employed in all situations.

In Chapter 5, the significant aspect behind the reference stress method is deliberated. Its initial application, to structures subjected to purely mechanical load, is then demonstrated for the problem considered in Chapter 4. In the presence of both mechanical and thermal

loads, an extension of the reference stress concept is then prescribed. These terms are then represented in terms of the effective reference stress quantities, enabling an assessment on the validity and appropriateness of current design and life assessment procedures [1] to be judged, under the various circumstances considered in Chapter 4.

In Chapter 6, an approach of investigating the behaviour of cracked structures under reverse-plasticity and reverse-plasticity/creep loading conditions is introduced. Using the HRR field criterion as the foundation, the near crack tip fields are then examined using a methodology based upon the LMM, numerically implemented in a two-stage decoupled analysis process. This enabled the behaviour of the crack tip fields, under reverse-plasticity and reverse-plasticity/creep loading conditions, to be individually analysed, under the varying magnitudes of load and temperature. Relationships between the crack tip fields and the cyclic loading histories are then identified, enabling the judgement on the conservativeness of current design and life assessment [1] procedures to be demonstrated.

Finally, in Chapter 7, conclusions to the objectives outlined in this thesis are presented, including a summary of the results generated. Suggestions on the possible future research areas to be conducted are also enclosed.

Chapter 2: Limit Analysis Methods

2.1. Introduction

In the subjects of limit analysis and plasticity theorems, their origins could be traced back to the 1940's and 50's plasticity schools. Then, the lack of effective computational methods for complex design problems provided a powerful incentive to discover new and distinct theorems. These findings, well documented in the current literature [22,50], gave fundamental insight into the behaviour of structures subjected to realistic and complex loads. Unsurprisingly, design codes and life assessment procedures for metallic structures, evolving from this period, relied heavily on the insights so obtained.

The growth of interest in limit analysis methods, in recent times, is, however, due to the need in directly computing the performance indicators (limit loads) of structures subjected to complex loadings. The capability of these methods in resolving structural integrity concerns, in current design and life assessment procedures [1], has boosted the prominence of these so-called direct methods, *i.e.* simplified solutions based on bounding theorems. This shift in attitude was made possible, with the advent of FEA methods [51], implemented within fairly flexible and reliable commercial FEA codes [10,11]. Thus, the incorporation of these direct methods within these codes is an aid to design, especially so, in determining the remaining strength of a structure once a flaw or crack is detected. This, in turn, would then enable the reference stress [1,19], a quantity often used in describing the behaviour of cracked structures, to be evaluated.

One particular direct method, widely used in industry for calculating limit loads for many years, is the Elastic Compensation Method (ECM) [14]. In its original form, this purely linear elastic analysis calculation involves adjusting the elastic moduli spatially to ensure that the linear elastic stresses are brought within yield, at a fixed strain distribution. A further elastic solution is then carried out using the current distribution of elastic moduli. At each stage, a lower bound on the limit load is then evaluated by scaling the solutions, so that the stresses lie within yield for the current elastic solution. In an iterative process, this sequence is terminated when the utmost lower bound limit load is achieved. Other variants of this method, that has been equally successful in evaluating the limit loads of cracked structures, includes the Reduced Modulus Method [52] and the Gloss r-node Method [15], with the full historical account of these methods detailed in the review paper of Mackenzie *et al* [53].

The above methods, despite their capabilities, have certain uncertainties associated with them. Firstly, most of these methods are supported by standard FEA codes, which itself is an upper bound method based upon the Rayleigh-Ritz optimisation technique. Furthermore, these codes tend to achieve global rather than point-wise equilibrium, which leads to serious implication on the methods' ability to converge to the utmost lower bound limit load, or worst still, it may not lie below the exact solution. The non-existence of any formal monotonic convergence proofs, further questions the methods' stability.

In view of overcoming these difficulties, Ponter *et al* [2,4] developed an iterative upper bound limit analysis method, which is based upon the concepts contained in the ECM. It basically involves defining a sequence of linear problems, where the linear coefficients are

chosen so that they match the yield condition. The iterative non-linear programming procedures developed, numerically implemented within the FEA code ABAQUS, would then generate sequences of upper bounds, converging monotonically to the least upper bound limit loads. Unlike previously, this methodology does deliver a convergence proof that the upper bounds will monotonically reduce to the least upper bound limit load [2]. Another advantage is in its ability in evaluating limit loads, for structures satisfying any arbitrary convex yield condition [4].

In this chapter, the re-interpretation of the ECM, as an iterative upper bound limit analysis method, is presented. Upon a brief introduction into the general fundamental theorems associated with limit analysis, the foundation behind the Linear Matching Method (LMM) is then discussed. Also included is the method's implementation within ABAQUS, software based upon FEA methods. For a structure subjected to purely mechanical loads, two different implementation procedures, suitability identified as Procedure A and Procedure B, are then presented. From the ensuing numerical solutions, comparisons were then made on the Procedures' accuracy, stability and convergence, leading to the identification of the superior methodology for further analysis.

2.2. Limit Analysis

Figure 2.1 shows the problem considered in the analysis. It consists of a body of volume, V, having a surface area, S. The surface is also divided into two parts: S_u, the part where constraints are prescribed, hence all displacement rates, $\dot{u}_i = 0$, and the remaining part,

S_P, onto which the loads are applied. The applied load is of the form, $\lambda P_i(x)$, where $P_i(x)$ is the shape of the load and λ is the scalar parameter, providing its magnitude.

The body is then assumed to be made up of an elastic-plastic material with a uniaxial yield stress, σ_y, satisfying the von-Mises yield condition,

$$f(\sigma_{ij}) = \bar{\sigma}(\sigma_{ij}) - \sigma_y = 0 \tag{2.1}$$

where $\bar{\sigma}(\sigma_{ij}) = \sqrt{\frac{3}{2}\sigma'_{ij}\sigma'_{ij}}$ is the von-Mises effective stress and $\sigma'_{ij} = \sigma_{ij} - \frac{1}{3}\sigma_{ij}\delta_{ij}$ are the deviatoric stresses. The plastic strain rates, $\dot{\varepsilon}^P_{ij}$, at yield are given by the associated flow rule,

$$\dot{\varepsilon}^P_{ij} = \dot{\alpha}\frac{df(\sigma_{ij})}{d\sigma'_{ij}} \tag{2.2}$$

where $\dot{\alpha}$ is the constant of proportionality. This can be expressed as the Prandtl-Reuss equation [54], given by,

$$\dot{\varepsilon}^P_{ij} = \frac{3}{2}\frac{\bar{\dot{\varepsilon}}}{\bar{\sigma}(\sigma_{ij})}\sigma'_{ij} \tag{2.3}$$

where $\bar{\dot{\varepsilon}}$ is the associated effective strain rate. In stress space, $\dot{\varepsilon}^P_{ij}$ forms a normal vector to the yield surface and for the Von-Mises yield condition, it implies that the plastic strain rates, $\dot{\varepsilon}^P_{ij}$, and the associated deviatoric stress at yield, σ'_{ij}, are proportional to each other.

The limit state of the body can then be defined as the value of $\lambda = \lambda_L$, where there exists an equilibrium stress field, σ_{ij}^P, which satisfies yield,

$$f(\sigma_{ij}^P) \leq 0 \tag{2.4}$$

where λ_L is the limit state parameter. At the same time, there exists a distribution of plastic strain rates, $\dot{\varepsilon}_{ij}^P$, which is compatible with the displacement rates, $\dot{u}_i = 0$, on S_u, such that, at all points in the body where $\dot{\varepsilon}_{ij}^P \neq 0$, σ_{ij}^P lies on the yield surface and is associated through the rate equations. It is well known that for the von-Mises yield condition, there exist a unique λ_L and associated $\dot{\varepsilon}_{ij}^P$ and σ_{ij}^P, except in the rigid regions, $\dot{\varepsilon}_{ij}^P = 0$, where σ_{ij}^P may not be unique.

In reality, however, the simultaneous satisfaction of both equilibrium and compatibility conditions, based upon an appropriate yield and flow rule criterion, are seldom achieved. This is, particularly so, in the analysis of structures having complex geometries and/or loading and/or boundary conditions. In its place, bounding theorems [22,50] are often utilised, producing either a lower bound or an upper bound limit to the true limit load.

2.2.1. Lower bound limit load

The lower bound limit load theorem states that a body will support the applied load, $\lambda_{LB} P_i$, if a stress field, σ_{ij}^*, can be found, which is in equilibrium with it, such that it satisfies yield at every point within V,

$$f(\sigma_{ij}^{*}) \leq 0 \tag{2.5}$$

then, $\lambda_{LB} \leq \lambda_L$, where λ_{LB} is the lower bound limit load parameter.

2.2.2. Upper bound limit load

The upper bound limit load theorem states that if the rate of internal energy dissipated in a body is equated with the work done externally on the body by the applied loads, the resulting estimate, $\lambda_{UB} \geq \lambda_L$, for a chosen deformation mechanism, where λ_{UB} is the upper bound limit load parameter. Thus, for an assumed compatible strain rate distribution, $\dot{\varepsilon}_{ij}^{c}$, with the displacement rates, $\dot{u}_i^c = 0$, on S_u, the theorem yields,

$$\lambda_{UB} \int_s P_i \dot{u}_i^c ds = \int_v \sigma_{ij}^c \dot{\varepsilon}_{ij}^c dv \tag{2.6}$$

where σ_{ij}^c is the stress at yield associated with $\dot{\varepsilon}_{ij}^c$.

Note: If the stress fields, σ_{ij}^{*} in (2.5) coincides with σ_{ij}^c in (2.6), then $\lambda_{LB} = \lambda_L = \lambda_{UB}$.

2.3. Linear Matching Method

2.3.1. Simulation technique for limit analysis

The method [2,4] attempts to relate a series of incompressible linear solutions to the limit state described above. The term, incompressibility, means that in an isotropic material,

the standard stress strain relationship becomes indeterminate. This argument would be clearer if it is written as two separate linear relationships, representing the deviatoric and hydrostatic stress and strain rate components respectively,

$$\sigma'_{ij} = \mu\dot{\varepsilon}'_{ij} \qquad \& \qquad hp = \frac{1}{3}\sigma_{ij}\delta_{ij} = K\dot{\varepsilon}_{kk} \tag{2.7}$$

where σ'_{ij} is the deviatoric stress, hp is the hydrostatic tension (mean stress), $\dot{\varepsilon}'_{ij}$ and $\dot{\varepsilon}_{kk}$ are the deviatoric and volumetric strain rates respectively. The shear modulus, μ, and bulk modulus, K, are related to the Young's modulus, E, through the following expressions,

$$\mu = \frac{E}{1+\nu} \qquad \& \qquad K = \frac{E}{3(1-2\nu)} \tag{2.8}$$

where ν is the Poisson's ratio. In dealing with incompressibility, *i.e.* volume conserving, indeterminacy occurs when the material is at $\nu = 0.5$ and the volume strain rate is zero, whilst the bulk modulus approaches infinity. It is therefore more convenient to deal with deviatoric quantities, as these are independent of the hydrostatic components, which themselves do not produce any strains in a rigid/perfectly-plastic material. This leads to the stress strain relationship in (2.7) to be given by,

$$\dot{\varepsilon}_{ij} = \frac{1}{\mu}\sigma'_{ij}, \qquad \dot{\varepsilon}_{kk} = 0 \tag{2.9}$$

where $\mu = \frac{2}{3}E$, identified in equation (2.8) using $\nu = 0.5$.

Essentially, the simulation technique in limit analysis requires varying spatially the shear modulus, μ. If it is possible, for the spatially varying shear modulus to find a solution that satisfies the von-Mises yield condition of (2.1),

$$f(\sigma_{ij}) = \overline{\sigma}(\sigma_{ij}) - \sigma_y = 0 \tag{2.10}$$

in the plastic region, V_p, of the body, and at the same time, in the rigid region, V_u, of the body, the stresses are kept within yield and the strain rates are zero, which involves letting the shear modulus approach infinity,

$$f(\sigma_{ij}) \le 0, \quad \dot{\varepsilon}_{ij} = 0, \quad \therefore \mu \to \infty \tag{2.11}$$

then the solution is essentially identical to the limit state solution, provided the following identities are made,

$$\sigma_{ij}^{P} = \sigma_{ij} \quad \& \quad \dot{\varepsilon}_{ij}^{P} = \dot{k}\dot{\varepsilon}_{ij} \tag{2.12}$$

where $\mu = \dfrac{\dot{k}}{\dot{\alpha}}$, with $\dot{k}$ being an arbitrary constant scaling rate parameter. This means that for any limit state solution, there exists a distribution of shear moduli, μ, for which the linear solution, σ_{ij}, is identical to the limit state solution, σ_{ij}^{P}.

In reality, however, the satisfaction of the conditions, presented in equations (2.10) and (2.11), is difficult to construct. This is primarily due to the fact that in its implementation within the finite element analysis codes, it requires the shear modulus to approach infinity in

the rigid part of the body. It is, however, possible for the shear modulus to be sufficiently large, which in turn, produces strain rates sufficiently small, so as not to contribute to the upper bound in (2.6). This results in the energy dissipation to approach zero in the rigid parts of the body. The simulation of such a method is described in an iterative procedure below, whereby it seeks a sequence of μ values, so that at each iterative step, the solution approaches more closely towards the correct solution.

2.3.2. Iterative method

The iterative method begins with a linear elastic stress solution, having an initial stress, $\bar{\sigma}(\sigma_{ij}^{k})$, and an associated strain rate field, $\dot{\bar{\varepsilon}}_{ij}^{0}$, with an arbitrary uniform shear modulus, μ^{k}. A new distribution of shear moduli, μ^{k+1}, is then evaluated so that, for fixed $\dot{\bar{\varepsilon}}_{ij}^{0}$, the stress point would be brought to the yield surface. This choice can be best understood from the construction shown in Figure 2.2. The new linear stress solution constructed would, thus, be an improvement to the previous iterative solution, provided they are related by the following relationship,

$$\mu^{k+1} = \mu^{k} \frac{\sigma_{y}}{\bar{\sigma}(\sigma_{ij}^{k})} \tag{2.13}$$

where k is the iterative number in an iterative process. This process is then continued until convergence occurs. At each iterative step, the lower and upper limit loads may then be evaluated as follows.

2.3.3. Iterative lower bound limit load

The iterative lower bound limit load parameter, λ_{LB}^{k}, may then be evaluated at each iteration, k, by scaling the magnitude of the applied load parameter, λ, according to the ratio of the yield stress, σ_y, and the maximum von-Mises effective stress, $\overline{\sigma}(\sigma_{ij}^{k})$, in the body,

$$\lambda_{LB}^{k} = \lambda \frac{\sigma_y}{\overline{\sigma}(\sigma_{ij}^{k})_{\max}} \tag{2.14}$$

2.3.4. Iterative upper bound limit load

The iterative upper bound limit load parameter, λ_{UB}^{k}, may then be evaluated at successive iteration, k, from the ratio of the internal energy dissipated in the body with the work done on the body, as described in equation (2.6), yielding,

$$\lambda_{UB}^{k} = \frac{\int_{v} \sigma_{ij}^{'c} \dot{\varepsilon}_{ij}^{ck} dv}{\int_{s} P_i \dot{u}_i^{ck} ds} \tag{2.15}$$

where $\sigma_{ij}^{'c}$ is the stress at yield associated with the compatible strain rate, $\dot{\varepsilon}_{ij}^{ck}$. For the characteristic yield condition, the von-Mises considered here, the condition requires that,

$$\overline{\sigma}(\sigma_{ij}) = \sqrt{\frac{3}{2}\sigma_{ij}^{'c}\sigma_{ij}^{'c}} = \sigma_y \tag{2.16}$$

where $\sigma_{ij}^{'c}$ may be written as,

$$\sigma_{ij}^{'c} = \sqrt{\frac{2}{3}}\sigma_y \frac{\dot{\varepsilon}_{ij}^{ck}}{\sqrt{\dot{\varepsilon}_{ij}^{ck}\,\dot{\varepsilon}_{ij}^{ck}}} \tag{2.17}$$

This leads to the iterative upper bound limit load parameter to be expressed in the form of,

$$\lambda_{UB}^{k} = \frac{\int_v \sigma_y \bar{\dot{\varepsilon}}^{ck} dv}{\int_s P_i \dot{u}_i^{ck} ds} \tag{2.18}$$

where $\sigma_{ij}^{'c}\dot{\varepsilon}_{ij}^{ck} = \sigma_y \bar{\dot{\varepsilon}}^{ck}$ and $\bar{\dot{\varepsilon}}^{k} = \sqrt{\frac{2}{3}\dot{\varepsilon}_{ij}^{ck}\dot{\varepsilon}_{ij}^{ck}}$.

2.3.5. Iterative upper bound limit analysis method

The above algorithms give rise to an iterative upper bound limit analysis method. The development of such a procedure was realized, through the investigations of Engelhardt [49]. He successfully developed an iterative procedure, capable of evaluating the upper bound limit loads in cracked structures. Using the FEA method [51] as the foundation, he also established that the methodology generates sequences of upper bounds, which monotonically reduces to converge to the least upper bound limit loads, in agreement with the convergence proofs of Ponter *et al* [2]. A brief description of this methodology, emphasising on the organization of the FEA codes, is described below.

A finite element model of a body is considered, whereby the strain field is given in terms of a nodal displacement vector, $\underline{u}^k$, in the usual notation, by,

$$\underline{\varepsilon}^k = [B]\underline{u}^k \qquad \& \qquad \underline{u}(x) = [N]\underline{u}^k \tag{2.19}$$

where $[N]$ is a matrix of suitable shape functions, used to give the displacements, $\underline{u}(x)$, within each element. The associated deviatoric stress, $\underline{\sigma}'^k$, is related to the deviatoric strain, $\underline{\varepsilon}^k$, through the constitutive relationship of the material, $[D]$,

$$\underline{\sigma}'^k = [D]^k \underline{\varepsilon}^k \tag{2.20}$$

where $[D]^k = \mu^k [d]$ and $[d]$ is just a matrix of constants.

Using these equations, it is possible to equate the strain energy density in the body in terms of the nodal displacements, yielding,

$$U^k = \frac{1}{2}\sigma_{ij}\varepsilon_{ij} = \frac{1}{2}\underline{u}^T [B]^T [D]^k [B]\underline{u} \tag{2.21}$$

The internal strain energy in the body can therefore be calculated, by integrating the energy density over the volume of the body,

$$\int_v U^k dv = \frac{1}{2}\underline{u}^T [K]^k \underline{u} \tag{2.22}$$

where the stiffness matrix of the body, $[K]^k = \int_v [B]^T [D]^k [B] dv$.

The solution to the finite element problem is, thus, provided by the nodal displacements, $\underline{u}^k$, for which the total potential energy, PE, has an absolute minimum, where,

$$PE = \int_v U dv - \lambda \int_s P_i u_i ds \tag{2.23}$$

Thus, the substitution of (2.22) into (2.23), differentiating and then equating the subsequent equation to zero, enables the minimum of the total potential energy to be identified. Essentially, the absolute minimum of (2.23) can be obtained from the solution to the following equation,

$$[K]^k \underline{u}^k = \lambda^k \underline{P} \tag{2.24}$$

Thus, the iterative process consists of generating a sequence of spatially varying shear modulus, μ^k, according to the relationship in (2.13). Since, the sequences of strain rate fields are compatible, then the sequences of

$$\lambda_{UB}^k \int_s \underline{P u}^k ds = \int_v \sigma_y \bar{\dot{\varepsilon}}^k dv \tag{2.25}$$

satisfies the condition that $\lambda_{UB}^k \geq \lambda_L$. The advantage of this iterative procedure is that in subsequent iterations, it is guaranteed that the iterative upper bound limit load parameter,

evaluated in equation (2.18), will yield $\lambda_{UB}^{k+1} \leq \lambda_{UB}^{k}$ [2], with the discontinuation of the iterative process occurring when convergence is achieved.

The application of the LMM, as an iterative upper limit analysis method, combines the convenience of using linear elastic stress solutions with the capability of non-linear programming method. The existence of strict convergence proofs [2] that the upper bound monotonically reduces to the least upper bound limit load is another characteristic of this upper bound method. At the present time, two different implementation approaches of this method have been developed, identified as Procedure A and Procedure B in this thesis. The former is a straightforward implementation, whereby the external loads are applied directly on the body [2], whilst the latter requires the application of the loads through external linear elastic stress solutions [4,49]. The features of these two procedures are discussed below, with particular emphasis of its implementation within the FEA code, ABAQUS. Although, both approaches are different, identical solutions are to be expected.

2.4. The Use of ABAQUS

ABAQUS [11], a product of HKS, is the powerful engineering simulation program utilised in this work. Based on FEA methods, this general-purpose software is widely used in industry to analyse engineering problems in such diverse areas of stress/strain analysis, heat transfer, thermal-electrical analyses, *etc*. Its extensive library of elements, with an equally impressive list of material models, coupled with the added ability to model your own material behaviour using user subroutines and option blocks, makes it an ideal choice.

Another significant capability of ABAQUS is in its ability to analyse not only linear, but non-linear problems. This is done incrementally, whereby the problem is divided into increments, small enough to be solved linearly. The solution to the non-linear problem is, thus, provided by the sum of these linear increments. In a standard elastic-plastic analysis, upon the generation of the FEA model, the utilization of ABAQUS involves essentially defining the constitutive behaviour of the material. In the elastic part, the material properties such as the Young's modulus, E, and the Poisson's ratio, ν, are generally declared. For the plastic part, the non-linear material behaviour is defined, through a set of stress values corresponding to a set of strains. For more complex analyses, ABAQUS is equipped with a host of subroutines, making it possible to define more involved material models, geometric behaviour, *etc.*

A typical ABAQUS analysis consists of three distinct stages. It begins with *pre-processing*, whereby a model of the physical problem is defined and an input file, created. In most situations, it is sufficient for the user to furnish the engineering data such as the structural geometry, material behaviour and loading conditions. However, in the proposed procedures, based upon the LMM, whereby the material's behaviour is user-defined, user subroutines such as UMAT need to be incorporated at this juncture. This is then followed by *simulation*; the stage in which the numerical problem defined in the input file, is solved. Once completed, the results obtained are then evaluated or *post-processed* using the output files generated.

2.5. LMM (Procedure A)

Primarily, ABAQUS is designed to carry out analysis rather than provide a safe operating limiting condition for a structure, the essence behind the upper bound limit analysis

method. Therefore, in the implementation of the LMM using this procedure [2], certain features in ABAQUS need to be re-defined and re-interpreted, in conjunction with the requirements associated with the method. These changes are necessary due to the utilization of user subroutines in the analysis. Their general use, essential in understanding the remaining work, is discussed below.

- ***Subroutine DLOAD:*** This subroutine allows the user to define non-uniform distributed loads. In an analysis, it is accessed at each load integration point, where the load case is defined, altered and updated after each increment.

- ***Subroutine UMAT:*** This subroutine is used to define complex material properties, not definable by a simple constitutive model through the Young's modulus, E, and Poisson's ratio, ν. It is accessed at each material gauss point, where the *USER MATERIAL option is prescribed. The user must then define the Jacobian, $[J]$, which is the relationship between the incremental stresses and incremental strains,

$$\Delta\sigma_{ij} = [J]\Delta\varepsilon_{ij} \tag{2.26}$$

Once this matrix is defined, it allows the computation of the incremental stresses from equation (2.26), using the incremental strains supplied by ABAQUS. These incremental stresses would then be updated and added after each increment, ultimately providing the total stress solution. (Note: The Jacobian matrices for plane stress, plane strain and axisymmetric analyses are given in Appendix A)

- ***Subroutine URDFIL:*** This is where the results files are accessed during an analysis. At the end of each increment, the user-requested results are written to the results files. These would be stored, extracted and updated as and when the analysis persists. In addition, this subroutine is also used as a terminating mechanism, *i.e.* stopping the analysis process, following the satisfaction of certain convergence criteria or the specified number of iterations.

2.5.1. ABAQUS implementation of the LMM (Procedure A)

In its implementation within ABAQUS, it was found that the procedure has to be tricked into producing a series of linear solutions [2,49]. This is to conform to the way ABAQUS solves non-linear problems by dividing them into linear increments and each increment is solved linearly. This meant that for each increments of load, ΔP, incremental stresses, $\Delta\sigma_{ij}$, are evaluated, as shown in Figure 2.3. The total solution is, therefore, the sum of these increments at the end of the analysis.

Within the procedure itself, however, these incremental values are viewed differently. Each of these increments is looked upon as part of a separate linear solution, hence the equivalencies in Figure 2.3. This implies that the material definition in UMAT, normally used to define the relationship between the incremental stresses and strains, now defines the relationship between the total stress and strain of a linear solution,

$$\Delta\sigma_{ij} = [J]\Delta\varepsilon_{ij} \quad \equiv\equiv\equiv \quad \sigma_{ij} = [J]\varepsilon_{ij} \tag{2.27}$$

Although, it makes no sense to the limit load calculation whatsoever, the total loads and stresses still need summing up. This is crucial in satisfying ABAQUS's own internal convergence criterion, achieving equilibrium, and leading it into "thinking" it is still solving a non-linear problem. Thus, the correct results are those written to files purposely opened by the user within the subroutines, rather than those presented by ABAQUS in its own data files. It is also important to note that the non-linearity of the problem is associated with the material, not geometry, as discussed in (2.9).

The first step in the analysis procedure is initialisation. This is where the material model within UMAT, *i.e.* the Young's modulus and hence the Jacobian, as well as the distributed load in DLOAD, is arbitrarily assigned a value. These are then written to files accessible via user subroutine URDFIL. This made it possible for the Jacobian, load and any other relevant data, to be updated, and via shared data blocks, made available to other user subroutines.

In the next iteration, ABAQUS will update the relevant boundary conditions. In this case, the static boundary conditions remain unchanged, but the kinematic boundary conditions, *i.e.* the load, must be updated. ABAQUS will therefore call upon subroutine DLOAD, at each load integration point, to calculate the new load, P_{UB}, where $P_{UB} = \lambda_{UB}^{k} P_i$, with the iterative upper bound limit load parameter, λ_{UB}^{k}, identified from (2.18). Meanwhile, at each material gauss point, the user subroutine UMAT will be summoned by ABAQUS. The current stress-strain relationship, $[J]$, will be evaluated and updated using equation (2.13), for that particular linear problem. This enables ABAQUS to evaluate the revised stiffness matrix, and hence the next linear solution of the model. This modified material behaviour, coupled with the strain

fields from ABAQUS, also allows the computation of the current stress fields. These are then summed up with previous incremental stresses, to obtain the total stress solution. The organization of this procedure is schematically shown on the block diagram in Figure 2.4. Numerically, this procedure is repeated until the user-declared convergence criterion is attained. An example of a fully commented version of the user subroutines utilised in this procedure is also included in Appendix B.

2.6. LMM (Procedure B)

An alternative iterative upper bound limit analysis procedure, which is also based upon the LMM, is described here. Unlike previously (Procedure A), whereby the external loads are applied directly on the body, hence generating stress fields in equilibrium with it, this procedure (Procedure B) [4] is interpreted differently. The loads are applied through external linear elastic stress solutions, $\lambda\hat{\sigma}_{ij}$, where $\hat{\sigma}_{ij}$ is the linear elastic stress solution at $\lambda = 1$. The problem posed in this situation is, thus, no longer represented by (2.9), but by the following equation,

$$\dot{\varepsilon}_{ij} = \frac{1}{\mu}\left(\lambda_{UB}^{k}\hat{\sigma}_{ij}^{'} + \overline{\rho}_{ij}^{'}\right), \qquad \dot{\varepsilon}_{kk} = 0 \tag{2.28}$$

This gives rise to the procedure, which now delivers a constant residual stress field, $\overline{\rho}_{ij}^{'}$, which is in equilibrium with the linear solutions, instead. The above argument also implies that the iterative upper bound limit load parameter, previously evaluated in (2.18), is now obtained from,

$$\lambda_{UB}^{k} = \frac{\int_{v} \sigma_y \bar{\dot{\varepsilon}}^{ck} dv}{\int_{v} \hat{\sigma}_{ij} \dot{\varepsilon}_{ij}^{ck} dv} \tag{2.29}$$

with the terms having the same meanings as before.

Originally, this procedure was developed as a means of computing shakedown limits [5]. This phenomenon refers to one of the possible behavioural modes experienced by a body, subjected to cyclic loading histories. The methodology basically involves identifying a constant residual stress field, which keeps the elastic stresses, the sum of the linear elastic stress solutions and the constant residual stress field, within yield. Its application in limit analysis, as an iterative upper bound limit analysis method, is made possible, as limit load is a special case of shakedown, as ascertained by Martin [22] and Koiter [25]. As such, since shakedown theory will be discussed in great detail in Chapter 3, the theoretical reasoning behind this iterative procedure will not be presented here.

2.6.1. ABAQUS implementation of the LMM (Procedure B)

This procedure [5,49], like the previous one, was also implemented within ABAQUS. The bulk of the procedure is similar, with the obvious difference being the absence of the subroutine DLOAD. Its inclusion is made redundant as the applied loads are now prescribed via external linear elastic stress solutions. These are linear elastic stress solutions associated with the loads, solved separately beforehand and written to a formatted direct-access file, in terms of the stress tensor, for each element at each gauss point.

The analysis begins with the file, where the external linear elastic stress solutions are stored, is accessed, retrieved and incorporated into subroutine UMAT. This allows the Jacobian to be evaluated using the moduli updated in (2.13). Unlike previously, the applied loads, here, are set to zero, so that the stress fields generated out of this computation is now the residual stress field.

The rest of the analysis is concerned with the identification of the iterative upper bound limit load parameter, λ_{UB}^{k}. At each iteration, subroutine UMAT would evaluate the volume integrands in (2.29). These integrals are then extracted, via shared data blocks, by subroutine URDFIL to calculate λ_{UB}^{k}. This is then returned to subroutine UMAT as a scaling factor on the linear elastic solutions in the next iteration. This additional step is essential in preventing the magnitudes of the stresses and strains from "blowing-up". If left uncontrolled, it would have repercussions on the ability of the procedure to produce accurate numerical solutions. The overall organization of this method could be further understood by examining the block diagram in Figure 2.5 as well as an example of a fully commented version of the program in Appendix C. (For further explanations, refer to Sections (3.3.1) and (3.3.2) of this thesis.)

2.7. Numerical Examples

So far, two different iterative upper bound limit analysis procedures, capable of identifying the limit loads in cracked structures, were discussed. Although these two iterative procedures evaluate the limit loads differently, the ultimate magnitudes of the converged upper bound limit loads is anticipated to be identical. In demonstrating this as well as the

various aspects of these two procedures, two examples were investigated. From the resulting solutions, comparisons were then made on their accuracy, stability and convergence rapidity, leading to the identification of the superior procedure for further analysis.

2.7.1. Double-edged crack plate

The problem consists of a plate having two symmetrically placed edge cracks, with each crack, of crack length, a, penetrating through a quarter of the plate's width. This plate is also under a uniaxial tensile load, P, as shown in Figure 2.6. In the actual FEA model itself, however, only a quarter of the plate was examined. This simplification is made possible by taking advantage of the symmetrical nature of the problem as well as the everlasting need in reducing computational effort.

Both plane stress and plane strain conditions were investigated. For each, an appropriate mesh needs to be identified. Among the factors considered are the element types, node numbers, integration types/numbers, *etc*. After an initial exploration with the different available combinations, the eight-noded quadrilateral plane stress element, CPS8, was chosen. For plane strain, the corresponding formulation is CPE8H, with the additional use of hybrid elements, to take into account the effect of incompressibility, as discussed in Section (2.3.1). Even with the use of hybrid elements, a Poisson's ratio of $\nu = 0.5$ cannot be used, but it allows the ratio to be very close to 0.5.

Figure 2.7 shows the two meshing arrangements employed in the analysis. The first is a mesh with 30 elements, while the other involves meshing with 20 times more elements.

Solutions for these two models were then generated and shown in Figure 2.8, as plots of upper bound limit loads against number of iterations. For both procedures, it substantiated the claim that the upper bound limit loads, P_{UB}, monotonically reduces with increasing number of iterations, where $P_{UB} = \lambda_{UB} P$, in agreement with the convergence proofs of Ponter *et al* [2]. This monotonically reducing behaviour is clearly observed in both the plane stress and plane strain analyses. The solutions also revealed their dependency on the mesh. For this reason, in FEA models, there is a tendency of meshing with more elements, with the expectation of producing better results. In our analysis, it was found that this hypothesis holds true, but only to a certain extent. Meshing beyond a reasonable limit would increase computing times as well as being cost-ineffective.

It should also be noted that the solutions were sensitive to incompressibility. Effecting plane strain analysis, it was established that P_{UB} is dependent upon the value of ν. This was studied by Engelhardt [49], who showed that the difference between P_{UB} at $0.5 - \nu = 10^{-13}$ and $\nu = 0.49$ is 7%. He suggested an explanation for these large discrepancies, whereby he concluded that incompressibility affects the stiffness more than the energy dissipation in a structure, since the energy dissipated due to volumetric changes is not taken into consideration in the upper bound limit load calculations. Thus, using the recommended value of $\nu = 0.4999999999$, the P_{UB} solution generated in this thesis is a reliable one. Any value closer to 0.5 would induce numerical errors, which would ultimately cause the analysis to fail.

The characteristics of these two procedures are, however, best described by their ability to achieve rapid convergence. Unlike other currently available methods, fairly good

converged solutions were reached within the first 20 iterations. These were then compared with the exact results obtained from Nuclear Electric Inc [20]. As shown in Figure 2.8, the percentage error, for the 600-elements mesh, was 8% for plane stress and 6% for plane strain. At the 40^{th} iteration, these errors have reduced to 6% and 5% respectively. In comparison with corresponding solutions for the 30-elements mesh, the percentage errors have reduced significantly. This demonstrates the effectiveness of the procedures, as it allows limit loads to be evaluated, with a reasonable amount of meshing elements in the model. The capability of these procedures is further reinforced with the anticipated identical P_{UB} solutions obtained from the two procedures. (The actual fully commented programming codes used in both procedures, for the various different analyses considered, are enclosed in attached CD)

2.7.2. Cracked cylinder

Figure 2.9 shows the problem considered in the analysis. It is concerned with a cracked cylinder, of radius, $5w$, and length, $10w$, subjected to an axial load, P. The internal crack, a, extends through the cylinder's thickness, w, all around its periphery. The FEA model shows its equivalent representation as an axisymmetric problem. As before, using symmetry, only half of the cylinder's length was analysed. In addition, by modifying the boundary conditions, the model was re-interpreted as a plane stress/plane strain plate in the presence of an edge crack.

To ensure uniformity, the axisymmetric, plane stress and plane strain FEA models, all have approximately the same number of elements, *i.e.* 5800 elements. Unlike before, there is a greater proportion of meshing elements occurring at the crack tip, as shown in Figure 2.10.

Using such selective mesh refinement arrangement, it was numerically found that improved upper bound solutions were obtained, in comparison with the meshing arrangements of Figure 2.7. This is not surprising as the upper bound limit load parameters, computed in (2.18) and (2.29), is very much dependent upon the effective strain, especially those occurring at the crack tip. Thus, reducing the contribution of the deformation mechanism in Figure 2.11 would ultimately result in enhanced solutions, in agreement with the investigation of Hentz [55]. In his work, he examined the relationship between the meshing density and the accuracy of the solutions, leading to the conclusion that an accurate P_{UB} is obtained if the number of meshing elements across the uncracked ligament is about 10-50 elements. His argument is mainly due to the major contributions the plastic region, *i.e.* that in the vicinity of the crack tip, makes in equations (2.18) and (2.29), in comparison with that from the rigid regions of the body, *i.e.* those away from the crack tip.

Limit load solutions were then generated, for ratios of $\frac{a}{w} = 0.0 - 1.0$, in multiples of 0.1, for the axisymmetric, plane stress and plane strain analyses considered. As there were no exact solutions available, comparisons were made with an assumed "exact" solution obtained from another analysis with much more substantial mesh refinements, with the configuration of this mesh shown in Figure 2.12. The consistency of the solutions generated using the adopted procedures, provided the confidence that this "exact" solution is very close to reality. This enabled the values of P_{UB}, obtained from the two meshing arrangements of Figures 2.10 and 2.12, to be compared. Figure 2.13 shows an example of one such comparison, for the cracked plane stress problem at $\frac{a}{w} = 0.4$. It can be clearly seen that the upper bound limit loads has improved tremendously, with the percentage error at the 40^{th} iteration reduced to $<1\%$.

Although not included in this thesis, similar behaviours were also observed in the examinations into the other analyses. Based upon the accuracy of these solutions, the meshing arrangement in Figure 2.10, was, thus, elected as the one to be used in subsequent chapters, in the investigations into the overall and crack tip behaviour of cracked structures.

At this point, an additional investigation in the identification of limit loads, using standard step-by-step analysis, was conducted. This is necessary in validating the accuracy of the previous results as well as enabling the capability of the LMM to be judged. Using the problem solved in Figure 2.13 as an example, a full step-by-step analysis calculation was performed, with the results obtained shown in Figure 2.14. The plot clearly shows that as the increments of applied load, P, is increased, the displacement, u, in the direction of the load also increases. This observance in behaviour continues until the load reaches the limit load, at which the step-by-step analysis process terminates. In our analysis, it was found that termination occurs at $P = 120.4\text{MPA}$, which is within 1% of the "exact" solution. This good correlation between the solutions was found to be in agreement with the previously discussed iterative solution, whereby at the 40^{th} iteration, the percentage is less than $<1\%$. This indicates the capability of the LMM in generating accurate limit loads solutions in cracked structures. Further examination also revealed that in the process of generating the limit load, instability occurs as the load approaches very close to the limit load. This is mainly due to the numerical difficulties encountered by ABAQUS in satisfying the equilibrium condition, leading to convergence problems. In reducing this effect, ABAQUS generates more increments as the limit load is approached. Such an instability problem is not observed in the application of the LMM. For simple cracked structures, such as those investigated here, the effect of instability on the limit load is found to be relatively insignificant. However, in the

context of evaluating limit loads for complex structural geometries and/or loading/boundary conditions, the advantage of the LMM is apparent. Lastly, the effects of analysis times on the solution processes were also investigated. In this department, the step-by-step analysis, with CPU time of about 5 minutes, has the advantage over the LMM, with CPU time of about 20-25 minutes. Although it takes a longer time in generating the limit load solutions, the accuracy of the solutions generated as well as the ability in coping with the instability issues, has made the LMM a better choice, ultimately outweighing the time factor.

The accuracy of these numerical solutions is further evident when compared with the solutions of Miller [20]. For a single-edge notched tension (SENT) plane stress specimen, he investigated the variations of limit loads, with increasing crack length. His limit load values were then compared with those from the numerical solutions, generated from the above procedures. This is shown in Figure 2.15, where P_L is the uncracked limit load. It is clearly shown that Miller's plane stress results correlates well with those of the numerical solutions. For axisymmetric and plane strain analyses, however, no such Miller's solutions exist. Nevertheless, the plot does show the conservative nature of the plane stress solutions, since much larger values of P_{UB} were attained for the axisymmetric and plane strain analyses. (The actual fully commented programming codes used in both procedures, for the various different analyses considered, are enclosed in the attached CD)

2.8. Concluding Remarks

In the identification of limit loads in cracked structures, this chapter proposed the employment of the LMM, as an iterative upper bound limit analysis method. Two different

implementations of this method were described, identified as Procedure A and Procedure B. One is the straightforward implementation, whereby the external loads are applied directly on the body whilst the other requires the application of the loads through external linear elastic stress solutions. The applications of these two procedures were then investigated on two cracked numerical problems, with the ultimate aim of identifying the superior procedure for further analysis.

In the numerical investigations, the characteristics of these two procedures were examined. It was found that both procedures were equally capable of generating the monotonically reducing sequence of upper bounds, eventually converging to the least upper bound limit loads. It was also observed that both procedures generated very stable solutions, with good converged P_{UB} obtained within the first 20 iterations. In general, the solutions obtained from these two procedures were found to be, by and large, identical. However, in the subsequent chapters, whereby the behaviour of cracked structures subjected to cyclic histories of loads and temperatures were investigated, Procedure B has the edge. Its ability to introduce loads and temperatures, via external linear elastic stress solutions, justifies our decision on its preference. From this point onwards, the mention of the linear matching method (LMM) refers to the solution process of Procedure B.

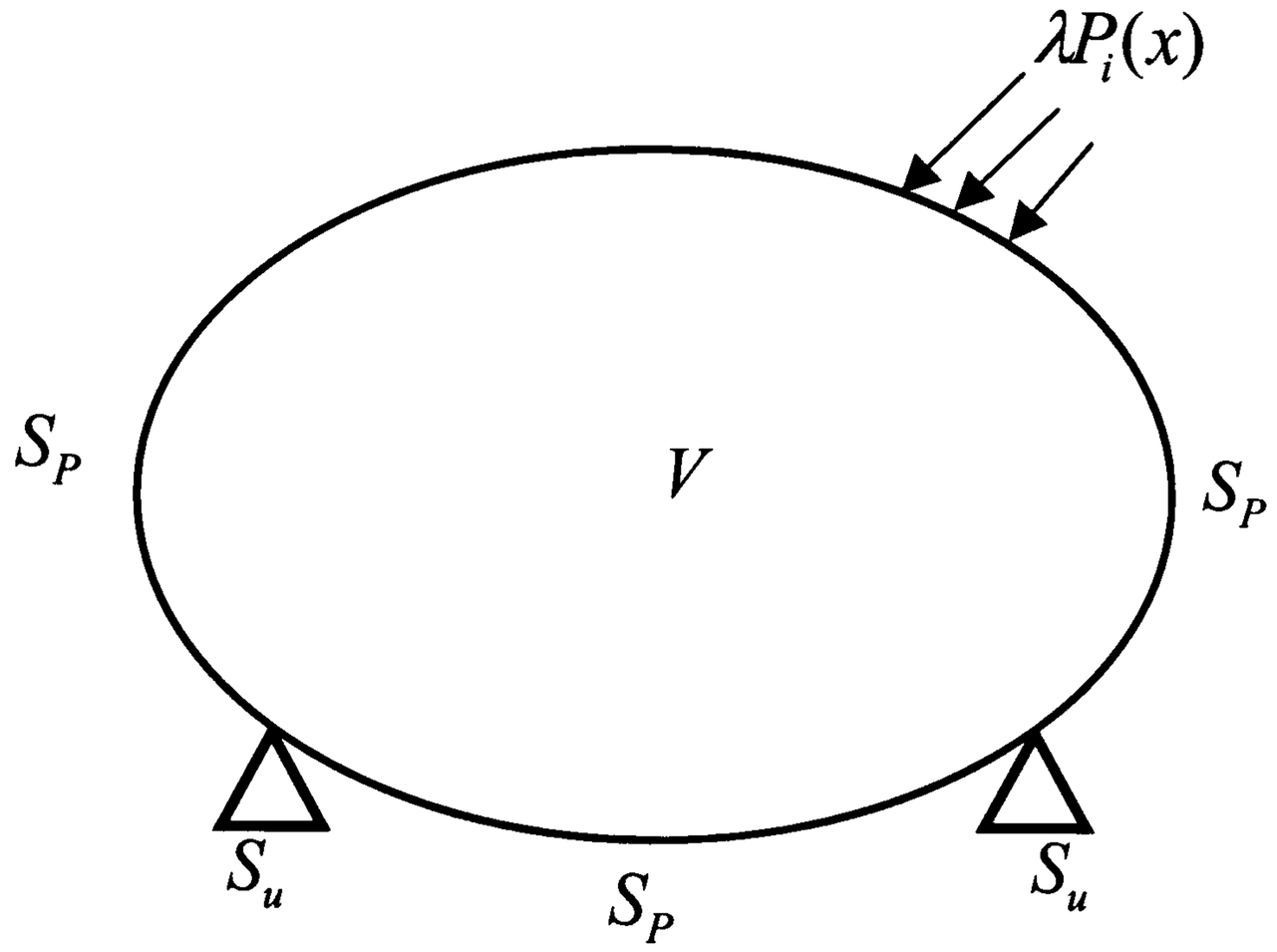

Figure 2.1: Schematic diagram of the general problem.

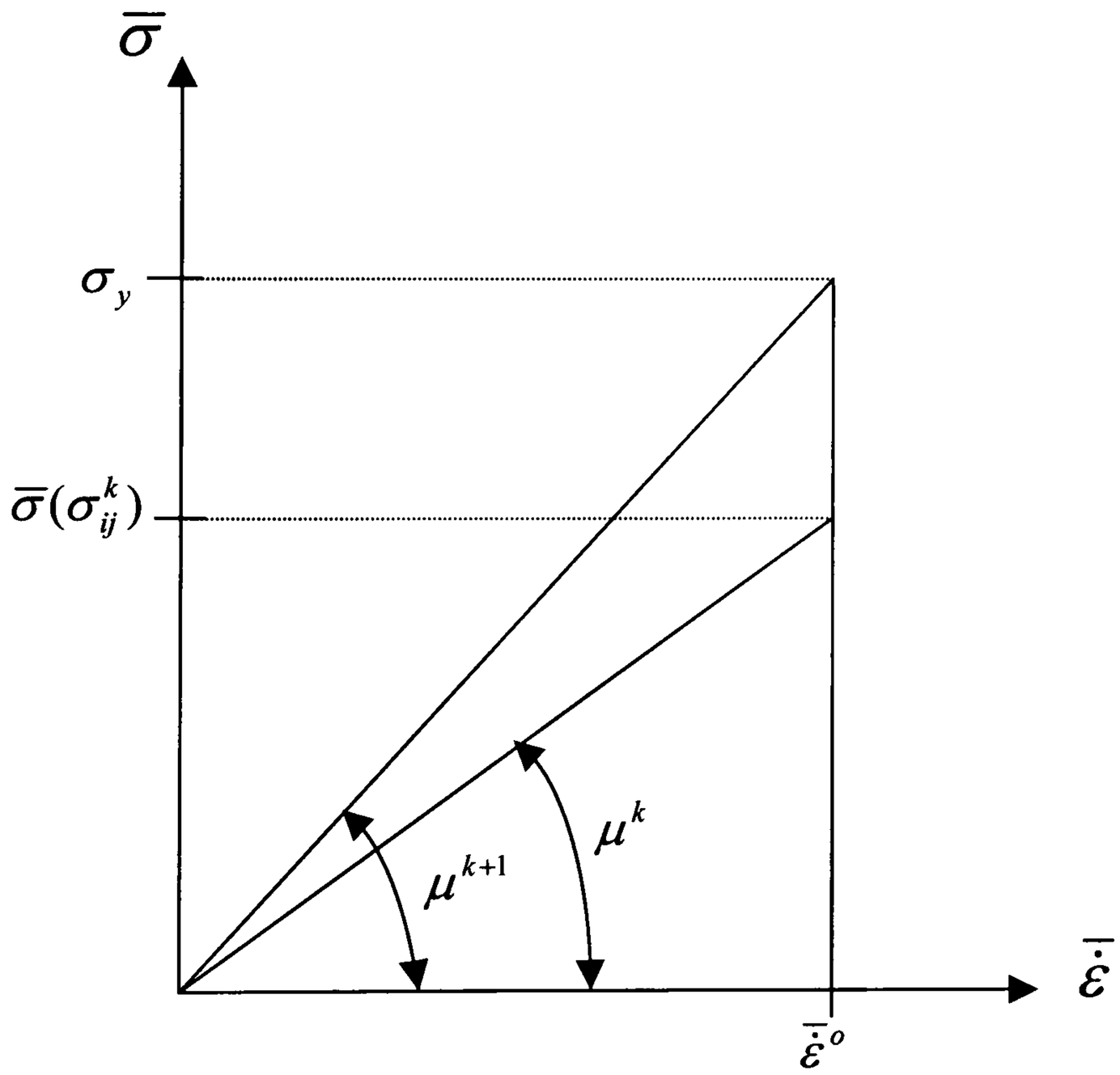

Figure 2.2: The iterative process, as represented in equation (2.13).

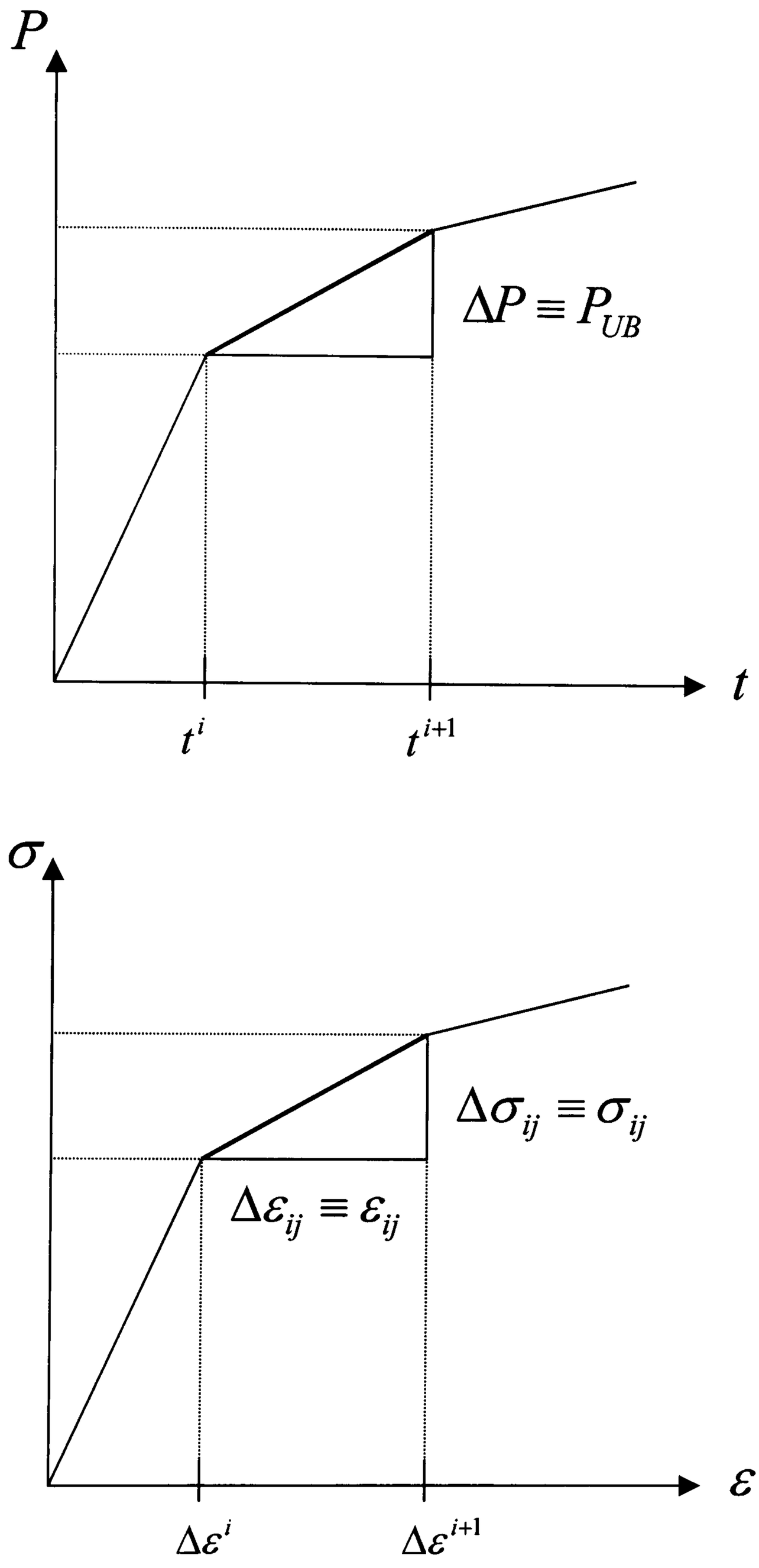

Figure 2.3: The analysis of non-linear problems using ABAQUS.

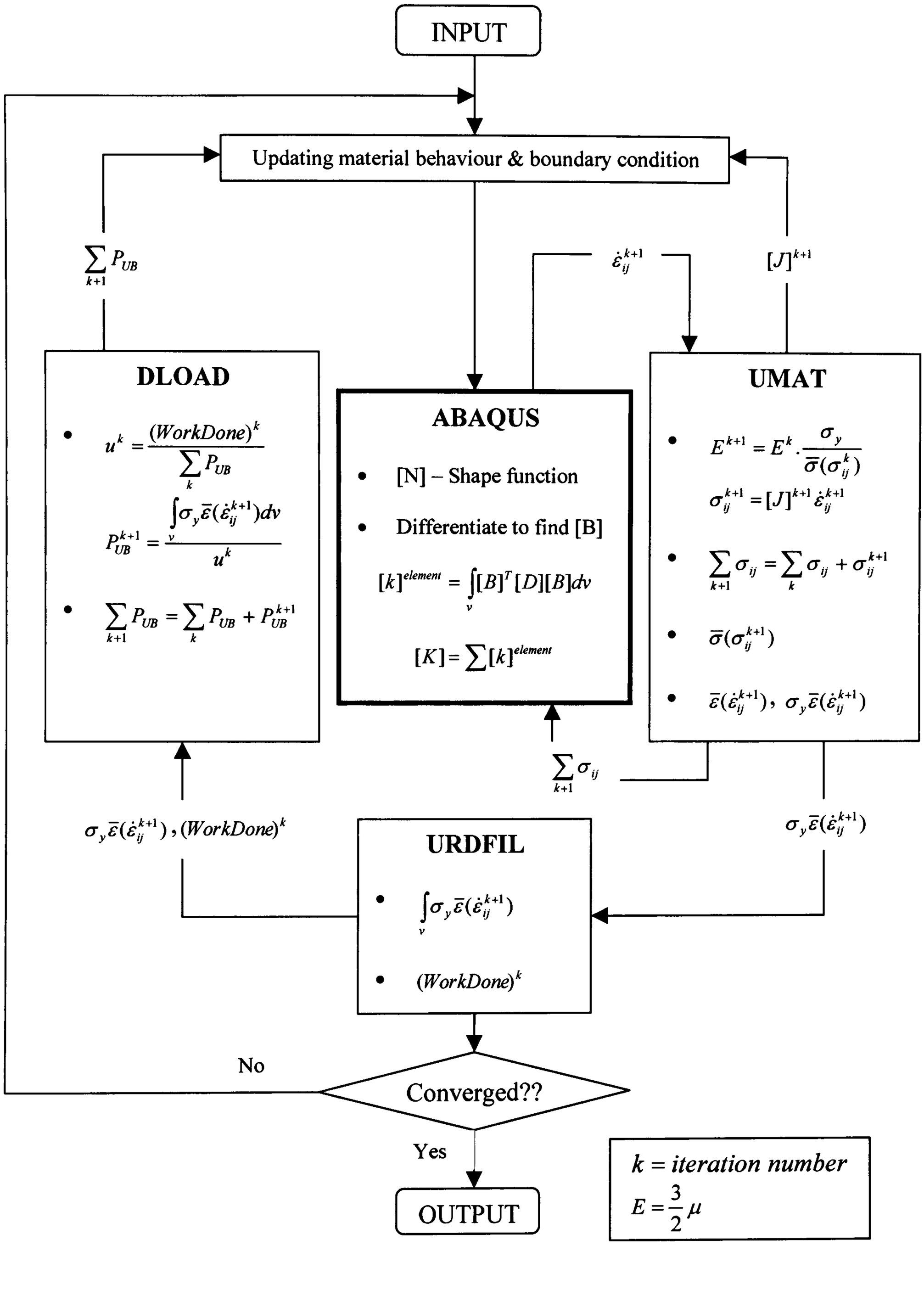

Figure 2.4: Interaction between ABAQUS and user subroutines for the LMM (Procedure A).

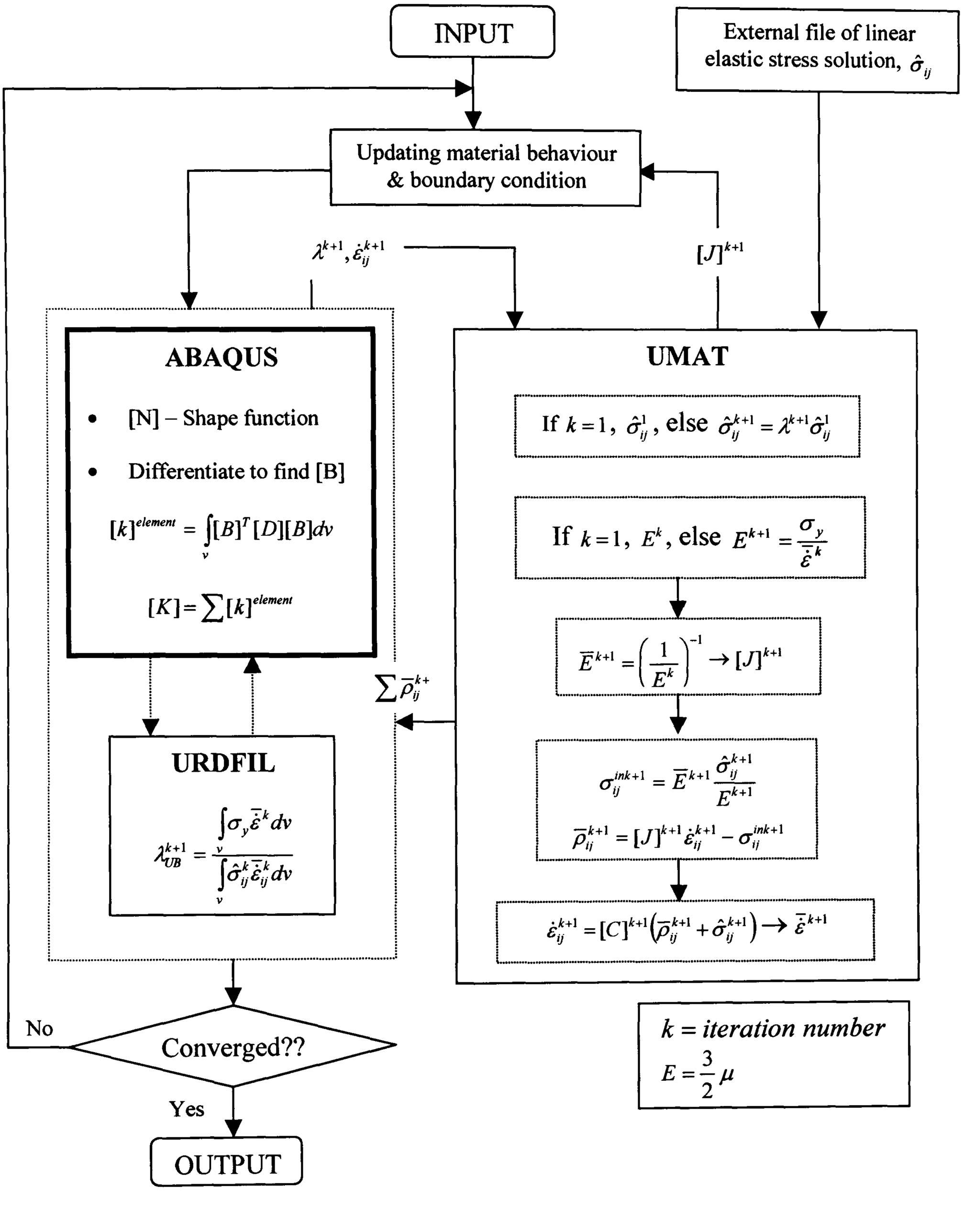

Figure 2.5: Interaction between ABAQUS and user subroutines for the LMM (Procedure B).

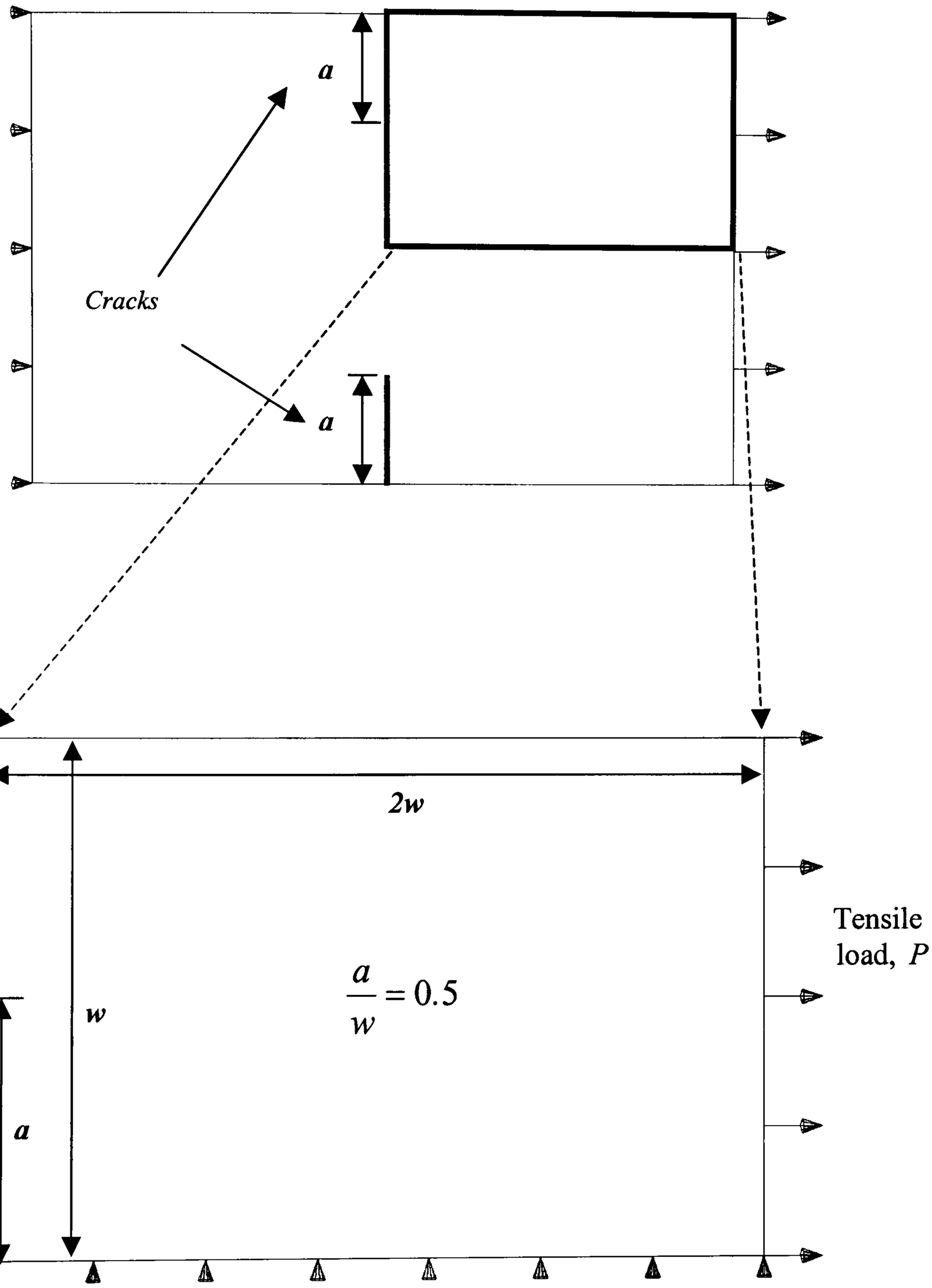

Finite element model

Figure 2.6: Double-edged crack plate.

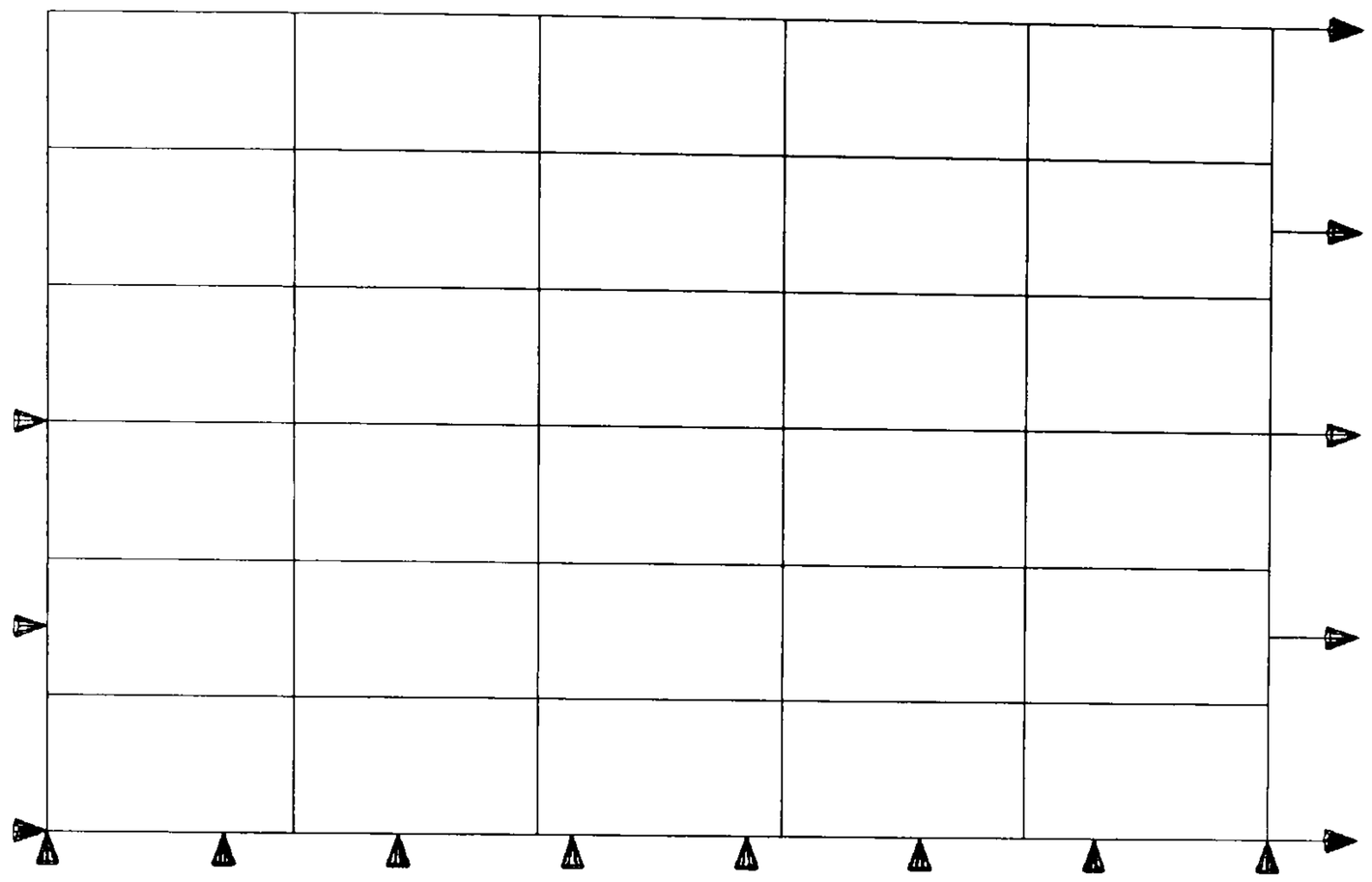

30 quadrilateral elements

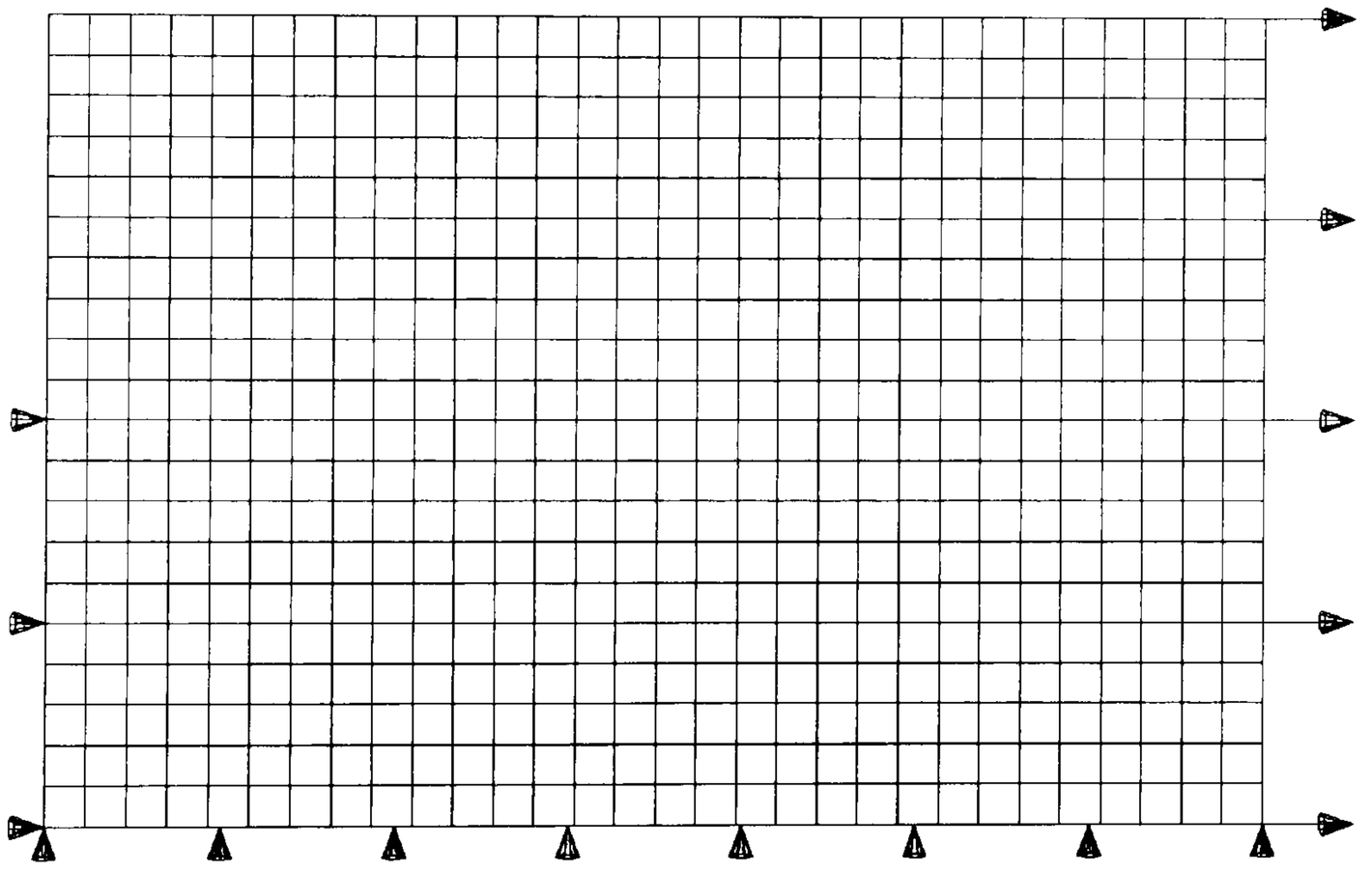

600 quadrilateral elements

Figure 2.7: The meshing arrangements employed in the analyses.

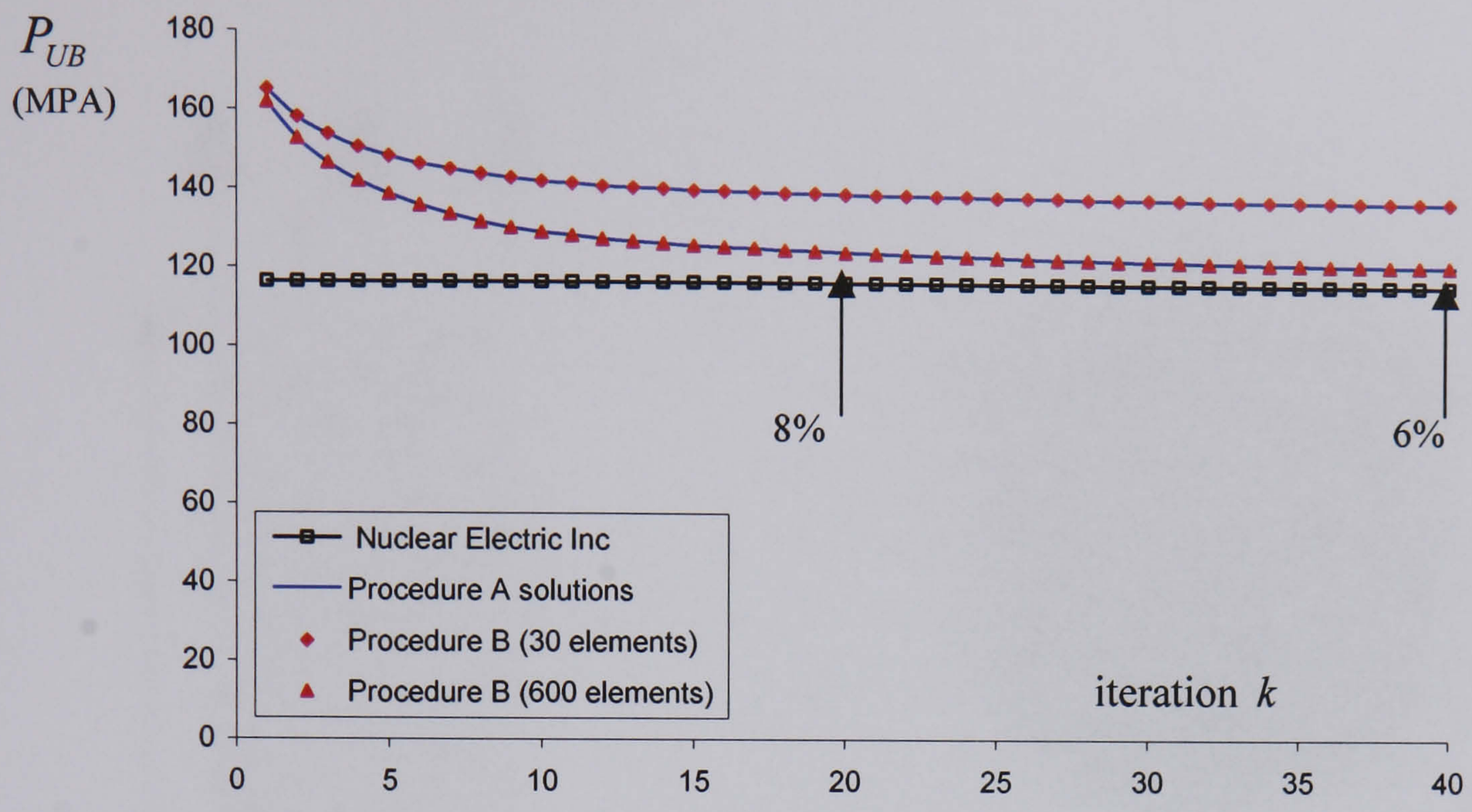

Plane Stress

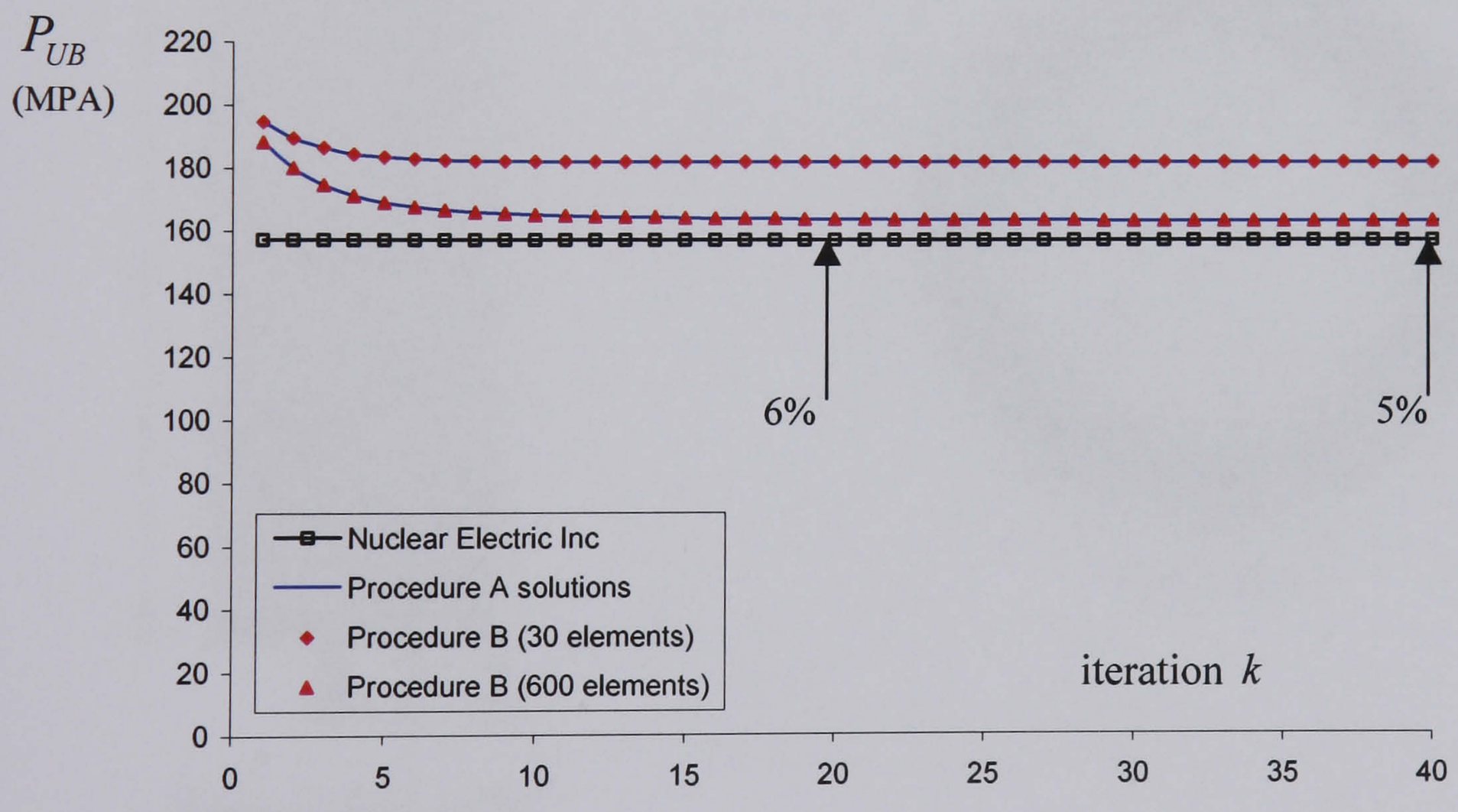

Plane Strain

Figure 2.8: Plots of upper bound limit loads vs number of iterations.

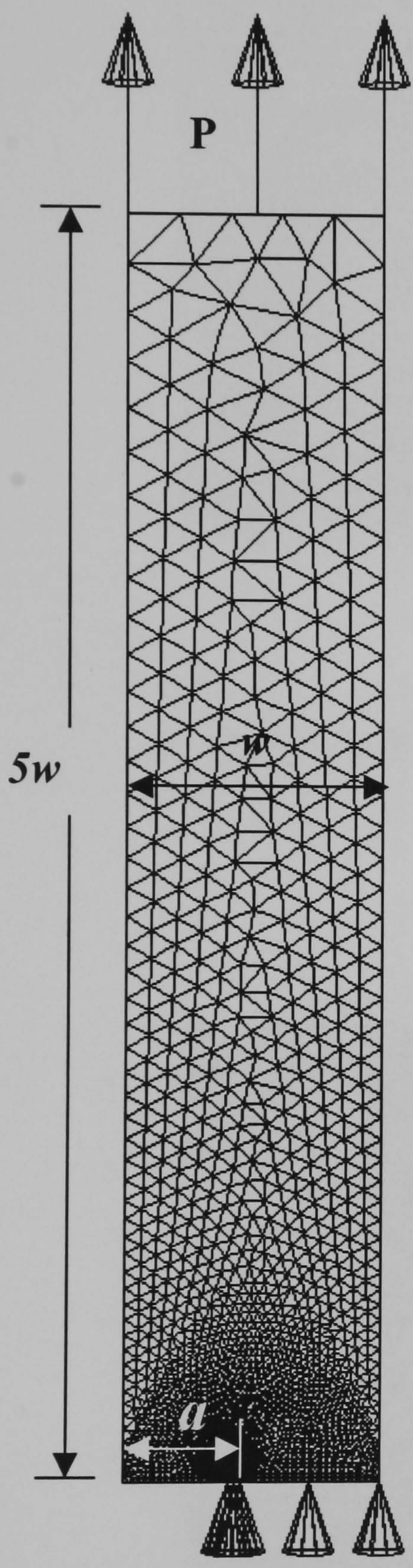

Finite element model

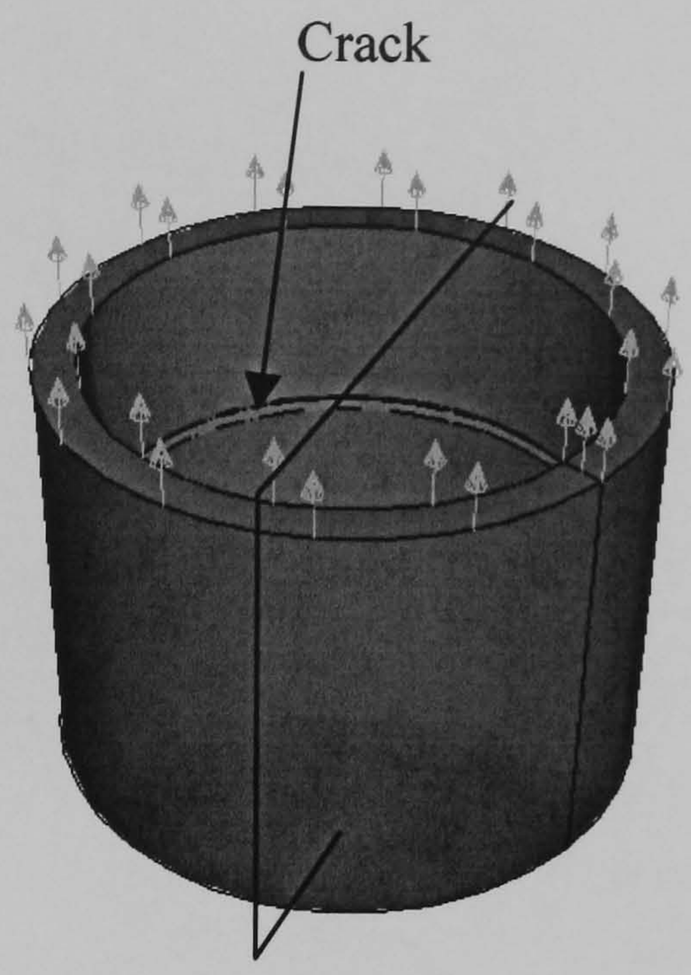

Cylinder

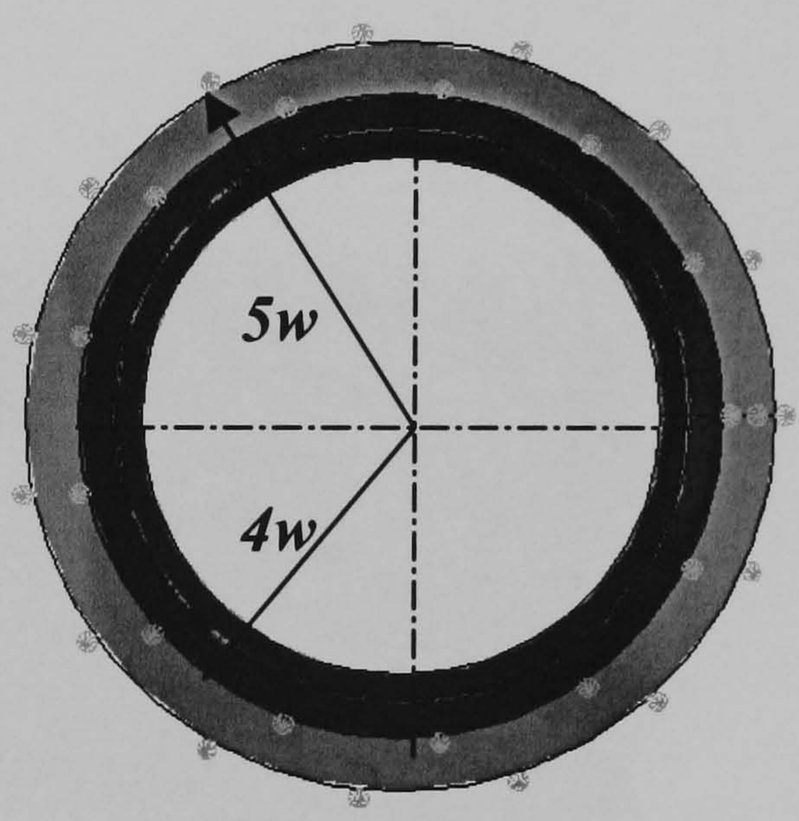

Plan View

Figure 2.9: Cylinder with crack.

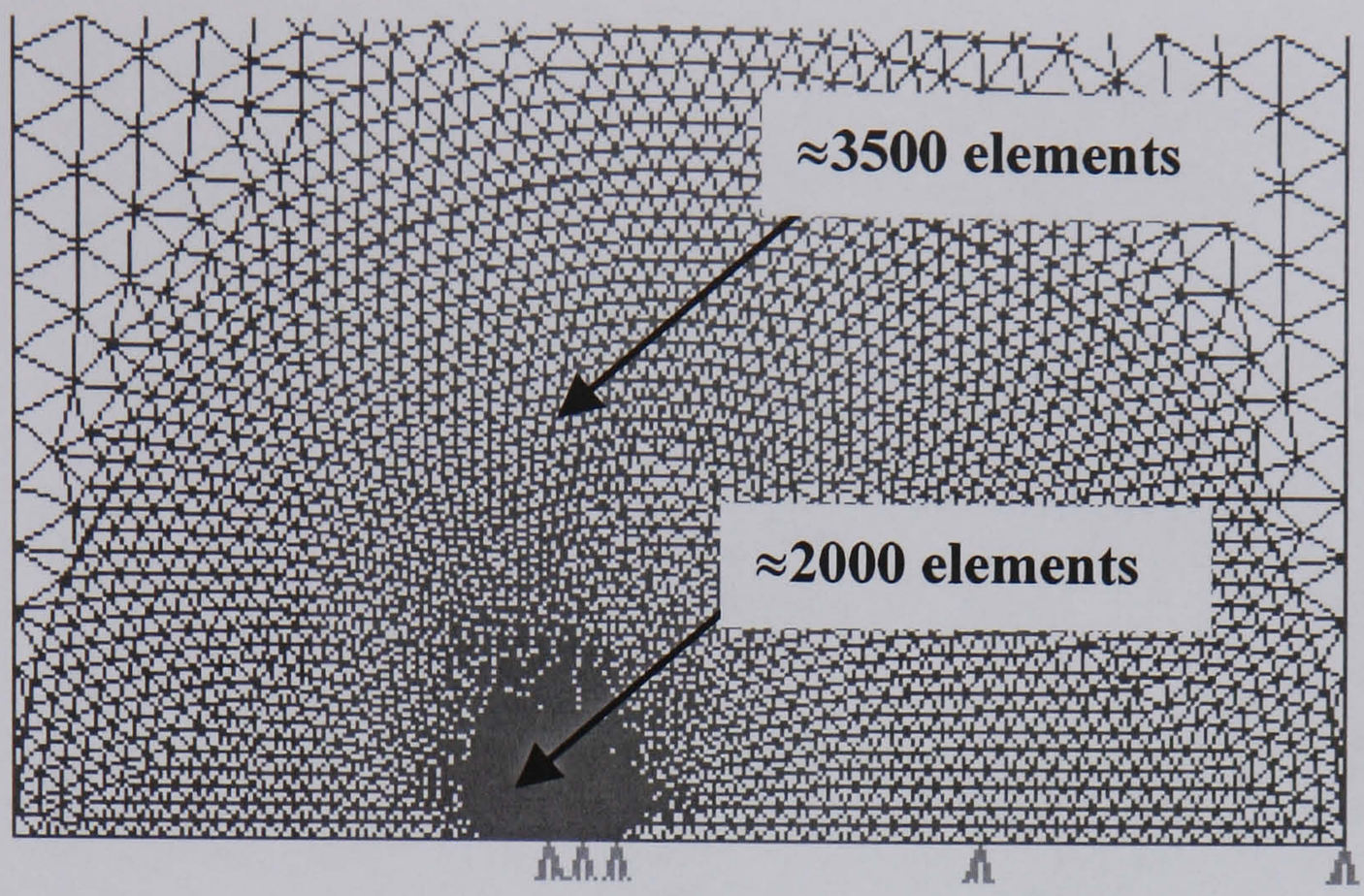

Figure 2.10: Finite elements mesh at the crack tip.

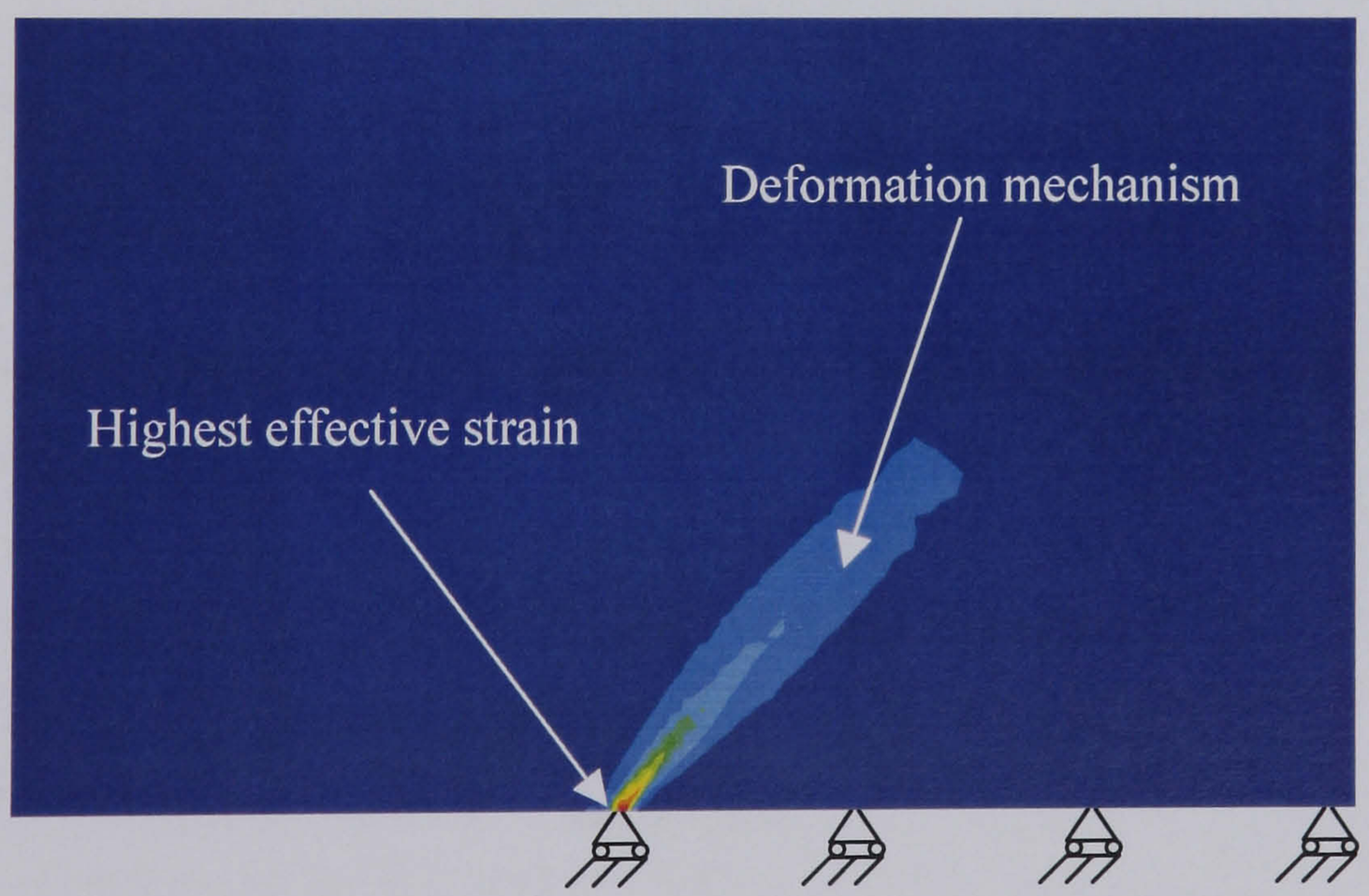

Figure 2.11: Plot of the von-Mises effective strain at the crack tip.

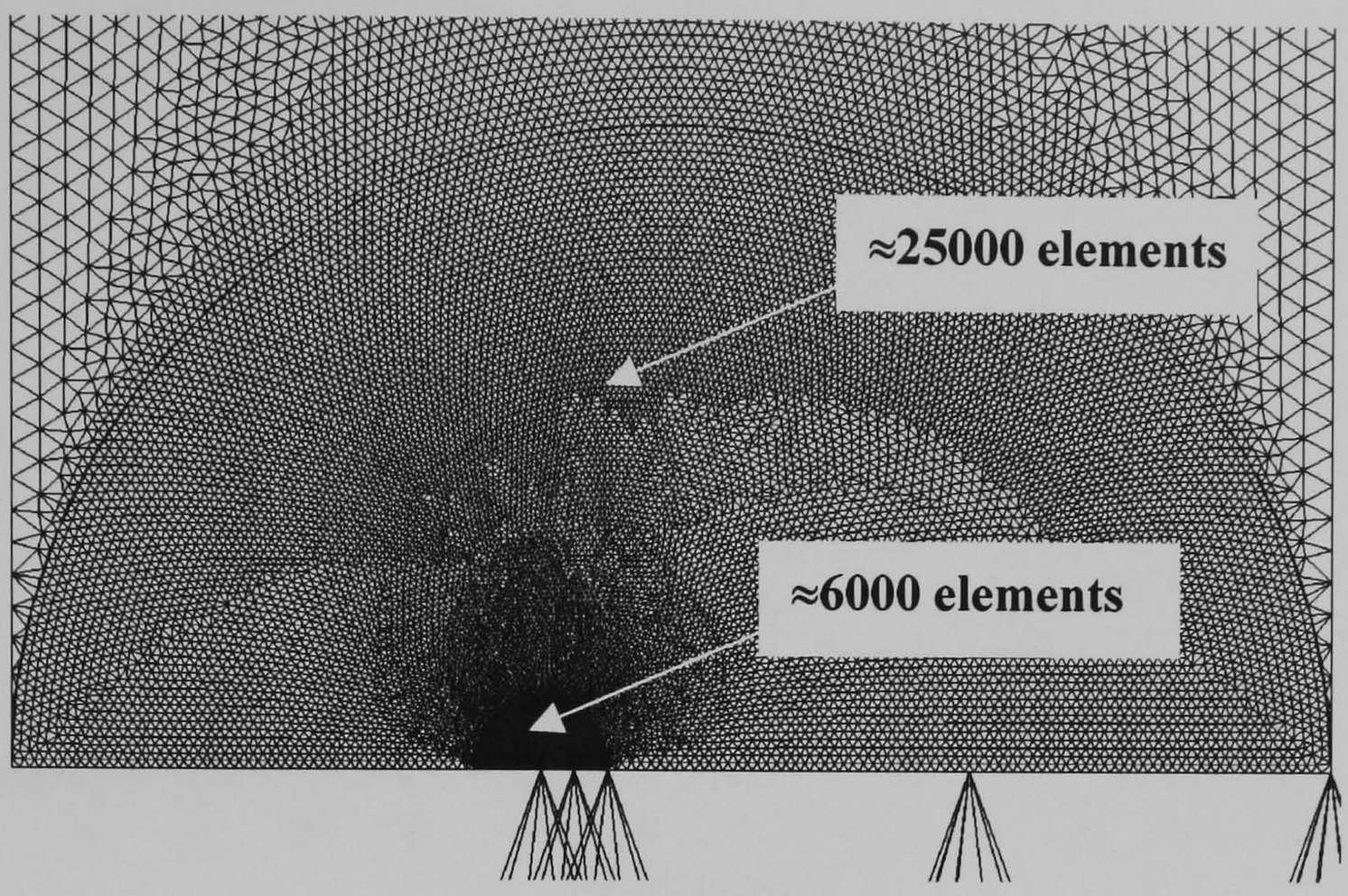

Figure 2.12: Meshing configuration at the crack tip
for evaluating the "exact" solution.

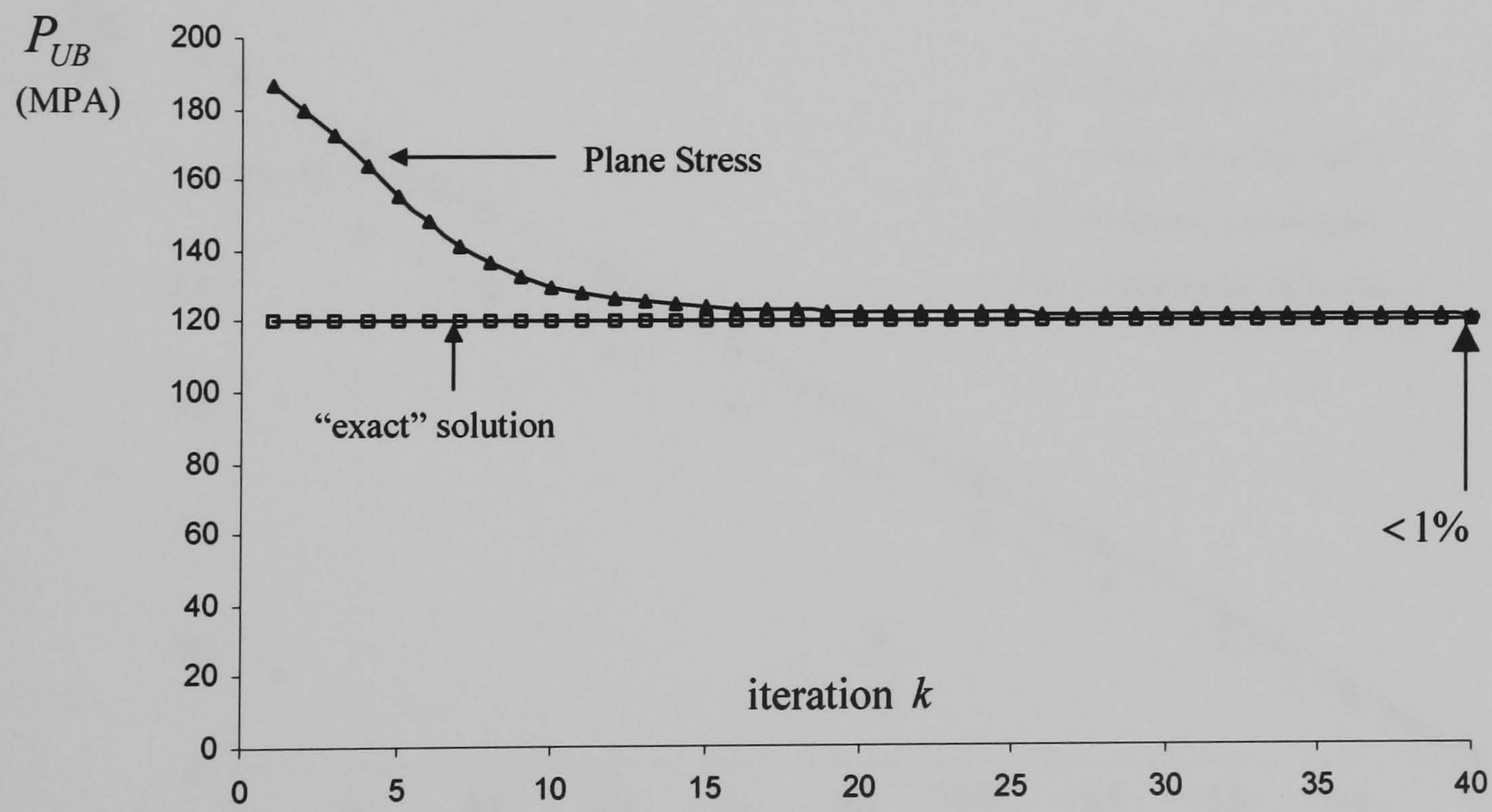

Figure 2.13: Upper bound limit loads vs number of iterations.

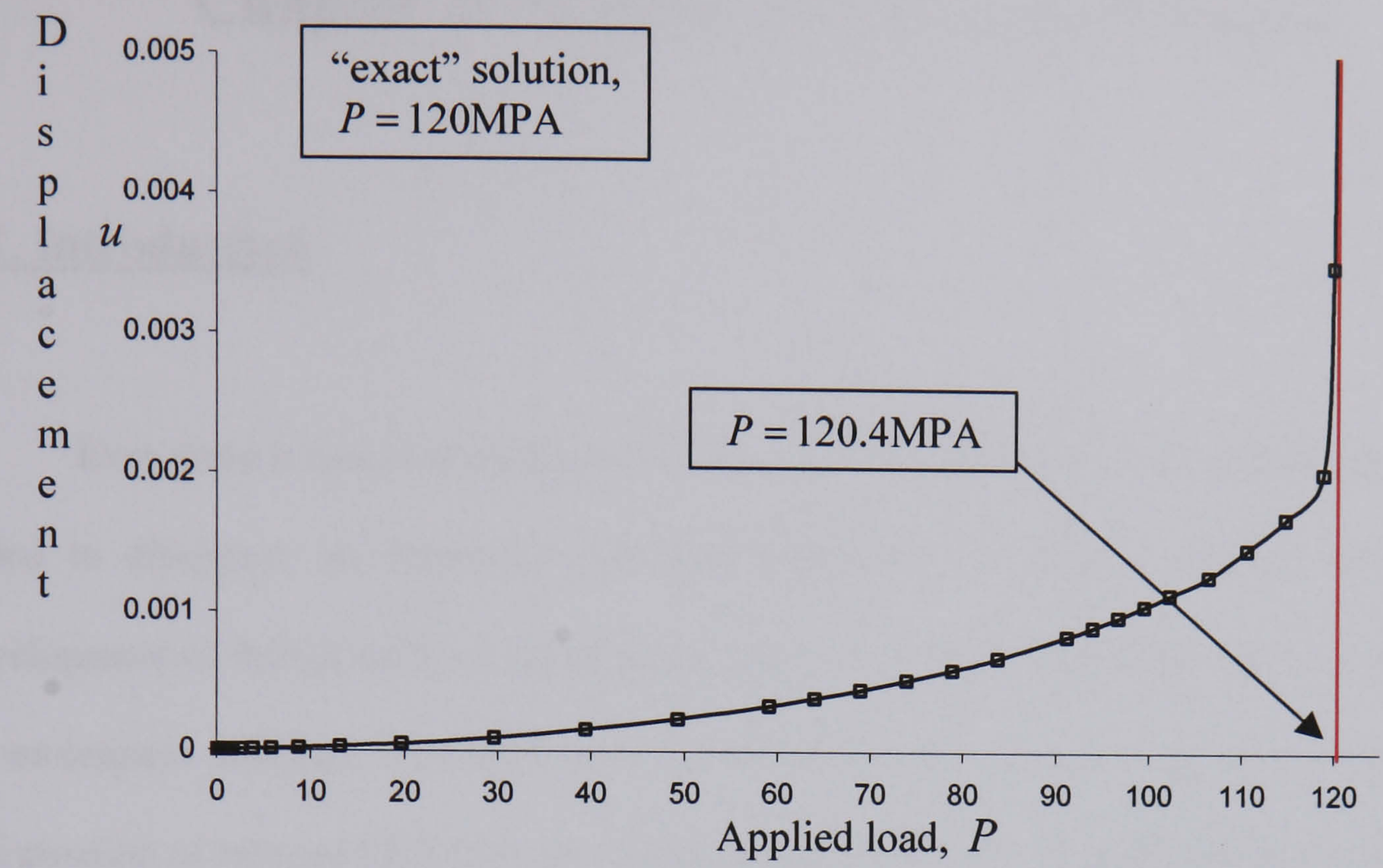

Figure 2.14: The identification of limit loads using step-by-step inelastic analysis in comparison with the results in Figure 2.13.

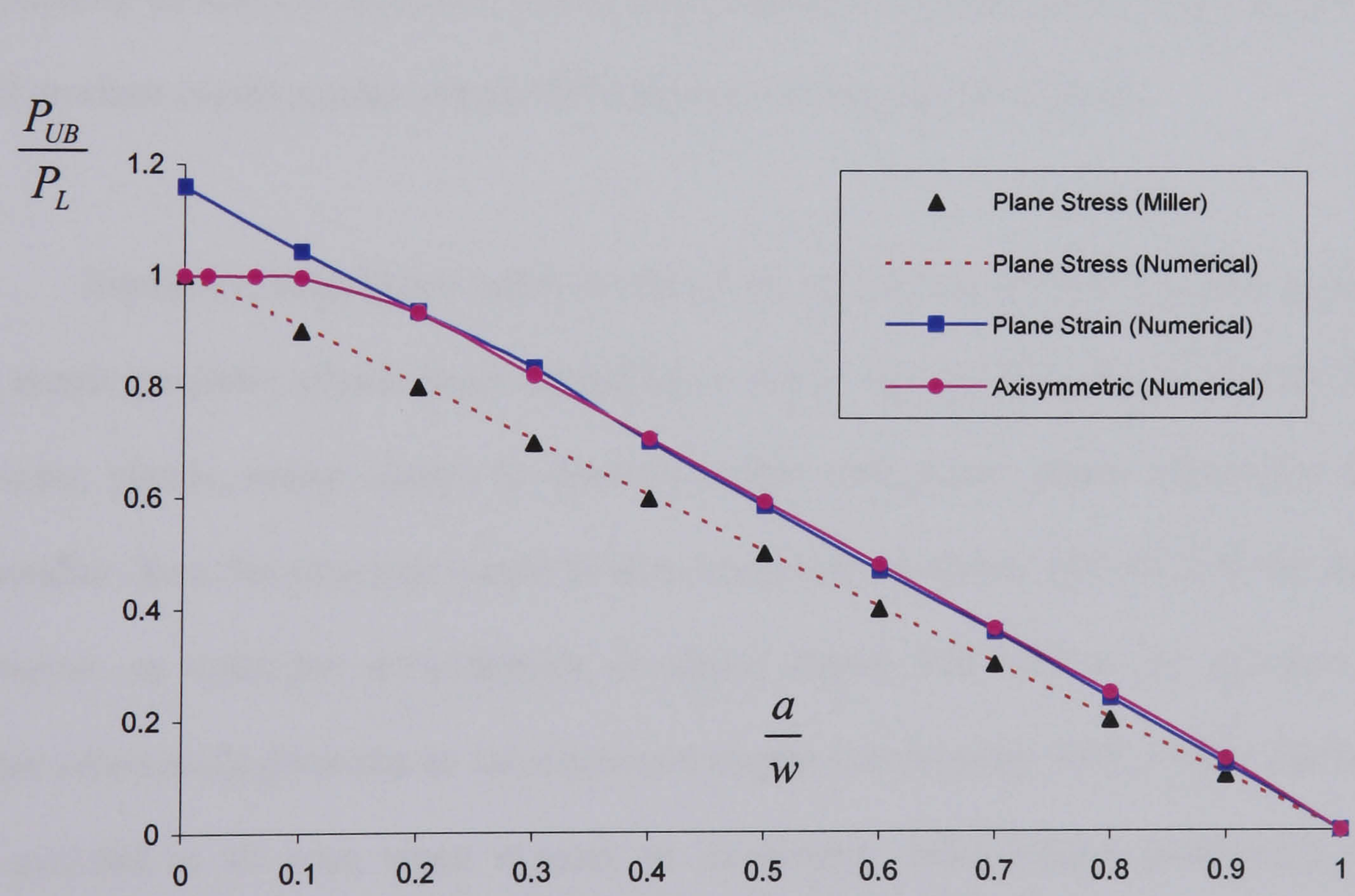

Figure 2.15: Comparisons between the limit loads for plane stress, plane strain and axisymmetric analyses.

Chapter 3: Shakedown Analysis Methods

3.1. Introduction

Ever since it was first mentioned in the late 1920's [56], interest in shakedown analysis failed to disappear, as important industrial problems still arose. Initially, utilized in the development of design rules for metallic structural frameworks, the theory has now progressed to encompass practical problems such as the design of nuclear reactor components [57], deformation of railway lines [58], pavement designs [59], *etc*. Its influence is to such an extent that it is often one of the tools of structural design and safety assessment in certain design standards [1]. Even, recent advances in FEA methods and the ever-ready availability of simulation techniques have not, in any way, diminish its importance, as shakedown concepts still produce useful results, which other analysis techniques failed to do.

Implicitly, shakedown refers to one of the possible behavioural modes experienced by an elastic-perfectly plastic body subjected to cyclic loading histories. If, during the loading process, plastic strains ceased to develop further and purely elastic behaviour is observed thereafter, then the structure is said to have *shaken down* and is safe [21,25]. On the contrary, however, an unlimited accumulation of plastic strains will lead to the structure failing by either *alternating plasticity* or *incremental collapse* (*ratchetting*) [60]. Whilst ratchetting must be avoided at all cost, since it leads to intolerable deformations, alternating or reverse-plasticity can be accommodated, provided during its design life, the effect of low cycle fatigue is taken into consideration.

Continued research interest in shakedown analysis methods is mainly due to their apparent advantage over step-by-step inelastic analysis methods [10,11]. For structures undergoing complex/difficult to model loading cycles, where the extremes of the loading histories are known, shakedown theory can simplify matters a great deal. It uses simple material models, *i.e.* elastic-perfectly plastic, and considers a load domain that contains all possible load paths between the extremes, thus eliminating the need to know the precise load path and material model. This leads to uncomplicated, cost-effective and efficient methods, reasons enough for their sustained attention.

Practically, the significance of these shakedown analysis methods is mainly related to the questions posed in the processes of engineering design and life assessment of structures subjected to cyclic loading histories, *i.e.* mechanical and thermal. The industry is calling out for a direct method capable of predicting the boundaries between shakedown, reverse-plasticity and ratchetting. The interaction diagrams developed would then provide a mean of assessing a structure's safe operating region. In addition, the effectiveness of such methods in generating direct answers to these questions would ultimately enhance their reputation as a replacement for currently used tabulated values and simple lower bound estimates [1].

In addressing the effect of shakedown, the present approach involves the employment of shakedown analysis methods, developed using the classical shakedown theorems of Melan [21] and Koiter [25]. The utilization of such procedures [53,61] has enabled shakedown limits to be accurately and efficiently evaluated in many structural components. In the identification of the corresponding reverse-plasticity and ratchetting limits, however, not much work has

been undertaken. In closing this gap, Ponter *et al* [6,7] developed minimum theorems for an arbitrary cyclic state, whereby the theorems, reduce to the classical shakedown theorem when the loading histories lies within the shakedown limit, and identifies the ratchetting limits when it does not. The availability of these extended theorems is, particularly, valuable in the present investigations into the behaviours of cracked structures subjected to cyclic histories of loads and temperatures. In such situations, the presence of the elastic stress singularity at the crack tip, leads to the breaking down of the shakedown condition, hence, the non-existence of any shakedown limit. However, the procedures for identifying the ratchetting limit still holds. This is mainly due to the need in accounting for low cycle fatigue, *i.e.* the toleration of cyclic plastic strains forming a reverse-plasticity mechanism in a confined region of the body without inducing any net strain growth. The ability of these procedures in evaluating ratchetting limits in these cracked structures would then enable the validity of current solutions [26,27,28], where cracks were replaced with notches, to be judged.

In this chapter, the foundation behind the Linear Matching Method (LMM), employed in the identification of the shakedown, reverse-plasticity and ratchetting limits, is discussed in great depth. Upon the introduction of the fundamental shakedown theorems for a general problem, its implementation is then presented for the upper bound shakedown theorem. For structures loaded in excess of shakedown, extended theorems for the identification of ratchetting limits are also explained. The applications of these methods are then investigated on the so-called Bree problem [37], with and without the presence of cracks. A further examination on a real industrial problem [1] is also conducted; allowing comparisons between the numerical solutions and those used in current design and life procedures to be made.

3.2. Shakedown Analysis

Figure 3.1 shows the problem considered in the analysis. The body is made up of an isotropic, elastic-perfectly plastic material, satisfying the yield condition of (2.1) and the associated flow rule of (2.3). Of volume, V, and surface area, S, the body experiences a history of cyclic mechanical load, $\lambda P_i(x_j,t)$, on S_P, and a temperature distribution, $\lambda\theta(x_j,t)$, within V, where λ is the load parameter. The remaining surface, S_u, is where constraints are prescribed, such that the displacements, $\dot{u}_i = 0$. In addition, a convex yield function is assumed such that the maximum work principle, given by,

$$(\sigma_{ij}^P - \sigma_{ij})\dot{\varepsilon}_{ij}^P \geq 0 \tag{3.1}$$

holds true, where σ_{ij}^P is the stress associated with the plastic strain rate, $\dot{\varepsilon}_{ij}^P$, at yield and σ_{ij} is any state of stress that satisfies (2.1). The associated linear elastic stress solution, corresponding to $\dot{\varepsilon}_{ij}^P = 0$, is denoted by $\lambda\hat{\sigma}_{ij}$, with,

$$\hat{\sigma}_{ij}(x,t) = \hat{\sigma}_{ij}^P(x,t) + \hat{\sigma}_{ij}^\theta(x,t) \tag{3.2}$$

where $\hat{\sigma}_{ij}^P(x,t)$ & $\hat{\sigma}_{ij}^\theta(x,t)$ are the linear elastic stress solutions for the mechanical and thermal loads respectively. In the following, the linear elastic stress solutions are chosen such that the load parameter, $\lambda \geq 0$. In addition, the elastic material properties are also assumed to be temperature-independent.

3.2.1. Lower bound shakedown theorem

Historically, it was Melan [21], who developed the first general shakedown theorem using the static approach. It was to determine whether shakedown would occur, or not occur, in an elastic-perfectly plastic structure subjected to a combination of loads, each varying independently between prescribed limits. The theorem states that, "*if a time-independent residual stress field,* $\overline{\rho}_{ij}(x)$, *can be found, such that* $\sigma^{*}_{ij}(x,t)$, *the sum of the residual stresses with the linear elastic stresses,* $\hat{\sigma}_{ij}(x,t)$, *do not violate the yield criteria at any point within the body under all possible load combinations, then the body would shakedown*", *i.e.*

$$f(\sigma^{*}_{ij}) < \sigma_y \tag{3.3}$$

where $\sigma^{*}_{ij}(x,t) = \hat{\sigma}_{ij}(x,t) + \overline{\rho}_{ij}(x)$

In practice, however, structures do not shakedown to a unique state, independent of the loading histories. Generally, during shakedown analysis, a distribution of residual stress fields is expediently chosen, such that, the largest possible load variations results. This implies that the application of this theorem leads to a lower bound, λ_{LB}, on the exact shakedown limit, λ_s.

3.2.2. Upper bound shakedown theorem

The upper bound shakedown theorem, based on kinematic principles, uses the analogy between the theories of limit analysis and shakedown. Otherwise known as Koiter's [25] theorem, it provides a necessary condition for the occurrence of shakedown by stating that, "*a*

structure under cyclic loadings would shakedown if the external work done by the loads is less than or equal to the internal work dissipated for all admissible strain rate cycles, $\dot{\varepsilon}_{ij}^{c}$".

This introduces the concept of an incompressible and kinematically admissible strain rate history, $\dot{\varepsilon}_{ij}^{c}$, which need not be compatible but is associated with a compatible strain increment, $\Delta\varepsilon_{ij}^{c}$, such that,

$$\int_{o}^{\Delta t} \dot{\varepsilon}_{ij}^{c} = \Delta\varepsilon_{ij}^{c} \tag{3.4}$$

This, in turn, is associated with the corresponding displacement increment fields, which satisfies the displacement boundary conditions,

$$\Delta\varepsilon_{ij}^{c} = \frac{1}{2}\left(\frac{d\Delta u_i^c}{dx_j} + \frac{d\Delta u_j^c}{dx_i}\right) \tag{3.5}$$

In terms of such a history, the upper bound shakedown theorem is given by,

$$\lambda_{UB} \int_{v} \int_{0}^{\Delta t} \hat{\sigma}_{ij} \dot{\varepsilon}_{ij}^{c} dt dv = \int_{v} \int_{0}^{\Delta t} \sigma_{ij}^{c} \dot{\varepsilon}_{ij}^{c} dt dv \tag{3.6}$$

where the upper bound shakedown limit, $\lambda_{UB} \geq \lambda_s$, with the equality achieved, if and only if, the exact deformation mechanism is chosen. The above equation, as in equation (2.18), is then simplified for the von-Mises yield condition, leading to,

$$\lambda_{UB} = \frac{\int_{v}\int_{0}^{\Delta t} \sigma_y \bar{\dot{\varepsilon}} dt dv}{\int_{v}\int_{0}^{\Delta t} \hat{\sigma}_{ij} \dot{\varepsilon}_{ij}^{c} dt dv} \tag{3.7}$$

where $\sigma_{ij}^{c}\dot{\varepsilon}_{ij}^{c} = \sigma_y \bar{\dot{\varepsilon}}$ and $\bar{\dot{\varepsilon}} = \sqrt{\frac{2}{3}\dot{\varepsilon}_{ij}\dot{\varepsilon}_{ij}}$.

3.3. Shakedown Limits for the von-Mises Yield Condition

As previously mentioned, shakedown refers to one of the various modes of behaviour a body may exhibit when subjected to a history of cyclic loading. Associated with such a phenomenon is a constant residual stress field, $\bar{\rho}(x)$, which causes the redistribution of stresses within the body. Hence, any deformation, *i.e.* plastic strains, induced by the initial linear elastic stresses exceeding the yield stress, will only be limited during the initial few cycles. Upon which, the resumption of the elastic behaviour is observed. Therefore, in the identification of the shakedown limits, a method capable of determining, among others, the time-independent residual stress field and the associated deformation strain field is required. This is attempted in the sections below.

3.3.1. Linear matching method

The shakedown method, like the previously discussed limit analysis methods [2,4], was also developed by Ponter *et al* [3]. It basically involves matching a linear rate problem to that of a plasticity problem, whereby sequences of linear solutions with spatially varying

moduli are produced. These, in turn, generate upper bounds, which monotonically reduce to the least upper bound shakedown limit, for the chosen class of displacement fields. Although, initially conceived for the von-Mises yield condition, subsequent simplification and generalisation makes it applicable to any arbitrary yield conditions [5]. The value of this method is further enhanced with the recently developed finite element analysis codes for three-dimensional structural problems [8].

In general, the method involves defining a sequence of linear problems where the linear coefficients are identified so that they match the yield condition. For the von-Mises yield criterion, the chosen strain rates are incompressible; hence, the linear problem is defined by the shear modulus, $\mu(x,t)$. Thus, corresponding to an initial kinematically admissible strain rate history, $\dot{\varepsilon}_{ij}^{i}$, this modulus is found by matching the linear material to that of a perfectly plastic material so that they both give the same effective stress, *i.e.*

$$\frac{3}{2}\mu\bar{\dot{\varepsilon}}^{i} = \sigma_{y} \tag{3.8}$$

For subsequent linear problems, a new kinematically admissible strain rate history, $\dot{\varepsilon}_{ij}^{f}$, is now defined, such that,

$$\dot{\varepsilon}_{ij}^{f'} = \frac{1}{\mu}\left(\lambda_{UB}^{i}\hat{\sigma}_{ij}^{'} + \bar{\rho}_{ij}^{f'}\right), \qquad \dot{\varepsilon}_{kk}^{f} = 0 \tag{3.9}$$

where $\bar{\rho}_{ij}^{f'}$ is a time-independent constant residual stress field. It is important to note that the superscripts, *i* and *f*, corresponds to the initial and subsequent (final) states respectively.

Therefore, integrating equation (3.9) yields,

$$\Delta\varepsilon_{ij}^{f'} = \frac{1}{\overline{\mu}}\left(\sigma_{ij}^{in'} + \overline{\rho}_{ij}^{f'}\right) \tag{3.10}$$

where $\frac{1}{\overline{\mu}} = \int_0^{\Delta t} \frac{1}{\mu(t)} dt$ and $\sigma_{ij}^{in'} = \overline{\mu}\left(\int_0^{\Delta t} \frac{1}{\mu(t)} \lambda_{UB}^{i} \hat{\sigma}_{ij}^{'}(t) dt\right)$

The solution to this incompressible linear problem yields a new upper bound, λ_{UB}^{f}, when $\dot{\varepsilon}_{ij}^{f}$ is substituted into (3.7). The existence of convergence proofs [3,5] shows that $\lambda_{UB}^{f} \leq \lambda_{UB}^{i}$, with equality occurring, if and only if, $\dot{\varepsilon}_{ij}^{f} \equiv \dot{\varepsilon}_{ij}^{i}$. This procedure, when repeated, would generate a monotonically reducing sequence of upper bounds, converging to the least upper bound shakedown limit.

3.3.2. Numerical procedure for the upper bound shakedown limit

The above-mentioned equations gives rise to a programming method, which solves problems where the bounded load domain is known. For the problem in Figure 3.1 involving two load types, $P(t_n)$ & $\theta(t_n)$, where $n = 1$ to r, the loading histories would thus describe sequences of straight-line paths between sets of extreme points in load space. This is schematically shown in Figure 3.2(a). Similarly, the linear elastic stress histories, $\hat{\sigma}_{ij}^{P}(t_n)$ & $\hat{\sigma}_{ij}^{\theta}(t_n)$, would also describe sequences of linear paths in stress space, as shown in Figure 3.2(b). This implies that the plastic strains can only occur at the vertices of the stress histories. Thus, the strain rate history now becomes the sum of the increments of plastic strains, *i.e.*

$$\Delta\varepsilon_{ij}^{c} = \sum_{n=1}^{r} \Delta\varepsilon_{ij}(t_n) \tag{3.11}$$

Modifying equation (3.10) accordingly yields,

$$\Delta\varepsilon_{ij}^{f'} = \frac{1}{\overline{\mu}}\left(\sigma_{ij}^{in'} + \overline{\rho}_{ij}^{f'}\right) \tag{3.12}$$

$$\frac{1}{\overline{\mu}} = \sum_{n=1}^{r} \frac{1}{\mu(t_n)} \text{ where } \mu(t_n) = \frac{\sigma_y}{\overline{\varepsilon}(\Delta\varepsilon_{ij}^{i}(t_n))} \quad \text{and} \quad \sigma_{ij}^{in'} = \overline{\mu}\left(\sum_{n=1}^{r} \frac{1}{\mu(t_n)} \lambda\hat{\sigma}_{ij}^{'}(t_n)\right)$$

Numerically, the iterative procedure [5,49] begins with initialisation. The material model in user subroutine UMAT, defined by the shear moduli, $\mu(t_n)$, at n vertices of the loading history, is arbitrarily assigned to a value, usually a constant. In addition, as explained in Section 2.6.1, the external linear elastic stress solutions are extracted and incorporated into the subroutine, such that $\hat{\sigma}_{ij}(t_n) = \hat{\sigma}_{ij}(t_n)_{ext}$.

In the next iteration, the subroutine UMAT will be summoned again by ABAQUS. This time, the shear moduli, at each material integration point, will be updated, using the relationship,

$$\mu(t_n)^{k+1} = \frac{\sigma_y}{\overline{\varepsilon}(\Delta\varepsilon_{ij}^{k}(t_n))} \text{ where } \frac{1}{\overline{\mu}^{k+1}} = \sum_{n=1}^{r} \frac{1}{\mu(t_n)^{k+1}} \tag{3.13}$$

This allows the Jacobian matrix, $[J]^{k+1}$, to be defined, enabling

$$\sigma_{ij}^{ink+1} = \overline{\mu}^{k+1}\left(\sum_{n=1}^{r}\frac{1}{\mu(t_n)^{k+1}}\lambda^{k+1}\hat{\sigma}_{ij}(t_n)\right) \tag{3.14}$$

to be evaluated. The matrices for $[J]^{k+1}$, in plane stress, plane strain and axisymmetric conditions, are presented in Appendix A. The constant residual stress field is then calculated,

$$\overline{\rho}_{ij}^{k+1} = [J]^{k+1}\Delta\varepsilon_{ij}^{k+1} - \sigma_{ij}^{ink+1} \tag{3.15}$$

which, in turn, made it possible for the strain increments associated with n vertices of the loading histories to be computed,

$$\Delta\varepsilon_{ij}^{k+1}(t_n) = [C]_n^{k+1}\left(\overline{\rho}_{ij}^{k+1} + \hat{\sigma}_{ij}^{k+1}(t_n)\right) \tag{3.16}$$

where $[C]_n^{k+1}$ is the stiffness matrix derived from $\mu(t_n)^{k+1}$. Before the commencement of the next iteration, ABAQUS will call upon user subroutine URDFIL, where the iterative upper bound shakedown limit, derived from equation (3.7), is determined.

$$\lambda_{UB}^{k+1} = \frac{\int_v \sigma_y \sum_{n=1}^{r}\overline{\varepsilon}(\Delta\varepsilon_{ij}^{k+1}(t_n)dv}{\int_v \sum_{n=1}^{r}\Delta\varepsilon_{ij}^{k+1}(t_n)\hat{\sigma}_{ij}^{k+1}(t_n)dv} \tag{3.17}$$

This procedure is shown interactively in Figure 3.3. The actual fully commented programs, for the numerical problems examined in Section 3.5, are enclosed in the attached CD.

In the previous chapter, the identification of the limit loads using Procedure B refers to the methodology described in this section. The utilization of this shakedown method to limit analysis problems is made possible due to the similarities existing between the iterative processes associated with limit analysis and shakedown. This is easily demonstrated by assuming that the load and temperature remains constant with time, *i.e.* at $n=1$. With this change, the above procedure becomes the limit analysis method employed in Section 2.6. This clearly shows that limit analysis is a special case of shakedown analysis, with the only exception is the need to consider load cycles in shakedown calculations rather than a static load.

3.4. Extended Shakedown Theorems

The aforementioned iterative upper bound shakedown method identifies a limit, generally corresponding to structural deformations in either reverse-plasticity or ratchetting. Theoretically, designing within this boundary is ideal, as it is failure-safe and less conservative than purely elastic analysis. Provided small accumulations of plastic strains are accommodated during the initial loading cycles, the use of such solutions is often realized in low temperature loading situations.

In high temperature applications, such as the operation of power plants, nuclear reactors, *etc*, however, structural components usually ended up being designed in the reverse-plasticity region. This transpires when the effective value of the amplitude of the variation of the elastic stresses exceeds twice the yield stress. The cyclic plastic strains developed, which alternates equally in tension and compression, forms a reverse-plasticity mechanism in a

confined volume of the structure, without inducing any substantial strain growth. This causes the sum of the elastic stresses, $\hat{\sigma}_{ij}(x,t)$, the constant residual stress field, $\overline{\rho}_{ij}(x)$ and the time-varying residual stress field, $\rho_{ij}(x,t)$, associated with this phenomenon, to be kept within yield only over some volume of the body. Unlike shakedown, the subsequent cyclic behaviour is not entirely elastic as there are restricted increments of plastic strains over some part of the body (reverse-plasticity), whilst behaving elastically (shakedown) in the remaining part.

Consequently, designing within this region involved accounting for two additional considerations. The first is the amplitude of the cyclic plastic strains, which provides information concerning fatigue crack initiation in low cycle fatigue. It must be ensured that during its designed life, the number of such cycles must be kept within the design limit. The other significant factor is the capacity of the body to withstand additional constant mechanical loads without failure. This would then provide an indication of the loading condition's proximity to the ratchet limit.

The correct evaluation of the reverse-plasticity and ratchetting limits requires an understanding of the behaviour of cyclically loaded structures in excess of shakedown. In filling this gap, Ponter *et al* [6] derived a minimum theorem for an arbitrary cyclic state, which reduces to the upper bound shakedown theorem when the loading history lies within a shakedown limit. In circumstances when the loading history is in excess of shakedown, the evaluation of the ratchet limit entails two sequential minimisation processes [7]. The first stage involves the evaluation of a varying residual stress field and the corresponding closed cycles of plastic strains. The second stage then becomes a conventional shakedown calculation for the ratchet limit, with the varying residual stress field taken into account. Subsequent

exploration of these theorems resulted in the derivation of the LMM-based computational procedures, employable within a finite element analysis scheme [7]. In the following, summaries of the essential ideas behind these formulations are presented.

3.4.1. Minimum theorem in excess of shakedown

Still continuing with the problem in Figure 3.1, whereby the cyclic behaviour of an elastic-perfectly plastic body with cycle time, $0 \le t \le \Delta t$, is analysed, *i.e.*

$$\dot{\varepsilon}_{ij} = \dot{\varepsilon}^{e}_{ij} + \dot{\varepsilon}^{P}_{ij} \tag{3.18}$$

where the elastic strains, $\varepsilon^{e}_{ij} = C_{ijkl}\sigma_{kl}$, with the tensor, C_{ijkl}, satisfying the usual symmetrical properties. The plastic strains, $\dot{\varepsilon}^{P}_{ij}$, are defined by the yield condition of (2.1) and the associated flow law of (2.3). In addition, the maximum work principle of (3.1) still holds true.

For this general problem, the existence of minimum theorems [6] allows the possibility of defining load histories lying within or beyond the shakedown limit. This is given by the functional,

$$I(\dot{\varepsilon}^{c}_{ij}, \lambda) = \int_{v}\int^{\Delta t}(\sigma^{c}_{ij} - \lambda\hat{\sigma}_{ij})\dot{\varepsilon}^{c}_{ij}\,dtdv \tag{3.19}$$

where σ^{c}_{ij} denotes the stress at yield and $\dot{\varepsilon}^{c}_{ij}$ is a kinematically admissible strain rate history such that the accumulated strain over the cycle,

$$\int_{o}^{\Delta t} \dot{\varepsilon}_{ij}^{c} = \Delta \varepsilon_{ij}^{c} \tag{3.20}$$

is compatible with a displacement field, Δu_{ij}^{c}, which, in turn, satisfies the displacement boundary conditions. Two additional restrictions are now placed on the magnitude of $\dot{\varepsilon}_{ij}^{c}$:

- Restriction 1: Corresponding to $\dot{\varepsilon}_{ij}^{c}$, a cyclic history of residual stress, $\rho_{ij}^{c}(x,t)$, is defined such that it satisfies the relationship,

$$\dot{\varepsilon}_{ij}^{cc} = C_{ijkl}\rho_{ij}^{c} + \dot{\varepsilon}_{ij}^{c} \tag{3.21}$$

where $\dot{\varepsilon}_{ij}^{cc}$ is also a kinematically admissible strain rate history. Note that:

$$\rho_{ij}^{c}(0) = \rho_{ij}^{c}(\Delta t) = 0 \tag{3.22}$$

- Restriction 2: Corresponding to $\rho_{ij}^{c}(x,t)$, a restriction is then placed on the absolute magnitude of $\dot{\varepsilon}_{ij}^{c}$, with the requirement that there exists a constant residual stress field, $\overline{\rho}_{ij}$, such that the composite stress history,

$$\sigma_{ij} = \lambda\hat{\sigma}_{ij} + \overline{\rho}_{ij} + \rho_{ij}^{c} \tag{3.23}$$

satisfies the yield condition, $f(\sigma_{ij}) \le 0$, for $0 \le t \le \Delta t$.

It was proven [7] that for a prescribed load history, *i.e.* a prescribed λ that,

$$I(\dot{\varepsilon}_{ij}^{c}, \lambda) \geq 0 \tag{3.24}$$

with the equality achieved, when, $\dot{\varepsilon}_{ij}^{c} = \dot{\varepsilon}_{ij}^{cr}$, the exact cyclic solution. As it happens, this argument is closely related to the shakedown theorems. At the shakedown limit, $\lambda = \lambda_s$, the magnitude of the strain rate history, $\dot{\varepsilon}_{ij}^{c}$, becomes sufficiently small for the changing component of the residual stress, $\rho_{ij}^{c}(x,t)$, to be insignificant. This resulted in the stress history in (3.23) and the yield condition, $f(\sigma_{ij}) \leq 0$, becoming the requirement of the lower bound shakedown theorem (Section 3.2.1). This leads to the condition in (3.24) now yielding, $I(\dot{\varepsilon}_{ij}^{c}, \lambda_s) \geq 0$ and $I(\dot{\varepsilon}_{ij}^{s}, \lambda_s) = 0$, where $\dot{\varepsilon}_{ij}^{s}$ is the exact shakedown mechanism. At this point, if the functional is described by $I(\dot{\varepsilon}_{ij}^{c}, \lambda_{UB}) = 0$, where $\lambda_{UB} \geq \lambda_s$, then the upper bound shakedown theorem is recovered (Section 3.2.2). Thus, for small $\dot{\varepsilon}_{ij}^{c}$, the aforesaid minimum theorem provided a generalisation of the lower and upper bound shakedown theorems.

In the case of loading in excess of shakedown, a parallel understanding of the nature of the ratchet boundary is required. This is provided by the requirement that there exist mechanisms that satisfy the condition of the theorem for finite $\dot{\varepsilon}_{ij}^{c}$ for which $\Delta\varepsilon_{ij}^{c} = 0$, *i.e.* although plastic deformation takes place in the cycle, there is no net accumulation of strain. Associated with such loading histories, a finite varying residual stress field, $\rho_{ij}^{c}(x,t)$, as a solution to (3.21), exists. If this is identified, then the analysis is reduced to a conventional shakedown problem where the prescribed loading history is augmented by some constant load,

which takes the structure to the ratchet limit. In these situations, the calculations are performed in two stages [6,7]. In the first stage, the varying residual stress field, associated with the applied varying loads, is evaluated. This is then followed by the location of the ratchet limit, in the second stage, where the elastic stress history takes into account the changes in the varying residual stress field. In the following, the implementations of these two numerical procedures are presented.

3.4.2. Numerical procedure for the varying residual stress field

The body, in Figure 3.1, is now assumed to be subjected to external loads, such that,

$$P_i(x_j,t) = \lambda \overline{P}_i(x_j) + P_i(x_j,t) \tag{3.25}$$

where $\overline{P}_i(x_j)$ is a constant load distribution and $P_i(x_j,t)$ and $\theta(x_j,t)$ are the cyclic histories associated with the mechanical load and temperature respectively. The associated linear elastic stress solution is defined by

$$\hat{\sigma}_{ij} = \lambda \hat{\sigma}_{ij}^{\overline{P}} + \hat{\sigma}_{ij}^{\Delta}(x,t) \tag{3.26}$$

where $\hat{\sigma}_{ij}^{\Delta} = \hat{\sigma}_{ij}^{P} + \hat{\sigma}_{ij}^{\theta}$, the varying elastic stress components due to $P_i(x_j,t)$ and $\theta(x_j,t)$.

The following argument is based on the general case where the elastic stress varies proportionally between two extreme values, $\hat{\sigma}_{ij}^{\Delta}(t_1)$ and $\hat{\sigma}_{ij}^{\Delta}(t_2)$, describing a straight-line path in stress space. Using this simplification, equations (3.20) & (3.22) now give,

$$\int_0^{t_1} \dot{\varepsilon}_{ij}^c dt = \Delta\varepsilon_{ij}^c \qquad \& \qquad \int_{t_1}^{t_2} \dot{\varepsilon}_{ij}^c dt = -\Delta\varepsilon_{ij}^c \tag{3.27}$$

and

$$\int_0^{t_1} \dot{\rho}_{ij}^c dt = \Delta\rho_{ij}^c \qquad \& \qquad \int_{t_1}^{t_2} \dot{\rho}_{ij}^c dt = -\Delta\rho_{ij}^c \tag{3.28}$$

Thus, by taking into consideration only $\Delta\varepsilon_{ij}^c$ and $\Delta\rho_{ij}^c$, the extremes of the reverse-plasticity mechanism can then be identified, providing sufficient information in the second stage.

In general, this LMM-based methodology [7] requires the solution of a sequence of linear problems. For an initial estimate of the strain increment, $\Delta\varepsilon_{ij}^c = \Delta\varepsilon_{ij}^{ci}$, a class of linear problems for a new estimate, $\Delta\varepsilon_{ij}^c = \Delta\varepsilon_{ij}^{cf}$, is then defined such that the linear coefficient, $\overline{\mu}^i$, is given by,

$$2\sigma_y = \left(\frac{3}{2}\right) 2\overline{\mu}^i \bar{\varepsilon}(\Delta\varepsilon_{ij}^{ci}) \tag{3.29}$$

The new distribution of the strain increment, $\Delta\varepsilon_{ij}^{cf}$, is then characterized as the solution to the following problem,

$$\Delta\varepsilon_{ij}^{cTf'} = \frac{1}{2\mu}\Delta\rho_{ij}^{f'} + \Delta\varepsilon_{ij}^{cf'}, \qquad \Delta\varepsilon_{kk}^{cTf} = \frac{1}{3K}\Delta\rho_{kk}^{f} \tag{3.30}$$

and

$$\Delta\varepsilon_{ij}^{cf'} = \left(\frac{1}{2\overline{\mu}^{i}}\right)\left(\Delta\hat{\sigma}_{ij}^{'} + \Delta\rho_{ij}^{cf'}\right) \tag{3.31}$$

where $\Delta\varepsilon_{ij}^{cTf}$ and $\Delta\rho_{ij}^{f}$ satisfies compatibility and equilibrium conditions respectively, with

$$\Delta\hat{\sigma}_{ij} = \hat{\sigma}_{ij}^{\Delta}(t_1) - \hat{\sigma}_{ij}^{\Delta}(t_2) \tag{3.32}$$

In an iterative process, the repeated application of this algorithm produces a sequence of solutions for $\Delta\varepsilon_{ij}^{ck}$, which converges to the absolute minimum of the functional. If two consecutive iterations, k and $k+1$, are now considered, then the relationship in (3.29) yields,

$$\overline{\mu}^{k+1} = \overline{\mu}^{k}\,\frac{2\sigma_y}{\overline{\sigma}(\Delta\hat{\sigma}_{ij} + \Delta\rho_{ij}^{ck})} \tag{3.33}$$

This procedure is shown interactively in Figure 3.4, with the actual fully commented programs, for the numerical problems examined in Section 3.5, enclosed in the attached CD. (Note: The values of the shear modulus, μ, and the bulk modulus, K, are obtained from materials data.)

3.4.3. Numerical procedure for the ratchet limit

The numerical procedure, used in the identification of the ratchet limit, is similar to those described for the upper bound shakedown limit (Section 3.3.2). The principal difference is the need to take into account the varying residual stress field calculated from the above procedure. In such cases, the upper bound shakedown theorem is given by,

$$\int_{v}\int_{0}^{\Delta t}\hat{\sigma}_{ij}\dot{\varepsilon}_{ij}^{c}dtdv=\int_{v}\int_{0}^{\Delta t}\sigma_{ij}^{c}\dot{\varepsilon}_{ij}^{c}dtdv \tag{3.34}$$

where $\hat{\sigma}_{ij}=\lambda_{UB}\hat{\sigma}_{ij}^{\overline{P}}+\hat{\sigma}_{ij}^{\Delta}(x_i,t)+\rho_{ij}^{c}(x_i,t)$. As only two distinct extremes of the elastic stress solutions, at instances t_1 and t_2, are considered, equation (3.34) yields,

$$\lambda_{UB}\int_{v}\hat{\sigma}_{ij}^{\overline{P}}\left(\Delta\varepsilon_{ij}(t_1)+\Delta\varepsilon_{ij}(t_2)\right)+\int_{v}\left\{\left(\hat{\sigma}_{ij}^{\Delta}(t_1)+\rho_{ij}^{c}(t_1)\right)\Delta\varepsilon_{ij}(t_1)+\left(\hat{\sigma}_{ij}^{\Delta}(t_2)+\rho_{ij}^{c}(t_2)\right)\Delta\varepsilon_{ij}(t_2)\right\}dv$$

$$=\int_{v}\left(\sigma_{ij}^{c}(t_1)\Delta\varepsilon_{ij}(t_1)+\sigma_{ij}^{c}(t_2)\Delta\varepsilon_{ij}(t_2)\right)dv \tag{3.35}$$

where $\rho_{ij}^{c}(t_1)=\Delta\rho_{ij}^{c}$, $\rho_{ij}^{c}(t_2)=0$ and $\Delta\varepsilon_{ij}^{c}=\Delta\varepsilon_{ij}(t_1)+\Delta\varepsilon_{ij}(t_2)$. Upon the re-arrangement of (3.35) for the von-Mises yield condition, the iterative upper bound ratchet limit multiplier can be written as,

$$\lambda_{UB}^{k+1}=\frac{\int_{v}\sigma_y\bar{\varepsilon}(\Delta\varepsilon_{ij}^{c})dv-\int_{v}\left\{\left(\hat{\sigma}_{ij}^{\Delta}(t_1)+\rho_{ij}^{c}(t_1)\right)\Delta\varepsilon_{ij}(t_1)+\left(\hat{\sigma}_{ij}^{\Delta}(t_2)\right)\Delta\varepsilon_{ij}(t_2)\right\}dv}{\int_{v}\hat{\sigma}_{ij}^{\overline{P}}\left(\Delta\varepsilon_{ij}(t_1)+\Delta\varepsilon_{ij}(t_2)\right)dv} \tag{3.36}$$

Thus, for the chosen class of displacement fields, the same iterative monotonically reducing sequence of upper bounds, converging to the least upper bound ratchet limit behaviour, is to be expected. This procedure is shown interactively in Figure 3.5, with the actual fully commented programs, for the numerical problems examined in Section 3.5, enclosed in the attached CD.

To this point, the exploitation of the numerical techniques is based upon the assumption of a perfectly plastic material. However, it is a well-known fact that the cyclic strain amplitude in a reverse-plasticity mechanism is sensitive to cyclic hardening. For many materials, this occurs when the amplitude of the effective stress, $\bar{\sigma}(\Delta\sigma_{ij})$, associated with the amplitude of the plastic strain, $\bar{\varepsilon}(\Delta\varepsilon_{ij}^{P})$, exceeds $2\Delta\sigma_y$. Thus, the inclusion of such an effect requires the development of a method based upon a constitutive equation, which predicts the required material's behaviour in the steady state. As an interim solution, however, it is possible to include the effects of cyclic hardening by assuming in (3.29), that

$$2\Delta\sigma_y = \bar{\sigma}\left(\Delta\sigma_{ij}(\Delta\varepsilon_{ij}^{c})\right) \tag{3.37}$$

where $\Delta\sigma_y$ is a monotonically increasing function of the effective strain amplitude, $\Delta\varepsilon_{ij}^{c}$. The ratchet limit so calculated would, thus, provide the largest load for which there exist a consistent history of stress that lies within yield. This implies in regions of cyclic hardening, the yield stress is related to the finite amplitude of strain, whereas elsewhere the history lies within the initial yield surface.

Figure 3.6, the cyclic and monotonic stress-strain curve for type 316SS, best describes these differences in material behaviours. It clearly shows that the perfect plasticity solution overestimates the material behaviour, since it does not suffer any cyclic hardening. At the other extreme, however, the assumption of isotropic hardening results in the material cyclically hardening to the elastic behaviour. These two solutions are, thus, sufficient to encompass or bound the entire range of a real material's behaviour. The accuracy of this

hypothesis was verified through the investigations of Ponter *et al* [23,24] on a two-bar structural problem.

3.5. Numerical Examples

The applications of the numerical procedures, discussed in Sections 3.3 and 3.4, are now demonstrated on two problems. The first is the classical Bree [37] problem, under both uncracked and cracked conditions. The second is the problem considered in R5 [1], whereby a pipe is subjected to an internal pressure in the presence of varying temperature.

3.5.1. Bree problem

This problem was, originally, used to simulate the behaviour of a nuclear reactor fuel can, subjected to very high thermal stresses in the presence of a constant pressure stress. Then, it was observed that the plastic strains produced, due to the cycling of the temperature gradient across the can wall during start-up and shutdown, has serious implications on the lifetime of a reactor. In overcoming this, Bree [37] developed theoretical solutions for a simplified plane stress model. These solutions, illustrated on the so-called Bree or interaction diagram, provided a means of distinguishing the different modes of material behaviour, corresponding to the severity of the thermal stresses. Thus, the availability of an atlas of such diagrams [62], considering the various combinations of thermal loadings and structural geometries, is of great assistance to designers, especially in the early design stage.

As an initial investigation, the same plane stress Bree problem is considered here. As shown in Figure 3.7, it consists of a plate, of width, w, subjected to a cyclic temperature gradient through the width, assumed to vary linearly between θ_0 and $\theta_0 + \Delta\theta$. In addition, the plate is under a constant axial stress, σ_p, and restrained from any in-plane bending. In the FEA model, the eight-noded quadrilateral meshing elements, CPS8, is used. The resulting interaction diagram is in Figure 3.8, in terms of the axial stress, σ_p, and the maximum thermo-elastic stress due to the fluctuating temperature difference, σ_t, both normalized by the uniaxial yield stress, σ_y. It can be clearly seen that the numerical shakedown and ratchet limits calculated by the proposed methods, are in good agreement with the theoretical solutions. This provided the confidence that the LMM-based methodologies, discussed in this chapter, were capable of generating correct and accurate results, justifying their continued use in other situations. Furthermore, these procedures were found to achieve rapid convergence, *i.e.* within 30-50 iterations, even when a very strict convergence criterion was employed.

The distinct feature on the interaction diagram is the separation of the different modes of material behaviour. In this particular analysis, it is divided into four main regions, namely,

- **E** - Elastic: In this region, it was found that any combinations of the elastic stresses, due to σ_p and σ_t, nowhere exceed the yield stress. The plate behaves entirely elastically with eventual failure due to high cycle fatigue.

- **S** - Shakedown: In this region, the stresses were found to exceed the yield stress, resulting in small increments of plastic strains. These deformations are, however, limited to the first few cycles, upon which the resumption of the elastic behaviour was observed. The

constant residual stress field, associated with this phenomenon, has caused the redistribution of the stresses within the plate. This effectively has the effect of pulling the stress fields, the sum of the elastic and residual stresses, into the yield surface.

- **P** - Reverse-plasticity: The transition to this region occurs when the effective elastic stresses exceeds twice yield. During each cycle, plastic strains were observed in volume, V_p, of the plate, but contained within the surrounding shakedown volume, V_s. This was made possible with the accommodation of the time-varying residual stress field, causing the stress distribution at the ends of the plate, to exceed twice the yield stress, whilst satisfying the shakedown condition at the center. Although, safe from plastic failure, the effect of low cycle fatigue must be taken into consideration.

- **R** - Ratchetting: This region is best characterized by the breaking down of the elastic, shakedown and reverse-plasticity conditions. In each cycle, plastic strains accumulate over a significant volume of the plate, leading to imminent structural failure from the unlimited accumulation of plastic strains.

Another significant advantage of the Bree problem is its ability to be re-interpreted as an axisymmetric or plane strain (mathematical/generalized) problem. This basically involves modifying the appropriate boundary conditions within the FEA model. In the axisymmetric model, it is now, as if, implying that a tube or cylinder is subjected to the prescribed loading conditions. In modelling thick sections for plane strain analysis, however, ABAQUS allows two types of meshing elements to be applied. The use of mathematical plane strain elements, CPE8H, assumes that the strain through the plate's thickness is zero, $\varepsilon_{zz} = 0$. Alternatively,

the employment of the generalized plane strain elements, CGPE8H, allows the through-thickness strains to remain constant in the model, $\varepsilon_{zz} = const$. Solutions to these additional circumstances were then generated and plotted on interaction diagrams in Figure 3.9. Also included are solutions for the respective analyses whereby the axial stress now varies, between zero and some maximum value, in-phase with the cyclic temperature gradient.

Identical solutions were observed for the axisymmetric and generalized plane strain analyses. With insight, this is not surprising as both use the same Jacobian matrix in describing the material behaviour. This leads to the conclusion that in the analysis of thermally loaded uncracked structures, the generalized plane strain formulation is a substitute for the axisymmetric analysis. In comparison with plane stress, however, these results were found to differ by about 16%. In cases where the axial stress varies, this difference has reduced to 8%. Both of these diagrams verify the conservative character of plane stress solutions explaining their regular use in structural design. Although, mathematical plane strain solutions resulted in much lower limits, there isn't any physical justification behind its utilization.

3.5.2. Bree problem with crack

The real motivation behind the development of these numerical methods is the need to characterise the remaining strength of cracked structures when subjected to the combined actions of mechanical and thermal loads. This is, in particular, in the context of the R5 method [1], for the high temperature life assessment procedures developed at British Energy in the UK. The utilization of present design guidelines, focussing on the prevention of the initial existence and subsequent propagation of cracks, is no longer appropriate. This is mainly due to

the presence of cracks or crack-initiating defects that are either inherent in the material or created during manufacturing and installation. Thus, the correct prediction of the structural response during loading conditions requires a method capable of accurately assessing these existing defects.

Here, the characteristics of these numerical procedures, in accounting for the effects of cracks, are investigated. The same standard Bree problem is considered, except with cracks included this time round. Depending upon the type of analyses, these cracks are either circumferential for axisymmetric, or edge cracks, for plane stress or generalized plane strain. The corresponding FEA models for these analyses are shown in Figure 3.10. The same FEA meshing arrangement at the crack tip, employed in Chapter 2 (Figure 2.10), is adopted here. This is justified on the basis of the accurate limit load solutions generated previously. The tube/plate is still subjected to uniaxial tension, σ_p, and a linear temperature gradient arising from a temperature difference of $\Delta\theta$. Denoted by σ_t, the thermo-elastic stress is now the maximum stress away from the crack, *i.e.* the value that would occur if the cracks were absent. These cracks of width, a, are also assumed to occur at the centre of the line of symmetry, allowing only half of the length to be modelled. It is important to note that the elastic stress solutions for the cracked body under the mechanical and thermal loads, utilized in these analyses, has a singularity at the crack tip.

In the analysis of such problems, the non-existence of any shakedown region is well documented, as shakedown limit can only occur at zero loads, *i.e.* $\sigma_t = 0$. This is due to the singularity in the elastic stress field at the crack tip. Numerically, this is proven with the use of a very fine mesh at the crack tip, like the one used in Chapter 2 (Figure 2.12). The numerical

procedure for identifying the ratchet boundary, however, still applies, as reverse-plasticity will be confined to a small region in the immediate vicinity of the crack tip. The results of such calculations, plotted on interaction diagrams, are shown in Figures 3.11, 3.12 and 3.13, corresponding to various increments of crack width. Two sets of solutions were included; those that assume perfect plasticity (PP) and an adaptation of the method to allow complete cyclic hardening (CCH) in the reverse-plasticity regions. The CCH solutions were obtained by substituting (3.37) into (3.29) and then repeating the iterative processes for the identification of the ratchet limits, described in Sections 3.3 and 3.4. Essentially, this additional procedure enables the effective stresses in the body to monotonically increase with increasing magnitude of the effective strains. The behaviour of realistic cyclic properties would be expected to lie between these two solutions (PP and CCH). As can be seen, the ratchet boundaries are insensitive to cyclic hardening, with differing solutions occurring only at high values of σ_t [63,64]. This outcome is not entirely unexpected, as the effect of cyclic hardening in cracked bodies, is generally confined in the immediate vicinity of the crack tip.

Of the three models analysed, the axisymmetric results were found to be distinctly different from the rest. This is especially so when the circumferential crack is greater than half of the tube's width. An explanation of such behaviour is attempted by observing the contour plots for the CCH von-Mises effective strains, $\bar{\varepsilon}(\Delta\varepsilon_{ij}^{c})$, at the ratchet limits. A selection of such plots is shown in Figures 3.14 and 3.15. It was found that when σ_t is small, the same deformation mechanism, seen in Chapter 2, was still observed. This behaviour was consistently observed for all crack widths, including the analysis of plane stress and generalized plane strain. The major difference occurs when $\sigma_t \geq 2\sigma_y$. A change in the

deformation mechanisms at the uncracked ligament was noticed. This behaviour was consistently observed as σ_t is increased, with additional reverse-plasticity strains appearing at the edge of the tube, if σ_t is high enough. A full collection of these plots, for all three two-dimensional analyses with varying crack widths, is enclosed in the attached CD. (Note: The contour plots were generated with a limit set on the maximum von-Mises effective strain $\bar{\varepsilon}(\Delta\varepsilon_{ij}^c)$. This is due to the high strain singularity experienced at the crack tip, which is the focussed area of investigation in Chapter 4.)

The variations in the ratchet limits, when σ_p is varying in-phase with the thermal loads, were also investigated. Solutions were generated for plane stress, generalized plane strain and axisymmetric loading conditions, plotted in the form of interaction diagrams in Figures 3.16 and 3.17. Only CCH solutions were computed, as in the course of writing this thesis, the implementation of the methodology for identifying the PP ratchetting limit is not available. The results indicate that the maximum mechanical load that the structures can carry, occur at some finite value of σ_t, not at the limit load, *i.e.* $\sigma_t = 0$. This behaviour is consistently observed in all the three analyses considered. These differences are best illustrated in Figure 3.18, the plot of the limit and maximum loads against varying crack widths, where P_L is the uncracked limit load. It was found that the utmost variation between the limit and maximum loads, for the respective analyses, was about 8%.

Another feature of these solutions is the convergence. As shown in Figure 3.19, the ratchet limits were found to reduce monotonically, converging to good solutions within the first 40-50 iterations. In comparison with those at the 100^{th} iteration, the percentage difference

is less than 1%. This behaviour is typical of the three analyses at the different crack widths. It still holds true for higher σ_t, even if the interaction diagrams generated stops at $\sigma_t = 3\sigma_y$.

3.5.3. R5 problem

The aim of this investigation is to compare the R5 [1] limit, employed within the current design and life assessment procedures, with solutions generated using the numerical methods described in this chapter. The same idealized structural geometry, investigated in R5 [1], is considered here. As shown in Figure 3.20, it consists of a homogeneous Type 316 stainless steel cracked pipe, subjected to repeated cyclic loadings, from an initially unstressed shutdown condition at ambient temperature of $20^0 C$ to an operating condition of $600^0 C$. In the presence of an internal pressure of 16MPa, the behaviour of this pipe, subjected to two different thermal stresses, were then examined. These were 200MPa in Example 1 and 300MPa in Example 2. The yield stresses were also assumed to vary with temperature, such that $\sigma_y^c = 184.2\,\text{MPa}$ and $\sigma_y^h = 126\,\text{MPa}$, where the superscripts denote the cold and hot parts respectively.

For the loading conditions corresponding to Example 1, the R5 [1] limit is obtained by assuming that the cracks do not exist. In such situations, the procedure then prescribes a means of identifying a shakedown limit, based upon the satisfaction of the lower bound shakedown theorem [21] of equation (3.3). Using the same assumption of an uncracked pipe, numerical shakedown limits were then generated, using the LMM-based methodologies described in the previous sections. The results from these two analyses are plotted in Figure 3.21, where

$\overline{\sigma}(\sigma^P)_{\max}$ and $\overline{\sigma}(\sigma^\theta)_{\max}$ are the maximum von-Mises effective stresses due to the internal pressure and thermal stresses respectively. For Example 1, the pipe's operation in "strict shakedown" is clearly demonstrated. Also observed is the good correlation between the R5 [1] limit and the numerical shakedown limit, with the slight conservativeness of the R5 limit not totally unexpected. This is mainly due to the employment of safety factors, perhaps excessively so, during the identification of this limit.

For the loading conditions corresponding to Example 2, the interaction diagram in Figure 3.21, shows that the pipe is now operating within the reverse-plasticity region. At the present time, there are no available procedures, prescribed within the current design and life assessment procedures, capable of identifying the equivalent R5 [1] ratchet limit. This gap can be filled with the use of the numerical methods discussed in this chapter. Figure 3.21 shows the numerical ratchetting limits, evaluated for the structural geometry considered, under both uncracked and cracked conditions. The plot distinctly shows a big difference between the loading conditions of Example 2 and the identified numerical ratchetting limits. In the current environment of operating structures at elevated temperatures, the loading conditions, applied on this structure, is extremely conservative, perhaps, unnecessarily so. It is hoped that the application of these LMM-based methodologies in identifying the shakedown and ratchetting limits, would ultimately lead to structures operating more efficiently and effectively.

3.6. Concluding Remarks

In relation to questions posed in the identification of shakedown, reverse-plasticity and ratchetting limits, this chapter proposed the linear matching method (LMM). Upon the

introduction of the fundamental shakedown theorems for a general problem, the numerical procedure, for the upper bound shakedown theorem [3,5,49], was then described. This was then followed by discussions into the extended theorems [6], for structures loaded in excess of shakedown. The associated numerical procedures [7], for the identification of ratchetting limits in both perfect plasticity and complete cyclic hardening conditions, were also presented.

The applications of these numerical methods were then examined on two problems; the Bree [37] problem, under uncracked and cracked conditions, as well as an additional industrial problem in R5 [1]. The solutions showed that the LMM-based methodologies were capable of generating accurate shakedown and ratchetting limits, within finite iterations. It was also able to cope very well with the different types of analyses conducted, *i.e.* plane stress, plane strain and axisymmetric, under various increments in crack widths. The insensitivity of the solutions to cyclic hardening was also observed, as both perfect plasticity and complete cyclic hardening ratchet limits yielded almost identical results. It is, however, the ability of the numerical procedure in dealing with the elastic singularity at the crack tip, which is the most outstanding feature of this method. Its capability in generating ratchet limit solutions, without needing to replace the cracks with notches, is a major achievement in the analysis into the behaviour of structures subjected to cyclic histories of loads and temperatures. This raised question marks on the validity of the so-called ratchet limit solutions [26,27,28], identified with notches in them.

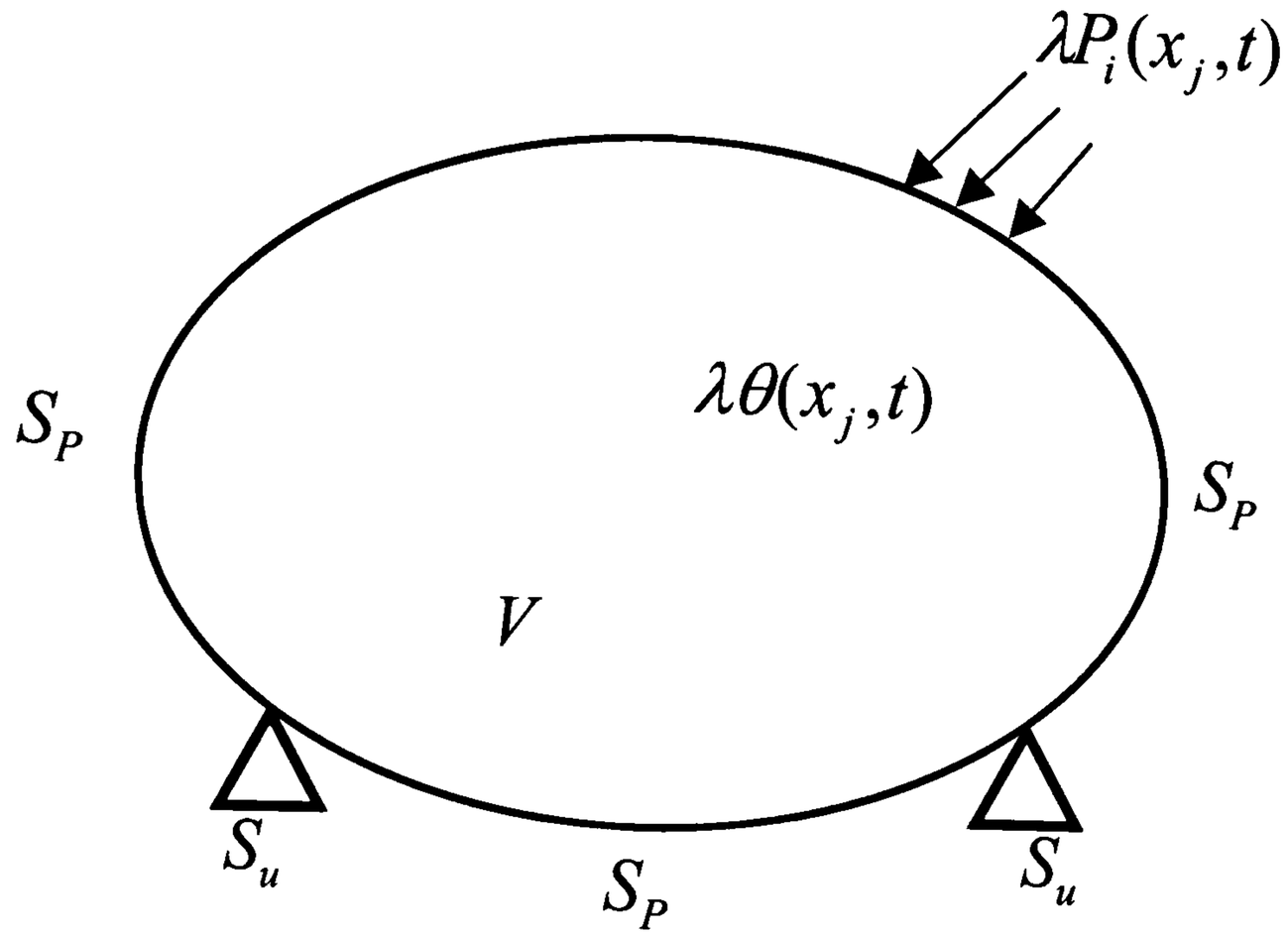

Figure 3.1: Schematic diagram of the general problem.

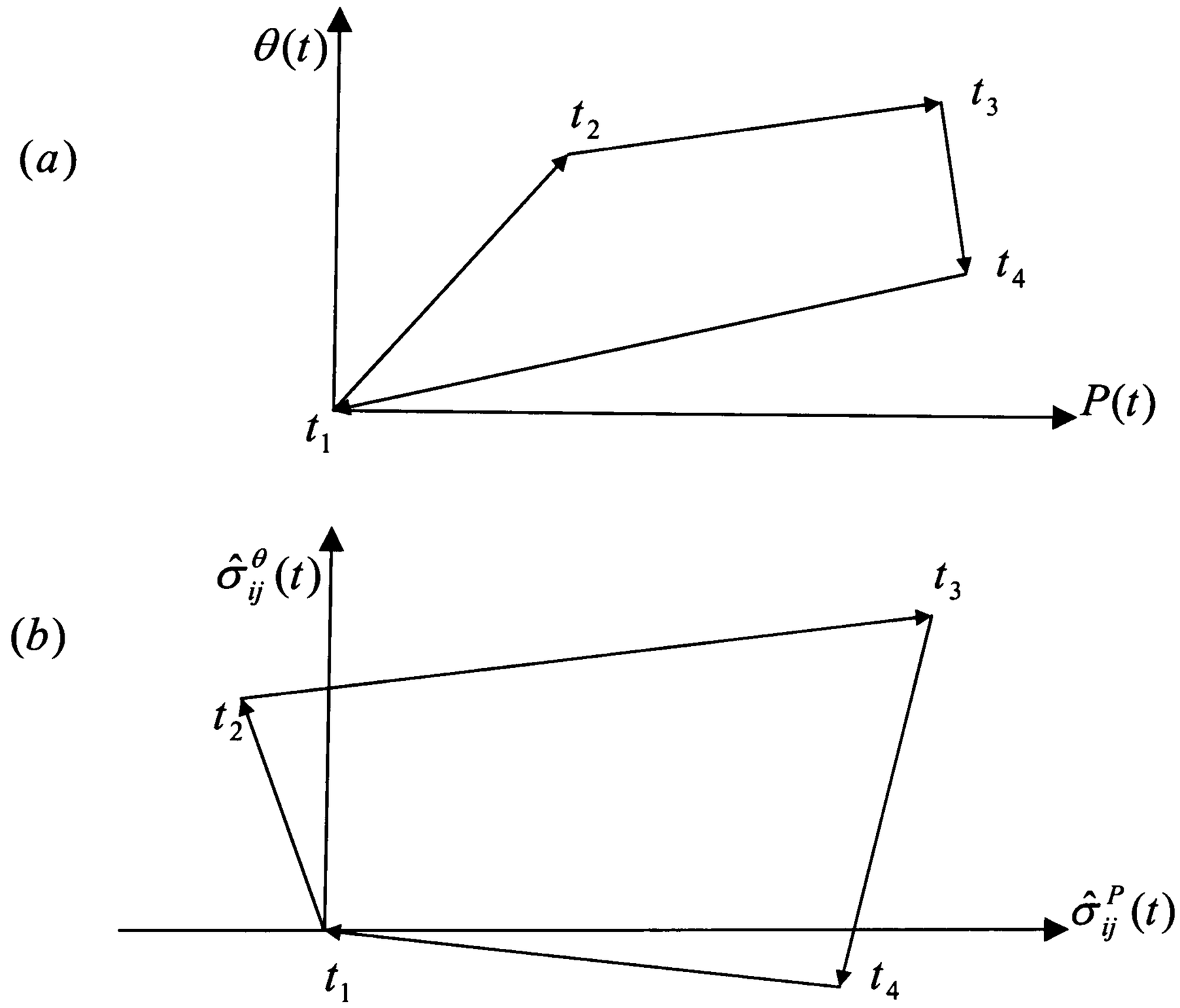

Figure 3.2: The cyclic loading history describing a sequence of straight lines in load space (a), producing a similar form for the elastic stress history in stress space (b).

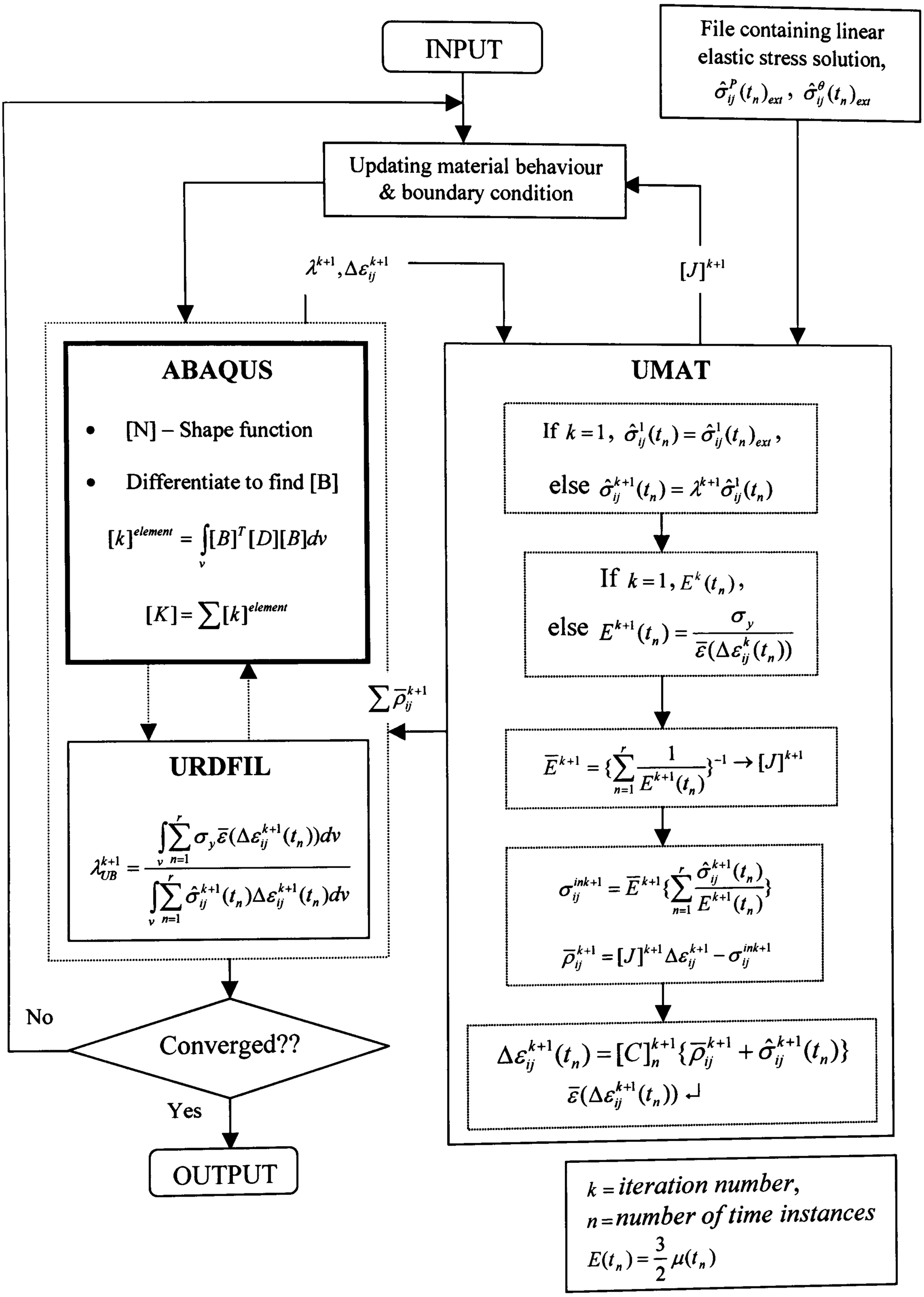

Figure 3.3: Interaction between ABAQUS and user subroutines for the upper bound shakedown limit method.

Figure 3.4: Interaction between ABAQUS and user subroutines for determining the varying residual stress field.

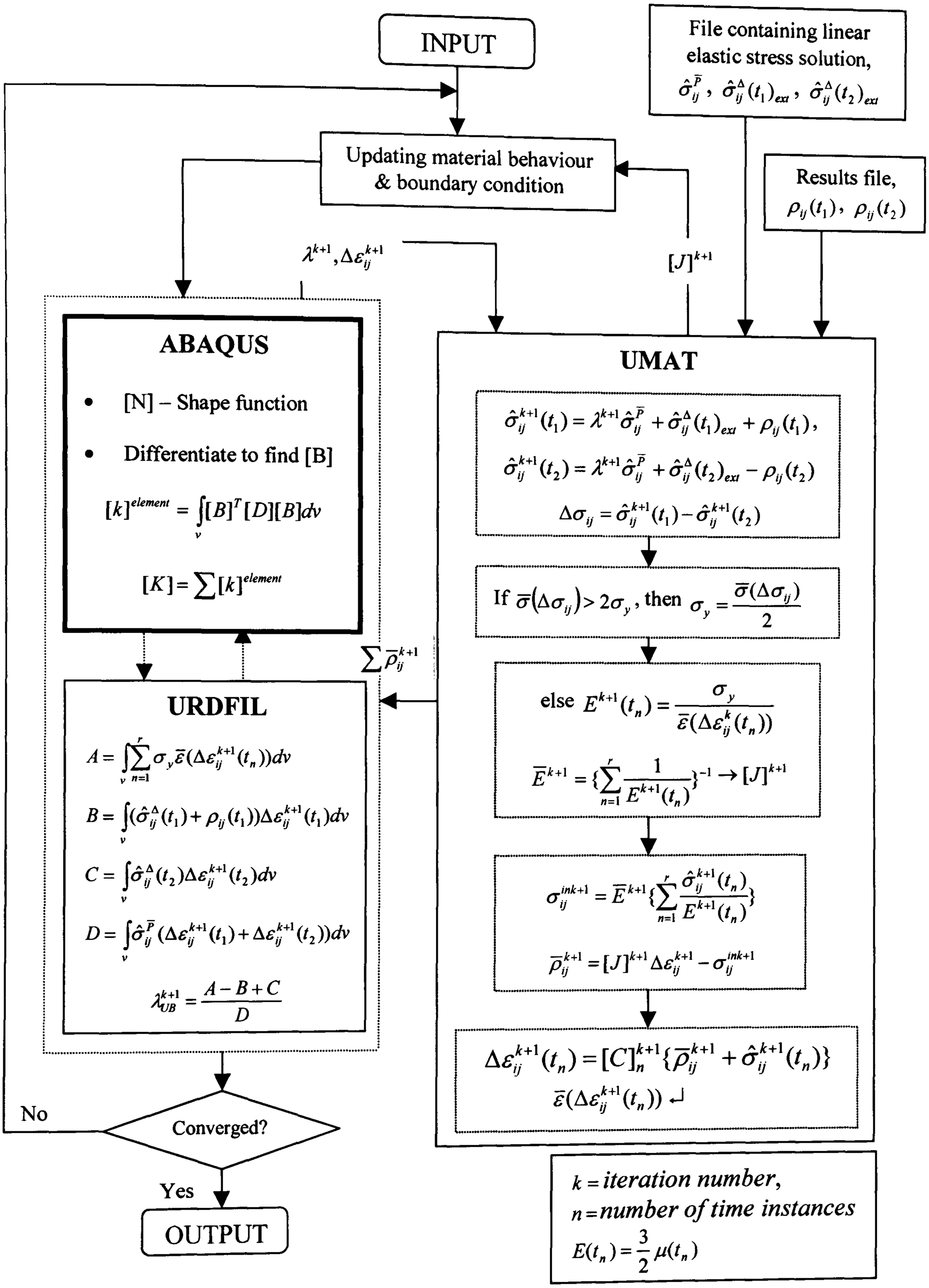

Figure 3.5: Interaction between ABAQUS and user subroutines for determining the ratchet limits.

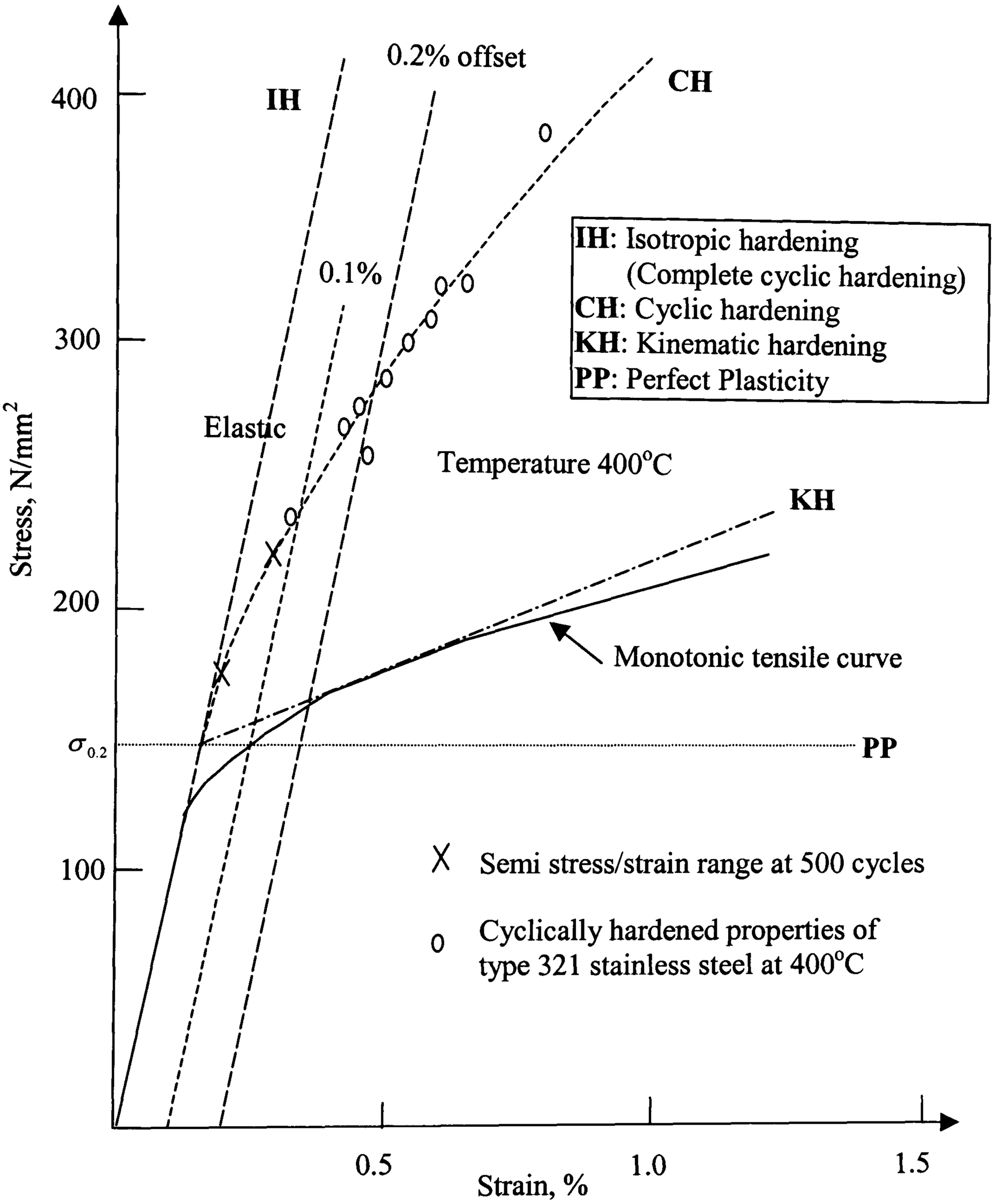

Figure 3.6: Cyclic and monotonic stress-strain curve for type 316SS.
(Courtesy of Ponter, A. R. S, and Karadeniz, S. [23,24])

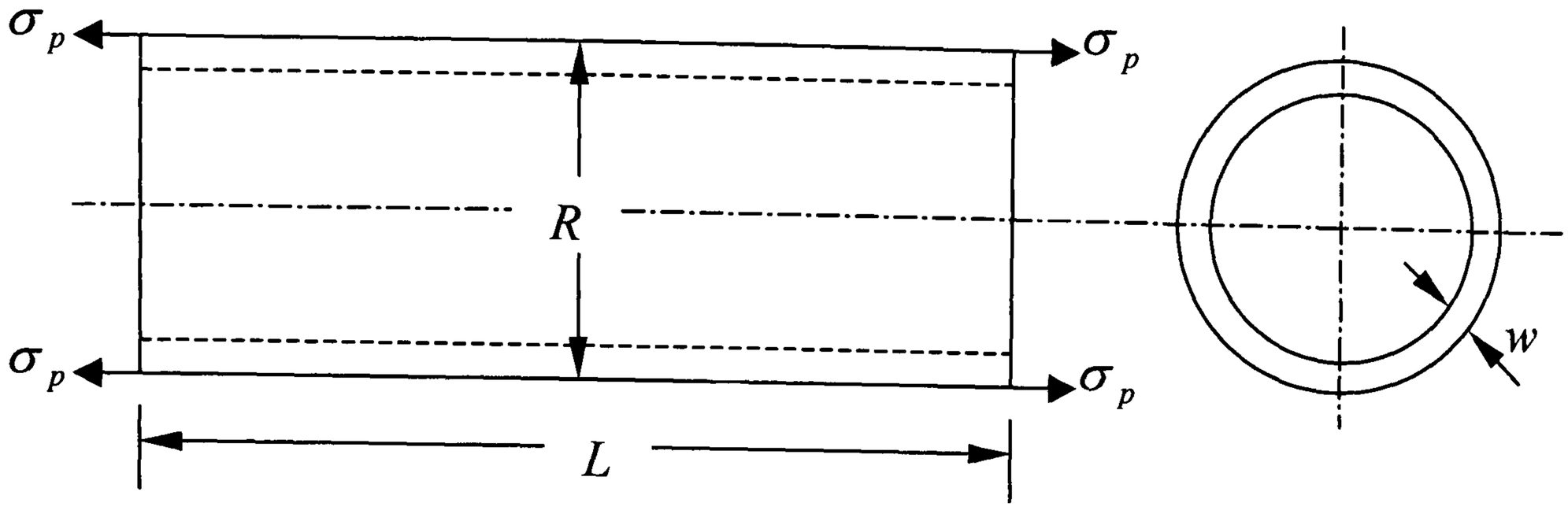

Fuels can problem

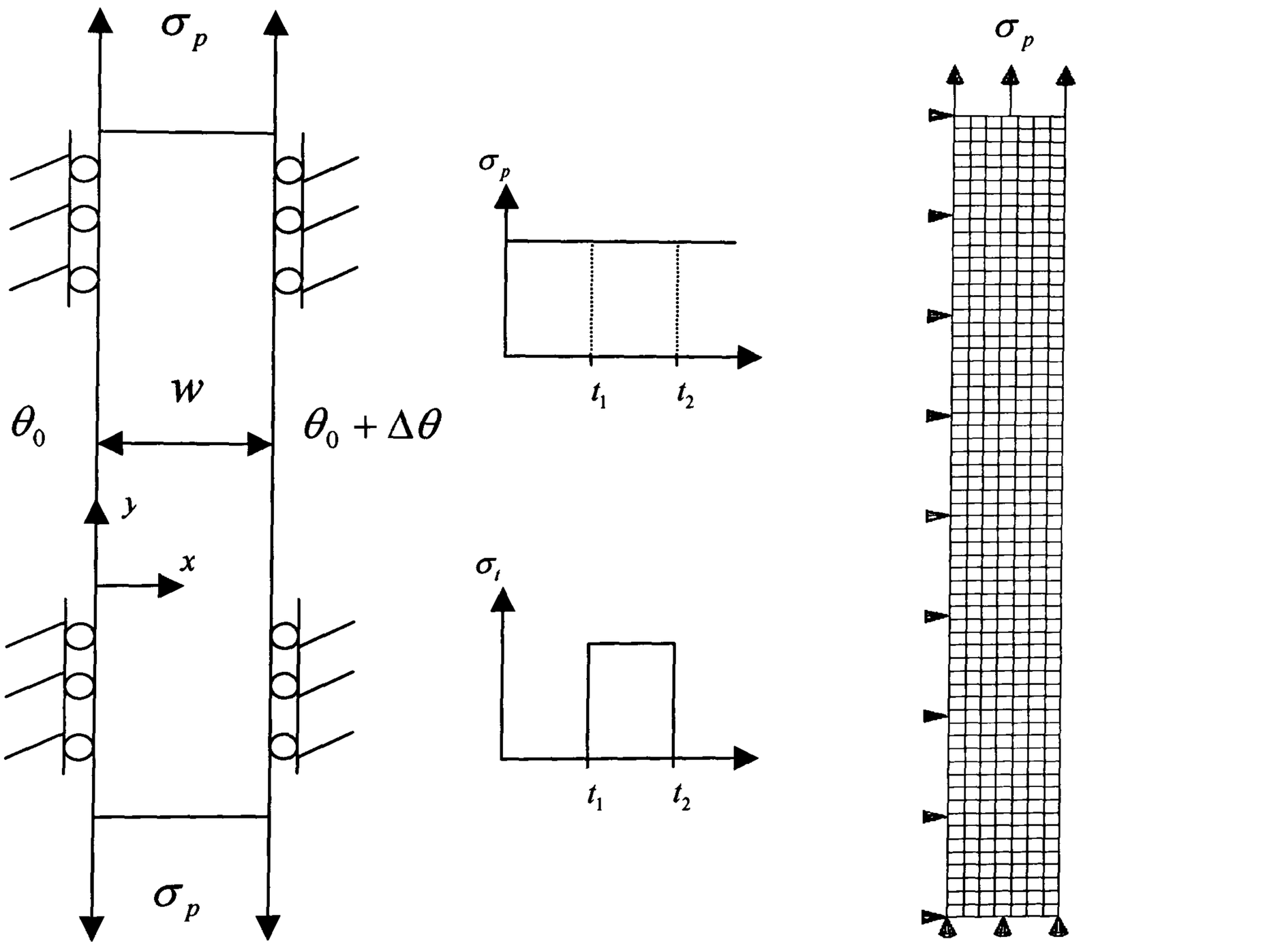

Bree problem (Plane Stress)

Finite element model

Figure 3.7: Schematic representation of the plane stress Bree problem.

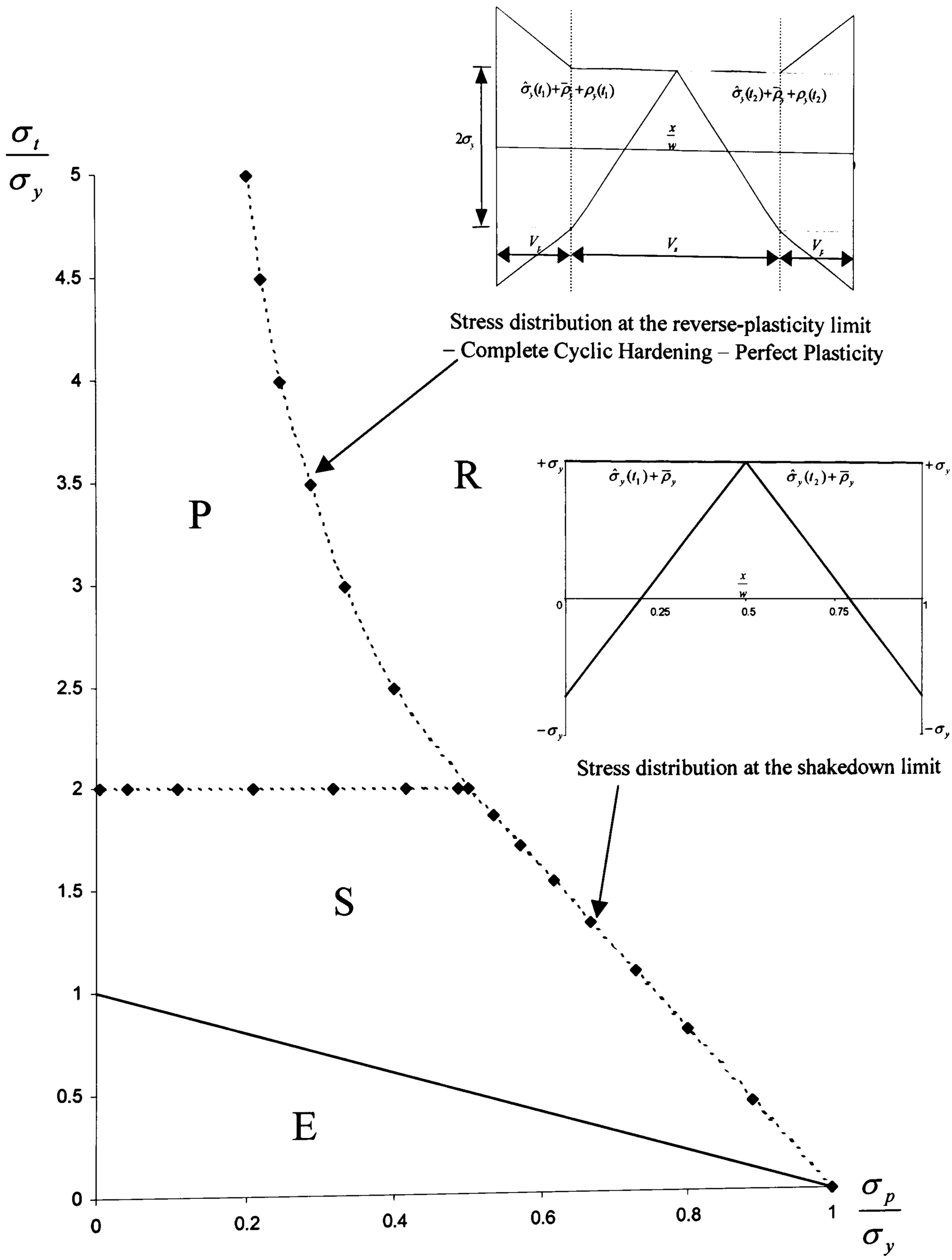

Figure 3.8: Interaction diagram for the plane stress Bree problem.
(♦ Numerical, ----- Theoretical)

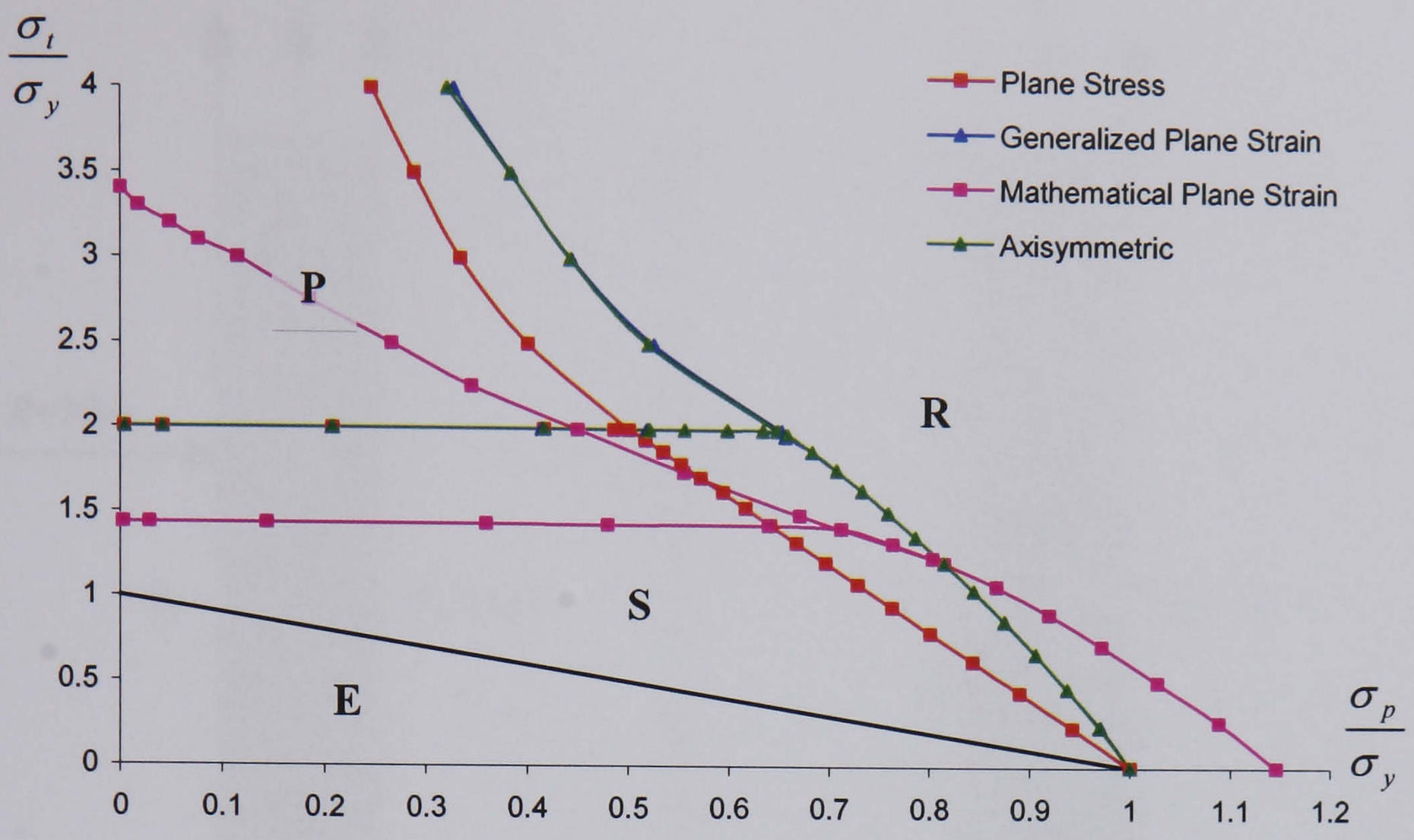

Axial stress remains constant at the two time instances.

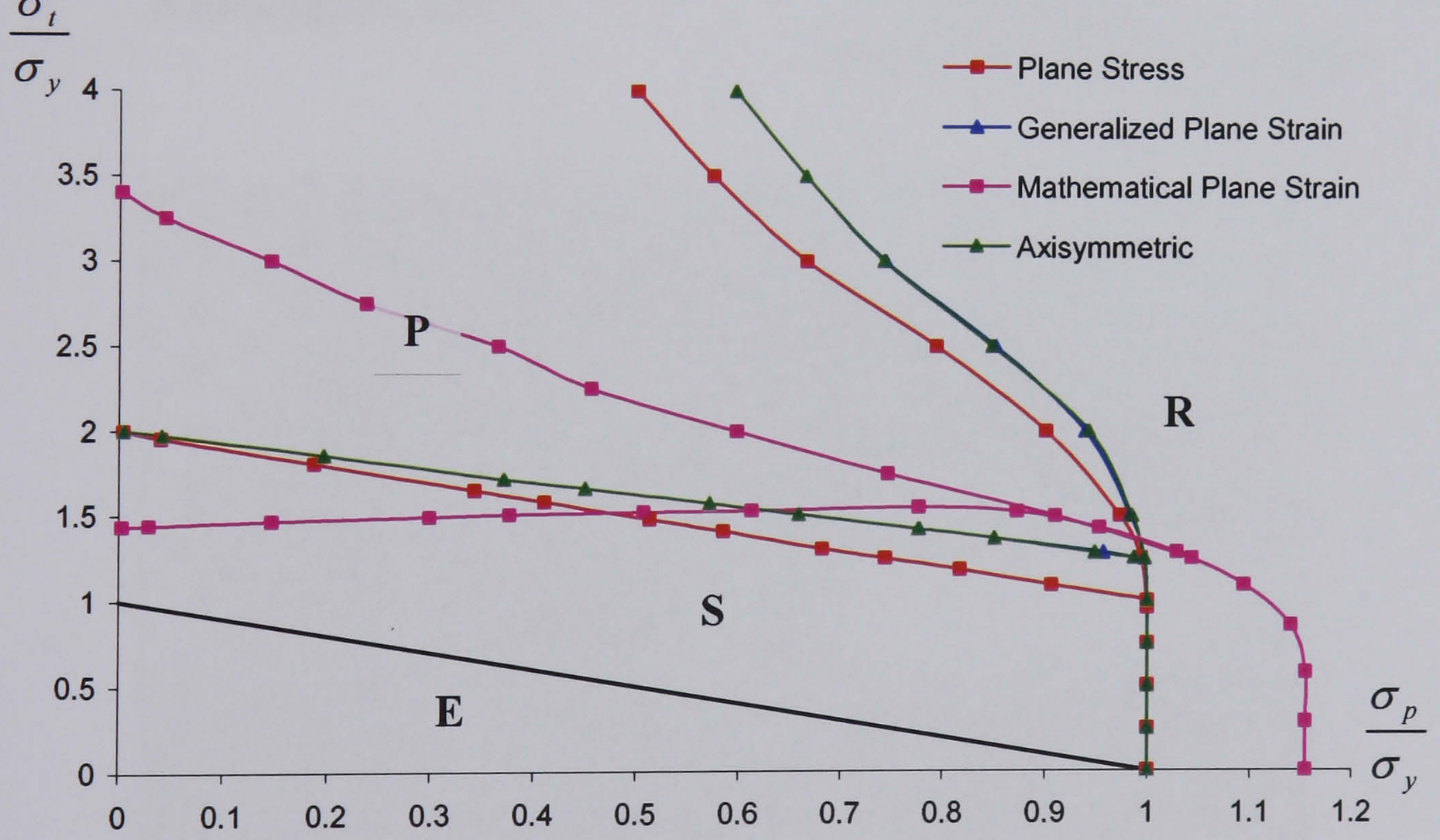

Axial stress varies in-phase at the two time instances.

Figure 3.9: Interaction diagrams for the different two-dimensional analyses.

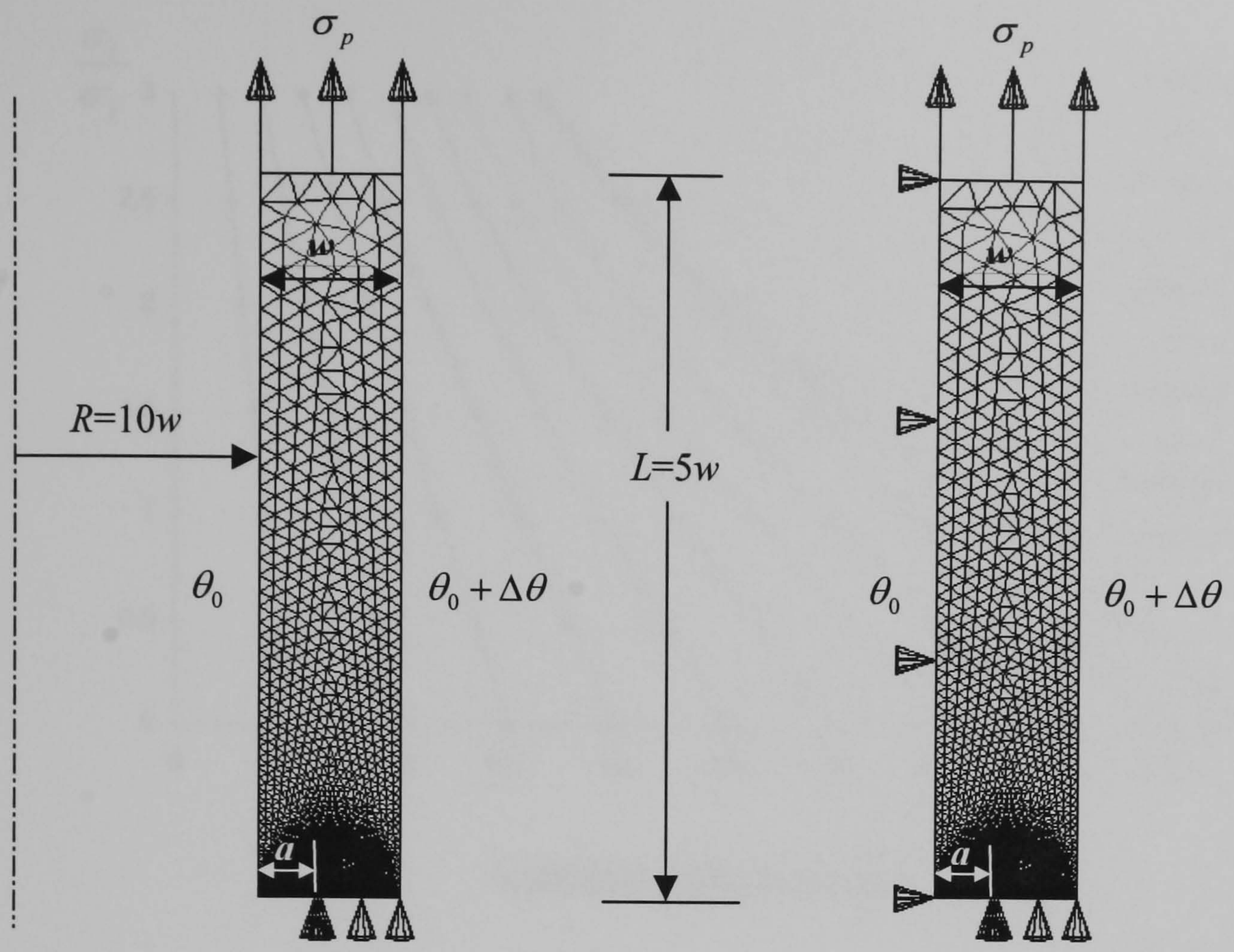

Axisymmetric model

Plane stress/
Generalized plane strain model

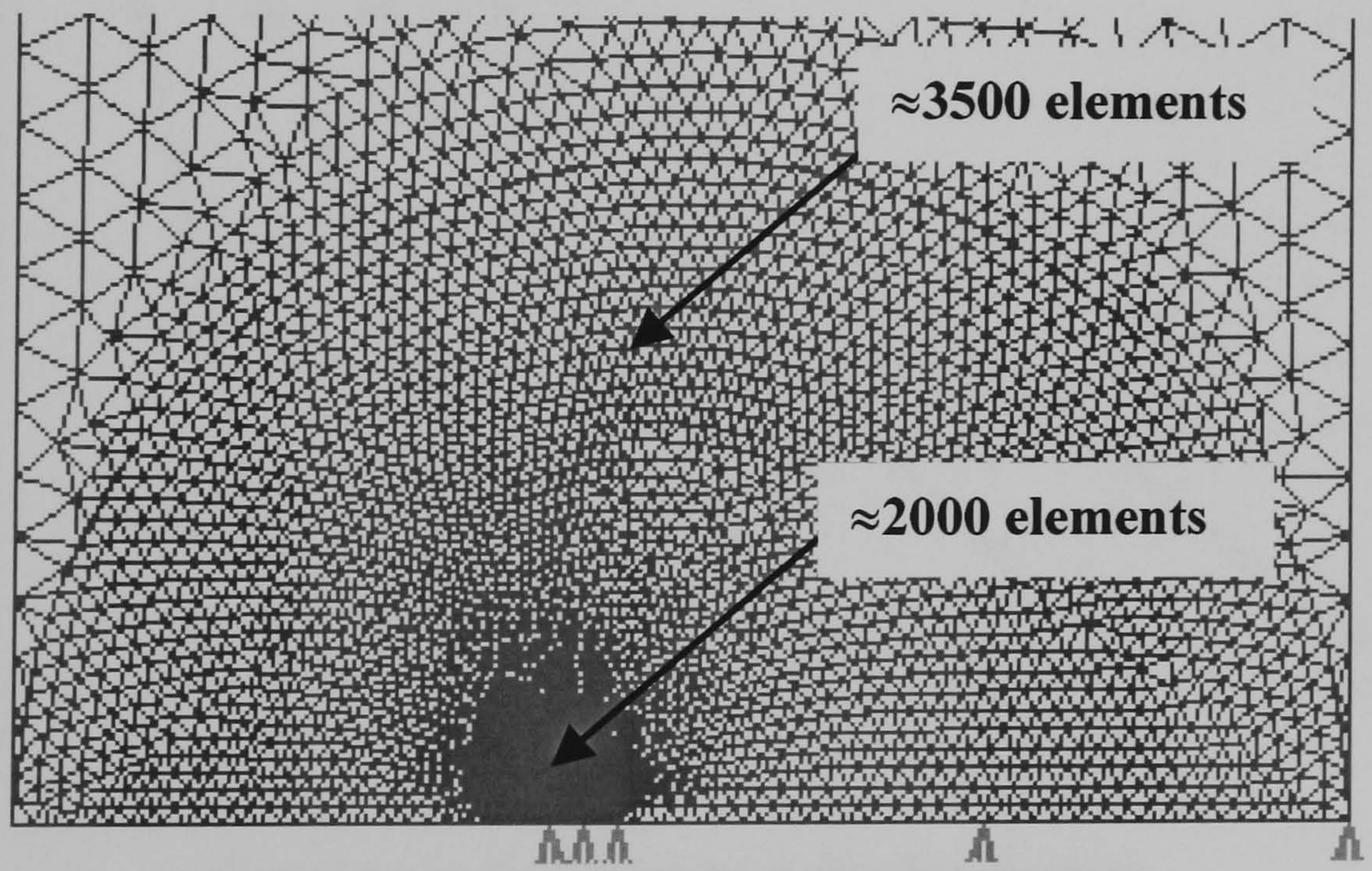

Mesh at the crack tip

Figure 3.10: Finite element analysis models for the cracked Bree problem.

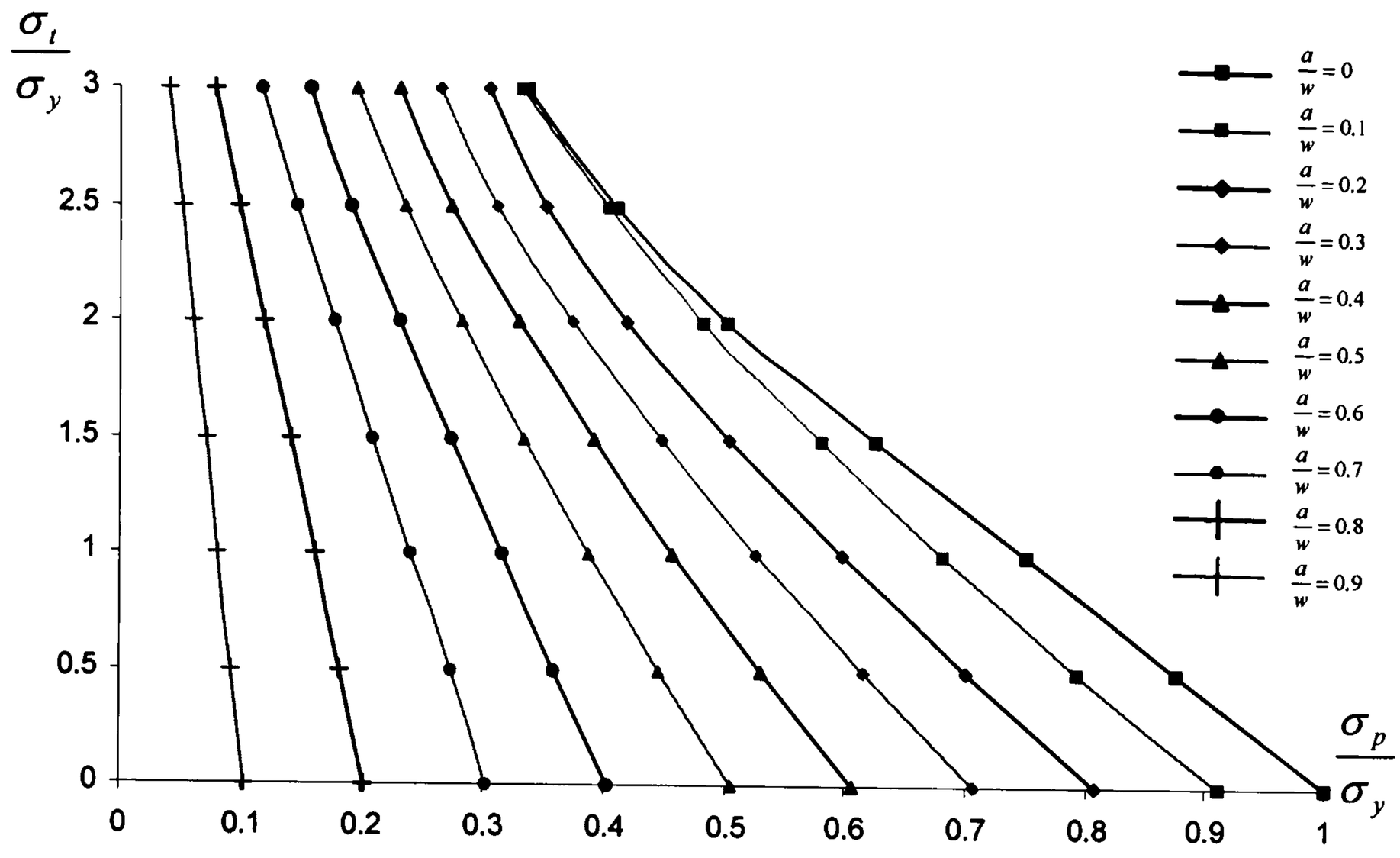

Complete cyclic hardening

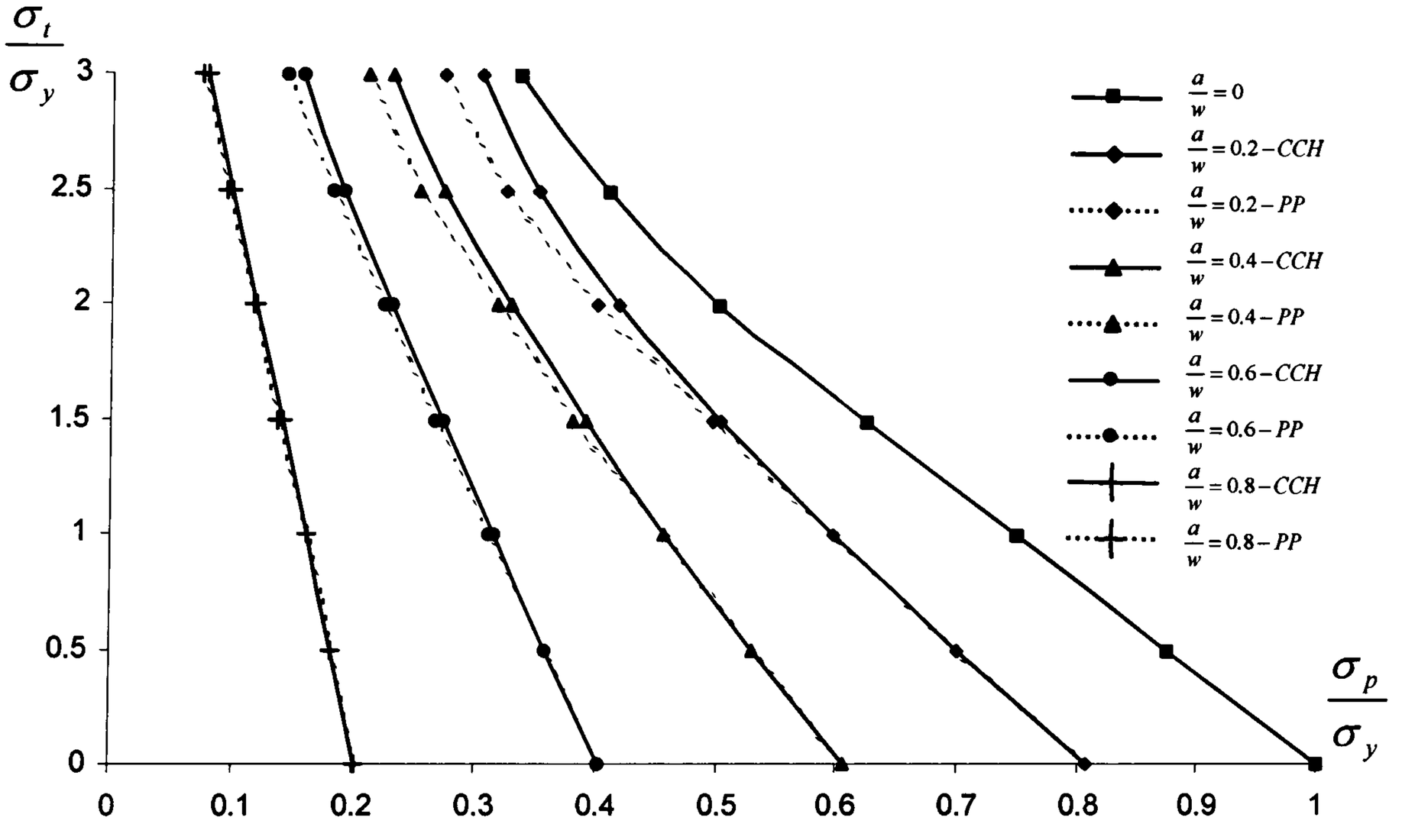

Complete cyclic hardening & Perfect plasticity

Figure 3.11: Ratchet limits for the cracked plane stress Bree problem.

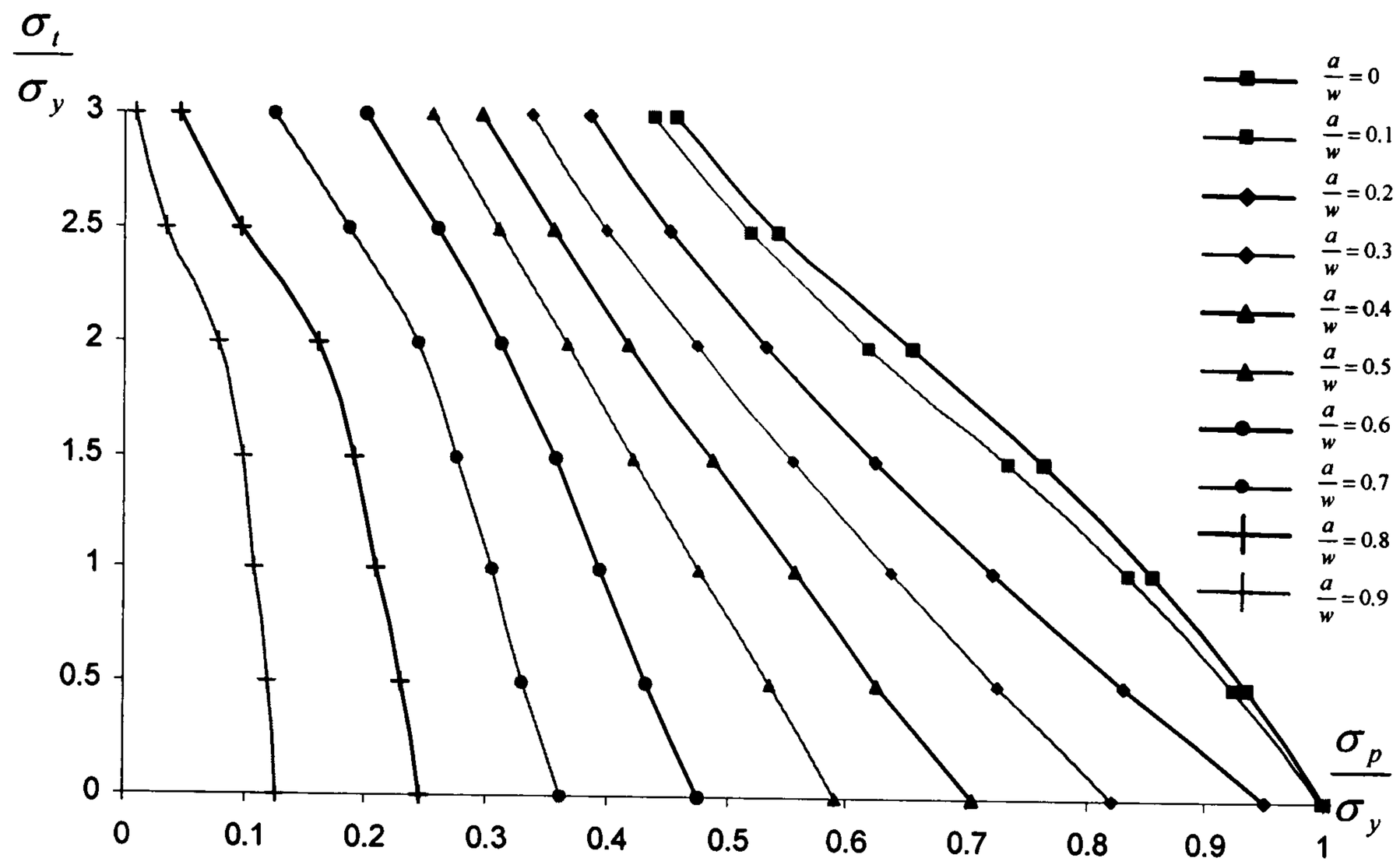

Complete cyclic hardening

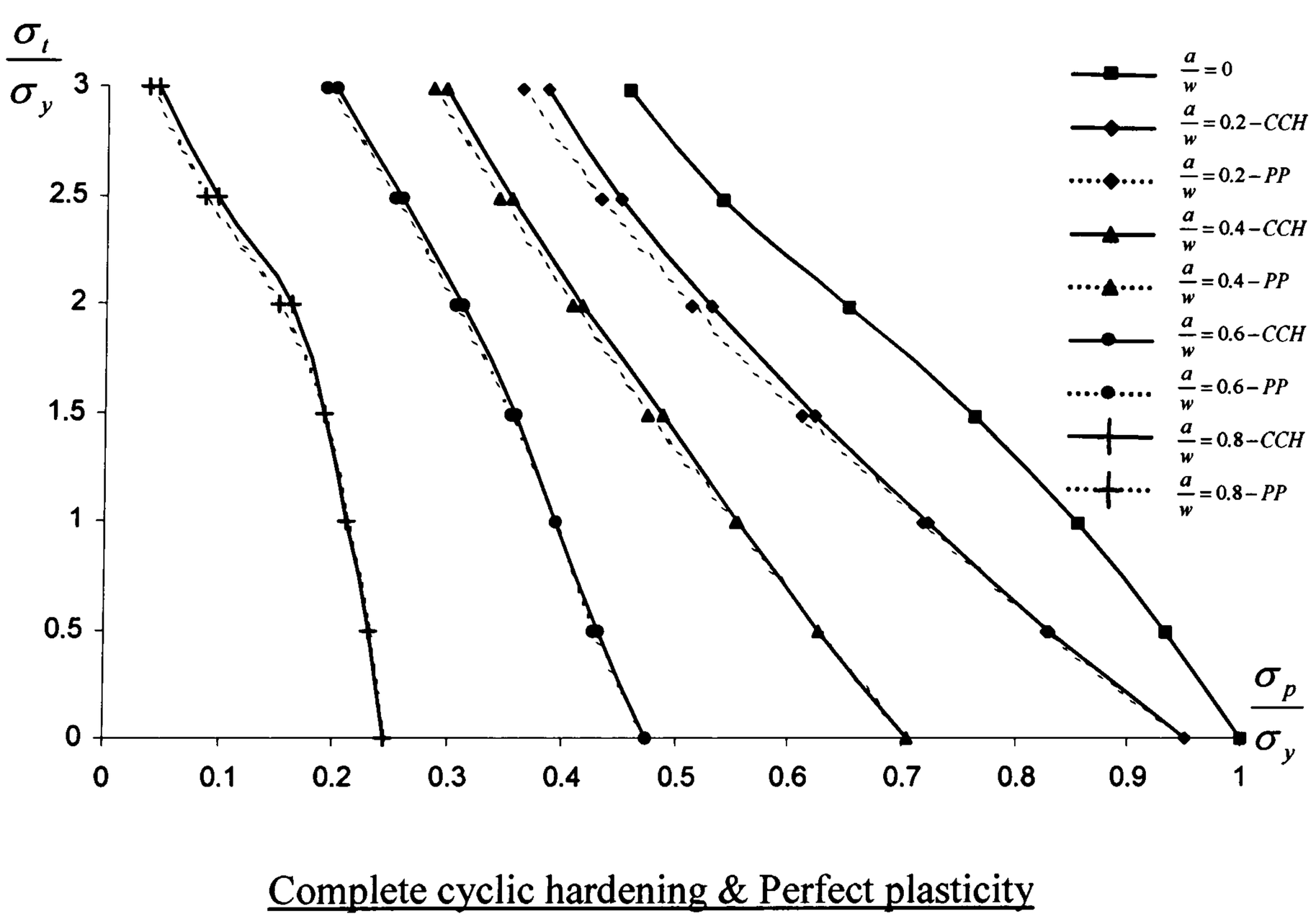

Complete cyclic hardening & Perfect plasticity

Figure 3.12: Ratchet limits for the cracked generalized plane strain Bree problem

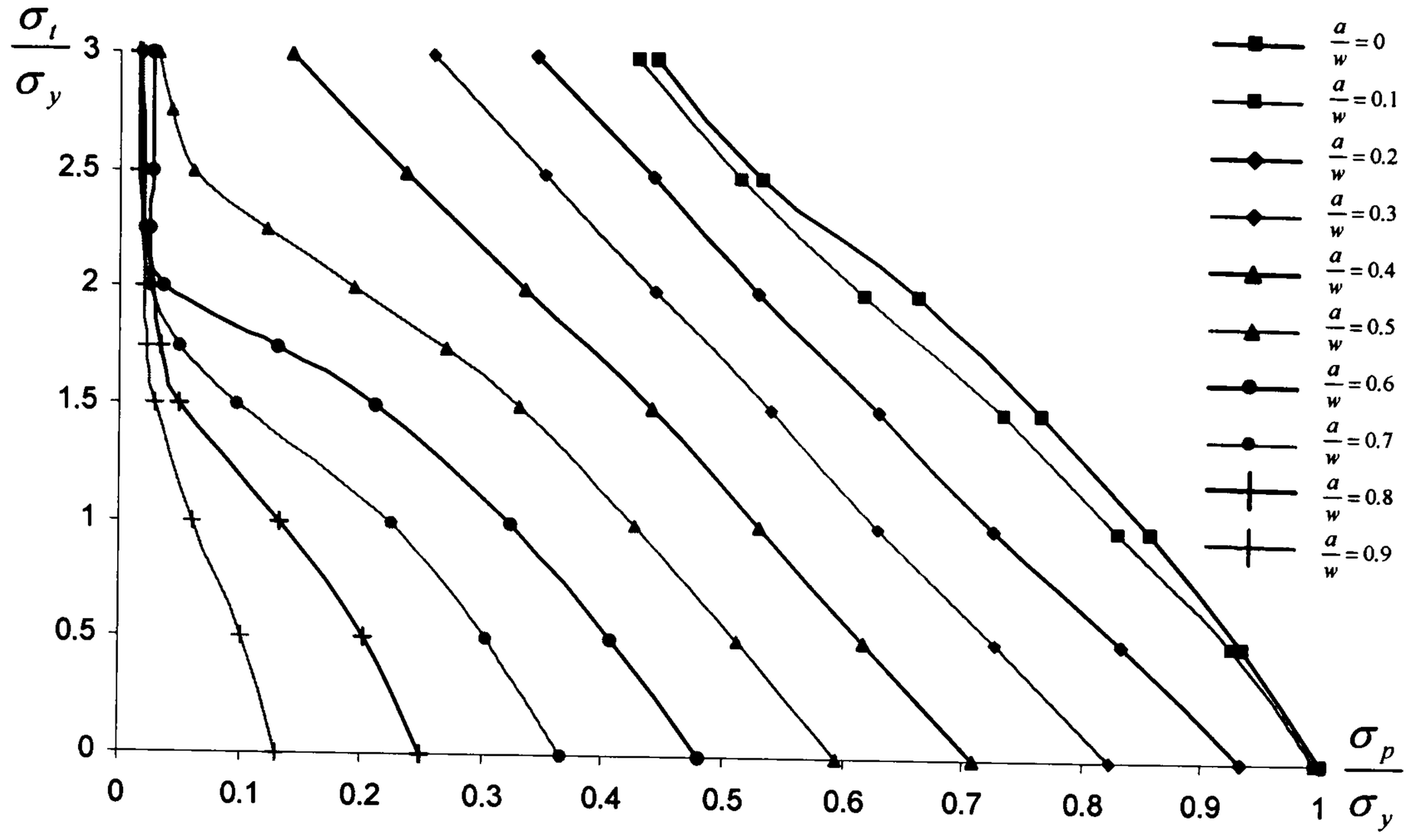

Complete cyclic hardening

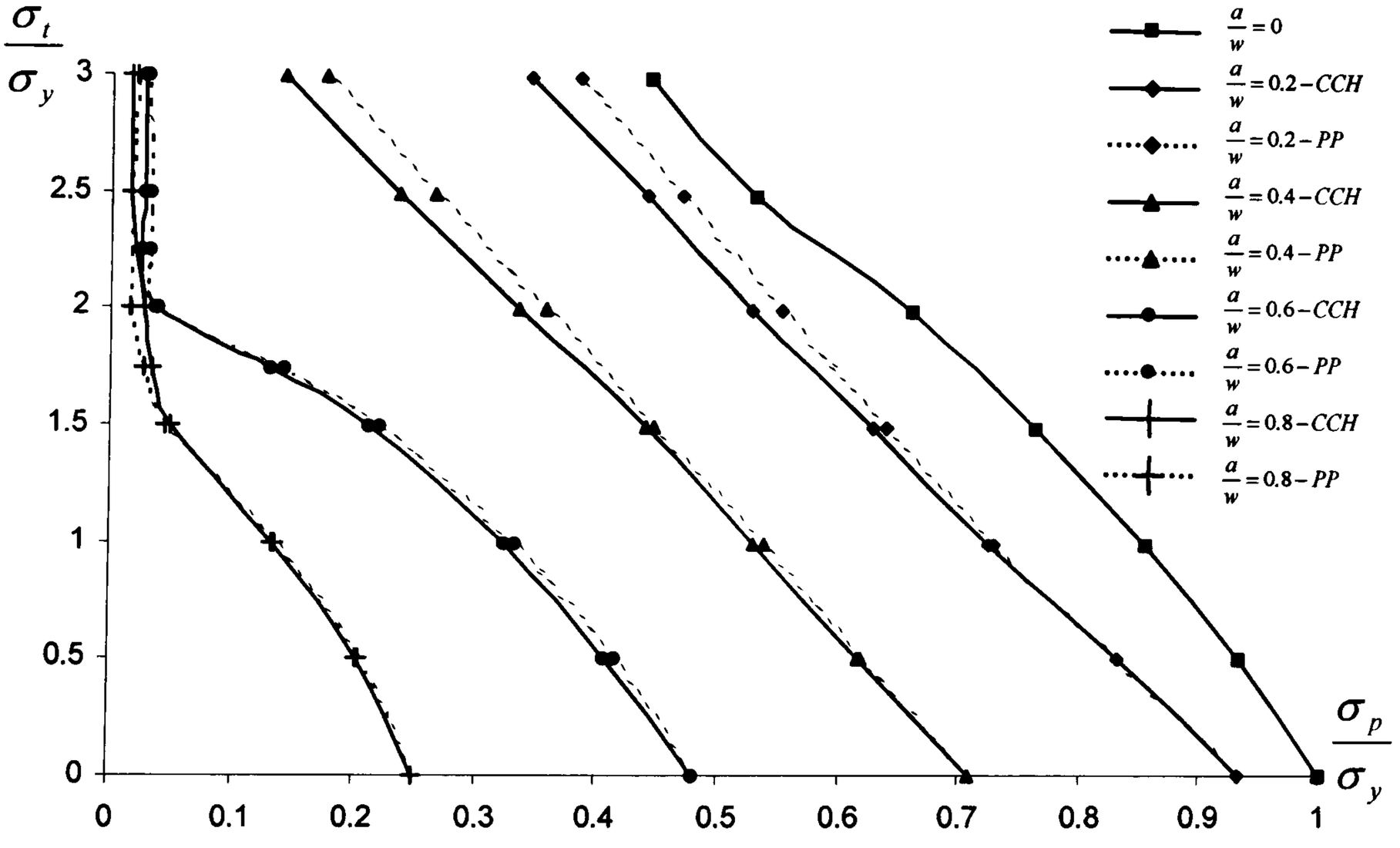

Complete cyclic hardening & Perfect plasticity

Figure 3.13: Ratchet limits for the cracked axisymmetric Bree problem.

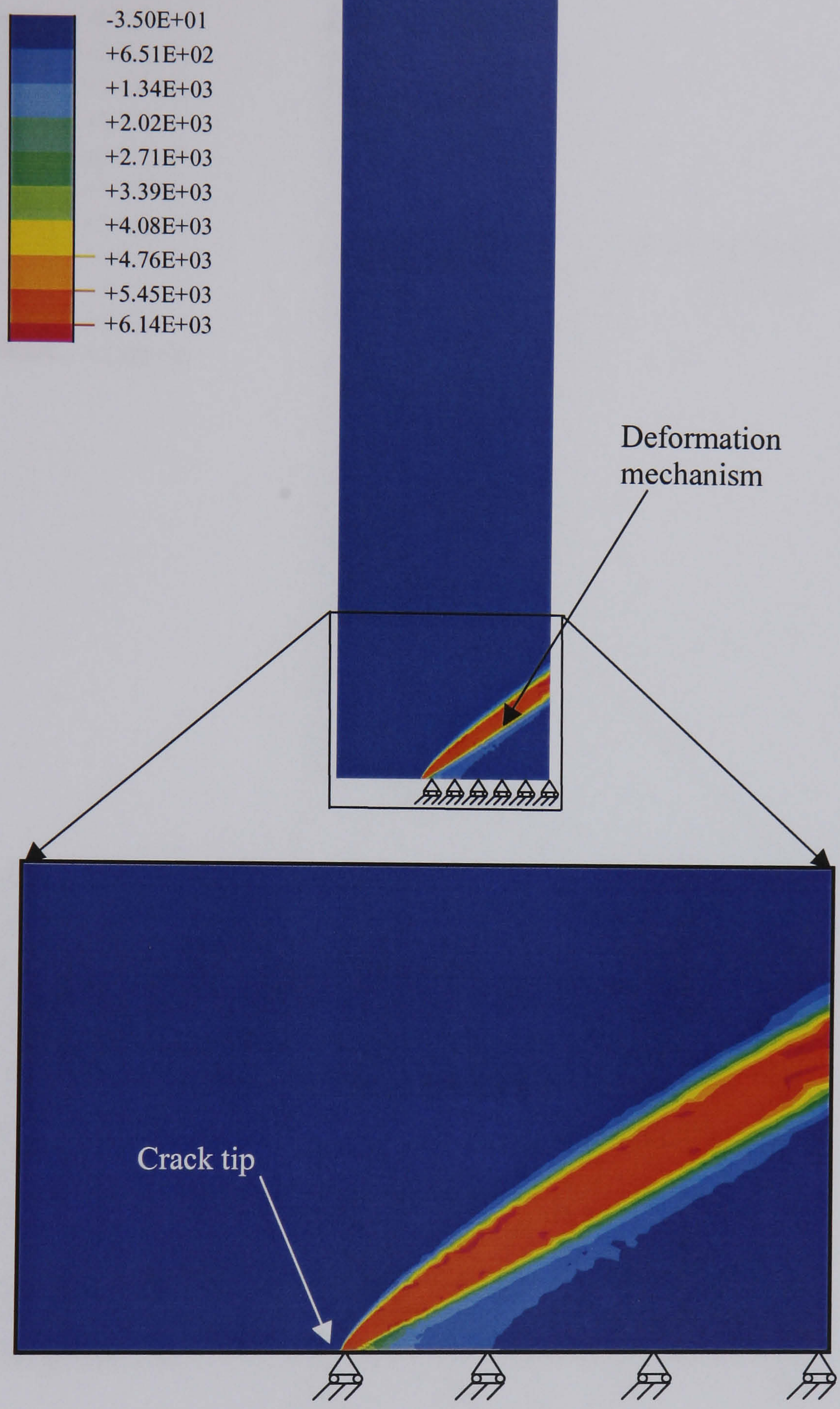

Effective strain at the crack tip

Figure 3.14: The von-Mises effective strain contours for the cracked axisymmetric tube at $\frac{a}{w} = 0.4$ and $\sigma_t = \sigma_y$.

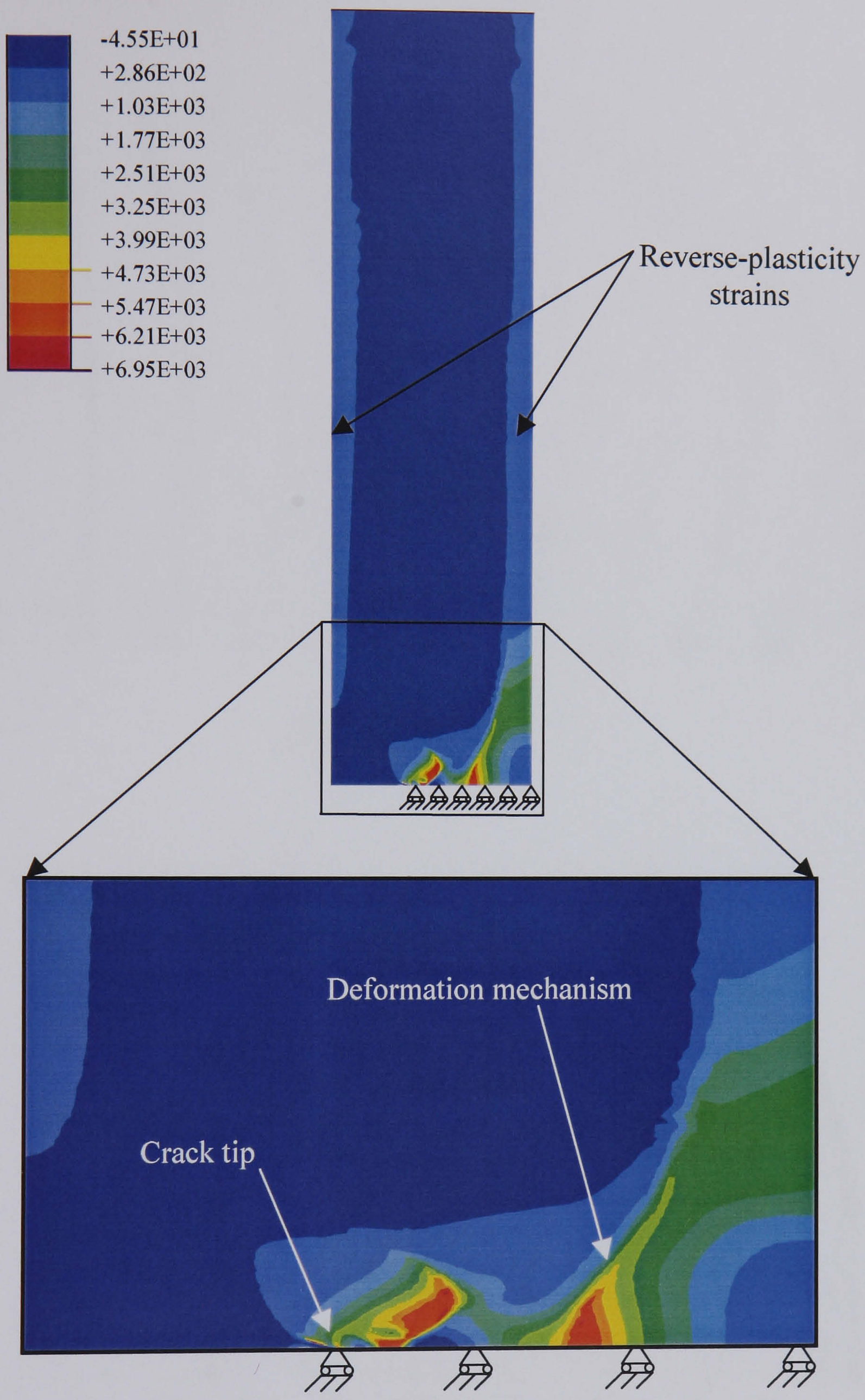

Effective strain at the crack tip

Figure 3.15: The von-Mises effective strain contours for the cracked axisymmetric tube at $\frac{a}{w} = 0.4$ and $\sigma_t = 3\sigma_y$.

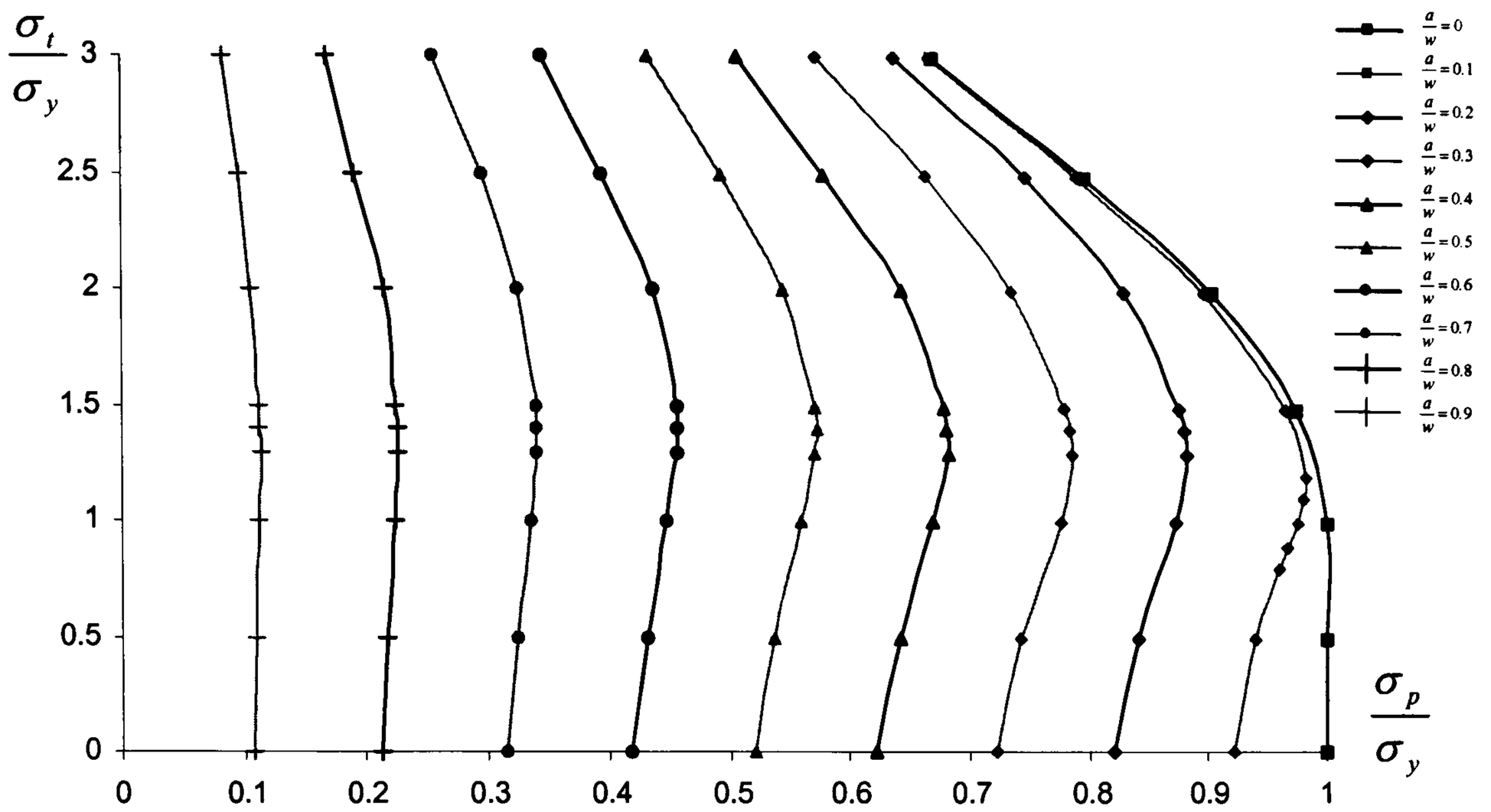

Plane Stress (CCH)

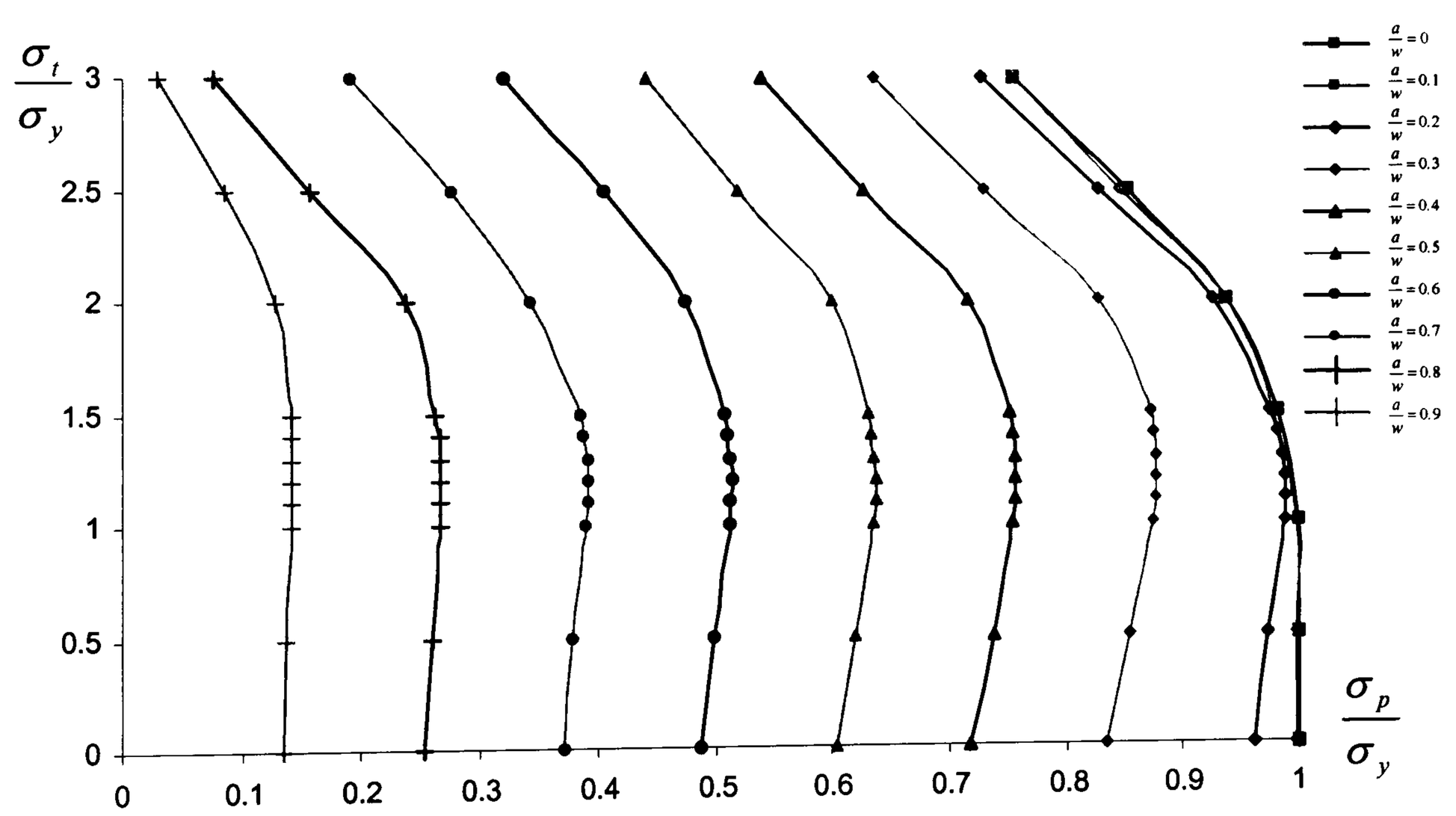

Generalized Plane Strain (CCH)

Figure 3.16: Ratchet limits under varying axial stress.

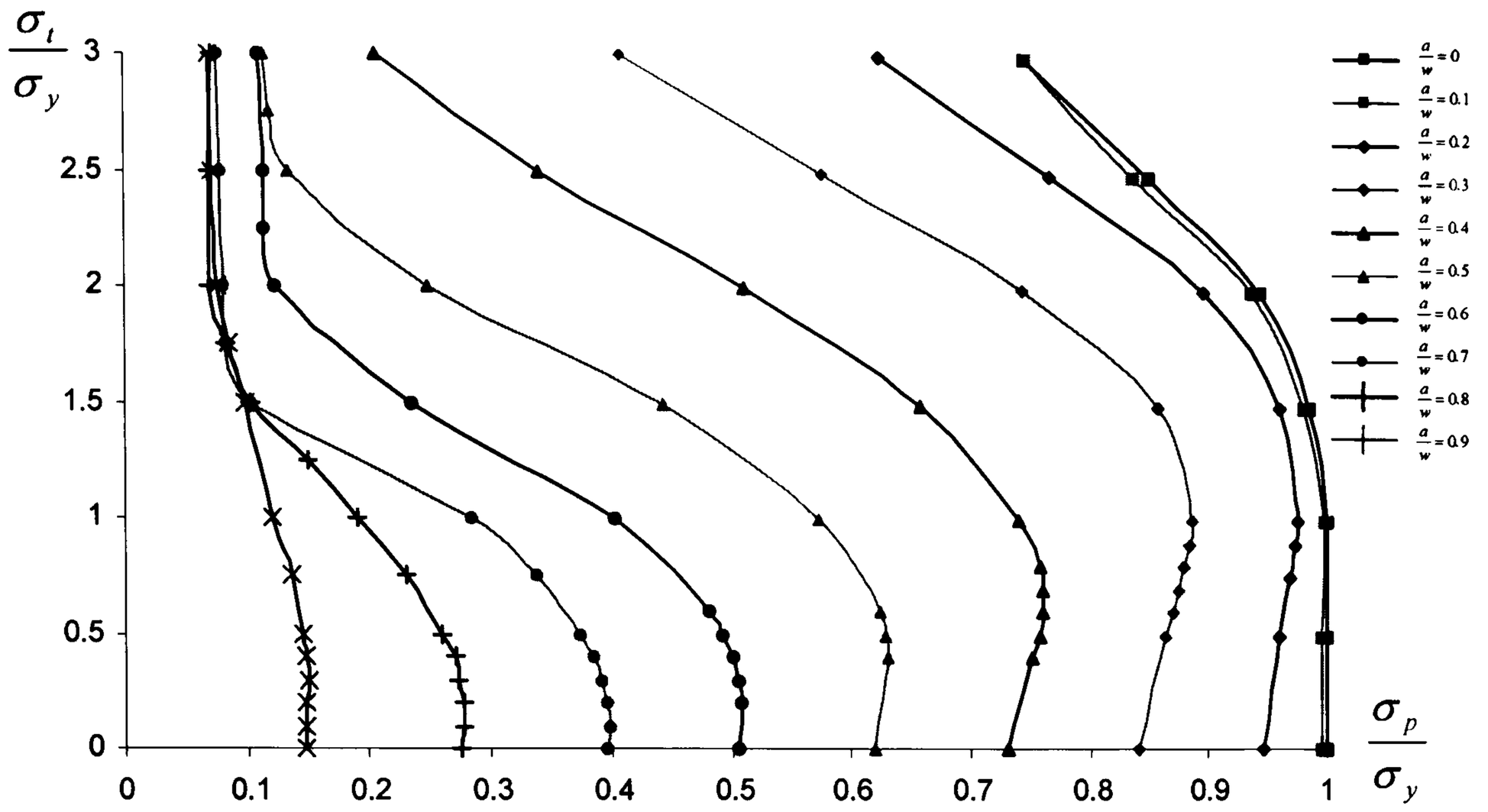

Axisymmetric (CCH)

Figure 3.17: Ratchet limits under varying axial stress.

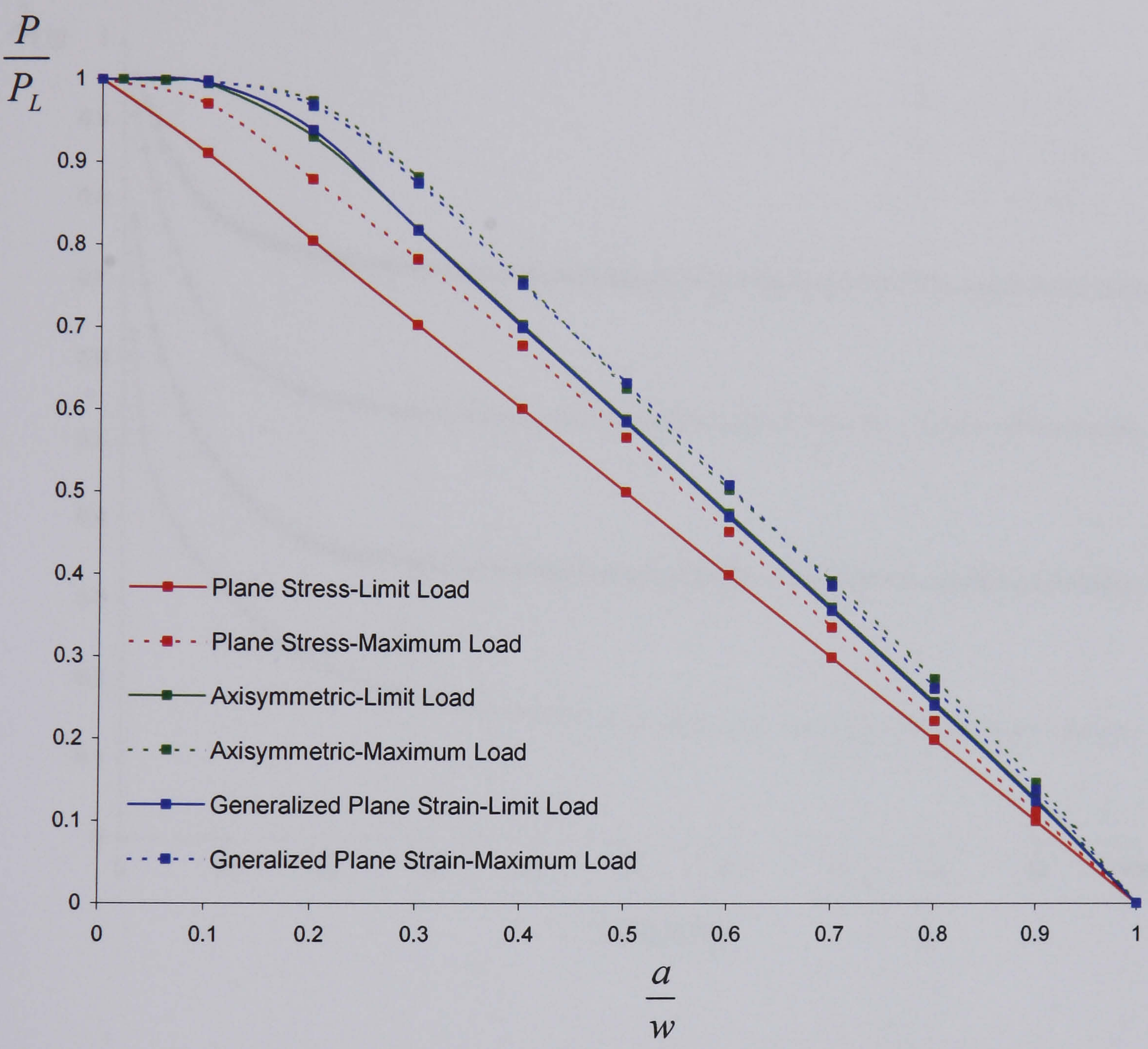

Figure 3.18: Comparisons between the limit and maximum loads for plane stress, generalized plane strain and axisymmetric analyses.
(Limit Load – identified at $\sigma_t = 0$,
Maximum Load – identified at some finite σ_t, *i.e.* $\sigma_t \neq 0$)

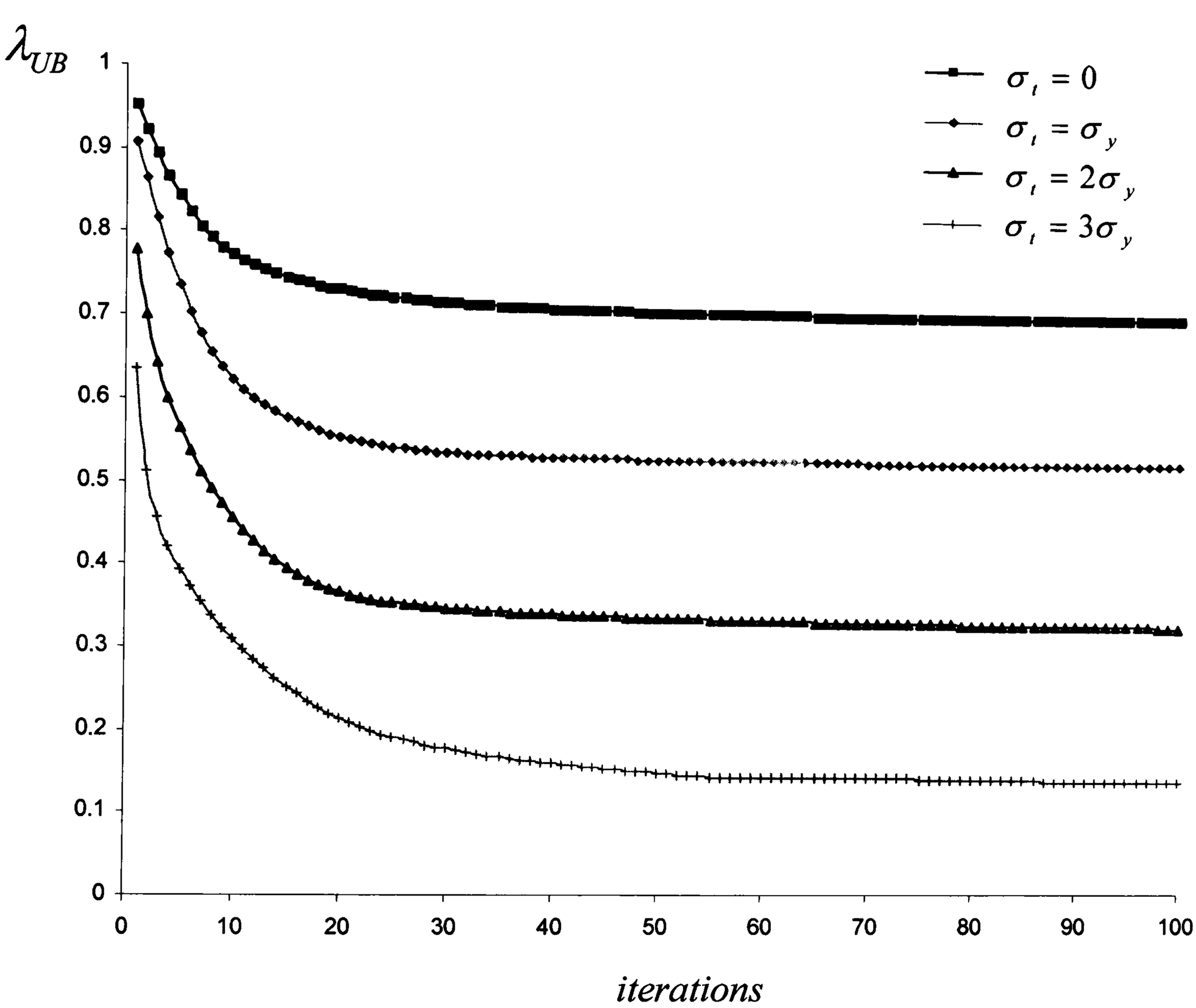

Figure 3.19: Plots of λ_{UB} for the ratchet limits against number of iterations for the cracked axisymmetric analysis at $\frac{a}{w} = 0.4$.

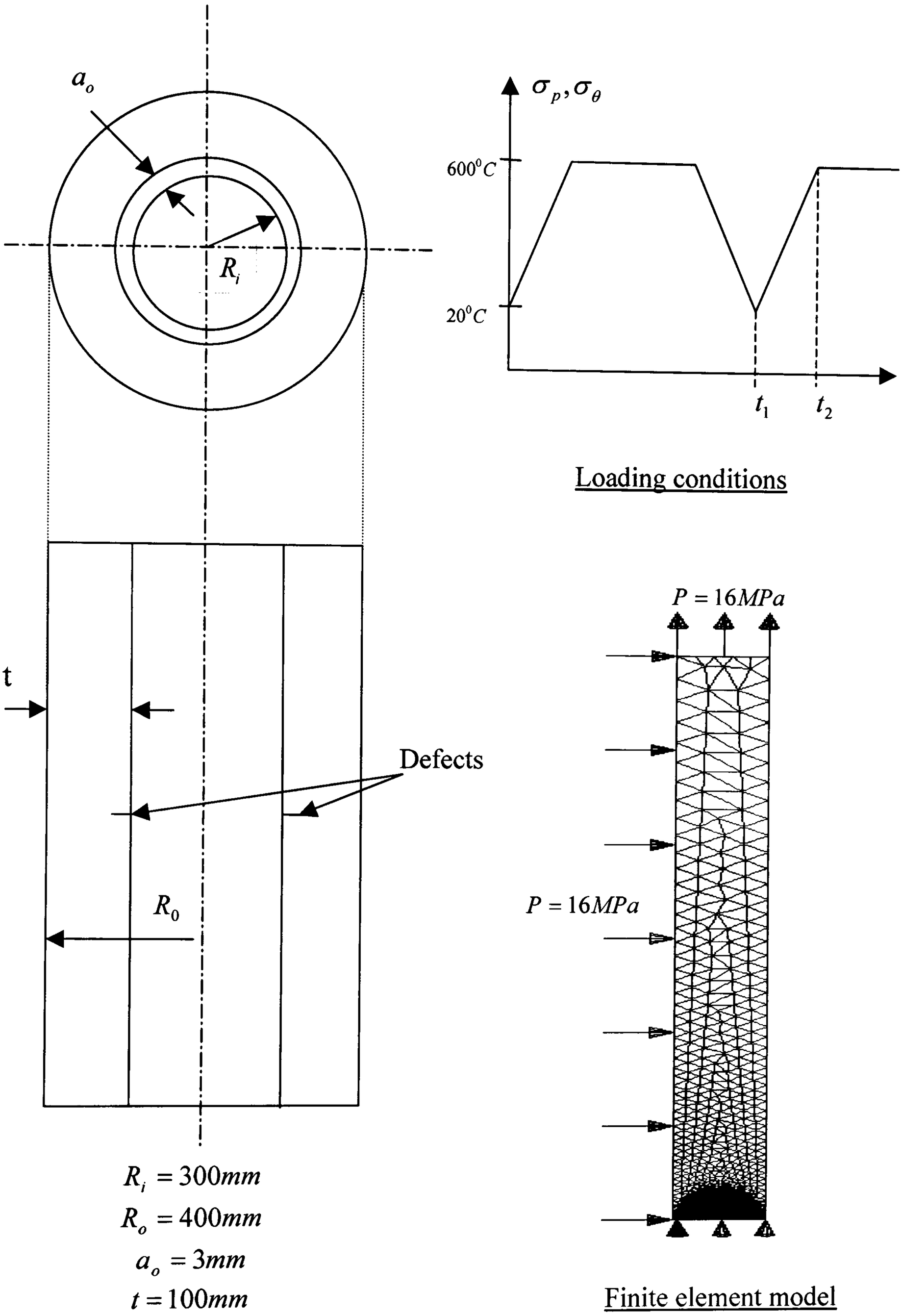

Figure 3.20: Idealized structural geometry of the R5 problem.

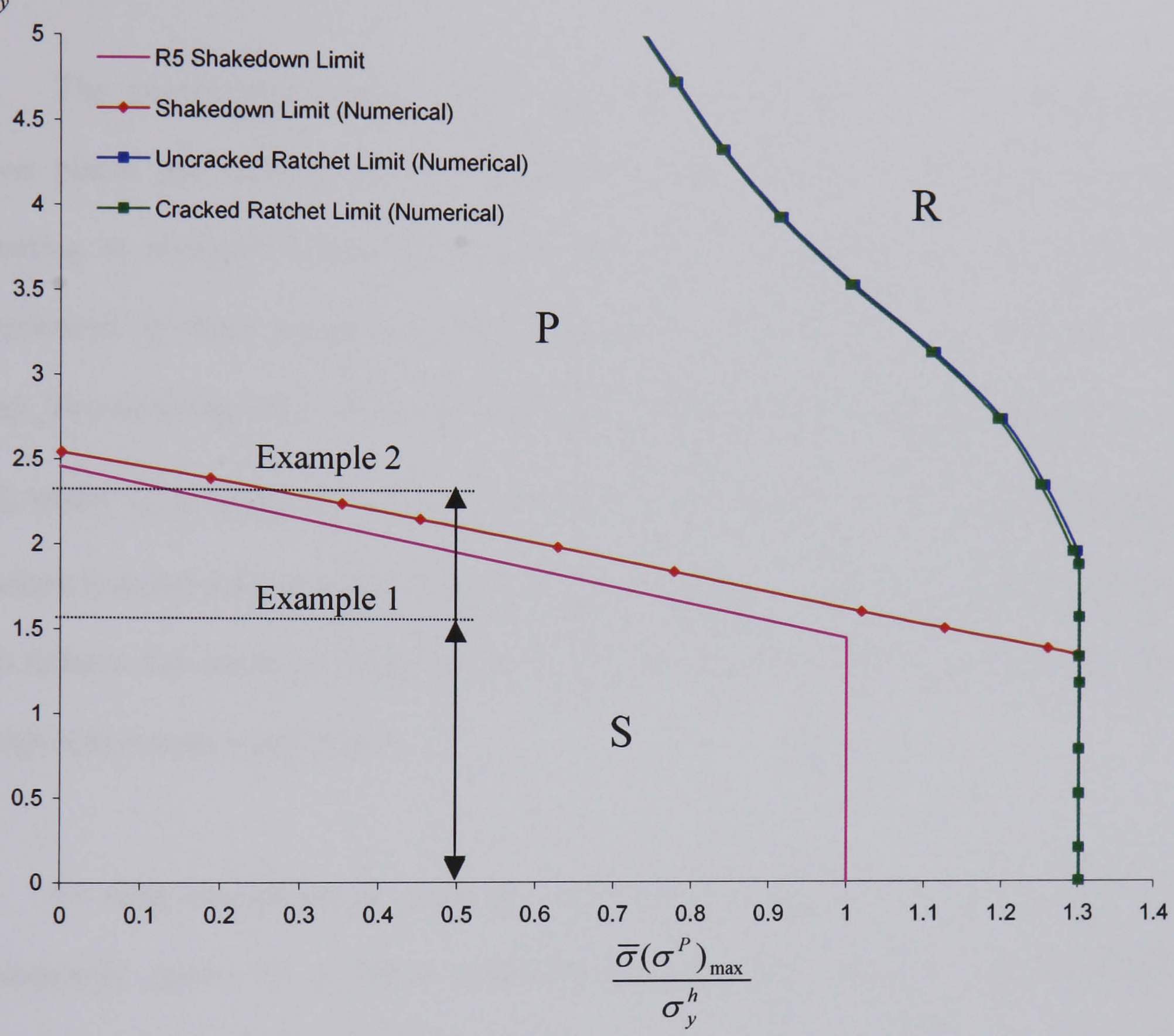

Figure 3.21: Comparisons between the numerical solutions generated and those currently used in the procedures for the R5 problem.

Chapter 4: Cyclic Creep Analysis Methods

4.1. Introduction

The ever-increasing demand in improving the efficiency and utilization of current power plants, gas turbines, chemical reactors, *etc*, has resulted in engineering components operating at elevated temperatures. In the presence of complex loading histories often experienced by these components, one of the dominant instigators of structural failures is creep. This time-dependent deformation process generally occurs at temperatures above $0.5T_m$ [19], where T_m is the absolute melting temperature of the material. On the assumption that the structure is defect free, the availability of present design guidelines [1,12,13] in accounting for such failures, has made it possible for this economically driven trend to progressively continue in high temperature applications.

In such circumstances, however, conditions are ideal for cracks to initiate and subsequently grow. As a result, engineering components undergo frequent mandatory inspections to assess their suitability for further use. If cracks are detected, some procedures are required to determine whether these cracks are acceptable or whether they constitute a risk to safety and must be repaired. Recent advances in the sensitivity of crack monitoring equipments have helped, allowing the detection of smaller and smaller cracks. In cases where inspection is not possible, hypothetical defects are often assumed to be present. Consequently, the defect assessment calculations performed thereafter, needs to be realistic because serious economic penalties could be incurred if the plant is taken out of service unnecessarily or

disastrous failures take place. This called for the development of an effective, efficient and reliable procedure, capable of assessing and, upon which, predict the remaining life of cracked components in current operational high temperature plants.

In the evolution of such methods, an understanding of creep in cracked structures is indispensable. An in-depth investigation into the near crack tip fields, under cyclic histories of loads and temperatures, and their influence on the cycle times and material behaviour are required. The conventional methodology is to develop constitutive laws for the material behaviour and to conduct detailed finite element studies of the response of the cracked structures. The problem with such an approach is that the constitutive models generated are either too elaborate or contain large number of variables, too complicated to implement. The validity of these models is, also, generally viewed with suspicion, as they are constructed from results obtained from experimental techniques, examined on a particular batch of material. Moreover, the employment of these laws computationally tends to be complex and expensive even for simple structural components, leading to difficulties in determining the relationship between the material behaviour and the structural performance.

In overcoming the above difficulties, an alternative approach was proposed by Le Mat-Hamata *et al* [29,30]. It involves investigating the behaviour of cracked structures, using the extremes of the applied cyclic loading histories, in conjunction with simple constitutive material models. For cracked structures subjected to cyclic variable loads, the investigations looked into the changes in the behaviour of the crack tip fields, with respect to changes in the cycle times, *i.e.* rapid and slow cycling [65], for constitutive models, such as Norton's power law and others [66,67,68]. Using such an approach, the results generated, revealed the near

identical overall creep deformation rates, found to be independent of the cycle times associated with the corresponding constitutive models. It was also established that this provided a more convenient way of relating the available experimental data to the behaviour of the near crack tip fields and the different features of the material response.

The above encouraging results formed the basis of the investigations carried out here, whereby an examination into the behaviour of the crack tip fields, subjected to the extremes of the applied cyclic histories of loads and temperatures, is conducted. The employed numerical procedure is the linear matching method, previously applied to limit load [2,4] and shakedown [3,5] problems, now used to generate the so-called rapid cycle creep solutions [69]. In short, these solutions assume that the cycle time is small compared to other characteristic times in the material. This provides an over-estimation on the creep deformation rates, ultimately yielding a conservative limit [65] on the results. It is believed that the exploitation of such numerical methods, based upon the prescribed approach, is capable of answering the safety and reliability concerns, existing in current structures operating at elevated temperatures. In addition, the capability of these procedures would also enable the appropriateness of current R5 [1] procedures, which treats the effect of thermal stress as an equivalent bending moment, to be validated.

In this chapter, the essential concept behind the rapid cycle creep solution [69,70] is discussed. This is then followed by the numerical implementation of the LMM-based methodology [49], for Norton's law and the Bailey Orowan [71] constitutive model. These two models were chosen, as they tend to bracket the behaviour expected of a real material [69]. Using the cracked axisymmetric Bree problem as an example, the characteristic of the

near crack tip fields, subjected to the extremes of the applied cyclic mechanical loads, was initially investigated. Similar investigation into the behaviour of the crack tip fields, under both cyclic mechanical and thermal loads was then conducted. These numerical procedures were then repeated, with variations in the structural geometries, loading histories and material properties, with the ultimate aim of indicating the versatility and appropriateness of such solutions. These results then act as input parameters in Chapter 5, whereby the behaviour of current R5 [1] procedures, which employ the reference stress formulation [1,19] as well as treats the effect of thermal stress as a bending moment, are examined.

4.2. Rapid Cycle Solution

In the analysis of a metallic body subjected to cyclic histories of loads and temperatures, the stress and strain histories generally evolves over a number of cycles before reaching a steady cyclic state. The associated deformation may then be conceived as consisting of two components, the displacements and strains accumulated during the transient and the steady state rate of incremental strain growth per cycle in the steady state. In practice, however, the assessment of performance in engineering structures tends to concentrate on the latter. There is, thus, an essential requirement for cyclic creep solutions capable of evaluating the accumulated creep strains during each cycle. This would then be related to a maximum strain rate, enabling the equivalent maximum load to be sought out that would result in strain rates no larger than the specified value.

Ponter & Cocks [65] came to the conclusion that two distinct extremes of cyclic creep solutions exist. The first is the rapid cycle creep solution, which occurs when the cycle times

are very short, compared with the characteristic time scales inherent in a particular constitutive material's model. There is no time for the stresses to redistribute, but the body will still exhibit a cyclic increase in creep strain. When the cyclic state is reached, the stress in the cycle has, however, been shifted so that the stress history is now the sum of the linear elastic stress solution and a constant residual stress field,

$$\sigma_{ij}(x,t) = \hat{\sigma}_{ij}(x,t) + \overline{\rho}_{ij}(x) \tag{4.1}$$

where $\hat{\sigma}_{ij}(x,t)$ are the linear elastic stress solutions due to the loads and temperatures and $\overline{\rho}_{ij}(x)$ is a constant residual stress field. The utilization of such solutions not only offers the benefit of simplicity but is also shown to provide an upper bound on the strain growth for finite cycle times in many circumstances [69]. On closer examination, the similarities between equation (4.1) and those described in shakedown theorems in equation (3.3) are apparent. It is known that the existence of a shakedown state is a characteristic of a material behaviour, described by time-independent constitutive equation. Thus, the rapid cycle creep solution can be thought of, as a special case of "time-dependent shakedown", at high temperatures where the effect of creep is significant.

At the other extreme, if the cycle times are much longer than the material characteristic time scales, a redistribution of the stresses to the steady state values occurs. Such solutions are often referred to as the slow cycle creep solutions and provide an underestimation of the creep strain rates occurring in a real structure. Although not considered here, Ponter and co workers [72,73] recently outlined a generalised approach in predicting such solutions at any cycle times. Unlike the rapid cycle solution, the creep behaviour is now the sum of the total

increment of strain and displacement per cycle and the amount of creep strain produced during the relaxation processes at the maximum temperature. The general form of the cyclic solution is, thus, given by,

$$\sigma_{ij}(x,t) = \hat{\sigma}_{ij}(x,t) + \overline{\rho}_{ij}(x) + \rho^{r}_{ij}(x,t) \tag{4.2}$$

where, as before, $\overline{\rho}_{ij}(x)$ is a constant residual stress field, here interpreted as the value of the residual stress field at the beginning of the cycle, and $\rho^{r}_{ij}(x,t)$ is the additional varying component. In the evaluation of these two components, a simple interrelation existing between them was used. It was found that if the changing component $\rho^{r}_{ij}(x,t)$ was known, then the evaluation of the corresponding constant component $\overline{\rho}_{ij}(x)$ was then interpreted as the solution of a rapid cycle solution where the elastic stresses were augmented by $\rho^{r}_{ij}(x,t)$. On the other hand, if $\overline{\rho}_{ij}(x)$, was known, then $\rho^{r}_{ij}(x,t)$ was found using step-by-step analysis through the cycle. Numerically, this convergent method [74] was successfully implemented within ABAQUS, through the combination of these two observations, where at each stage, a load parameter is adjusted so that a displacement rate condition is always satisfied.

These two cyclic creep solutions gives rise to the notion of bounding theorems [69]. For the rapid cycle creep solution, the advantage of the upper bound theorem is evident, as the analysis only involves the computation of a constant residual stress field, $\overline{\rho}_{ij}(x)$, rather than the step-by-step analysis of the cyclic loading histories due to both mechanical and thermal loads. The accurate estimation of the upper bound creep strain rates, thus, requires the

application of the appropriate form of constitutive equations. In this thesis, Norton's law and Bailey-Orowan recovery model, based upon the same constant stress data,

$$\dot{\varepsilon}_{ij} = \dot{\varepsilon}_0 \left(\frac{\overline{\sigma}(\sigma_{ij})}{\sigma_0} \right)^n \frac{3}{2} \frac{\sigma'_{ij}}{\sigma_0} \tag{4.3}$$

are considered, where $\overline{\sigma}(\sigma_{ij})$ is the von-Mises equivalent stress and σ'_{ij} is the deviatoric stress tensor. These two models are chosen, as they tend to bracket the behaviour expected of a real material, based upon the experimental and analytical conclusions of Ponter [69].

4.2.1. Norton's law creep model

This is the most commonly used function in describing the steady state creep deformation or, otherwise known as, secondary creep. The power law, attributed to Norton, computes the steady state creep strain rates, $\dot{\varepsilon}_{ij}$, under constant temperature using the expression,

$$\dot{\varepsilon}_{ij} = \dot{\varepsilon}_0 \left(\frac{\overline{\sigma}(\sigma_{ij})}{\sigma_0} \right)^n \tag{4.4}$$

where σ_{ij} is the applied stress, $\dot{\varepsilon}_0$ is the strain rate under constant stress and temperature, σ_0 and n is the creep exponent. The reason for its popularity is its simplicity in stress analysis applications. Another great advantage this formulation has over others is the ability to maintain the 'shape', regardless of the stress magnitudes. This means that the stress

distribution is a function of the magnitudes of the applied loads. Thus, for a cyclic history of the form (4.1), the creep strain rate accumulated over a cycle, $\Delta\varepsilon_{ij}$, is given by,

$$\Delta\varepsilon_{ij} = \int_0^{\Delta t} \dot{\varepsilon}_{ij}(\sigma_{ij}(t))dt \qquad \text{for } 0 \le t \le \Delta t \tag{4.5}$$

4.2.2. Bailey Orowan recovery model

The Bailey-Orowan creep model [71] is based on the assumption of a flow potential, $\overline{\Omega}$, which depends upon the von-Mises effective stress, $\overline{\sigma}(\sigma_{ij})$, and flow stress, S, such that,

$$\overline{\Omega}(\sigma_{ij}, S) = F\left(\overline{\sigma}(\sigma_{ij}) - S\right) + G(S,\theta) \tag{4.6}$$

with $\frac{\partial G}{\partial S} = \frac{r}{h}$, where r and h are power law functions of S, governing the thermal softening and strain hardening of the material respectively. The corresponding rate equations for this constitutive relationship [70] are given by,

$$\dot{\varepsilon}_{ij}^{P} = \frac{\partial\overline{\Omega}(\sigma_{ij}, S)}{\partial\sigma_{ij}} \qquad \& \qquad \dot{S} = -h(S)\frac{\partial\overline{\Omega}(\sigma_{ij}, S)}{\partial S} \tag{4.7}$$

The substitution of equations (4.6) into (4.7) now yields,

$$\dot{\varepsilon}_{ij}^{P} = f(\overline{\sigma}(\sigma_{ij}) - S)\frac{\partial\overline{\sigma}(\sigma_{ij})}{\partial\sigma_{ij}} \quad \& \qquad \dot{S} = h(S)\left\{f(\overline{\sigma}(\sigma_{ij}) - S) - \frac{\partial G}{\partial S}\right\} \tag{4.8}$$

where $f = \dfrac{dF}{d\bar{\sigma}(\sigma_{ij})}$ is interpreted as a step function, whereby, if $\bar{\sigma}(\sigma_{ij}) = S$, $f(\bar{\sigma}(\sigma_{ij}) - S) \geq 0$, otherwise if $f(\bar{\sigma}(\sigma_{ij}) - S) = 0$, then the condition $\bar{\sigma}(\sigma_{ij}) > S$ is not allowed.

For conditions where $\sigma_{ij} = const$, *i.e.* $\bar{\sigma}(\sigma_{ij}) = const$, the steady state creep behaviour is defined by $\bar{\sigma}(\sigma_{ij}) = S$ and $\dot{S} = 0$. This leads to equations (4.8) becoming,

$$f(\bar{\sigma}(\sigma_{ij}) - S) = \frac{dG}{dS} = \frac{dG}{d\bar{\sigma}(\sigma_{ij})} \tag{4.9}$$

and

$$\dot{\varepsilon}_{ij}^{P} = \frac{dG}{d\bar{\sigma}(\sigma_{ij})} \frac{\partial \bar{\sigma}(\sigma_{ij})}{\partial \sigma_{ij}} = \frac{\delta \Omega^{*}}{\delta \sigma_{ij}} = \dot{\varepsilon}_{ij} \tag{4.10}$$

where Ω^{*} is the steady state potential for the steady state creep strain rate, $\dot{\varepsilon}_{ij}$,

$$\Omega^{*}(\sigma_{ij}) = G(\bar{\sigma}(\sigma_{ij}), S) = k \frac{\bar{\sigma}(\sigma_{ij})^{n+1}}{n+1} \tag{4.11}$$

with $\dfrac{r}{h} = \dfrac{dG}{d\bar{\sigma}(\sigma_{ij})} = k\bar{\sigma}(\sigma_{ij})^{n}$. Obtained from equation (4.10) is a definition of Norton's law in terms of the effective stress and strain rate,

$$\bar{\dot{\varepsilon}}(\dot{\varepsilon}_{ij}) = k\bar{\sigma}(\sigma_{ij})^{n} = \frac{r}{h} \tag{4.12}$$

provided $k = \dfrac{\dot{\varepsilon}_0}{\sigma_0^n}$.

From previous discussions, a definition of the stress history for the rapid cycle solution was presented in equation (4.1). For this particular model, the identification of the constant residual stress field is based on the condition that the average rate of inelastic strain accumulated over a cycle, $0 \le t \le \Delta t$,

$$\tilde{\dot{\varepsilon}}_{ij} = \lim_{\Delta t \to 0} \frac{1}{\Delta t} \int_0^{\Delta t} \dot{\varepsilon}_{ij}^P (\hat{\sigma}_{kl} + \overline{\rho}_{kl}) dt \tag{4.13}$$

is compatible with an average rate of displacement, $\tilde{\dot{u}}_i$. This limit for the Bailey-Orowan recovery model corresponds to the strains occurring at an instant, t_0, in the cycle, allowing the previous equation to be written as,

$$\frac{\Delta \varepsilon_{ij}}{\Delta t} = \dot{\varepsilon}_{ij} (\hat{\sigma}_{kl}(t_0) + \overline{\rho}_{kl}) \tag{4.14}$$

where t_0 is the instant of the maximum von-Mises effective stress,

$$\overline{\sigma}(\hat{\sigma}_{kl}(t) + \overline{\rho}_{kl}) \le \overline{\sigma}(\hat{\sigma}_{kl}(t_0) + \overline{\rho}_{kl}) \tag{4.15}$$

However, the applicability of (4.14) is only limited to a single instant for $\overline{\sigma}(\sigma_{ij})$ to reach its maximum value. In the general case, $\overline{\sigma}(\sigma_{ij})$ has a number of extreme values corresponding to the different times, t_i, where $i = 1,2,...,r$,

$$\bar{\sigma}(\sigma_{ij}(t_1)) = \bar{\sigma}(\sigma_{ij}(t_2)) = \ldots = \bar{\sigma}(\sigma_{ij}(t_r)) = \bar{\sigma}^f, \qquad \bar{\sigma}(\sigma_{ij}(t)) \leq \bar{\sigma}^f \tag{4.16}$$

For such cases, the accumulation of the creep strains over the cycle, $\Delta\varepsilon_{ij}$, is given as a weighted sum of the steady state creep values corresponding to each of the time instances,

$$\Delta\varepsilon_{ij} = \Delta\varepsilon_{ij}(t_1) + \Delta\varepsilon_{ij}(t_2) + \ldots + \Delta\varepsilon_{ij}(t_r) \tag{4.17}$$

This implies that the appropriate form of (4.12) for the Bailey-Orowan model is,

$$\bar{\dot{\varepsilon}}(\dot{\varepsilon}_{ij}(t_i)) = \dot{\varepsilon}_0 \left(\frac{\bar{\sigma}^f}{\sigma_0} \right)^n \tag{4.18}$$

Furthermore, by exploiting the analogy existing between the rapid cycle solutions and those of shakedown, Ponter *et al* [5,49] provided a definition for $\bar{\sigma}^f$, the newly labelled flow stress, evaluated from,

$$\bar{\sigma}^f = \sigma_0 \left\{ \frac{1}{\dot{\varepsilon}_0} \sum_{i=1}^{r} \bar{\dot{\varepsilon}} \left(\frac{\Delta\varepsilon_{ij}^i}{\Delta t} \right) \right\}^{\frac{1}{n}} \tag{4.19}$$

4.2.3. Numerical procedure for the rapid cycle solution

The numerical implementation of the rapid cycle solution [49] is based upon the utilization of the linear matching method. The constitutive equations for Norton's law and the Bailey-Orowan model presented in (4.4) and (4.18) respectively, are individually matched

with those of a linear rate problem so that they both give the same effective stress. The similarities existing between these solutions and those of shakedown, allows the bulk of the iterative procedure, described in Section 3.3, for the upper bound shakedown limit, to be applied here. This is shown interactively in Figures 4.1 and 4.2. Furthermore, the availability of convergence proofs for the rapid cycle solution [70], in recent times, further enhances its reputation as a programming method, as the solutions preserves the same monotonically reducing behaviour, converging to the least upper bound creep deformation limit.

Although the class of problems solved here are the same as those for shakedown, the solution's criterion for the load parameter, λ, is no longer a shakedown limit. This is due to the existence of cyclic creep solutions for any values of λ. For such problems, a design criterion is usually defined by placing a restriction on the maximum average creep strain rate throughout the volume, $\frac{\Delta\varepsilon_T}{\Delta t}$. Within the iterative procedure itself, a factor, z_f, is introduced,

$$z_f = \frac{\Delta\varepsilon_T}{\bar{\dot{\varepsilon}}(\Delta\varepsilon_{ij})\Delta t} \tag{4.20}$$

ensuring the satisfaction of this criterion for each and every strain rate history, where $\bar{\dot{\varepsilon}}(\Delta\varepsilon_{ij})$ is the maximum effective creep strain rate in the problem. In conforming to this requirement, the cyclic creep solutions, generated for a particular value of λ, now needs to be scaled accordingly, so that,

$$\lambda^{k+1} = \lambda^k (z_f)^{\frac{1}{n}} \tag{4.21}$$

where $\lambda^{k+1} \leq \lambda^k$ is defined as the upper bound cyclic creep limit.

In the cyclic creep analysis of cracked structures, however, a re-definition of the terms in (4.20) is required. The condition that the design criterion conforms to the maximum effective creep strain rate, $\bar{\dot{\varepsilon}}(\Delta\varepsilon_{ij})$, in the problem is no longer appropriate, due to the high strain singularity experienced at the crack tip. On the other hand, the accuracy of the solutions is compromised if the location of the designated maximum effective creep strain rate, $\bar{\dot{\varepsilon}}(\Delta\varepsilon_{ij})$, is remotely away from the crack tip. Thus, an accurate representation of the crack tip conditions requires an equally accurate means of identifying the location of the designated maximum effective creep strain rate. An approach, proven to be successful on both fronts, is discussed below.

4.3. Cyclic Creep Analysis of Cracked Structures

The problem investigated is shown in Figure 4.3. It consists of a symmetric half of a cracked axisymmetric Bree problem, with the ratio of crack length, a, to width, w, of 0.4. As before, the tube is also subjected to a uniaxial tension and a linear temperature gradient arising from a temperature difference of $\Delta\theta$. In the ensuing solutions, these are denoted by σ_p and σ_t, the maximum mechanical and thermo-elastic stresses away from the crack respectively, *i.e.* the value that would occur if the crack were absent.

As in all computational effort, making certain assumptions on the model analysed is unavoidable. In the following analysis, only two time intervals are considered, $0 \leq t \leq \beta\Delta t$ and

$(1-\beta)\Delta t \le t \le \Delta t$, during each of which the loads remained constant. Thus, in terms of typical times, t_1 and t_2, within these two intervals, the accumulation of the creep strain rate over the cycle, $\Delta\varepsilon_{ij}$, is given by,

$$\Delta\varepsilon_{ij} = \dot{\varepsilon}_{ij}(\sigma_{ij}(t_1))\beta\Delta t + \dot{\varepsilon}_{ij}(\sigma_{ij}(t_2))(1-\beta)\Delta t \tag{4.22}$$

for Norton's creep law. The corresponding formulation for the Bailey-Orowan recovery creep model is,

$$\Delta\varepsilon_{ij} = \dot{\varepsilon}_{ij}(\sigma_{ij}(t))\Delta t \tag{4.23}$$

for the case when the maximum effective stress, $\bar{\sigma}(\sigma_{ij}(t))$, occurs at either $t = t_1$ or $t = t_2$, leading to either $\bar{\sigma}^f = \bar{\sigma}(\sigma_{ij}(t_1))$ or $\bar{\sigma}^f = \bar{\sigma}(\sigma_{ij}(t_2))$ respectively. However, if the maximum occurs at both time instances, t_1 and t_2, then,

$$\Delta\varepsilon_{ij} = \dot{\varepsilon}_{ij}(\sigma_{ij}(t_1))\eta\Delta t + \dot{\varepsilon}_{ij}(\sigma_{ij}(t_2))(1-\eta)\Delta t \tag{4.24}$$

where $\bar{\sigma}(\sigma_{ij}(t_1)) = \bar{\sigma}(\sigma_{ij}(t_2)) = \bar{\sigma}^f$ and the constant, η, a value between $0 \le \eta \le 1$, is defined by the continuum problem. In this particular analysis, a balanced cycle is assumed, with $\beta = 0.5$. Furthermore, the material properties are also taken to remain constant throughout the cycle. Although, not a representation of a real material, this provides a simple starting point in understanding the behaviour of cracked structures under cyclic creep histories of loads and temperatures.

4.3.1. HRR fields

As an initial examination, the problem in Figure 4.3 is considered, with only σ_p, the mechanical load, applied. In such situations, extensive theoretical and experimental studies have been undertaken [31,32] in describing the behaviour of the deformation fields at the crack tip. The postulation, which spurred the development of fracture mechanics theorems in that era, is the work of Hutchinson [75] and Rice and Rosengren [76]. In an isotropic, elastic-plastic material, satisfying the power-law hardening expression,

$$\varepsilon = \alpha \varepsilon_y \left(\frac{\sigma}{\sigma_y} \right)^N \tag{4.25}$$

the asymptotic form of the stationary crack tip fields, subjected to a tensile load, was derived, where α is a material constant, N is the power-law hardening exponent, σ_y and ε_y are the yield stress and the associated yield strain respectively. Rice [34] then presented the existence of the so-called path-independent integrals or J-integrals, as a characteristic of the fields around the crack tip. The implication of these findings is the ability to now define the near crack tip stress and strain distributions in the form,

$$\sigma_{ij} \rightarrow \left(\frac{1}{r} \right)^{\frac{N}{N+1}} f_{ij}(\theta), \quad \varepsilon_{ij} \rightarrow \left(\frac{1}{r} \right)^{\frac{1}{N+1}} f_{ij}(\theta) \tag{4.26}$$

where r and θ are the radial and angular distances away from the crack tip. In the current investigation into the steady state creep behaviour of the cracked Bree problem, equation (4.26), often referred to as the HRR fields, is still applicable. This conclusion was reached [19]

on the basis of similarities in the stress distribution of a plastically deforming body in (4.25), with that of a body deforming in steady state creep in (4.4), provided the exponents, $N = n$. The reason for this is the identical equilibrium and compatibility equations governing the creeping body and those in the plastic body, with the exception of the strain rate and displacement rate in the creeping body replacing the strain and displacement in the plastic body.

The above argument necessitates the employment of an accurate meshing technique at the crack tip. The application of such a routine would enable the variations of the stress and strain distributions with the coordinates, r and θ, to be evaluated, allowing the subsequent identification of the best-matched HRR field. Within the context of finite element analysis, various meshing techniques have been suggested. Some involves the use of specially developed finite elements [77,78], while others attempted at an improved solution with the inclusion of a rosette around the crack tip [79]. There have also been cases where the effect of the singularity is accounted for with numerical methods [80,81]. Although useful in specific circumstances, their general applications in all cases are questionable. With this in mind, an alternative meshing technique is proposed. It involves adopting the same intensity in the finite element crack tip mesh, previously employed in Figure 2.10 (Chapter 2) and Figure 3.10 (Chapter 3), but now organized in a fan-like meshing arrangement. This is shown in Figure 4.3, meshed using the regular six-noded triangular hybrid element (CAX6H).

The most significant aspect of the employed meshing scheme is the ability to generate cyclic creep solutions, along radial paths, r, at different angles, θ, away from the crack tip. Within the context of the investigations, into the behaviour of mechanically and thermally

induced crack tip fields, carried out in this chapter, this meshing arrangement is of immense importance. This is mainly due to the need in identifying the so-called best-matched HRR field, *i.e.* the field near the crack tip, that best satisfies the HRR condition of equation (4.26). Although in the following investigations, it would be shown that equation (4.26) is satisfied at all values of θ, at a distance r away from the crack tip, there is, however, a path that best matches the HRR condition. This is best-matched HRR field. In the following, the uncovering of such a field is described. Its identification would then enable a sampling point, within this field, to be identified, allowing the possible evaluation of the creep fracture mechanics parameter, C^*, from this point. The location of this sampling point, which would occur at a specific value of r and θ, would also enable the design criterion in equation (4.20) to be determined, where $\bar{\dot{\varepsilon}}(\Delta\varepsilon_{ij})$ is now designated as the maximum effective creep strain rate at the sampling point. The justification behind this argument is presented below.

4.3.2. Mechanical load

For the initial case of constant mechanical loads, rapid cycle creep solutions were then generated, for differing values of $\theta = 0^0 - 80^0$, in multiples of 10^0, along radial paths, r, away from the crack tip. One such solution is shown in Figure 4.4, based upon Norton's law with $n = 3$, where $\bar{\dot{\varepsilon}}(\Delta\varepsilon_{ij})$ is the von-Mises effective creep strain rate accumulated over the cycle and $\bar{\sigma}(\sigma_{ij})$ is the von-Mises effective stress. It can be clearly seen that, for all values of θ, the solutions compares favourably well with the HRR field, *i.e* in accordance with the HRR condition of (4.26), except for gauss points very close to the crack tip within the first two or three elements. This same HRR-field-satisfying behaviour was also observed in solutions

obtained for $n = 5$ & $n = 7$, as shown in Figures 4.5 and 4.6 respectively. It was, however, found that within these HRR-field-satisfying solutions, there exists a best-matched HRR field. This was identified at $\theta = 70^0$ and encompassed by five meshing elements within the finite element mesh (Figure 4.3). This location is in close agreement with the findings of Takeshi *et al* [30], who discovered that the maximum effective stress and strain occurs at $\theta = 71.6^0$.

Although the solutions presented, so far, were for the Norton's law, identical HRR-field-satisfying solutions were also established for the Bailey-Orowan model. In the case of constant loads, as considered here, these observations are not surprising, as predicted by equations (4.22) and (4.24). These matches in solutions, for two different creep models, further reinforce the confidence on the numerical methods' capability in identifying the HRR fields in other situations.

The numerical analyses were then repeated, on the same cracked problem, but with the mechanical loads now cyclically varying, between zero and some maximum value, over the two time intervals. Under such loading conditions, it was observed that the HRR condition of equation (4.26) was still satisfied, for all values of θ, for $n = 3,5\,\&\,7$ and for the two constitutive models considered, with the best-matched HRR field still identified at the aforementioned locations. These promising initial results into the behaviour of the crack tip fields under purely mechanical loads provided the conviction that the LMM-based numerical methods is capable of generating similar accurate solutions, in the impending investigations into the behaviour of cracked structures subjected to both cyclic loads and temperatures.

In the previous section, it was mentioned that the behaviour of the crack tip fields in elastic-plastic materials is often characterized by the integral, J. In steady state creep fracture

mechanics, however, the equivalent term is the parameter, C^* [19]. This was the result of the previously discussed strong analogy existing between the plastically deforming and creeping materials. The implication of this similitude is the ability to now define the near crack tip strain rate and stress fields, in terms of effective quantities, using,

$$\bar{\dot{\varepsilon}}(\Delta\varepsilon_{ij}) = \dot{\varepsilon}_o \left(\frac{C^*(n)}{I_n \sigma_0 \dot{\varepsilon}_0 r} \right)^{\frac{n}{n+1}} \bar{\varepsilon}(\tilde{\varepsilon}(\theta, n)) \tag{4.27}$$

$$\bar{\sigma}(\sigma_{ij}) = \sigma_o \left(\frac{C^*(n)}{I_n \sigma_0 \dot{\varepsilon}_0 r} \right)^{\frac{1}{n+1}} \bar{\sigma}(\tilde{\sigma}(\theta, n)) \tag{4.28}$$

where I_n is a dimensionless constant, $\bar{\varepsilon}(\tilde{\varepsilon}(\theta,n))$ & $\bar{\sigma}(\tilde{\sigma}(\theta,n))$ are dimensionless functions of θ and n respectively. These quantities are identifiable through various means [19,30], but here, these were obtained from tables evaluated by Shih [82]. Nonetheless, the evaluation of $C^*(n)$ from equations (4.27) and (4.28), still needs the corresponding numerical values of $\bar{\dot{\varepsilon}}(\Delta\varepsilon_{ij})$ and $\bar{\sigma}(\sigma_{ij})$ at a particular point, *i.e.* a value of r and θ, away from the crack tip. In this chapter, this so-called sampling point is at $\theta = 70^0$ and $r = 0.00865w$, identified within the previously discussed best-matched HRR field. Using this specific location, the parameters, $C^*(n)$, were then computed for $n = 3,5\,\&\,7$, where $\bar{\dot{\varepsilon}}(\Delta\varepsilon_{ij})$ and $\bar{\sigma}(\sigma_{ij})$ are the numerical values at the sampling point, obtained from the analyses conducted using the material properties of $\dot{\varepsilon}_0 = 0.05/\text{h}$ and $\sigma_0 = 100\text{MPa}$.

In the calculations, it was found that under constant mechanical loads, the values of $C^*(n)$, evaluated from equations (4.27) and (4.28), were identical, *i.e.* $C^*(n)$ can be

evaluated from using either $\dot{\bar{\varepsilon}}(\Delta\varepsilon_{ij})$ or $\bar{\sigma}(\sigma_{ij})$. Furthermore, comparisons between these numerical values and those estimated via the reference stress formulation [1,19] were also found to be within the range expected of such analyses. These issues will be discussed in greater detail in the next chapter.

4.3.3. Mechanical and thermal loads

In the case where both mechanical and thermal loads are considered, the theory that identifies C^* as the appropriate creep fracture mechanics parameter, *i.e.* the existence of path-independent integral does not exist. In closing this gap, an approach whereby C^* is interpreted in the same manner as K is understood in linear elastic fracture mechanics (LEFM), as the intensity of the accumulated strain concentration over the cycle, is suggested. For such an approach to be valid, the radial distribution of the von-Mises effective accumulated creep strain rate near the crack tip, needs to be reasonably described by the satisfaction of the HRR field condition of equation (4.26). The satisfactory fulfilment of this condition would then enable loading states along a contour in a (σ_p, σ_t) diagram to be identified, whereby the conditions at the crack tip, by this criterion, is identical. Numerically, this implies that the designated maximum effective creep strain rate, $\dot{\bar{\varepsilon}}(\Delta\varepsilon_{ij})$, used in the design criterion of (4.20), would now correspond to the magnitude of the von-Mises effective creep strain rate at the sampling point, identified within the previously defined best-matched HRR field.

For the cracked problem in Figure 4.3 subjected to the prescribed loading conditions, rapid cycle creep solutions were then generated, for the loading histories corresponding to the

contour in the (σ_p, σ_t) space in Figure 4.7, where $\sigma_y = 200\text{MPa}$. A selection of $\bar{\dot{\varepsilon}}(\Delta\varepsilon_{ij})$ plots is shown in Figures (4.8) to (4.10), for both models at $n = 3,5\ \&\ 7$. In all these cases, the variations of the effective accumulated creep strain rate are close to that of the HRR field condition of (4.26). The best-matched HRR field, however, still occurs at the previously identified locations, *i.e.* when $\sigma_p = \sigma_y$, as shown in Figure 4.3. In addition, the differences in the HRR gradients, for the majority of the loading histories, were found to be less than 10%, with only a few exceptions, especially for the Bailey Orowan model, exceeding this threshold. On the entirety, although these solutions were not as exact as before, they are still within the acceptable range expected of numerical analyses.

On that note, a similar expression for C^* was developed, using the same sampling point as before, but under the identity,

$$\bar{\dot{\varepsilon}}(\Delta\varepsilon_{ij}) = \bar{\dot{\varepsilon}}\left(\frac{\Delta\varepsilon_{ij}}{\Delta t}\right) \tag{4.29}$$

where $\bar{\dot{\varepsilon}}(\Delta\varepsilon_{ij})$ is now the average rate of strain growth at the crack tip, corresponding to that given by the best-matched HRR field. Thus, substituting the identity of (4.29) into (4.27), the values of $C^*(3)$, $C^*(5)$ and $C^*(7)$ were then computed, for the different combinations of loading histories presented. As the solutions are all homogeneous of degree, n, a scaling factor, λ, was introduced, yielding the correct condition at the crack tip, such that it scales $(\lambda\sigma_p, \lambda\sigma_t)$. A relationship, such as those given in Figure 4.7, was then outlined, resulting in plots of contours of constant $C^*(n)$ to be identified. These contours are shown in Figure 4.11. The results, however, seemed to indicate a dependency upon both the creep index, n, and the

constitutive equations used. For these solutions to be useful, they need to be presented in a form, which is insensitive to both the creep exponents and the constitutive equations. This task is undertaken in the next chapter, whereby the solutions are represented in terms of reference stress quantities [1,19].

4.4. Further Analysis

The above calculations demonstrated the possibility of obtaining the crack tip parameters, equivalent to $C^*(n)$, for cracked structures subjected to both cyclic histories of loads and temperatures. The adopted methodology identifies strain increments over a loading cycle that varies radially away from the crack tip, in the same manner as the HRR field condition of (4.26). The encouraging results, so far, acquired, however, needs to be validated with solutions, taking into consideration variations in loading histories, material properties, structural geometries, *etc*, before general conclusions could be reached. The results of these additional investigations are examined below. Some of these solutions would also be re-represented in the next chapter, in terms of the reference stress quantities [1,19].

4.4.1. Higher creep exponent

One distinct feature of the outlined LMM-based numerical procedures is their ability to generate solutions at much higher creep exponents. This is shown in Figure 4.12, in the form of contours of constant $C^*(n)$, for the creep exponents of $n = 3,5,7 \,\&\, 15$. Furthermore, unlike other available numerical methods, solutions were found to converge well within the first 20 iterations. The monotonically reducing sequence of solutions, prescribed by the proofs [70]

that the solutions converges to the least upper bound creep limit, were still observed even for $n = 15$. This behaviour was found to be typical in solutions generated by both constitutive models, at the different loading combinations of (σ_p, σ_t).

4.4.2. Variation in loading histories

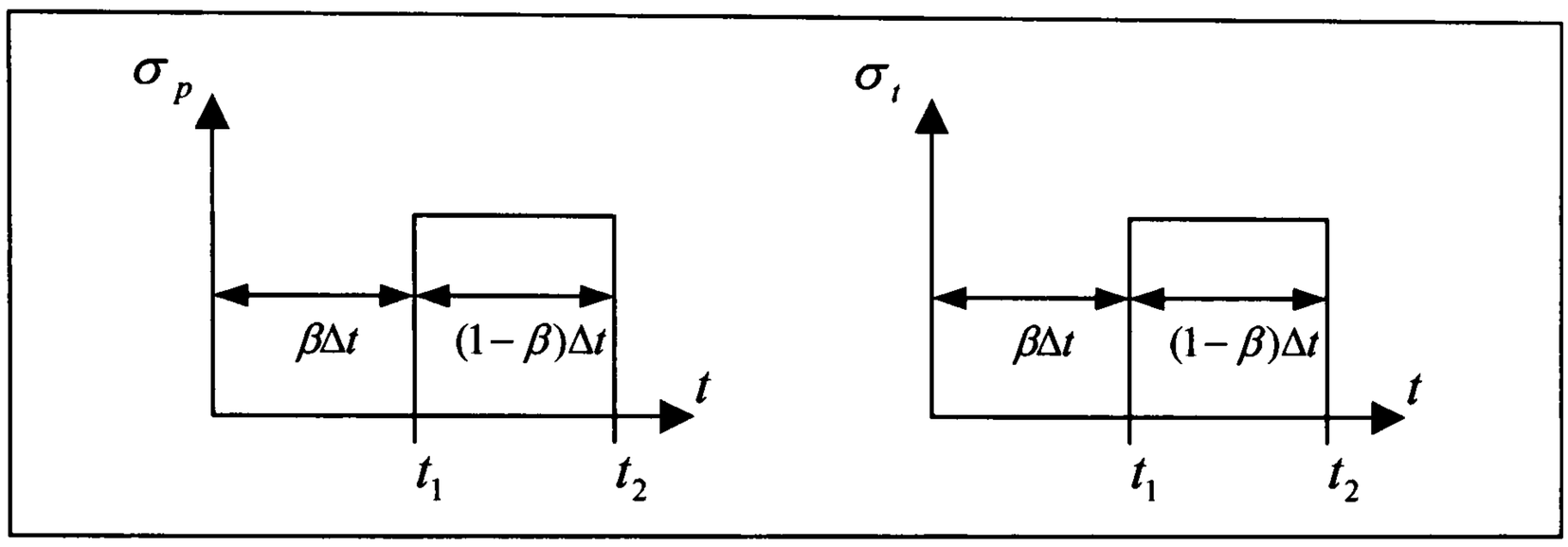

Table 1: Variations in the loading histories

The changes in the solutions, with respect to variations in the loading histories on the same cracked Bree problem of Figure 4.3, were also investigated. Here, the mechanical load no longer remains constant, but varies between zero and some maximum value over the cycle time, $0 \le t \le \Delta t$. Without taking into consideration the effect of temperatures, this situation was investigated before in Section 4.3.2. In this circumstance, however, the mechanical load is assumed to be varying in-phase with those of the thermal loads, as shown in Table 1.

The previously described numerical procedures were then repeated here. The rapid cycle solutions generated, for both models, were found to satisfy the HRR field condition of (4.26) reasonably well, with the best-matched HRR field still observed at $\theta = 70^0$ and encompassed by the five meshing elements (Figure 4.3). This holds true for the different

combinations of (σ_p, σ_t) considered in the analyses (Figure 4.7). This, thus, enabled the parameter, $C^*(n)$, to be evaluated, from the magnitudes of $\bar{\dot{\varepsilon}}(\Delta\varepsilon_{ij})$ at the sampling point using equation (4.27). As before, using the design criterion of (4.20), plots of contours of constant $C^*(n)$ were then identified, as shown in Figure 4.13. The plot further reinforces the statement that the solutions are dependent upon the creep index and the constitutive equations. In comparison with earlier solutions, more pronounced deviations were observed; more so for the Bailey-Orowan than Norton's law. The requirement for an insensitive definition of these contours, independent of the constitutive equations and creep exponents, is even more vital in this situation.

4.4.3. Varying material properties

So far, the solutions produced were based upon the assumption that the material properties remain constant throughout the loading cycle. In real materials, however, these properties would be expected to change with respect to changes in temperatures. In modelling this behaviour, the constitutive equations in (4.4) and (4.18), needs to be modified accordingly. Thus, under the effect of varying temperature, the appropriate formulation for Norton's law is,

$$\bar{\dot{\varepsilon}}(\Delta\varepsilon_{ij}) = \left(\frac{\bar{\sigma}(\sigma_{ij})}{\sigma_0}\right)^n \dot{\varepsilon}_0(\theta) \tag{4.30}$$

with $\bar{\sigma}(\sigma_{ij})$ being replaced by $\bar{\sigma}^f$ in the Bailey-Orowan model. In this situation, the term, $\dot{\varepsilon}_0(\theta)$, represented by,

$$\dot{\varepsilon}_0(\theta) = \dot{\varepsilon}_0(\theta_0) e^{-\frac{\Delta H}{R}\left(\frac{1}{\theta}-\frac{1}{\theta_0}\right)} \tag{4.31}$$

needs to evaluated, where θ is the temperature varying across the width of the tube. In its identification, the following creep law model, provided by British Energy [1], is adopted,

$$\bar{\dot{\varepsilon}}(\dot{\varepsilon}_{ij}) = Be^{\frac{-Q}{(T+250)+273}} \bar{\sigma}(\sigma_{ij})^n \tag{4.32}$$

where $B = e^{-12.7}$, $Q = 19700$, T is temperature in ^0C, $\bar{\sigma}(\sigma_{ij})$ is effective stress in MPa and $\bar{\dot{\varepsilon}}(\dot{\varepsilon}_{ij})$ is the effective creep strain rate per hour. The material is assumed to be Type 316 stainless steel, corresponding to the material properties in Table 2 below.

Heat transfer properties	Thermal conductivity (W/mm/c)	0.01365
	Specific heat (J/Kg/C)	465.4
	Density (Kg/mm3)	7.966E-06
Linear elastic properties	Young's modulus (GPa)	208
	Thermal expansion (/C)	15.37E-06
	Yield Stress (MPa)	200

Table 2: Material properties for the Type 316 stainless steel adopted.

Solutions were then generated for both models for $\dot{\varepsilon}_0(\theta_0) = 4.80906\text{E-}09/\text{h}$. These were then plotted in Figure 4.14, in the form of contours of constant $C^*(n)$. Irrespective of the loading histories considered, *i.e.* σ_p = constant or σ_p = varying, the results indicate a big difference in solution between Norton's law and the Bailey-Orowan model. This mirrors the observations of Ponter [69], leading to the agreement that the behaviour of real materials

would lie between these two models. (Note: This investigation was not pursued further beyond this point.)

4.4.4. Different crack lengths

In this section, the behaviour of the crack tip fields for short cracks were investigated. The same axisymmetric Bree problem, presented in Figure 4.3, is considered, with the exception that the ratio is now $\frac{a}{w} = 0.04$. In meshing the crack tip, the same fan-like meshing arrangement was still adopted. The previously described numerical procedures were then applied to this problem, with the generated results plotted in Figures 4.15 to 4.17, for both Norton's law and the Bailey Orowan constitutive model, at $n = 3,5 \,\&\, 7$. In all these solutions, the variations of $\bar{\dot{\varepsilon}}(\Delta\varepsilon_{ij})$ were still found to satisfy the HRR field condition of (4.26) reasonably well, with the best-matched HRR field now identified at $\theta = 70^0$ and encompassed by the three meshing elements between $0.00866w \le r \le 0.01045w$. This enabled the crack tip fracture parameters, $C^*(n)$, to be computed from equation (4.27), using the magnitudes of $\bar{\dot{\varepsilon}}(\Delta\varepsilon_{ij})$ at the sampling point, *i.e.* $\theta = 70^0$ and $r = 0.00953w$. These additional results are shown in Figure 4.18, as plots of contours of constant $C^*(n)$. Also included are solutions whereby the cracked problem is subjected to the loading histories described in Section 4.4.2, whereby the mechanical and thermal loads are cyclically varying in-phase with each other. Although the overall behaviour of these solutions was still dependent upon the creep exponents and the constitutive models used, the deviations were, however, found to be distinctly less than before.

4.4.5. Plane stress geometry

So far, the investigations conducted were on the cracked axisymmetric Bree problem, subjected to the different structural/loading conditions. Similar examinations were also carried out for the cracked plane stress Bree problem, under variations in loading histories and crack lengths. Although no solutions were included here, the proposed procedures, for describing the behaviour of the mechanically and thermally induced crack tip fields, were still found to be applicable. The results of these additional analyses are, however, presented in the next chapter using the reference stress concepts [1,19].

4.5. Concluding Remarks

In describing the behaviour of crack tip fields, subjected to the extremes of the applied cyclic histories of loads and temperatures, this chapter proposed the utilization of the rapid cycle creep solution [69,70]. Numerically implemented using the LMM, for the constitutive models of Norton and Bailey-Orowan, the procedure requires the identification of increments of strain over a cycle of loading that vary radially from the crack tip, in the same manner as the HRR field. The necessary fulfilment of this condition would then enable a design criterion to be identified, which in essence is a representation of the safe operation of the whole structure.

The investigations conducted revealed that such an approach is valid. It was observed that the satisfaction of the HRR field condition of equation (4.26) was reasonably achieved, for both the mechanical and thermal loads, under variations in creep exponents, loading

histories, crack lengths and constitutive equations. This made it possible for the crack tip fracture parameter, $C^*(n)$, to be identified, at a sampling point within the so-called best-matched HRR field. The contours of constant crack tip conditions, so evaluated, were then found to be dependent upon both the creep exponents and the constitutive models. These behaviours were also reproduced in both structural geometries, *i.e.* the cracked axisymmetric and plane stress Bree problems, considered.

These results form the basis of the investigations carried out in Chapter 5, whereby the solutions are re-interpreted in terms of the reference stress [1,19], independent of the creep exponents and the constitutive equations. The presentation of these solutions, in such form, would thus enable the behaviour of current R5 [1] procedures, which treats the effect of thermal stress as a bending moment, to be appraised.

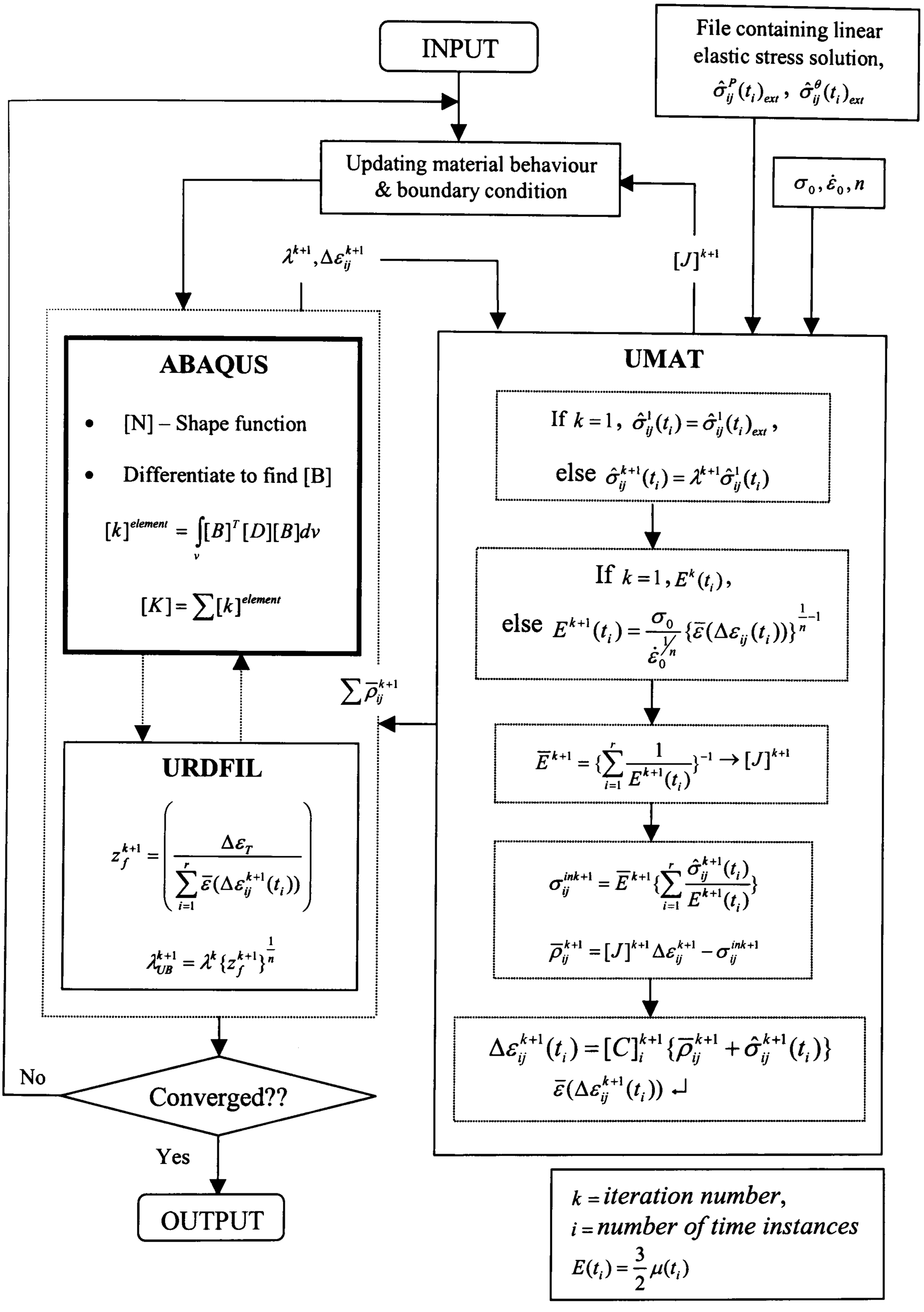

Figure 4.1: Numerical procedure for the rapid cycle solution using the Norton's law model.

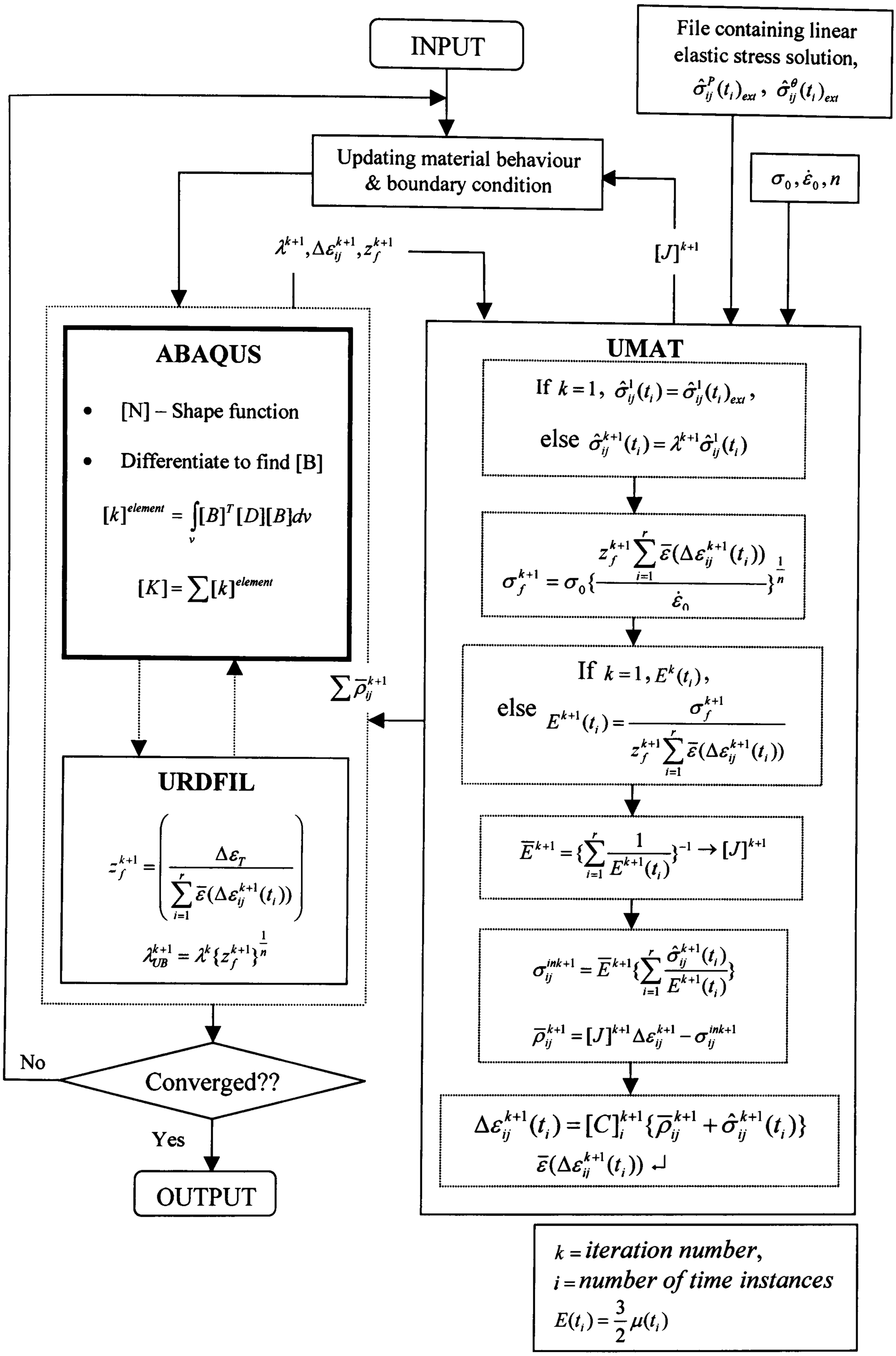

Figure 4.2: Numerical procedure for the rapid cycle solution using the Bailey-Orowan model.

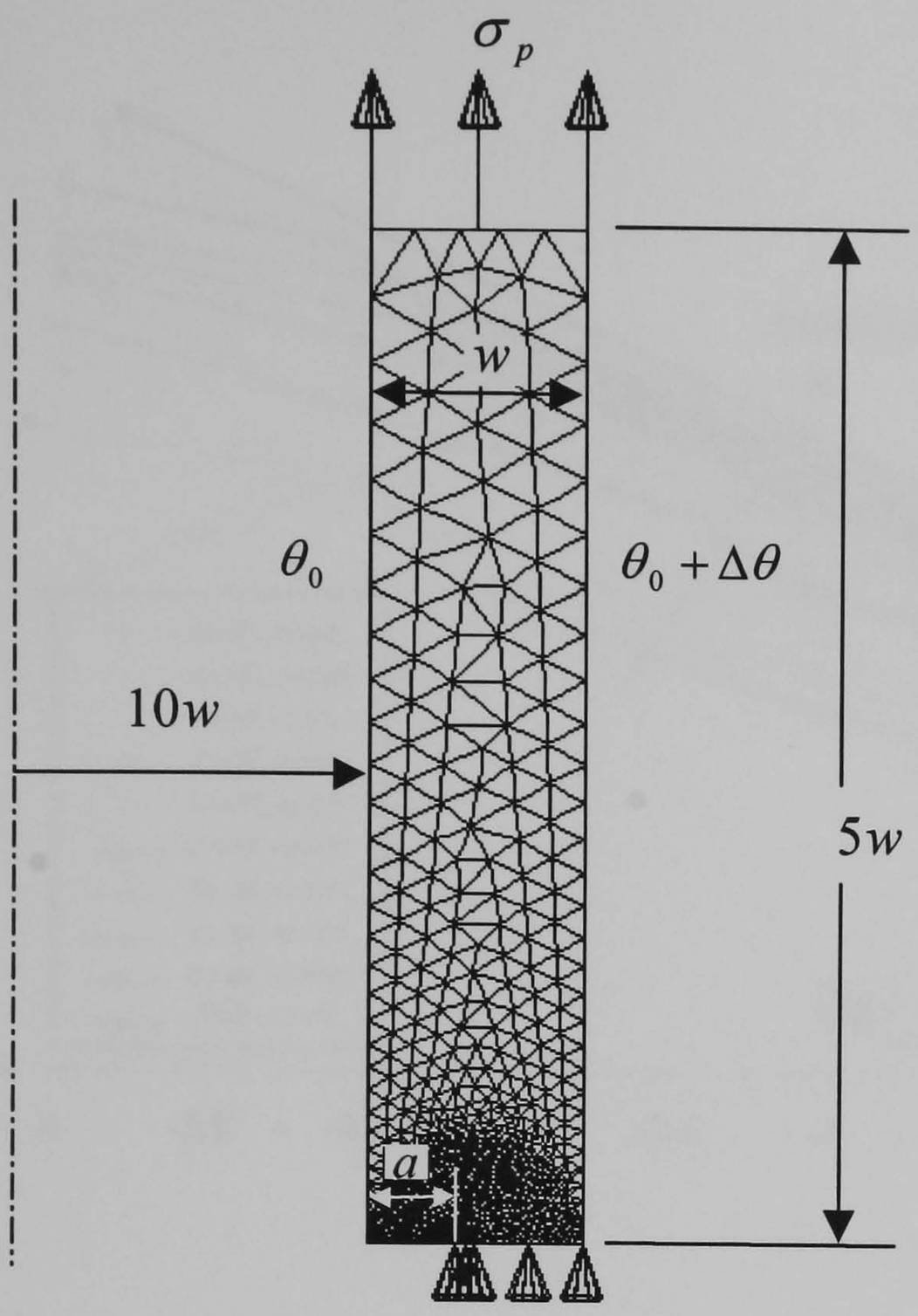

FEA model

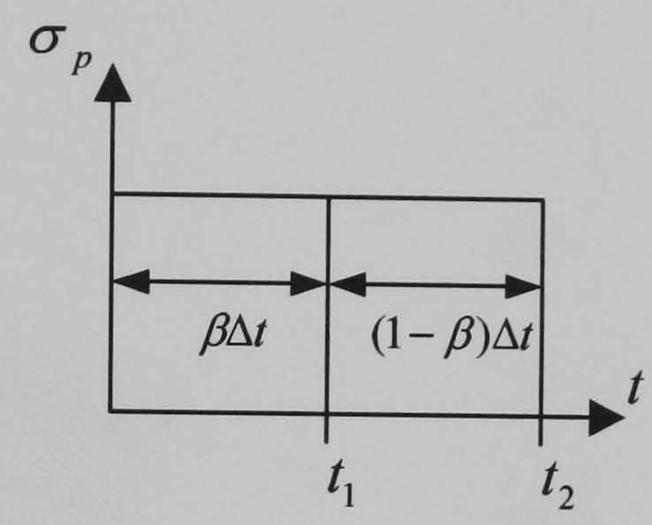

Loading conditions

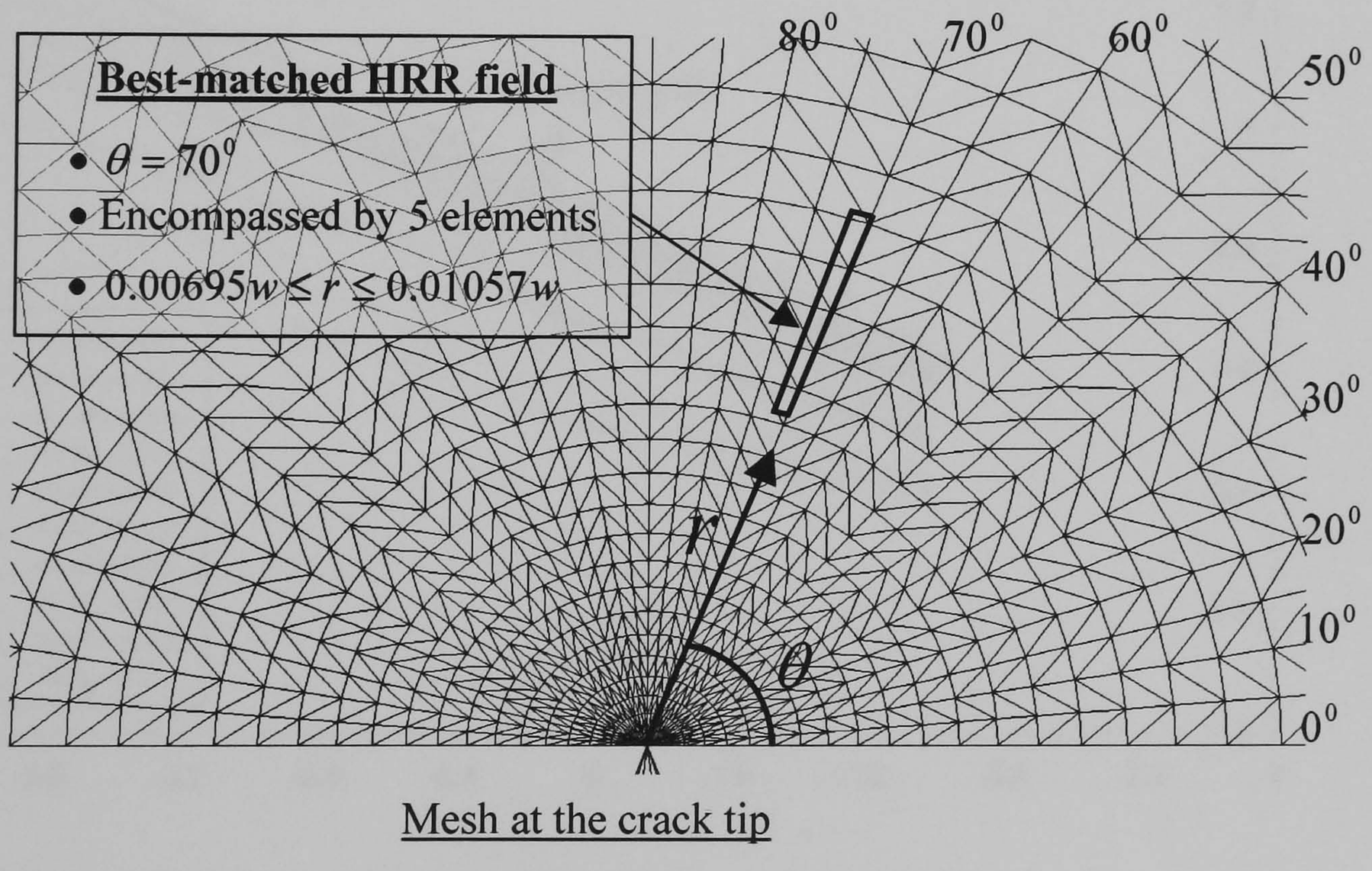

Mesh at the crack tip

Figure 4.3: The cracked axisymmetric finite element model used in the cyclic creep analyses.

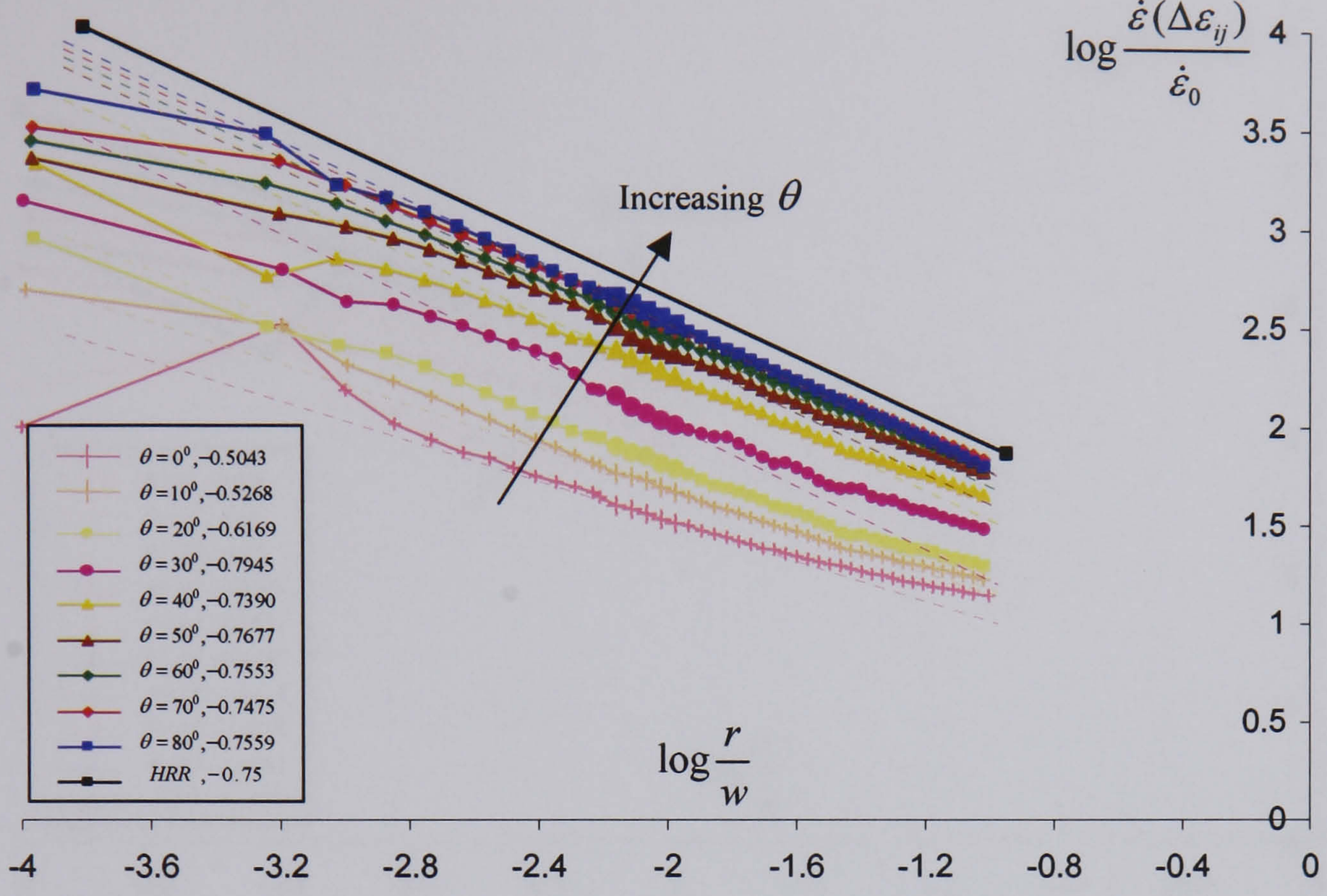

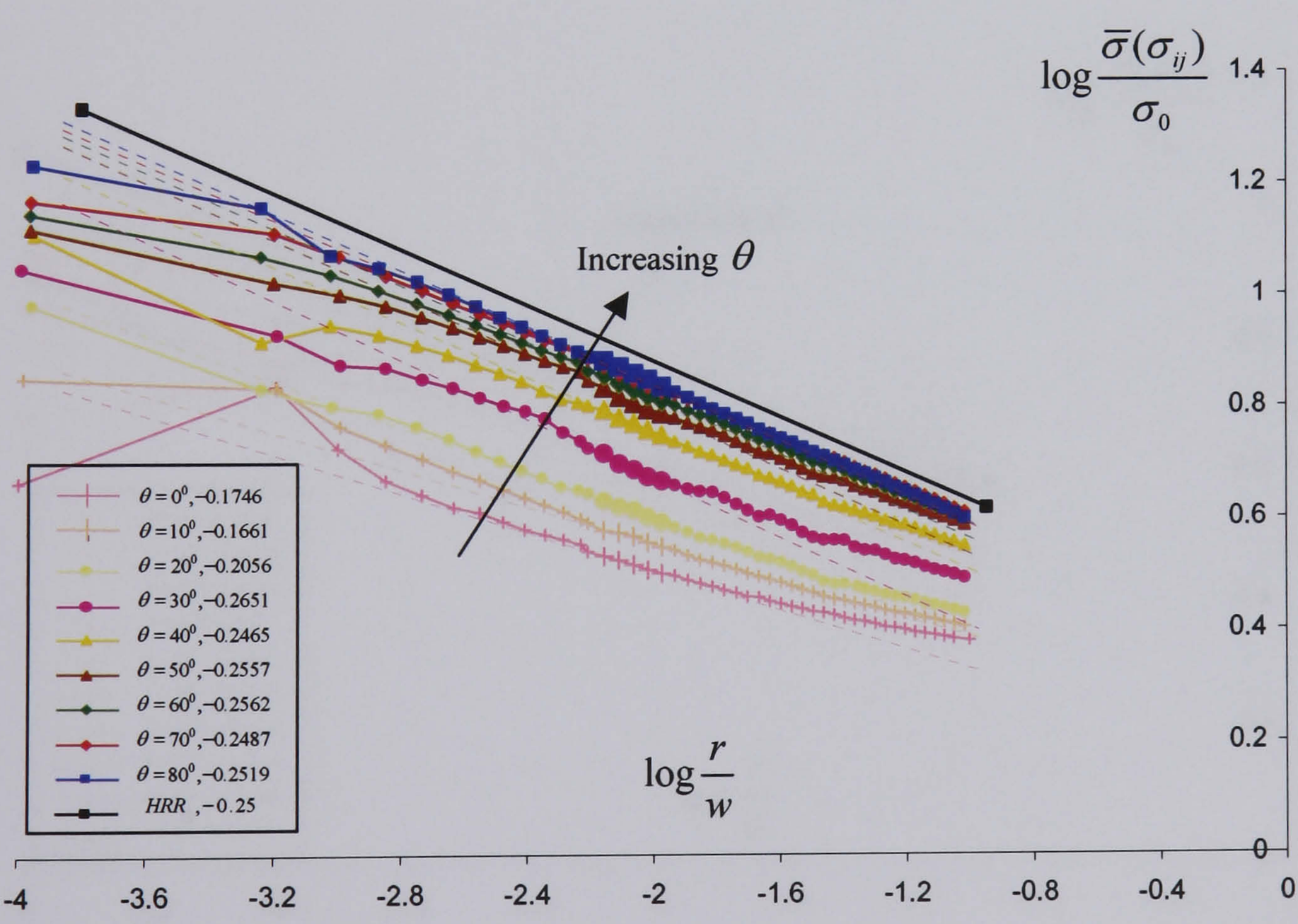

Figure 4.4: Rapid cyclic creep solutions under constant mechanical load, for differing values of θ at $n = 3$. (Norton's law)

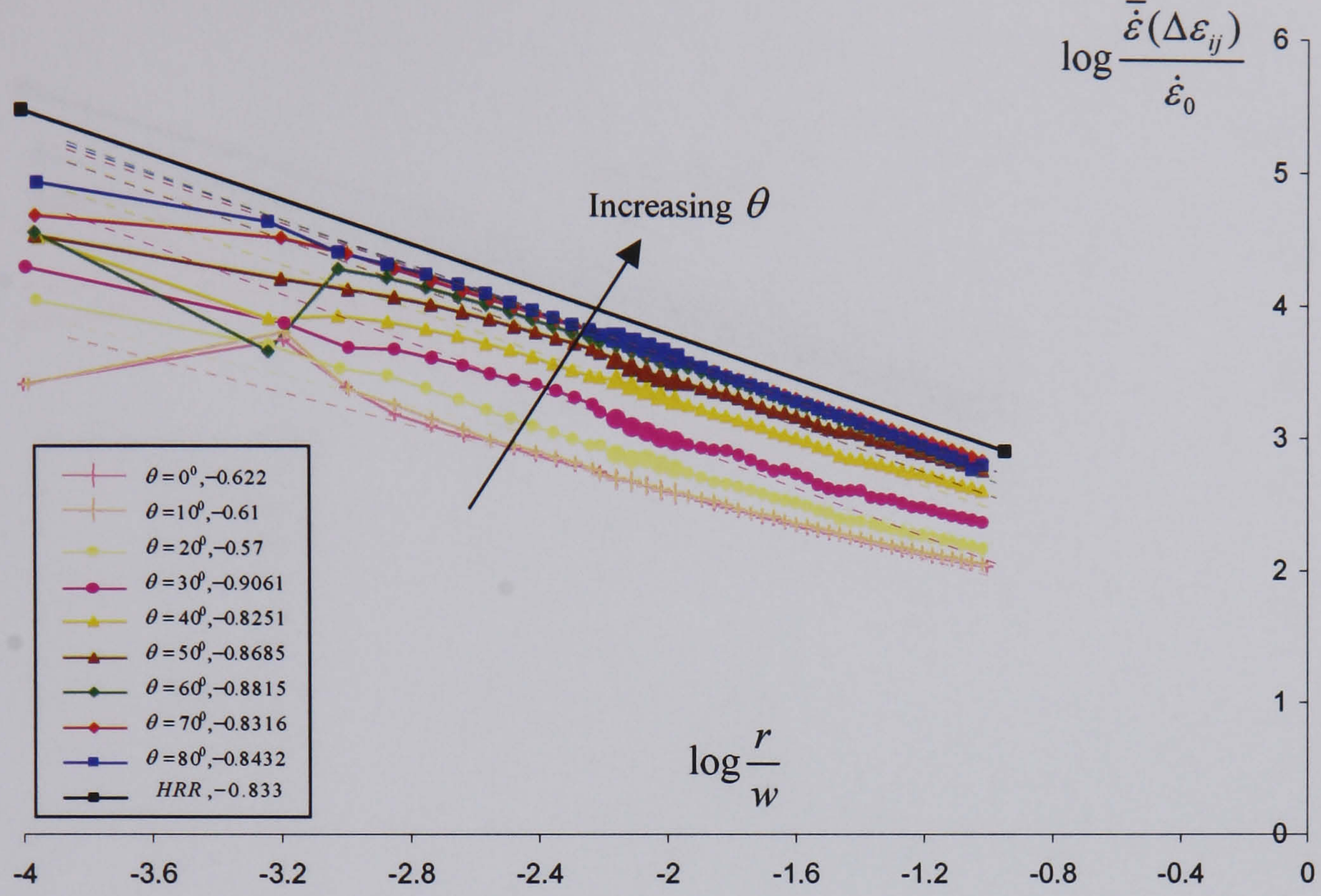

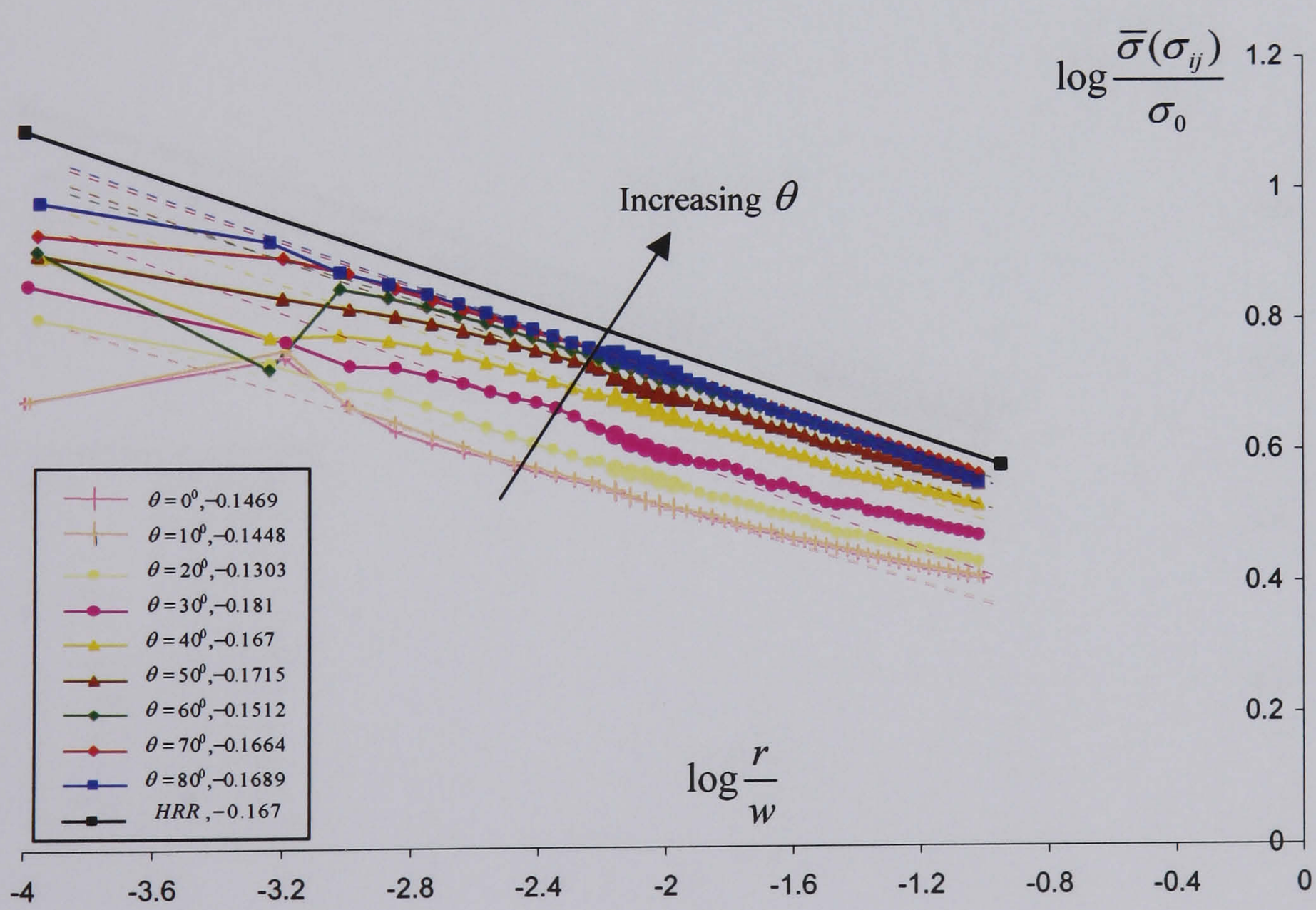

Figure 4.5: Rapid cyclic creep solutions under constant mechanical load, for differing values of θ at $n = 5$. (Norton's law)

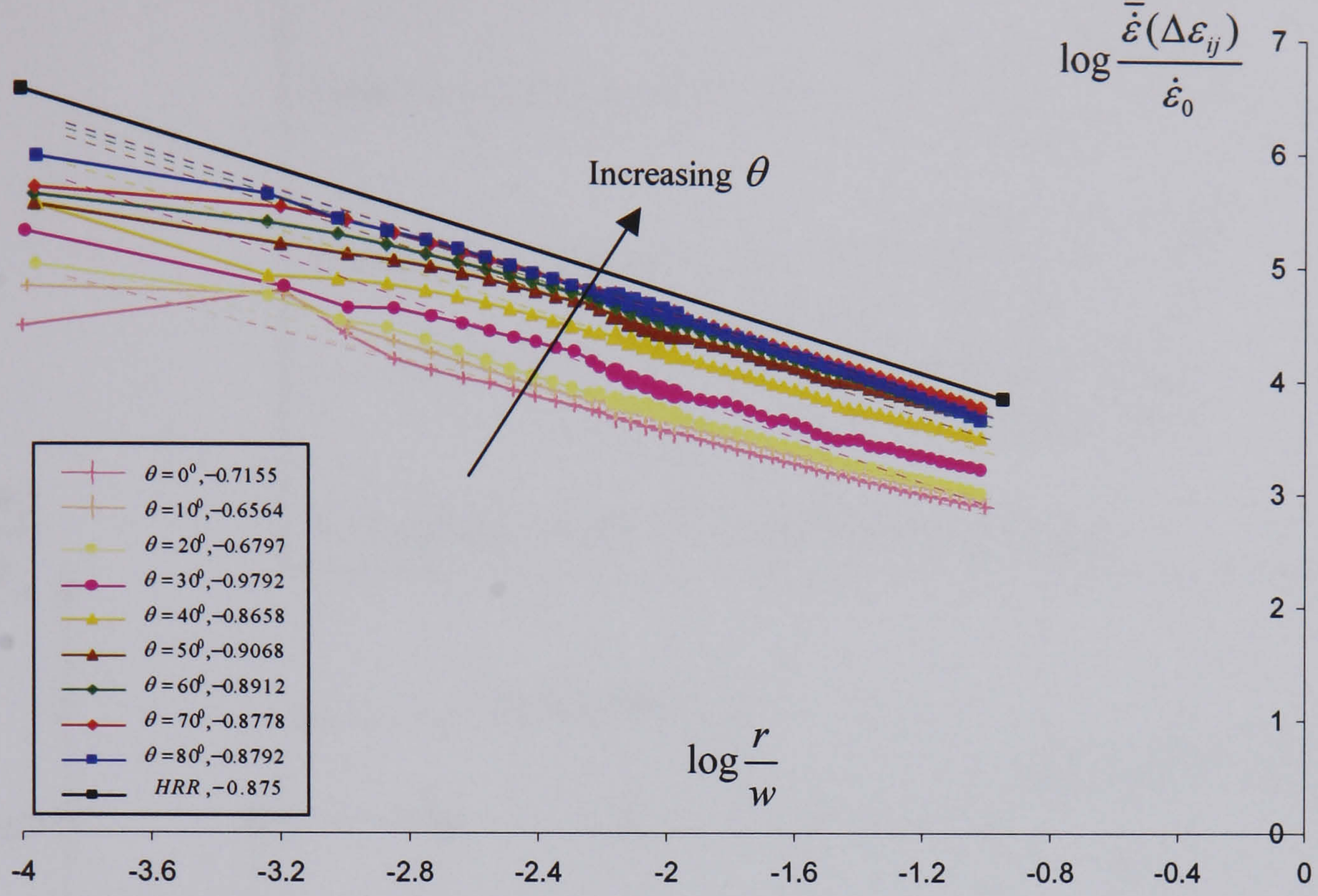

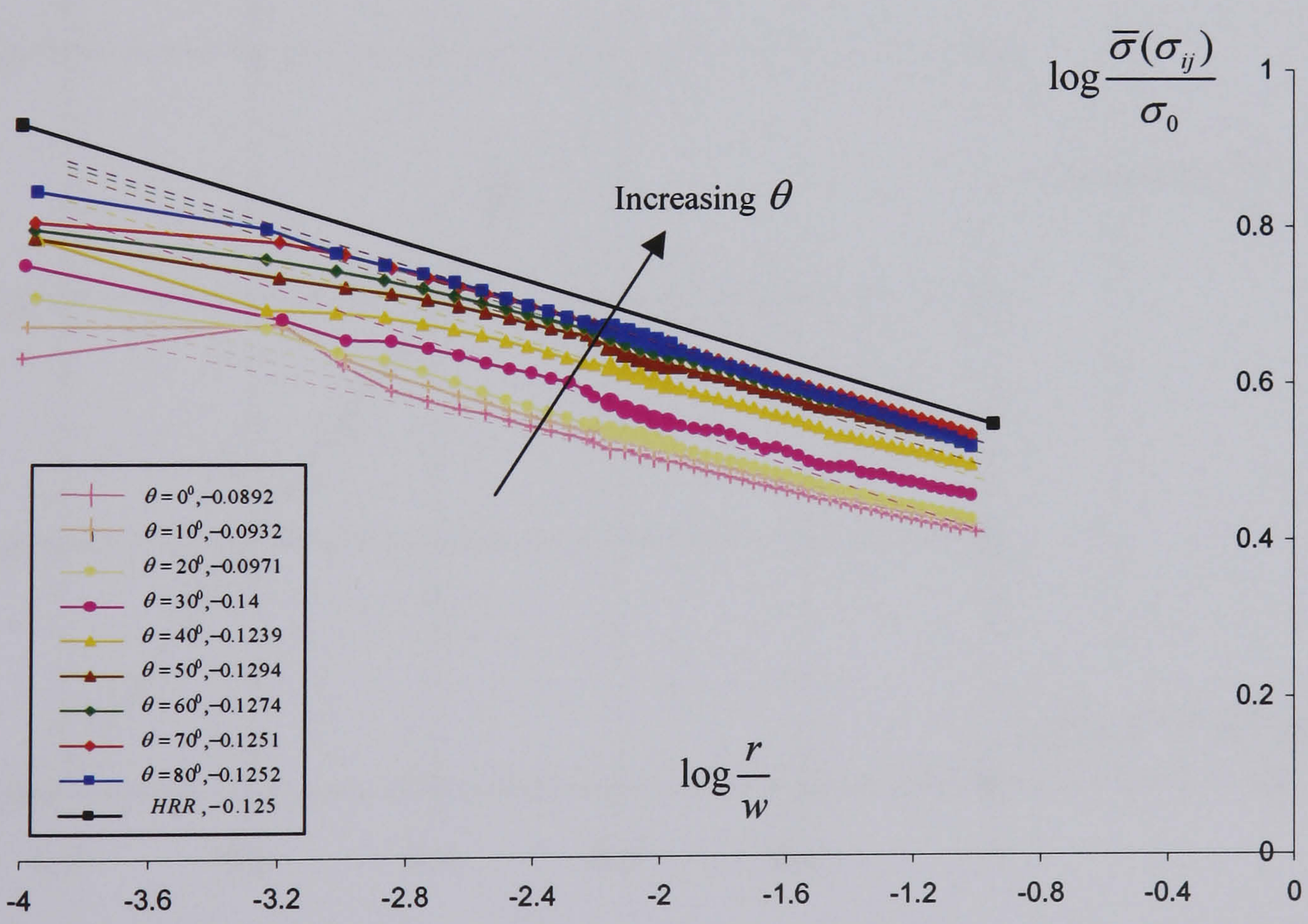

Figure 4.6: Rapid cyclic creep solutions under constant mechanical load, for differing values of θ at $n = 7$. (Norton's law)

Contour of constant $\bar{\dot{\varepsilon}}(\Delta\varepsilon_{ij})$, $\lambda = \left(\dfrac{\bar{\dot{\varepsilon}}(\Delta\varepsilon_{ij})^{(\sigma_p=\sigma_y,\sigma_t=0)}}{\bar{\dot{\varepsilon}}(\Delta\varepsilon_{ij})^{(x,y)}} \right)^{\frac{1}{n}}$

Contour of constant $C^*(n)$, $\lambda = \left(\dfrac{C^*(n)^{(\sigma_p=\sigma_y,\sigma_t=0)}}{C^*(n)^{(x,y)}} \right)^{\frac{1}{n+1}}$

where (x, y) are the different combinations of (σ_p, σ_t) considered in the analysis

• - Loading conditions in the numerical analyses

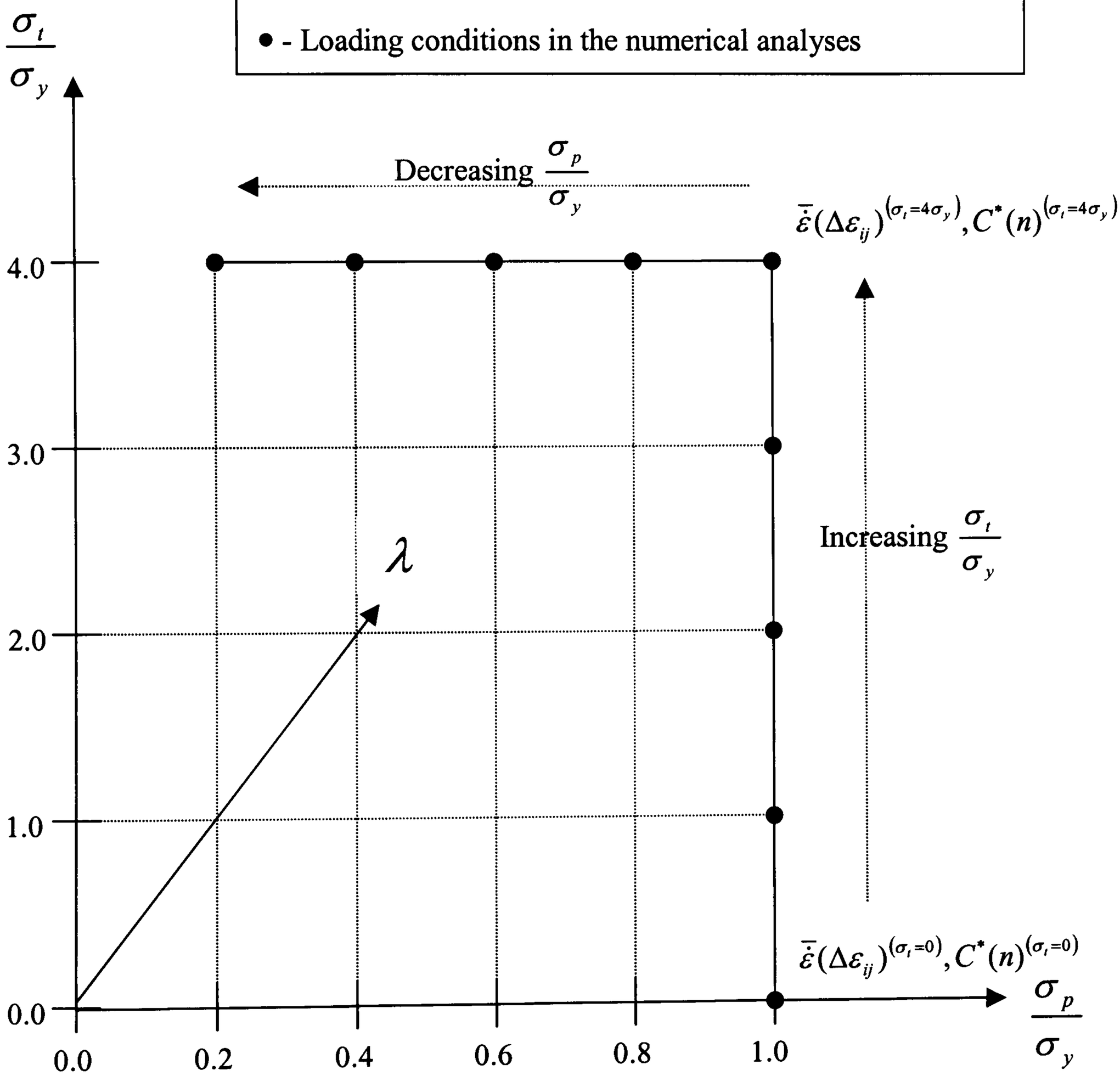

Figure 4.7: The load combinations of (σ_p, σ_t) considered in the analysis.

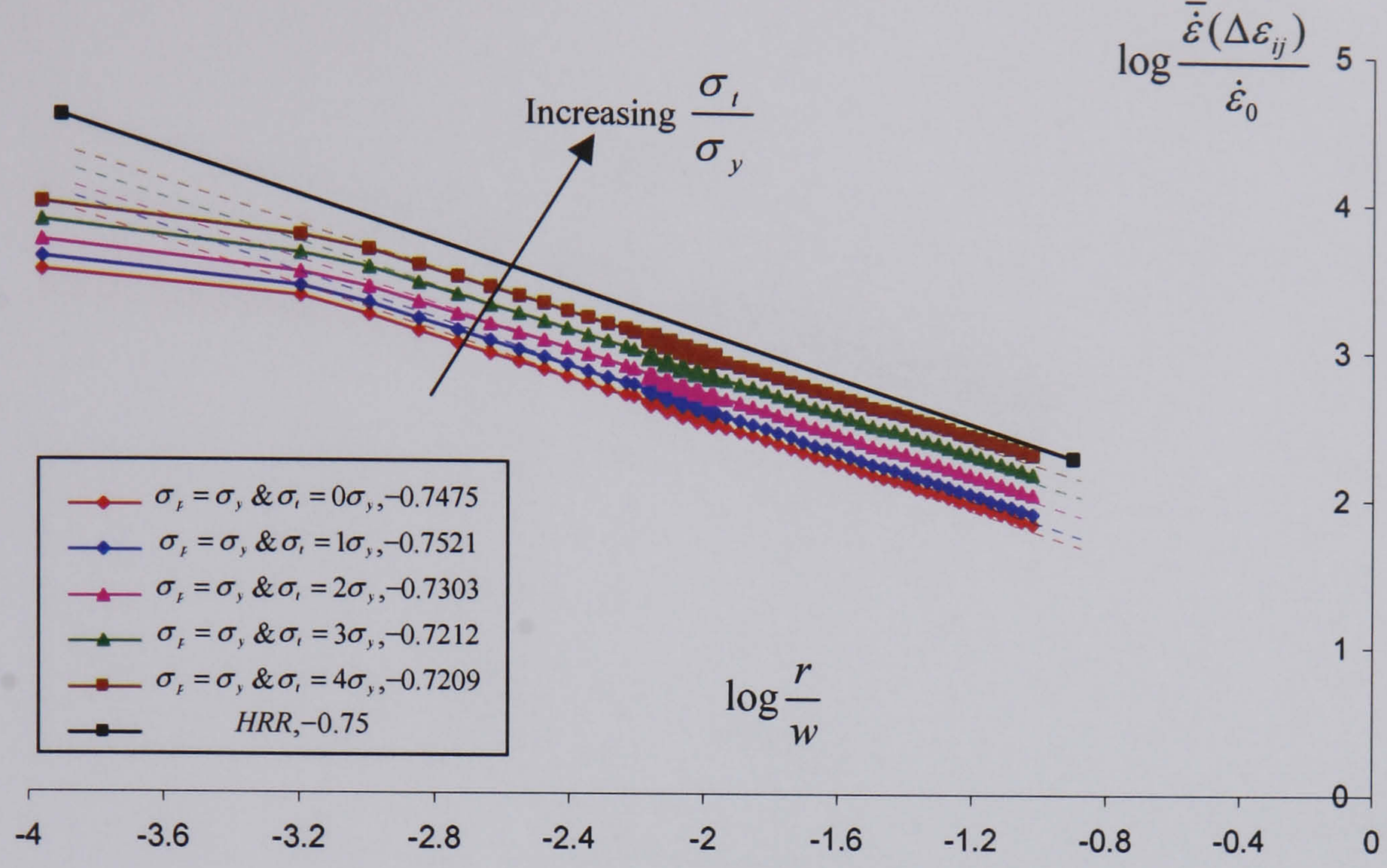

Norton's law model

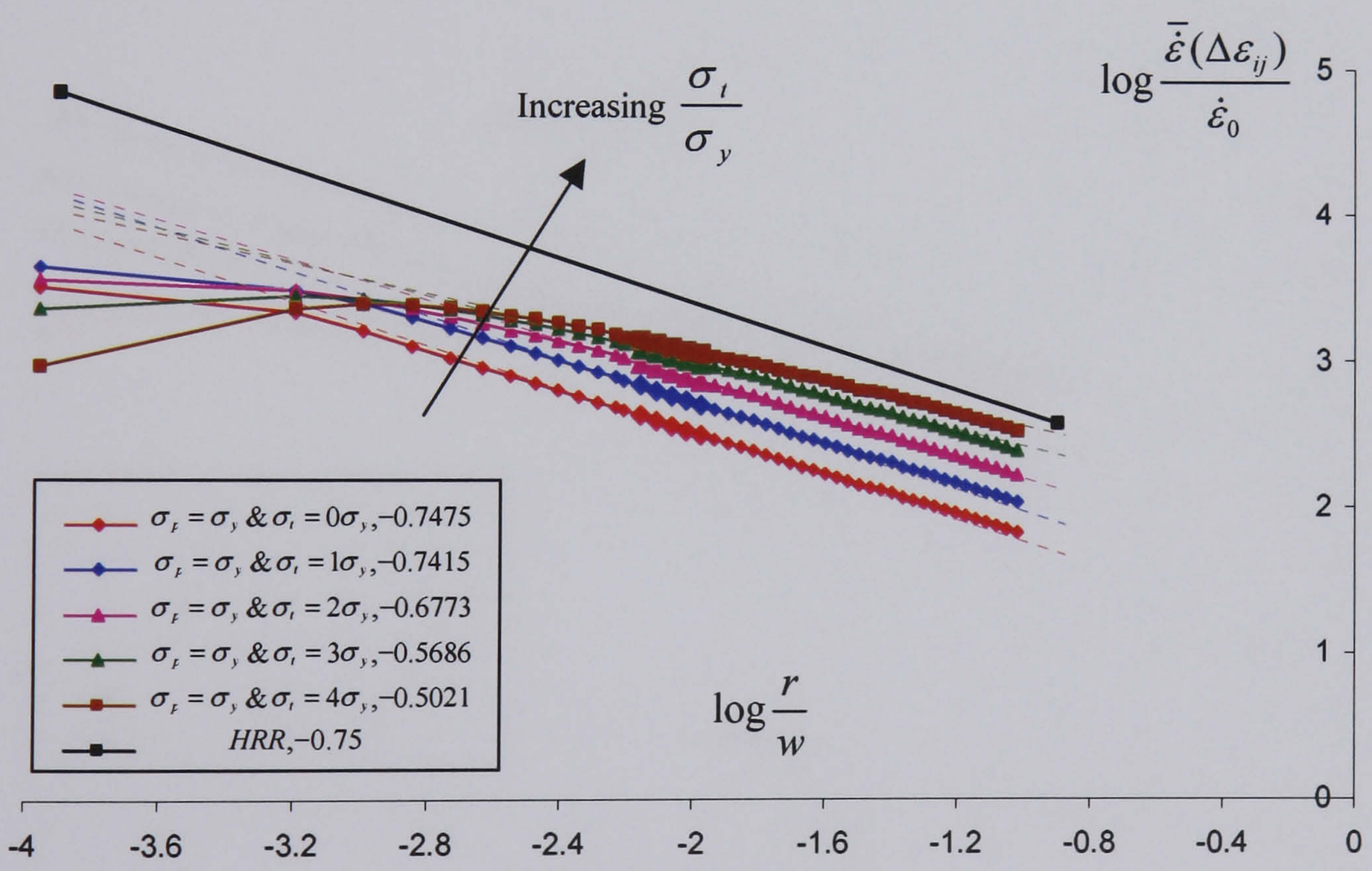

Bailey-Orowan model

Figure 4.8: Rapid cycle solutions for the different loading combinations of (σ_p, σ_t) at $n = 3$.

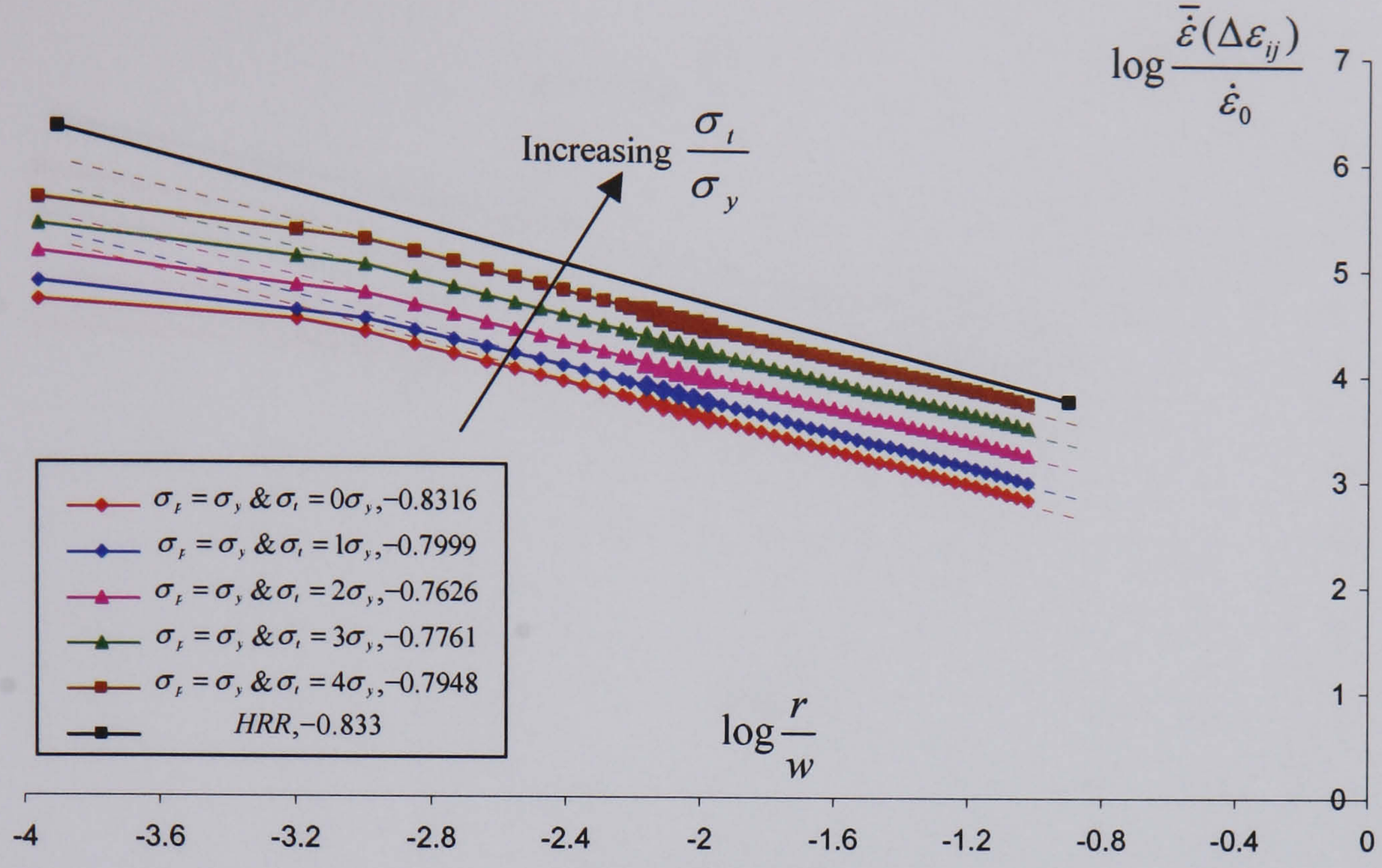

Norton's law model

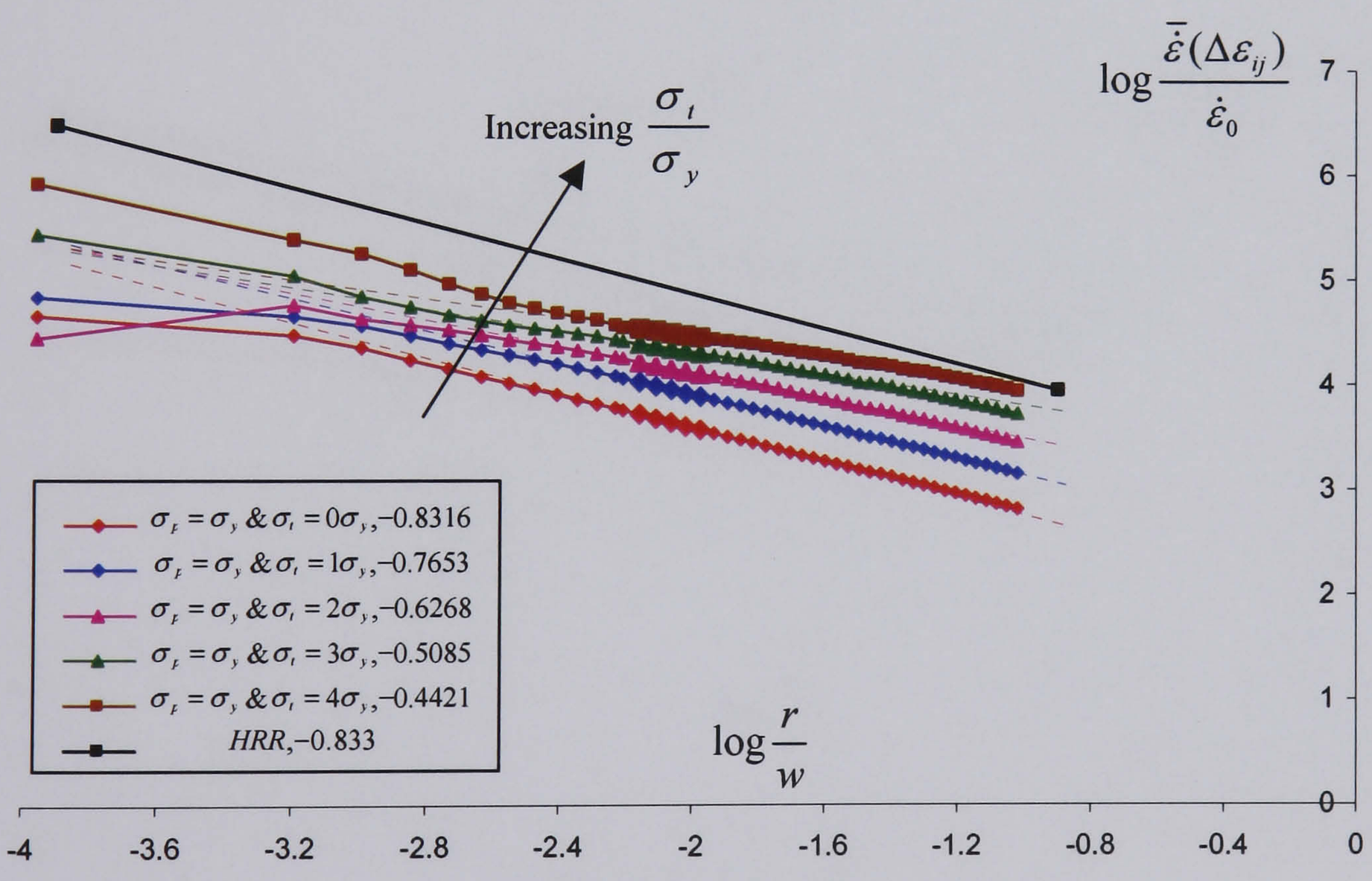

Bailey-Orowan model

Figure 4.9: Rapid cycle solutions for the different loading combinations of (σ_p, σ_t) at $n = 5$.

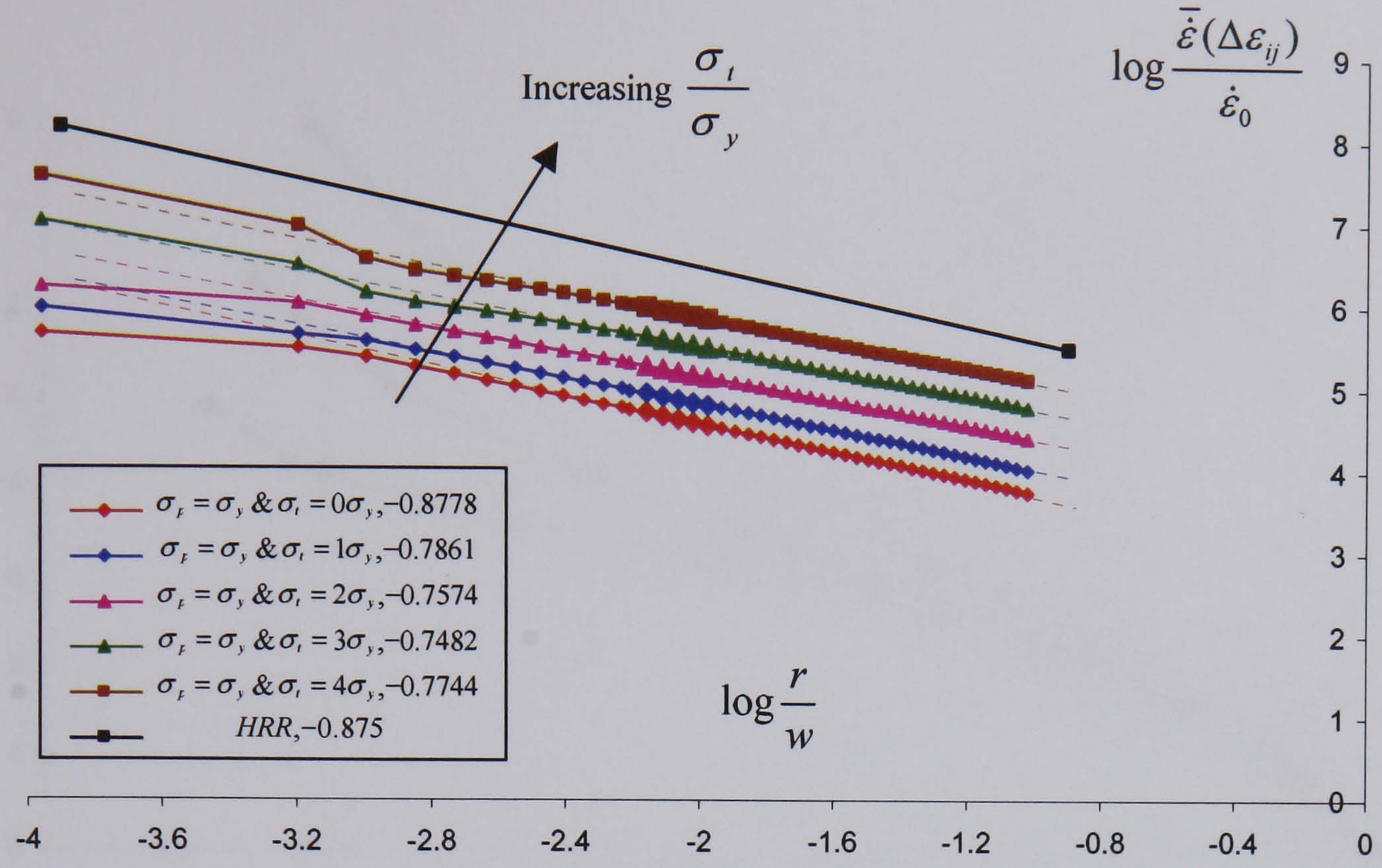

Norton's law model

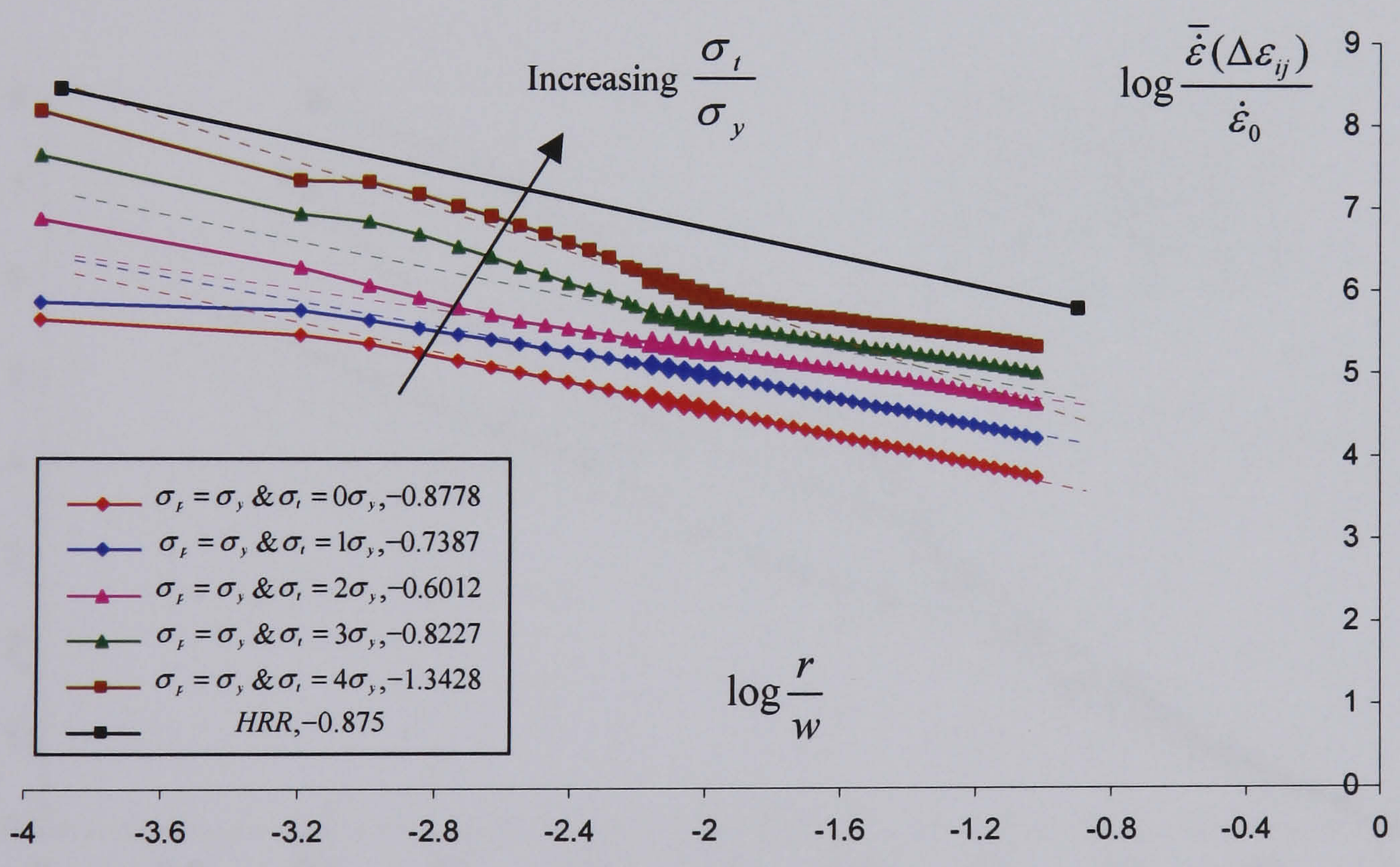

Bailey-Orowan model

Figure 4.10: Rapid cycle solutions for the different loading combinations of (σ_p, σ_t) at $n = 7$.

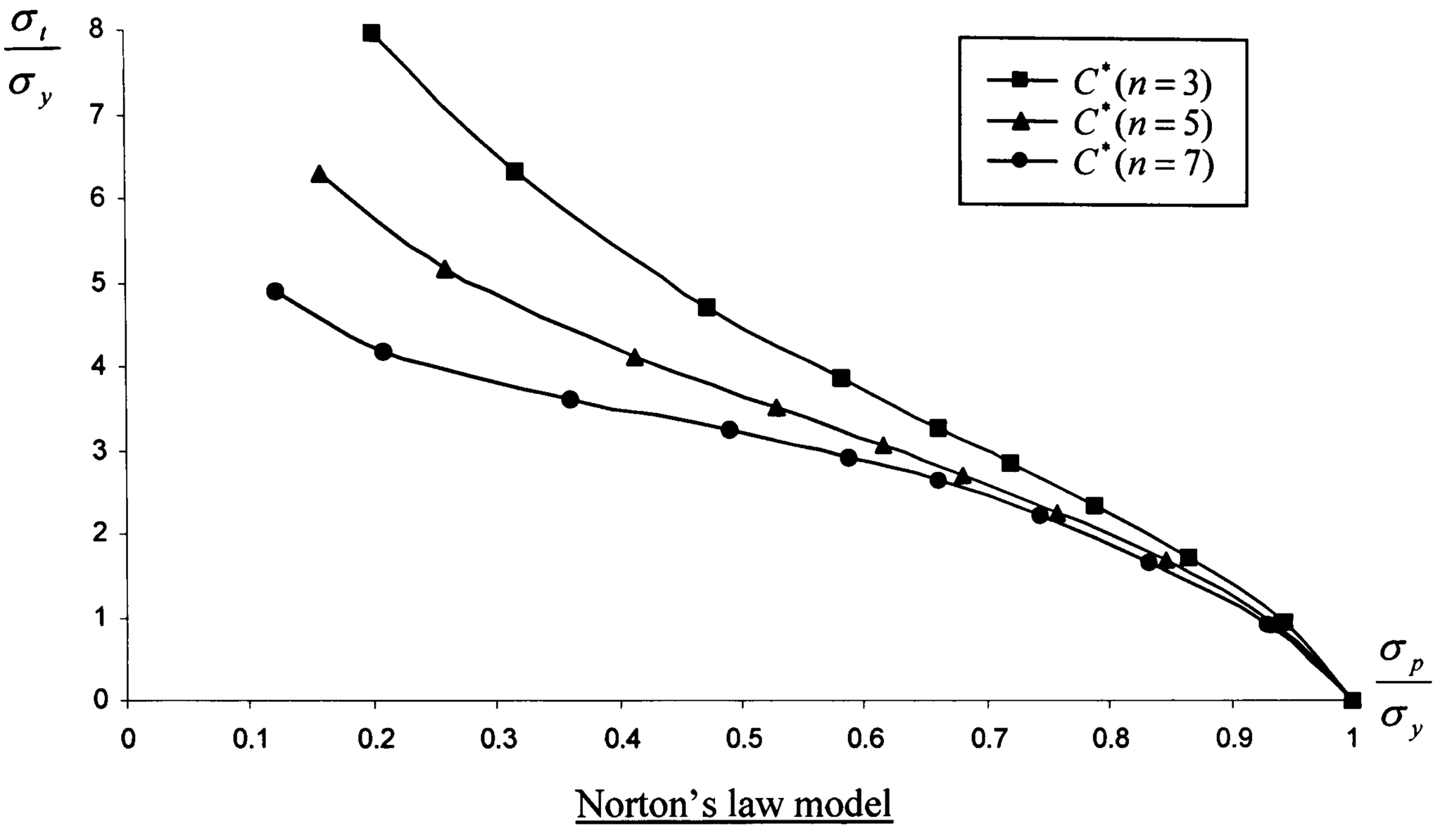

Norton's law model

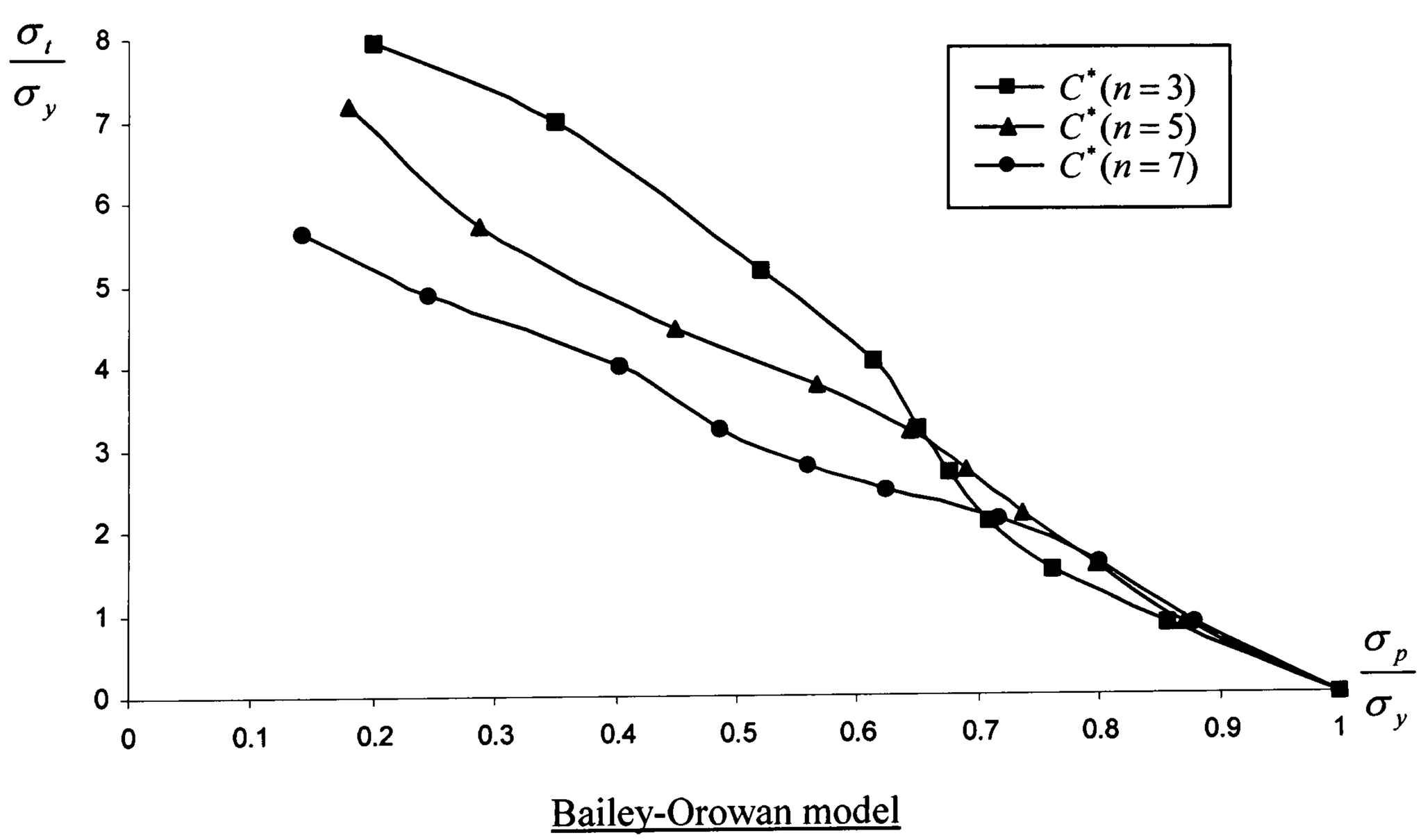

Bailey-Orowan model

Figure 4.11: Plot of contour of constant C^* for $n = 3,5 \& 7$.

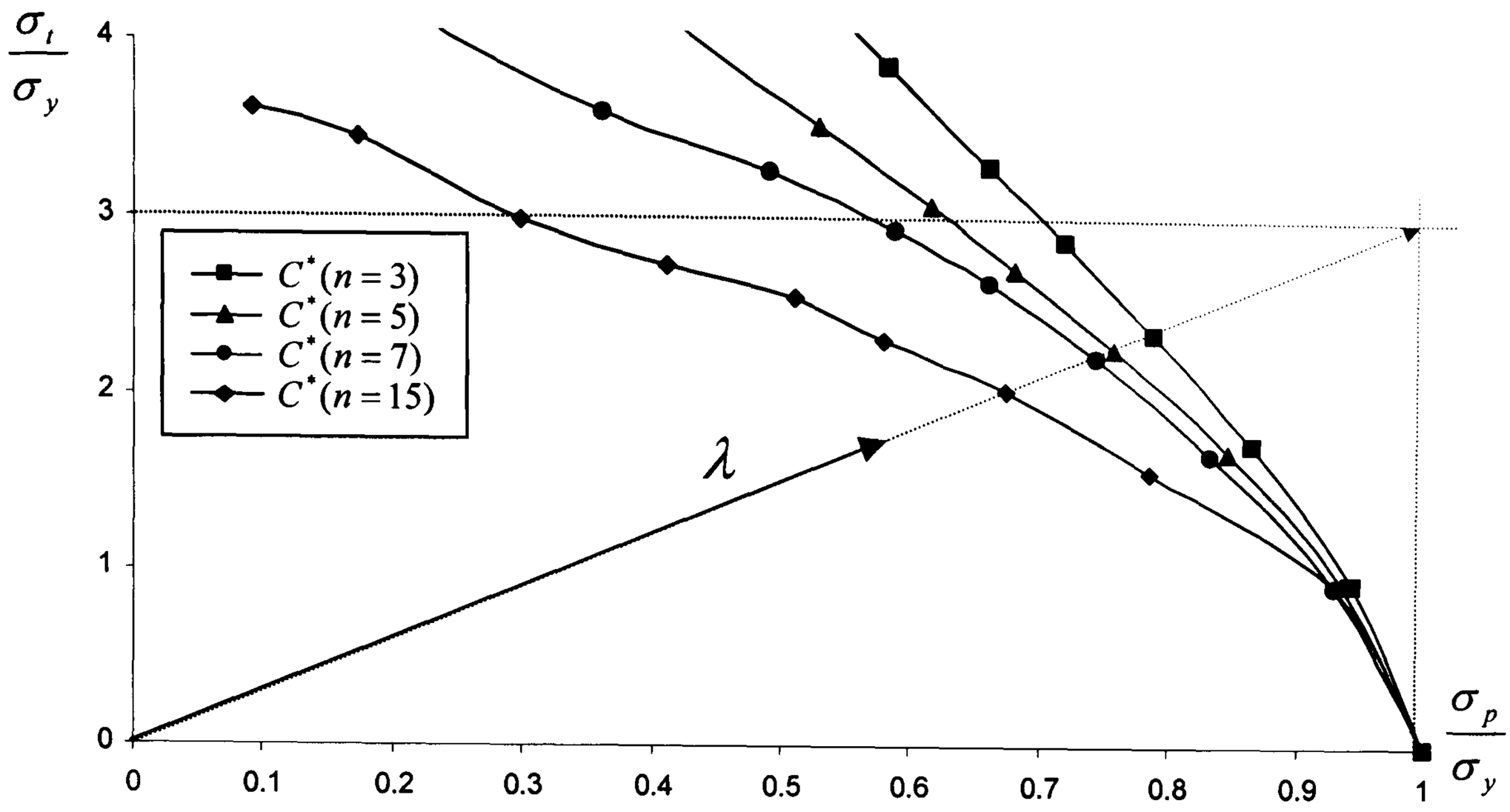

Contour of constant C^*

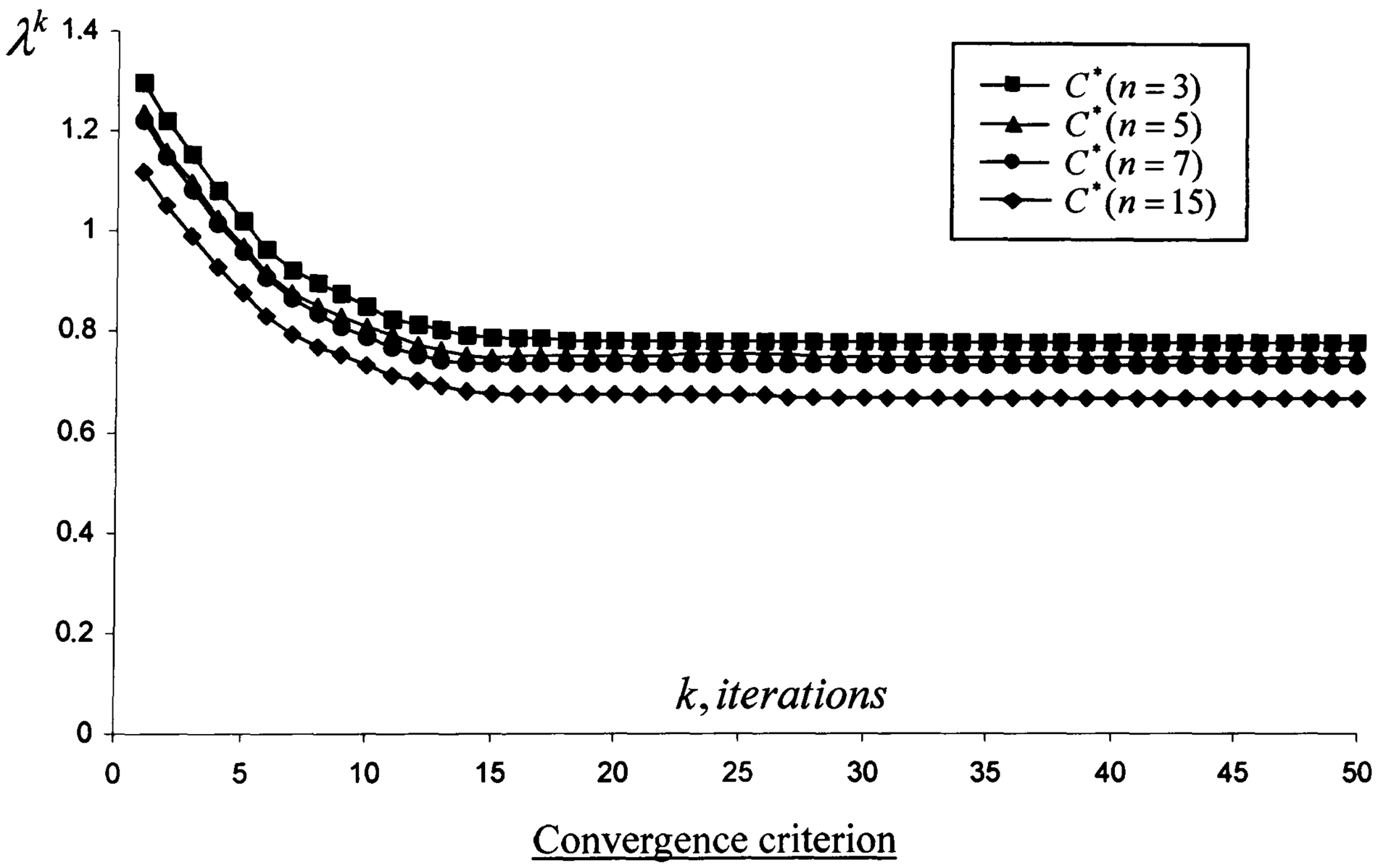

Convergence criterion

Figure 4.12: Comparison between the convergence criterions for the Norton's law model at $(\sigma_p = \sigma_y, \sigma_t = 3\sigma_y)$.

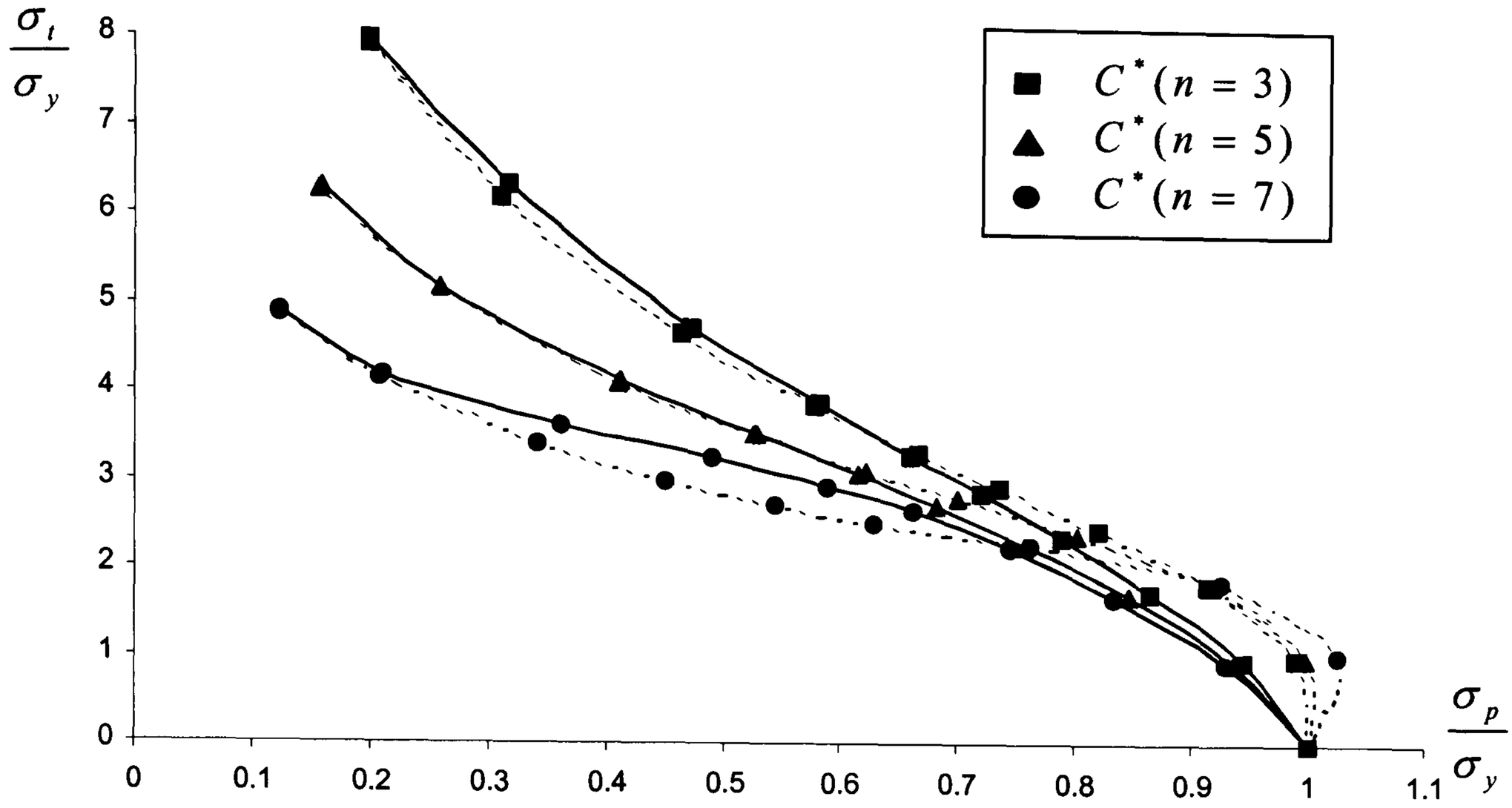

Norton's law model

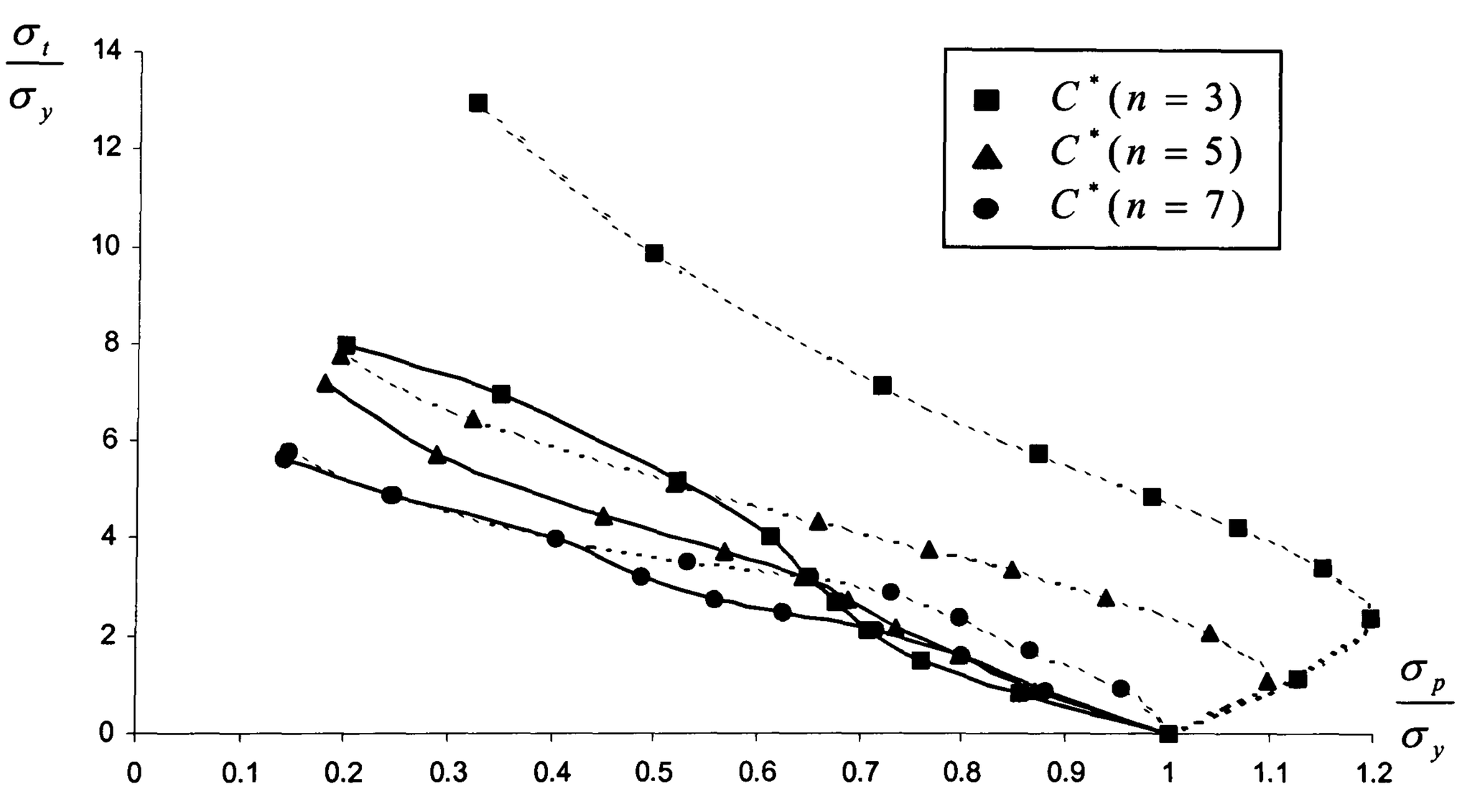

Bailey-Orowan model

Figure 4.13: Comparisons between contours of constant C^* for variations in the loading histories. (—σ_p =constant, ----σ_p =varying)

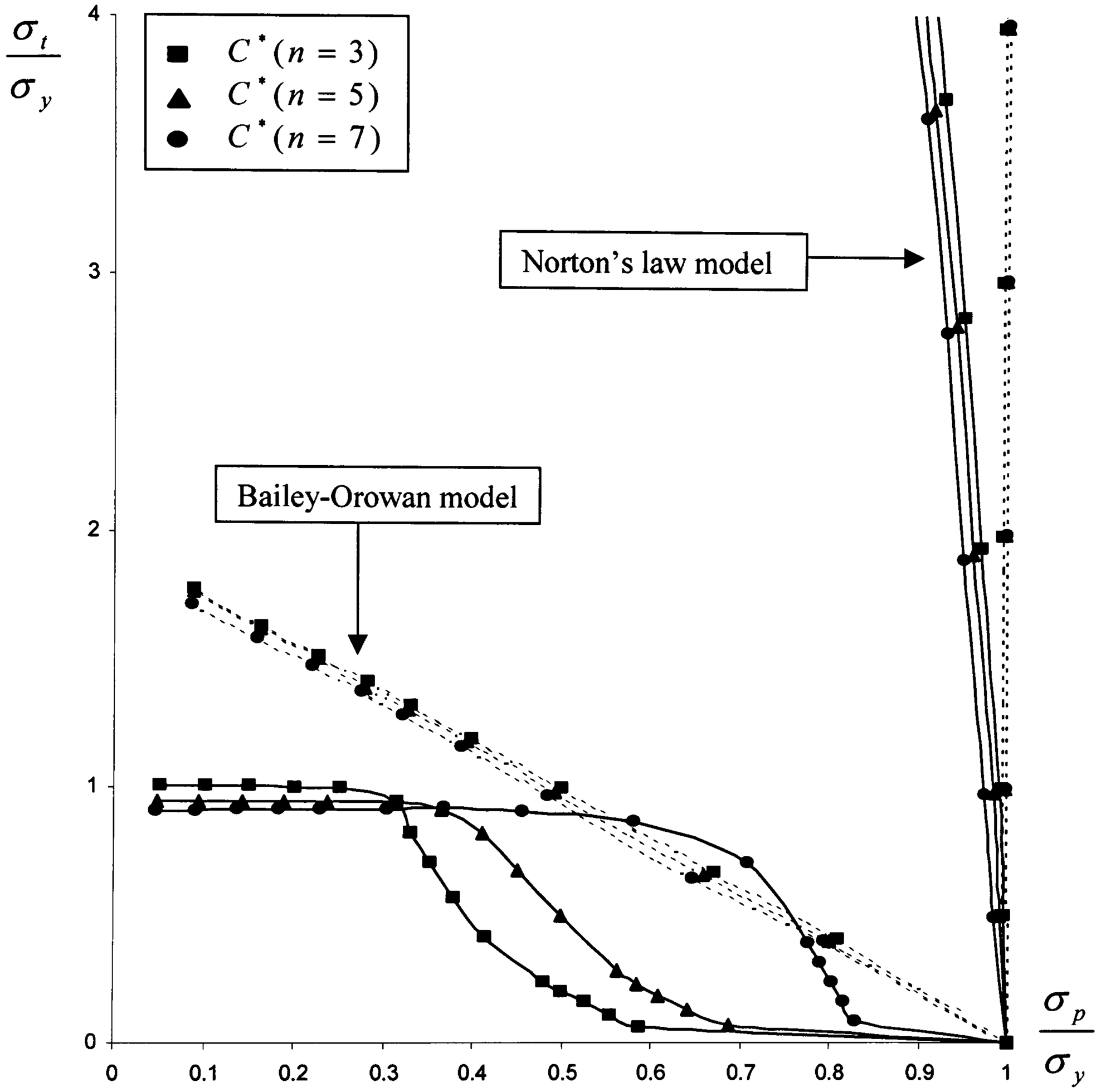

Figure 4.14: Comparisons between the plots of contours of constant C^* for both constitutive models with varying material properties.
(—σ_p = constant, ----σ_p = varying)

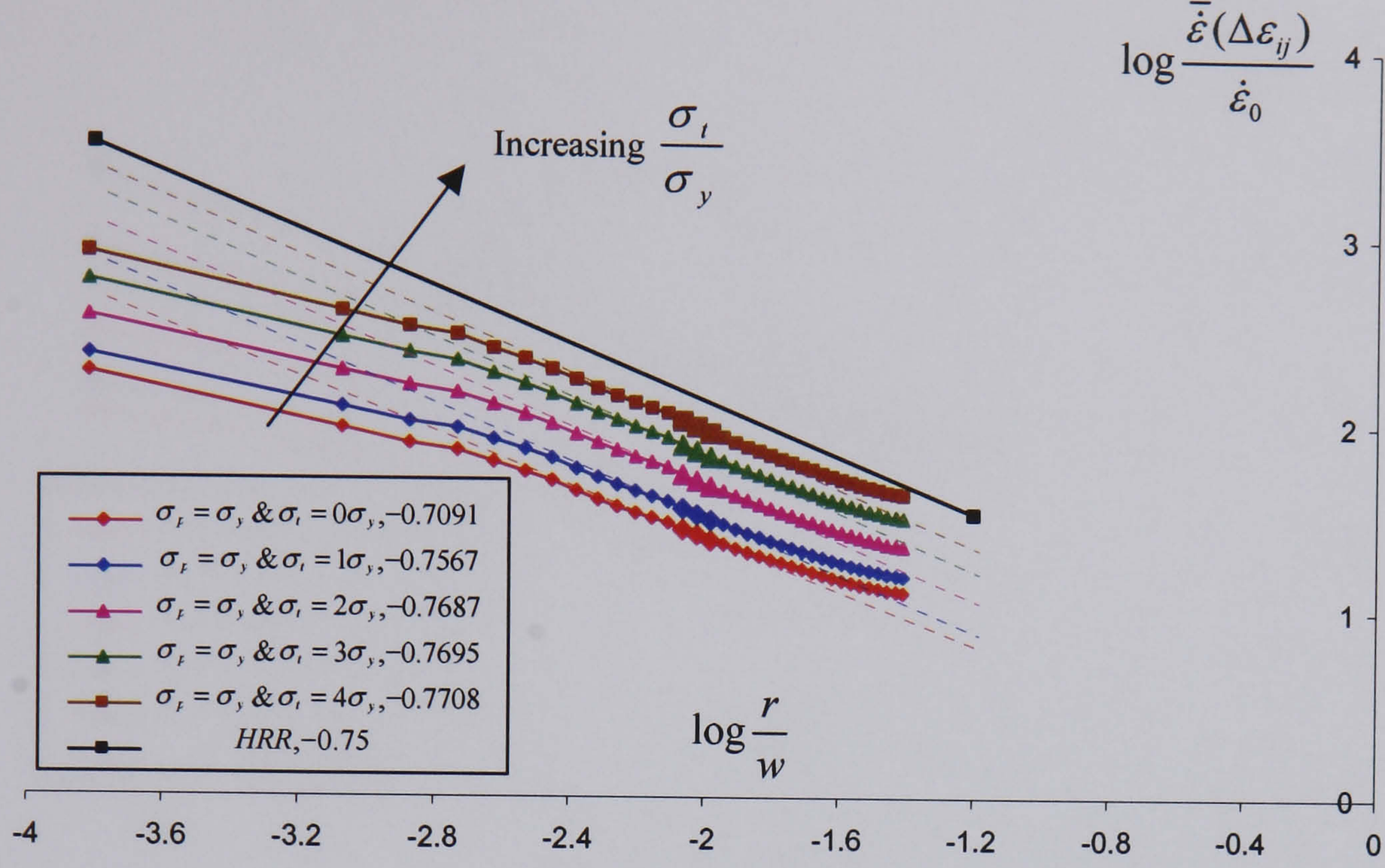

Norton's law model

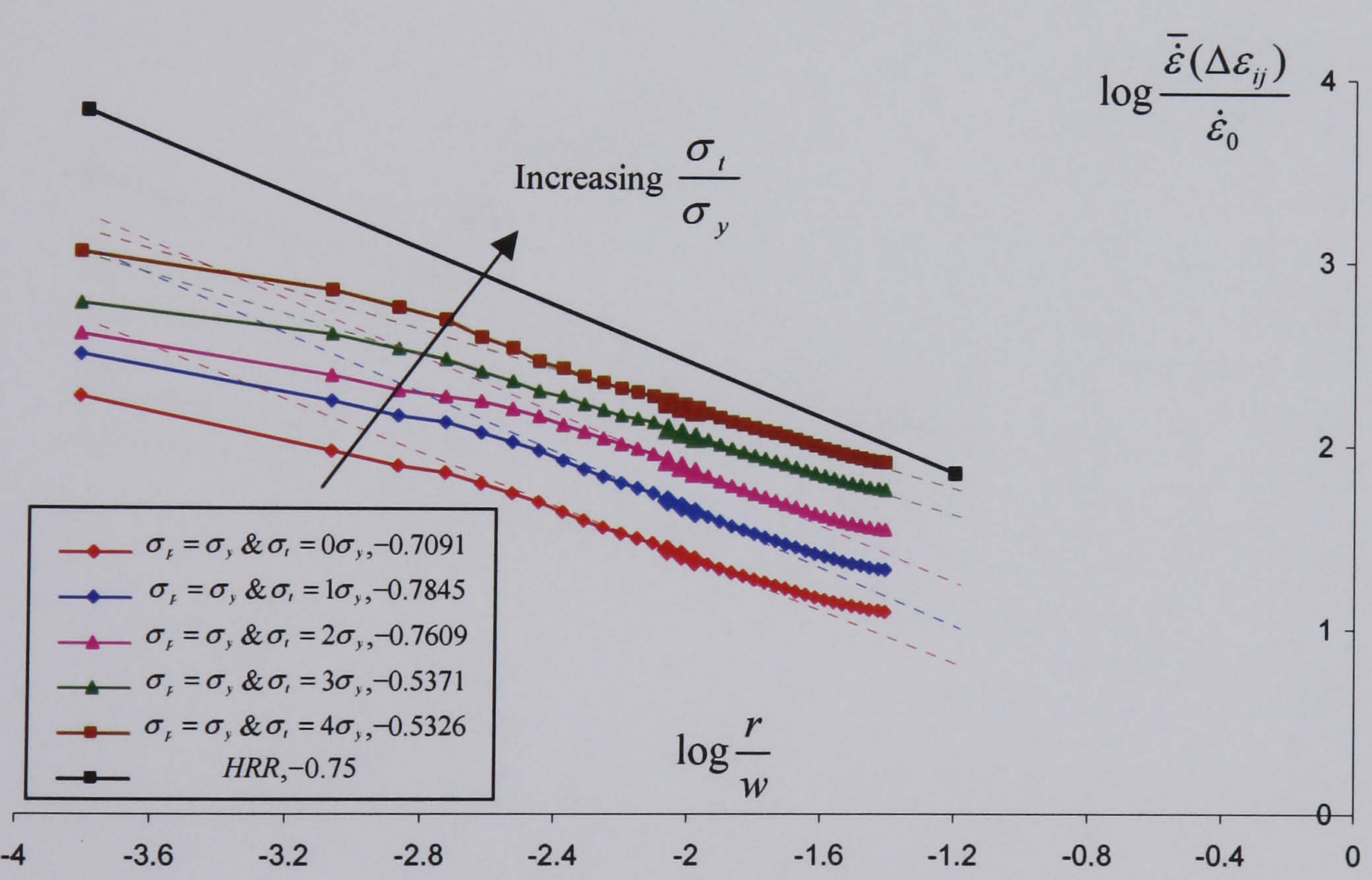

Bailey-Orowan model

Figure 4.15: Rapid cycle solutions for the different loading combinations of (σ_p, σ_t) at $n = 3$ for $\frac{a}{w} = 0.04$.

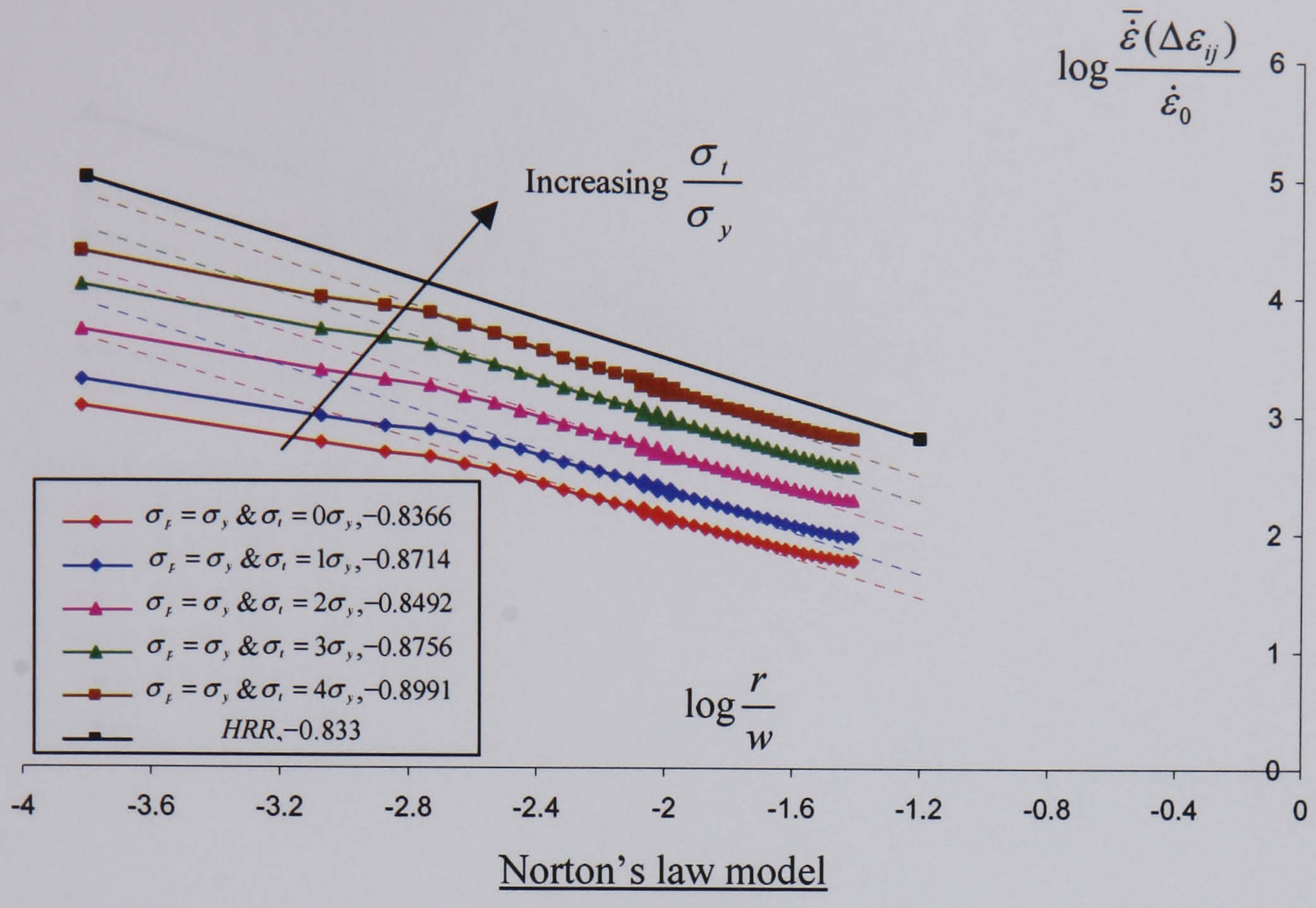

Norton's law model

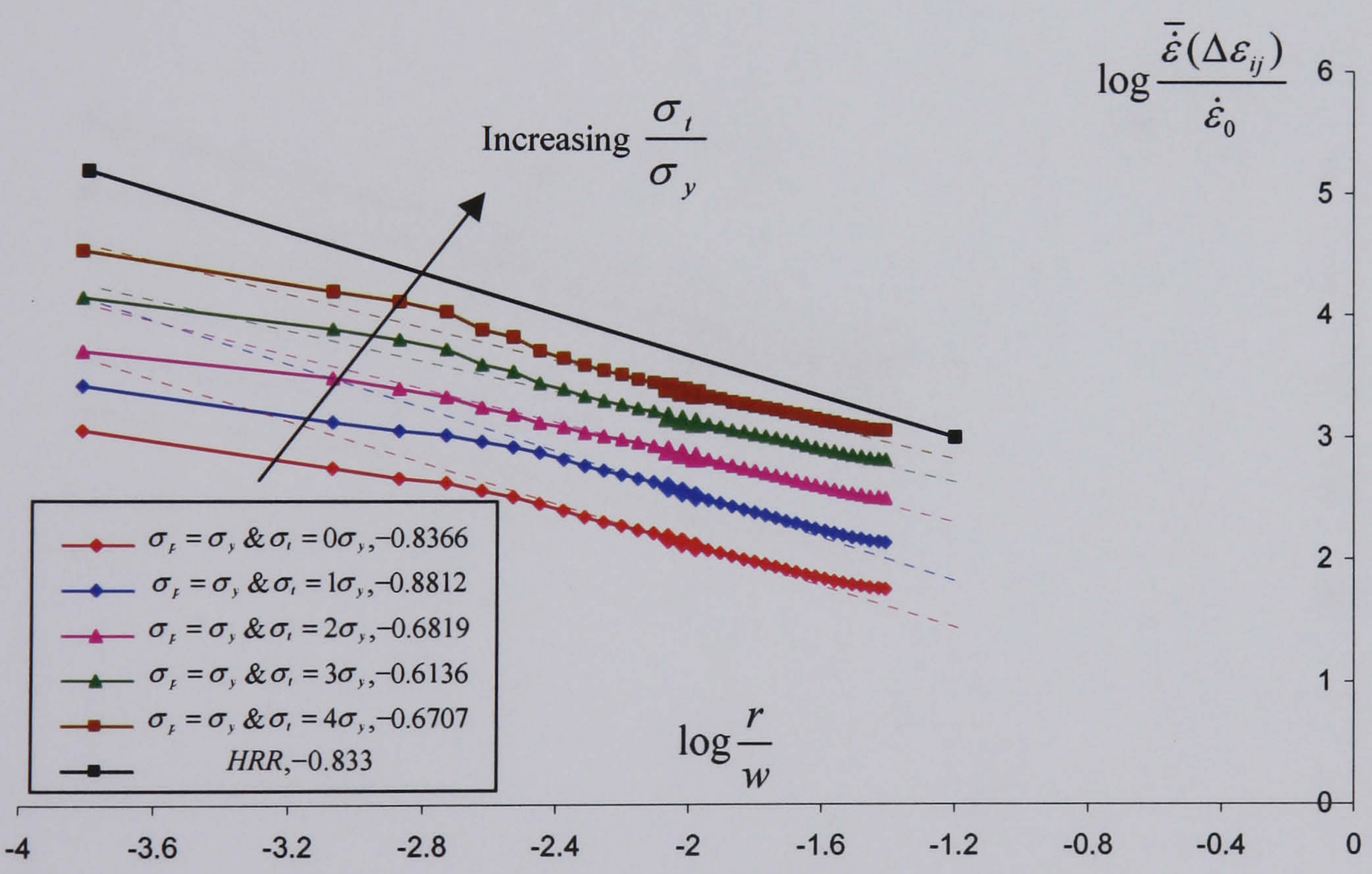

Bailey-Orowan model

Figure 4.16: Rapid cycle solutions for the different loading combinations of (σ_p, σ_t) at $n = 5$ for $\frac{a}{w} = 0.04$.

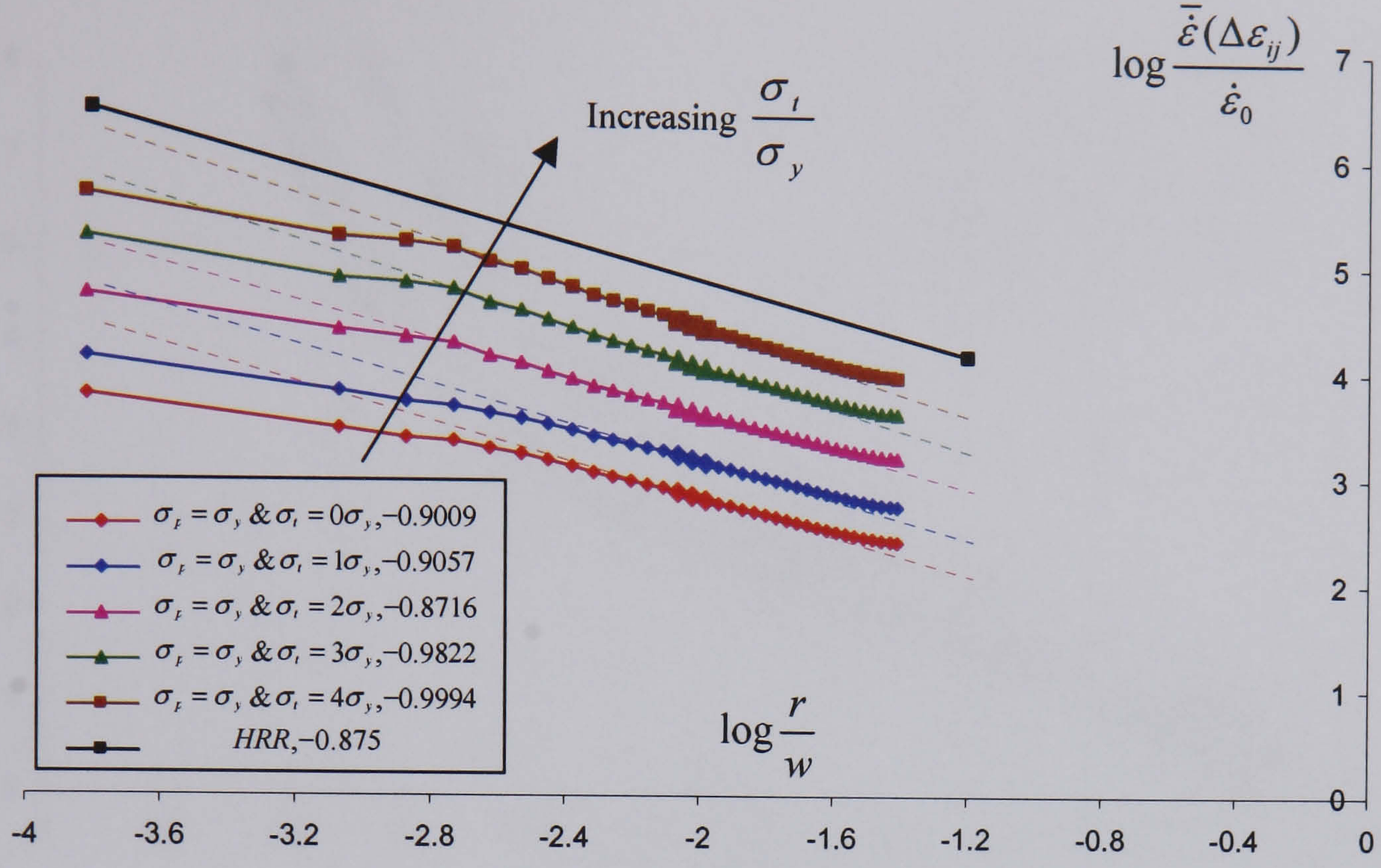

Norton's law model

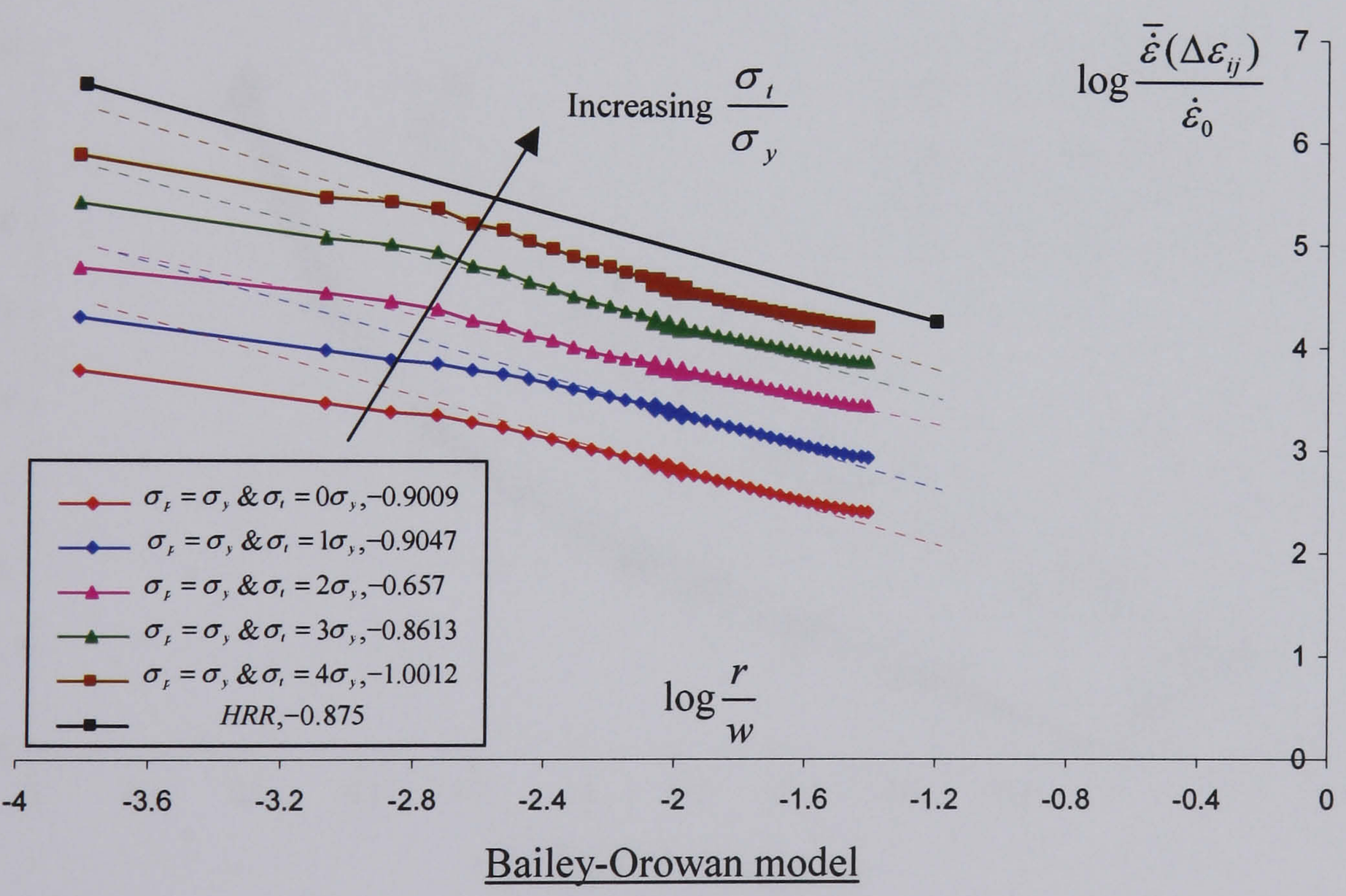

Bailey-Orowan model

Figure 4.17: Rapid cycle solutions for the different loading combinations of (σ_p, σ_t) at $n = 7$ for $\frac{a}{w} = 0.04$.

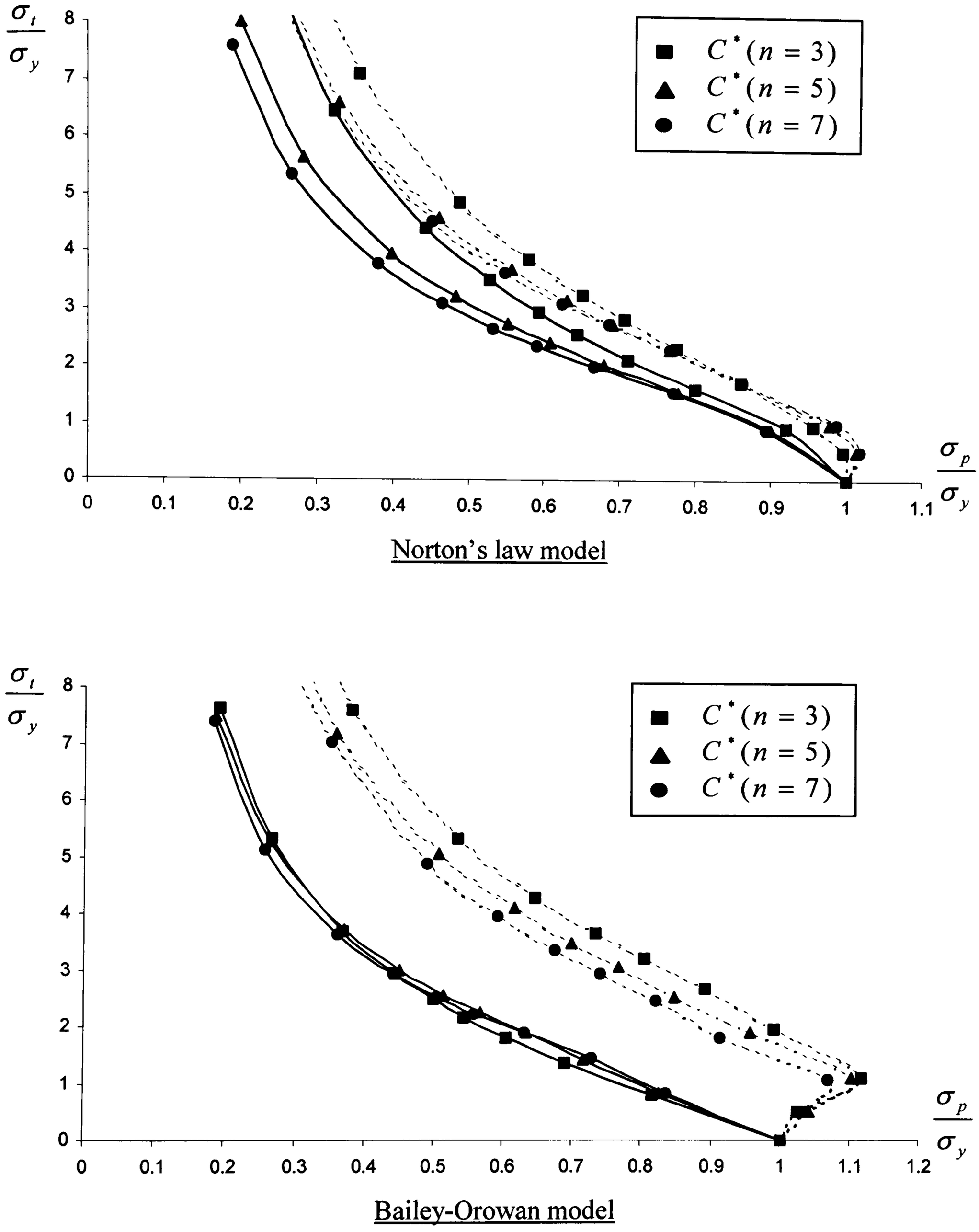

Figure 4.18: Contours of constant C^* for $\frac{a}{w} = 0.04$ under both loading conditions. (—σ_p = constant, ----σ_p = varying)

Chapter 5: Reference Stress Methods

5.1. Introduction

In the previous chapter, an investigation into the behaviour of the near crack tip fields, in cracked structures subjected to cyclic histories of loads and temperatures, was described. It was established that an accurate representation of the crack tip behaviour was possible, with the identification of the so-called best-matched HRR field. However, for such solutions to be useful, it needs to be represented in a form, independent of the loading histories, constitutive equations, creep exponents, *etc*. The designated quantity would then dictate the overall behaviour of the structure, enabling comparisons to be made with other known available solutions.

In representing the characteristics of these cracked structures, the term used is the reference stress [1,19]. It was initially developed as means of describing the creep deformation in steadily loaded structures for shell and beam problems [83,84]. The results from these structural geometries revealed that it is possible to relate the stress fields at $n=\infty$, to provide reliable estimates of work rates for lower values of n, where n is the creep exponent. Although initially conceived for a body deforming in steady state creep, the strong analogy between creeping and plastically deforming materials, as discussed previously, resulted in the general definition of the reference stress, in isothermally loaded structures, to be given by,

$$\sigma_{ref} = \frac{P}{P_L}\sigma_y \tag{5.1}$$

where P is the applied load and P_L is the plastic collapse load (limit load) corresponding to the uniaxial yield stress, σ_y. As the limit load is proportional to the yield stress, the value of σ_{ref} is, therefore, significantly dependent upon the accurate evaluations of these limit loads. This is one of the reasons behind the investigations, into the limit loads of cracked structures, undertaken in Chapter 2.

Continued research interest in this field is in the development of simplified methods for estimating the reference stress. Most of these methods are compromised between the pessimism of using elastic stress analysis and the cost and complexity associated with cyclic inelastic computation (step-by-step analysis). The simplified reference stress method [1,19] adopted here, describes the quantities of interest in a complex component, in terms of a reference stress and corresponding creep data at the reference stress level. Although, it was originally developed for describing the creep deformation in steadily loaded structures, the technique has since been extended to cover cyclic loadings, creep rupture and the effects of defects [83,85,86]. In most cases, this method was found to overestimate the stress levels in a component, with the ever-ready availability of detailed inelastic analysis computations, in situations requiring more accurate assessment.

In this chapter, the relevant concepts behind the reference stress method [1,19] are presented. Its initial application, on cracked structures in the presence of constant mechanical loads, is then demonstrated, allowing judgment on the accuracy of the previously calculated magnitudes of $C^*(n)$ to be made. This is then followed by an extension to this method, necessary in describing the behaviour of cracked structures subjected to both mechanical and

thermal loads. These solutions, when represented in terms of the effective reference stress, σ_{ref}^{eff}, provided a means of appraising current R5 [1] procedures, which treats the effect of thermal stress as an equivalent bending moment, under the various conditions considered in Chapter 4.

5.2. Simplified Reference Stress Method

The utilization of the reference stress method is initially described for the problem in Figure 4.3. It is for the cracked axisymmetric Bree problem, subjected to a constant uniaxial tension in the presence of varying temperature, with the material properties assumed to remain constant throughout the cycle, at ratio of $\frac{a}{w} = 0.4$.

5.2.1. Mechanical load

In the analysis of cracked structures under purely mechanical loads, the application of the simplified reference stress method [1,19] is based upon the notion that the steady state creep fracture mechanics parameter, $C^*(n)$, may be approximated by,

$$C^*(n) = \sigma_{ref} \dot{\varepsilon}_{ref} R' \tag{5.2}$$

where σ_{ref} is the reference stress defined by equation (5.1) and $\dot{\varepsilon}_{ref}$ is the creep strain rate at the reference stress, evaluated from,

$$\dot{\varepsilon}_{ref} = \left(\frac{\sigma_{ref}}{\sigma_0} \right)^n \dot{\varepsilon}_o \tag{5.3}$$

where $\dot{\varepsilon}_0$ and σ_0 are material constants. The characteristic length, $R^{'}$, used in equation (5.2), is given by,

$$R^{'} = \frac{K^2}{\sigma_{ref}^2} \tag{5.4}$$

where K is the stress intensity factor in linear elastic fracture mechanics. As both K and σ_{ref} are directly proportional to the applied load, P, the value of $R^{'}$ is, therefore, independent upon the magnitude of loads, but varies considerably with the crack size, a.

At this juncture, the above-mentioned sequence of equations allows the parameter $C^*(n)$ to be evaluated. These magnitudes, estimated in (5.2), were obtained, using the values of σ_{ref} and $R^{'}$ calculated in (5.1) and (5.4) respectively, which, in turn, are dependent upon the values of P_L and K. The implication of this procedure is the ability to now estimate $C^*(n)$, in any circumstances, as long as P_L and K are known. On top of that, the accuracy of $C^*(n)$ could also be assessed, by making comparisons between these approximations and those calculated in the previous chapter. These results are illustrated below.

The quantities required in performing such calculations, for the cracked axisymmetric Bree problems, associated with the two crack lengths considered, are shown in Figure 5.1. Also presented are the corresponding terms required for the cracked plane stress Bree

problems. In these plots, the values of the limit loads, P_L, were obtained from the numerical analyses conducted in Chapter 2, *i.e.* Figure 2.14, whilst the corresponding values of the stress intensity factors, K, were identified from the linear elastic stress solutions. The knowledge of these two parameters, thus, enabled the magnitudes of $C^*(n)$ to be evaluated, with the results from these two analyses, tabulated in Figure 5.2.

Two solutions were compared, namely C^*_{ref} and C^*_{cal}. The magnitudes of C^*_{ref} were evaluated using the prescribed procedures, *i.e.* substituting equations (5.1) and (5.4) into (5.2). The other magnitudes C^*_{cal} were those calculated in the previous chapter, whereby the magnitudes of $\bar{\dot{\varepsilon}}(\Delta\varepsilon_{ij})$ at the best-matched HRR field, is substituted into equation (4.27). The comparisons between these two solutions showed that irrespective of the types of analyses conducted or the sizes of the crack lengths considered, the values of C^*_{ref} were always larger than those of C^*_{cal}. This is not surprising as C^*_{ref} is an upper bound calculation [1,19], designed to overestimate the values of $C^*(n)$ calculated in cracked structures. The comparisons also revealed that the differences between C^*_{ref} and C^*_{cal} solutions rarely exceed a factor of 2. This feature in the solutions is of particular significance as it proves the accuracy of C^*_{cal} solutions. The availability of literatures indicating that the differences between C^*_{ref} and C^*_{cal} should not be more than 2 or 3 [19], as observed in the figure, justified the adopted approach of describing the crack tip conditions at the best-matched HRR field. Furthermore, the good correlations observed, also demonstrated the capability of the LMM-based methodologies in producing accurate and reliable results. (Note: The material properties used in this analysis are the same as those used before, *i.e.* $\dot{\varepsilon}_0 = 0.05/\text{h}$ and $\sigma_0 = 100\,\text{MPa}$).

5.2.2. Mechanical and thermal loads

In the event when both mechanical and thermal loads are considered, the definition of the reference stress in (5.1) is no longer appropriate. In accounting for such behaviour, the R5 [1] procedures currently employs a limit, identified using the assumption that the behaviour of thermally loaded structures is identical to those subjected to an equivalent bending moment, in the presence of the applied constant loads. In terms of thermal stresses, this limit can be expressed by,

$$\left(\frac{P}{P_L}\right)^2 + \frac{2}{3}\left(\frac{\sigma_t}{\sigma_y}\right) = 1 \qquad (5.5)$$

where the terms has the same meanings as before. In validating the above conjecture as well as the need in filling this void in the reference stress formulation, an extension of the reference stress method, applicable to both mechanical and thermal loads, is described below.

The procedure for the extended simplified reference stress method begins with initially identifying $C^*(1)$, *i.e.* $C^*(n)$ at $n=1$ from equation (5.2), yielding,

$$C^*(1) = \frac{\dot{\varepsilon}_o}{\sigma_o} K^2 \qquad (5.6)$$

which is only dependent upon the stress intensity factor, K. In this analysis, the values of K, required in equation (5.6), is obtained from the linear elastic stress solutions, evaluated at the

previously identified sampling point, $\theta = 70^0$ and $r = 0.00865w$, within the best-matched HRR field, from,

$$\bar{\sigma}(\sigma_{ij}) = \frac{K}{\sqrt{2\pi r}} \bar{f}(f_{ij}(\theta)) = E\bar{\dot{\varepsilon}}(\Delta\varepsilon_{ij}) \tag{5.7}$$

where $E = \frac{\sigma_o}{\dot{\varepsilon}_o}$. The identification of K, thus, requires re-running the numerical procedures for the rapid cycle creep solutions at $n = 1$, for both Norton's law and the Bailey Orowan model presented in Figures 4.1 and 4.2 respectively. The values of $\bar{\dot{\varepsilon}}(\Delta\varepsilon_{ij})$, obtained at the sampling point, is then substituted into equation (5.7), where K is computed, enabling $C^*(1)$ to be evaluated in equation (5.6).

Under both mechanical and thermal loads, the values of $C^*(1)$, evaluated in equation (5.6), may then be identified as having an effective K value, which will be dependent upon both the loading conditions and the constitutive equations, provided the strain distribution at the crack tip is identical. This is clearly observed in Figure 5.3, the additional $\bar{\dot{\varepsilon}}(\Delta\varepsilon_{ij})$ plots at $n = 1$, for the deep cracked axisymmetric Bree problem. In both constitutive models, the variations of the effective accumulated creep strain rate still show good correlations with the HRR field condition of (4.26). The necessary satisfaction of this condition, thus, enables $C^*(1)$ to be evaluated from (5.6), in conjunction with (5.7). The important thing to note out of these additional solutions is the differing behaviours the two constitutive equations exhibits, with respect to changes in σ_t. For Norton's law, $C^*(1)$ is virtually independent of σ_t, whereas in the Bailey Orowan relationship, $C^*(1)$ increases with increasing σ_t.

The above arguments provided a means of defining a reference stress, valid in structures subjected to both mechanical and thermal loads. It involves substituting equation (5.6) into (5.2), and upon re-arranging the terms; a newly defined reference stress is obtained, as given by the following expression,

$$\sigma_{ref} = \left(\frac{C^*(n)}{C^*(1)} \sigma_0^{n-1} \right)^{\frac{1}{n-1}} \tag{5.8}$$

In the analyses, it was found that equation (5.8) is a much more convenient form of writing the reference stress. Thus, using this definition, the values of σ_{ref} were then evaluated, for the different combinations of (σ_p, σ_t), using the calculated values of $C^*(n)$ at $n = 3,5\,\&\,7$ from the previous chapter and $C^*(1)$ from equation (5.6). A relationship, similar to those described in Figure 4.7, was then derived for identifying contours of constant σ_{ref},

$$\lambda = \left(\frac{\sigma_{ref}^{(\sigma_p=\sigma_y, \sigma_t=0)}}{\sigma_{ref}^{(x,y)}} \right) \tag{5.9}$$

where $\sigma_{ref}^{(\sigma_p=\sigma_y, \sigma_t=0)}$ is the reference stress at purely mechanical loads and $\sigma_{ref}^{(x,y)}$ are reference stresses at the different combinations of mechanical and thermal loads. This allowed plots of contours of constant σ_{ref} to be identified, in both models, as shown in Figure 5.4.

The reference stress solutions in the aforementioned figure shows a dependency upon the creep exponents, n, and the two constitutive equations used, *i.e.* Norton's law and the

Bailey Orowan model. The reason for this disagreement was understood by plotting the equation,

$$(n-1)\log\sigma_{ref} = \log\left(\frac{C^*(n)}{C^*(1)}\sigma_0^{n-1}\right) \tag{5.10}$$

at the different loading combinations, as shown in Figures 5.5 and 5.6. For the reference stress to be $n-$independent, the plots have to display straight lines that intercept the $y-$axis at zero. However, in these solutions, it clearly shows that in both models, this is not the case. The primary deviation is due to the good straight lines passing through the values of $C^*(3)$, $C^*(5)$ and $C^*(7)$, but not passing through the origin, *i.e.* the primary difficulty is the value of $C^*(1)$. Nevertheless, it is still possible to obtain an $n-$independent σ_{ref}, provided the calculated values of $C^*(1)$ is now replaced by the effective values, $C^*_{eff}(1)$, *i.e.* the values extrapolated off the straight lines. With this change, the pursuit for an $n-$independent σ_{ref}, represented by σ^{eff}_{ref}, was realized. This is shown in Figure 5.7, as plots of contours of constant σ^{eff}_{ref}, for both models. The contours generated were found to be not only independent of the creep exponents, n, but insensitive to the constitutive equations as well.

Numerically, the implication of $C^*_{eff}(1)$ is that it varies with σ_t and between the two material descriptions. The physical significance of $C^*_{eff}(1)$ could be understood by calculating an equivalent K_{eff} value from equation (5.6). This enables three different definitions of K values to be evaluated and compared, namely,

- K_{cal} - Evaluated from the calculated value of $C^*(1)$ using equation (5.6).
- K_{eff} - Evaluated from the effective value of $C^*_{eff}(1)$ using equation (5.6).
- K_{elas} - Evaluated using linear superposition from,

$$K_{elas} = K^P_{elas} + K^\theta_{elas} \tag{5.11}$$

where K^P_{elas} and K^θ_{elas} are the stress intensity factors associated with the mechanical and thermal loads respectively, obtained from the linear elastic stress solutions. These K values were then compared in Figure 5.7, for both models, normalised with respect to, $K_{norm} = \sigma_p \sqrt{a}$. The results shows that the largest value of K is given by those evaluated through linear superposition, $K = K_{elas}$, whereas the effective values, $K = K_{eff}$, were observed to be generally greater than those directly computed values, $K = K_{cal}$. Thus, the appropriate K values are those bounded between the upper bound of $K = K_{elas}$ and the lower bound of $K = K_{cal}$.

Figure 5.7 also revealed the conservative nature of current design rules and life assessment procedures [1], in accounting for the high temperature response of cracked structures in cyclic creep loading conditions. In comparison with the σ^{eff}_{ref} solutions, the non-compliance of the deduction used in generating the R5 [1] limit, which treats thermal stresses as equivalent bending moments, is apparent. The solutions from the employed extended reference stress method clearly showed that the R5 solution is conservative by a factor of 2. This conclusion is justified, on the basis of the two different constitutive models, Norton's law and the Bailey Orowan model, presenting virtually matching solutions.

5.3. Other Circumstances

The procedures for the extended reference stress method were then applied to other cases considered in Chapter 4. Figure 5.8 shows the solutions for the cracked axisymmetric Bree problem at $\frac{a}{w} = 0.04$. The results still shows that the R5 limit is conservative, even more so in this situation. The insensitivities of the reference stress solutions to the constitutive equations were also observed. Also evident is the almost identical solutions the contours of constant σ_{ref}^{eff} shows with respect to the ratchet limit. In terms of K, the overestimation of K_{elas} is still exhibited, with the values of K_{cal} providing a lower limit at the other extreme. As before, the effective values, denoted by K_{eff}, were found to lie in between these two evaluations. The behaviour of these solutions was further reinforced with corresponding solutions obtained for the cracked plane stress Bree plate problem. These additional plots are shown in Figures 5.9 and 5.10, for the crack lengths of $\frac{a}{w} = 0.4$ and $\frac{a}{w} = 0.04$ respectively. Irrespective of the crack lengths considered, it was found that the contours of constant σ_{ref}^{eff} seemed to reproduce the solutions observed in the corresponding cracked axisymmetric analyses. This is also mirrored in the way the values of K were displayed. More importantly, the results gave the impression that, in terms of reference stress quantities, the behaviour of cracked structures under cyclic loading histories, are generally independent of the structural geometry, *i.e.* plane stress and axisymmetric.

The reference stress solutions, for the cracked axisymmetric and plane stress Bree problems, subjected to varying mechanical loads in the presence of thermal loads, were also evaluated. These are shown in Figures 5.11 and 5.12, in comparison with previous solutions whereby the mechanical loads remained constant. For the most part, much higher σ_{ref}^{eff} limits were obtained, which is not surprising as the loading conditions are not as intense as before. The exception is for the cracked axisymmetric problem at $\frac{a}{w} = 0.4$, which shows almost identical contours. This particular result points to the direction that, in deep cracks, there is a cut-off limit occurring at $\sigma_t \approx 3\sigma_y$. In short cracks, the corresponding maximum limit was observed at $\sigma_t \approx 6\sigma_y$.

5.4. Concluding Remarks

The calculations, in Chapter 4 and 5, demonstrated that it is possible to obtain crack tip parameters, equivalent to $C^*(n)$, for cracked structures subjected to both mechanical loads and temperatures. The procedure requires the identification of increments of strain over a cycle of loading that varies radially from the crack tip, in the same way as the HRR field. It was shown, in Chapter 4, that the adopted rapid cycle creep solutions for the two constitutive equations, Norton's law and the Bailey-Orowan model, yield the same steady state creep behaviour. This led to the reproduction of the HRR field gradients in both cases. Under the effect of variable temperatures, however, the rapid cycle creep solutions tend to yield an upper bound to the creep deformation rates. This implies that the computed values may, hence, be regarded as conservative for finite cycle times.

In this chapter, the calculated values of $C^*(n)$ were then interpreted in terms of a reference stress, independent of the creep index, n. To obtain a consistent definition of a reference stress, it was found necessary to replace the computed values of $C^*(n)$ at $n=1$, by an effective value, extrapolated from the values of $C^*(n)$ at $n=3,5\,\&\,7$. With this modification, it was shown to be possible to define reference stress values that are insensitive to n and the constitutive equations. Although, the effective values $C^*(n)$ at $n=1$ shows some variation between the constitutive equations, these may be overestimated by a linear combination of the values for load and temperature, calculated separately. For the problem considered, a part through cracked cylinder subjected to axial load and radial temperature gradient, the values of the effective stress calculated in this way indicate that, for thermal loading problems, the reference stress method described in R5 may be conservative by a factor of about 2. This result also applies if the geometry is reinterpreted as a plane stress problem.

These encouraging results indicated that a more rational approach to crack tip properties under cyclic creep loading conditions is possible, by the methodology described in these two chapters. Although successful in the problems examined, there is clearly a need to investigate the behaviour of the crack tip fields under more carefully defined geometries, material properties, thermal transients conditions, *etc*, before general conclusions can be reached on the appropriateness of current R5 [1] procedures.

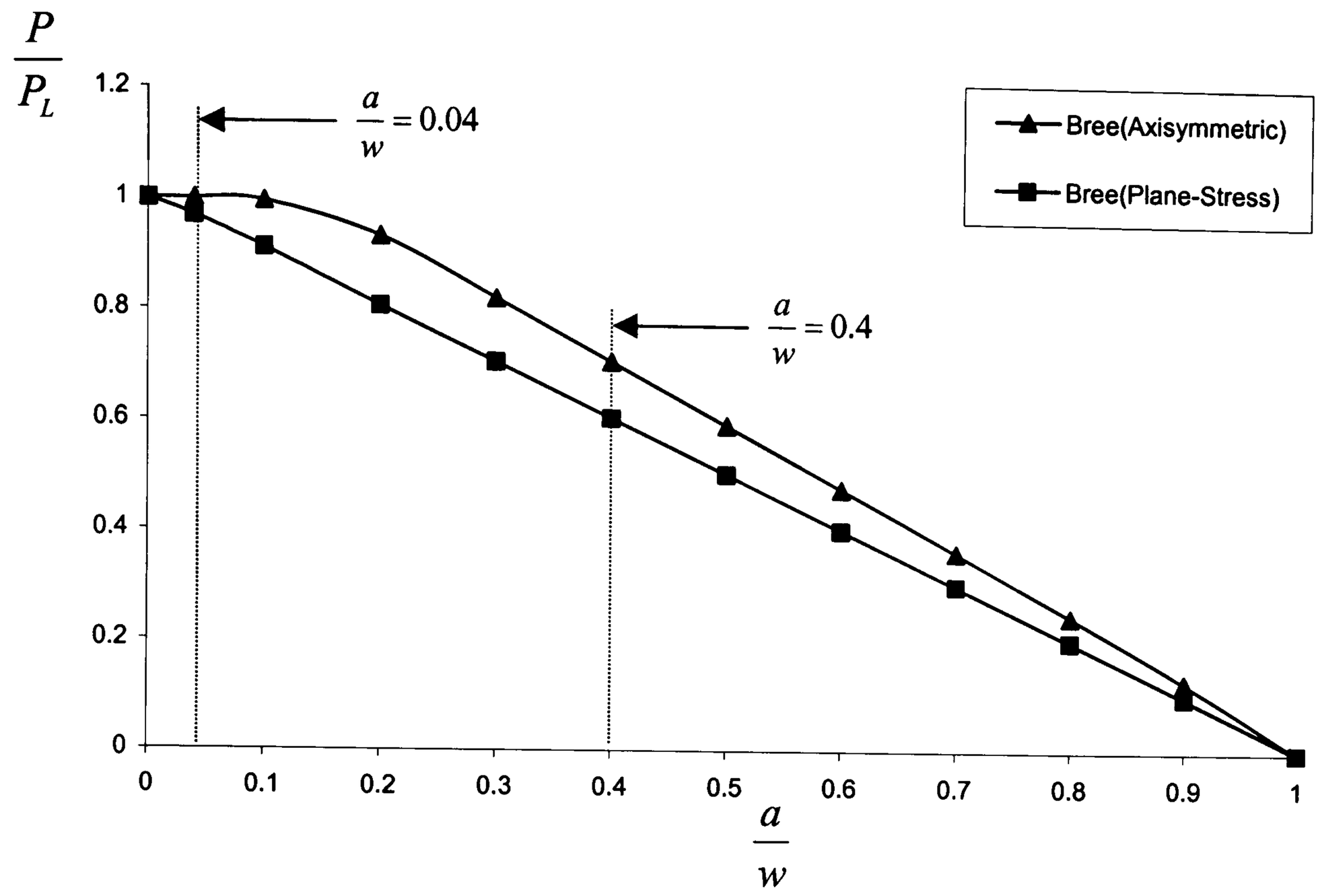

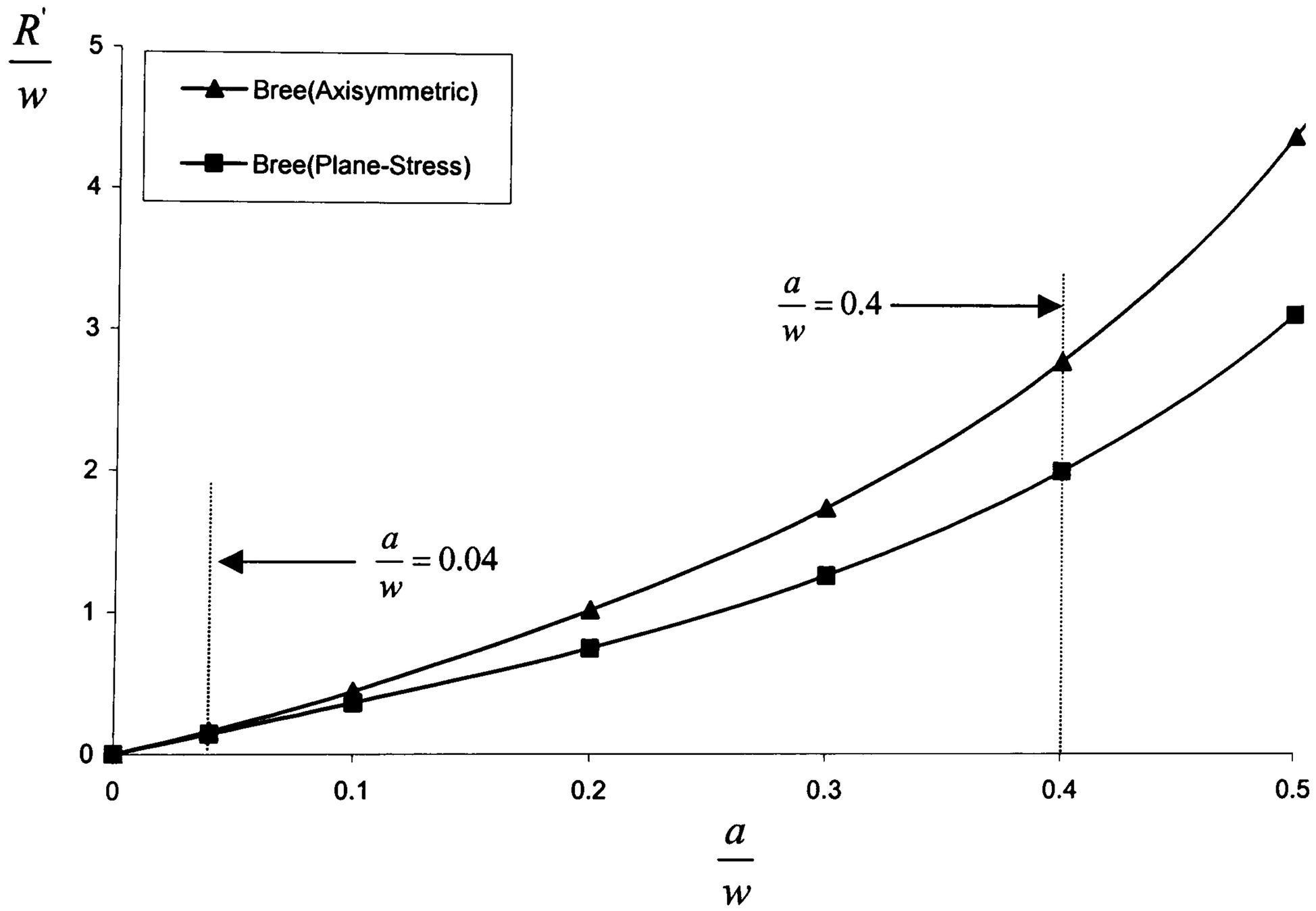

Figure 5.1: Differences between the axisymmetric and plane stress analyses.

	$C^*_{ref}\ (MPamh^{-1})$			$C^*_{cal}\ (MPamh^{-1})$		
Bree	**n=3**	**n=5**	**n=7**	**n=3**	**n=5**	**n=7**
Plane Stress	6018	65709	717360	2539	33908	344435
Axisymmetric	4470	35720	285441	4088	30869	243248

Results for $\frac{a}{w} = 0.4$

	$C^*_{ref}\ (MPamh^{-1})$			$C^*_{cal}\ (MPamh^{-1})$		
Bree	**n=3**	**n=5**	**n=7**	**n=3**	**n=5**	**n=7**
Plane Stress	66	280	1198	53	258	1088
Axisymmetric	65	262	1050	52	242	995

Results for $\frac{a}{w} = 0.04$

Figure 5.2: Comparisons between the different values of $C^*(n)$.
(C^*_{ref} - Reference stress estimates of $C^*(n)$ from equation (5.2),
C^*_{cal} - Calculated values of $C^*(n)$ from equation (4.27))

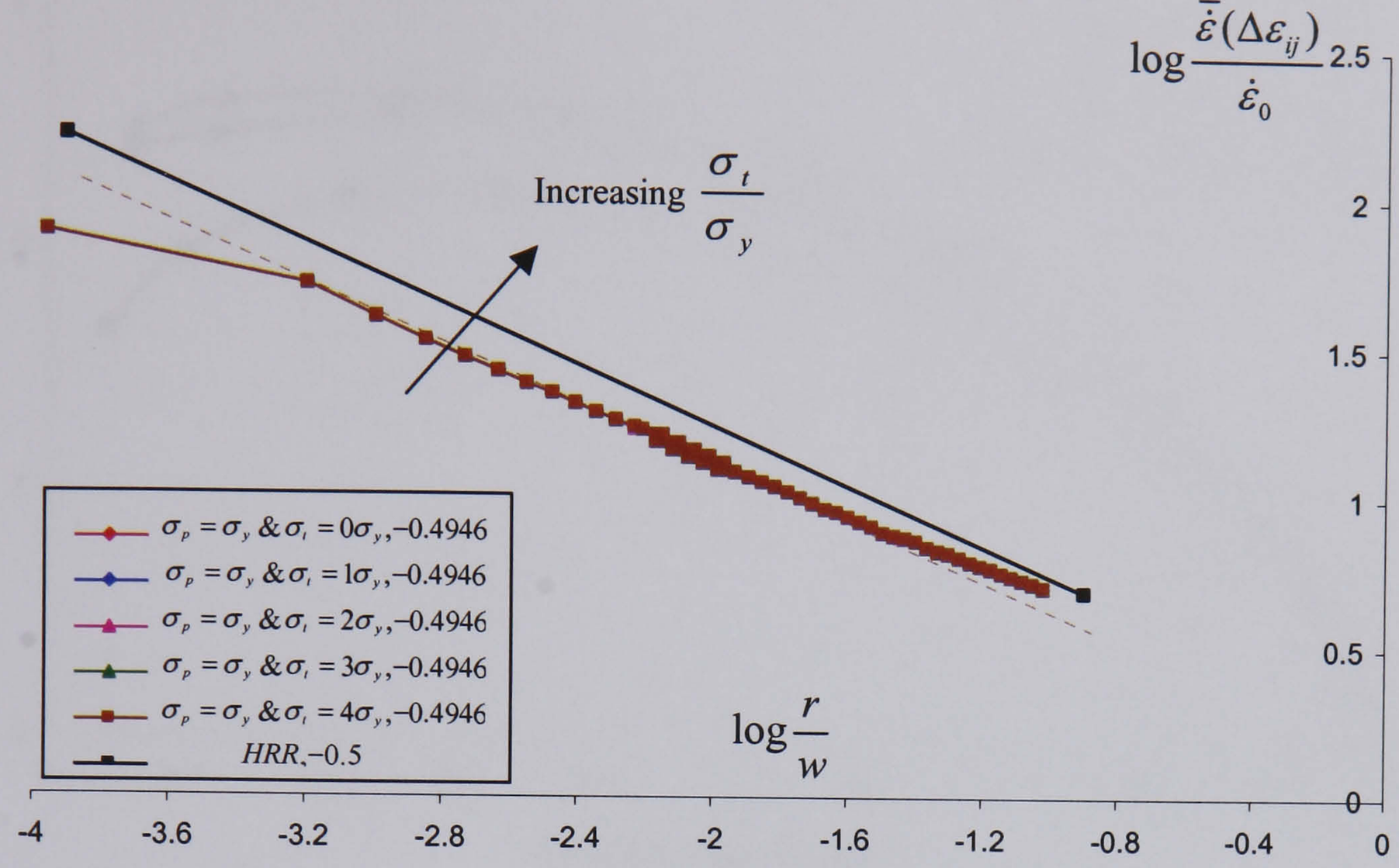

Norton's law model

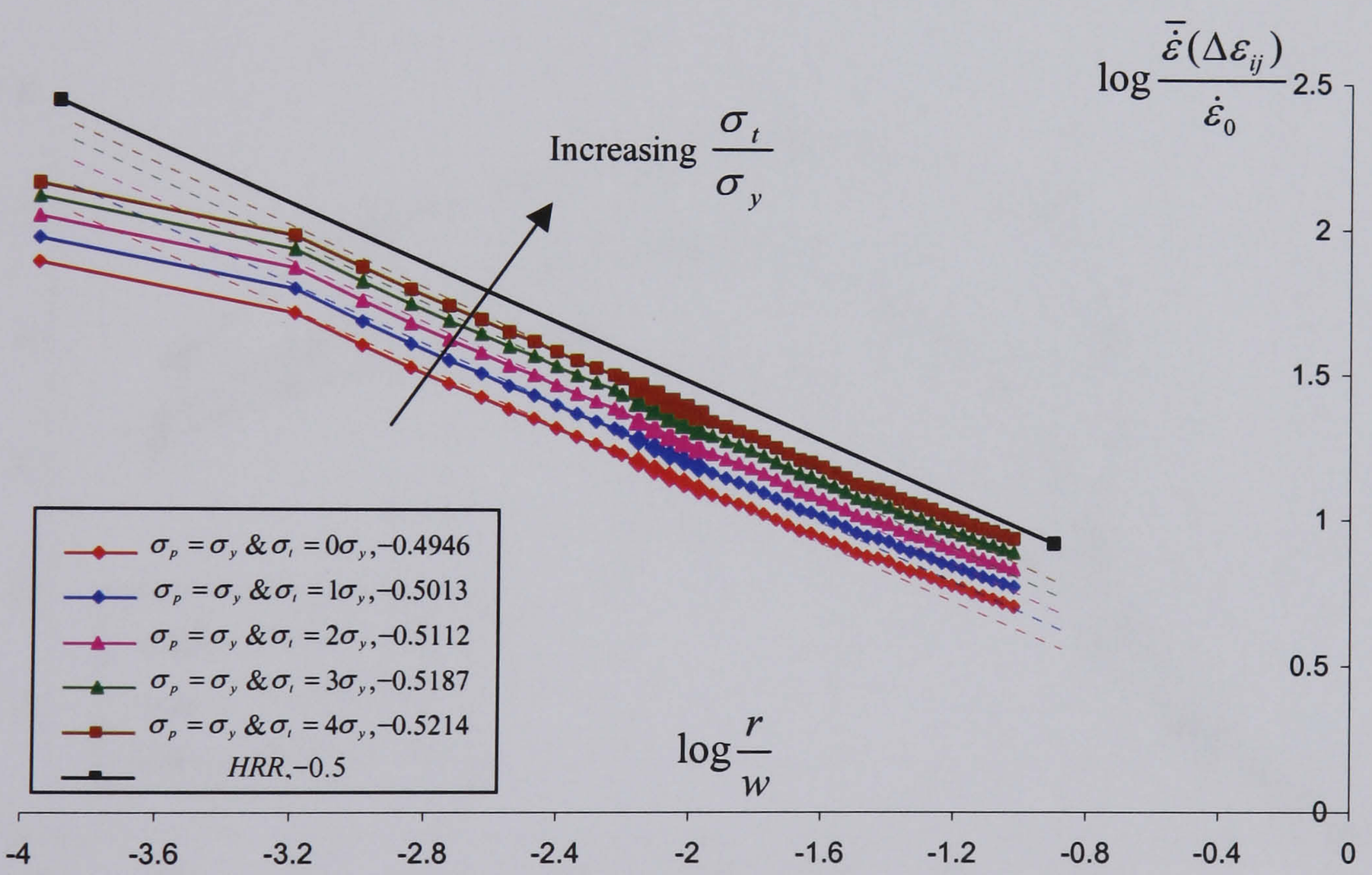

Bailey-Orowan model

Figure 5.3: Rapid cycle solutions for the different loading combinations of (σ_p, σ_t) at $n = 1$.

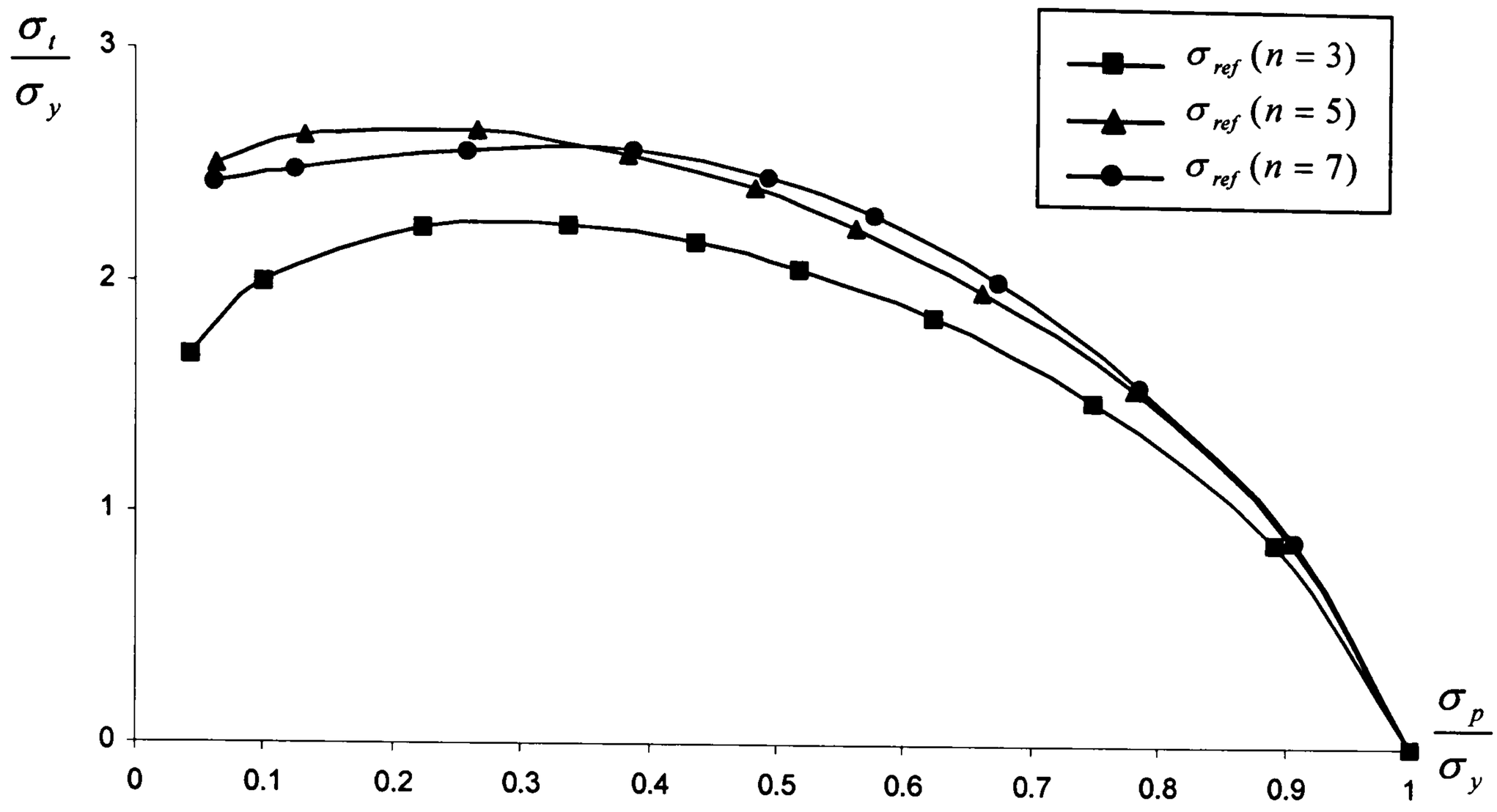

Norton's law model

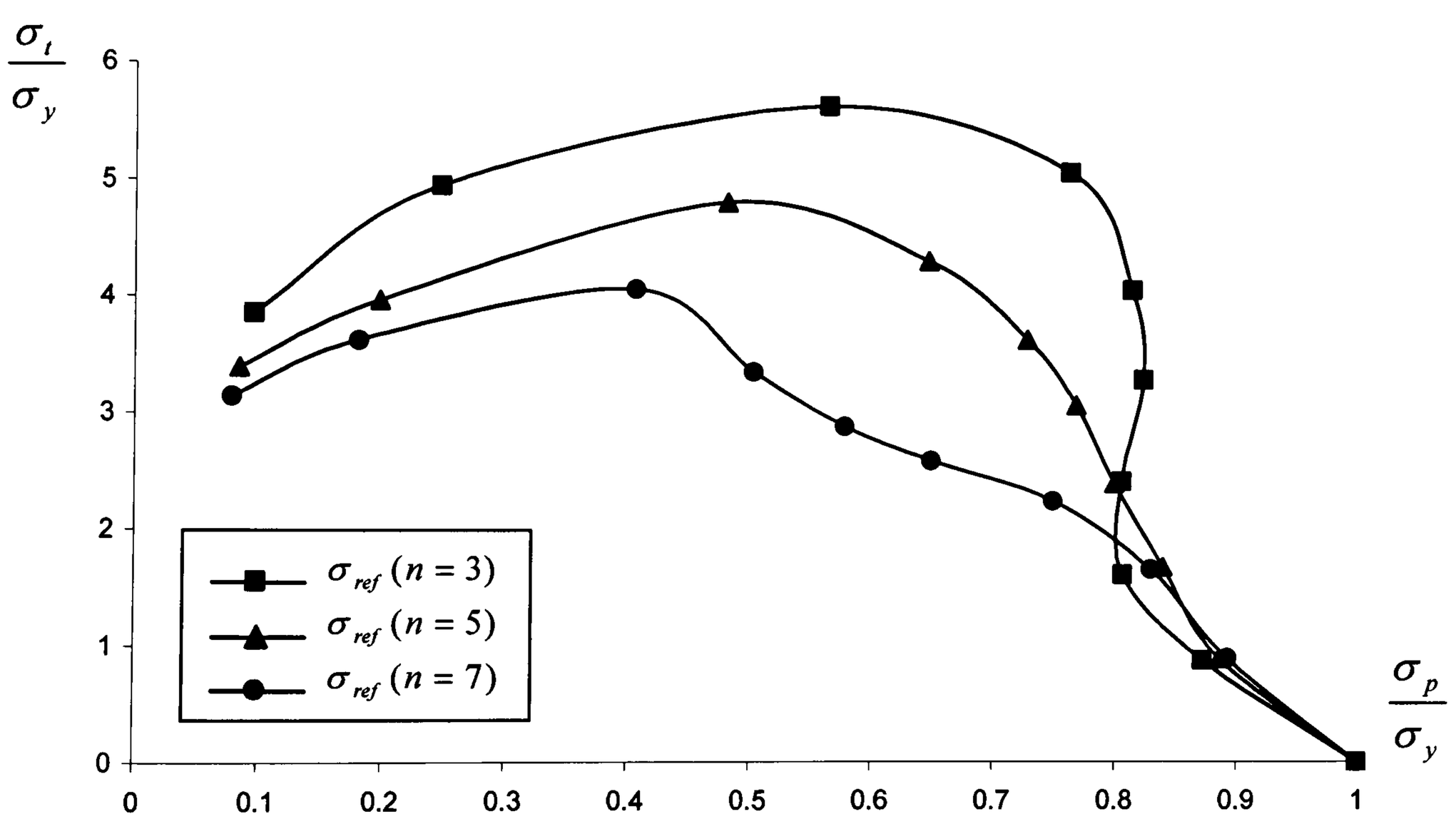

Bailey-Orowan model

Figure 5.4: Plot of contours of constant σ_{ref} for $n = 3,5 \& 7$.

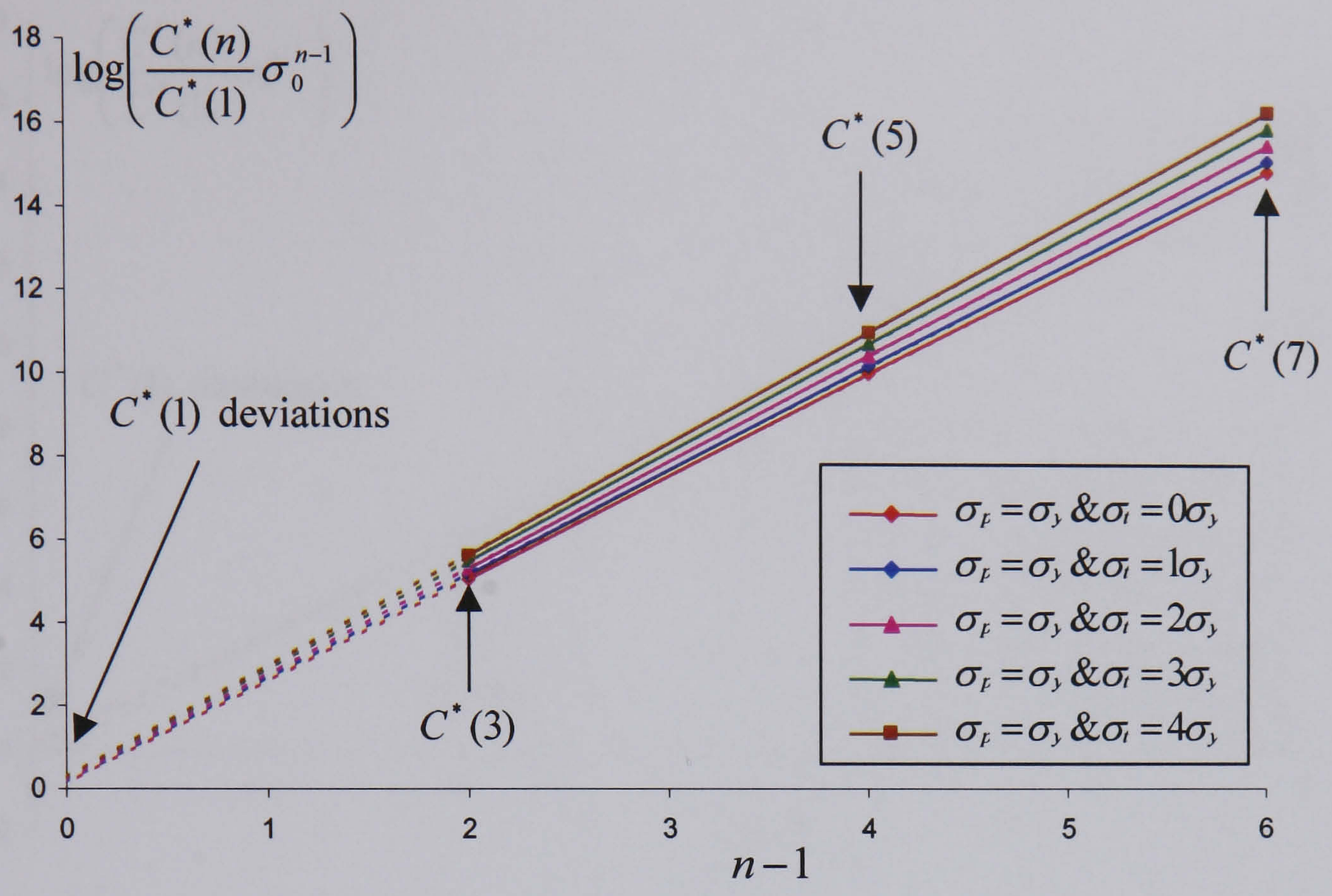

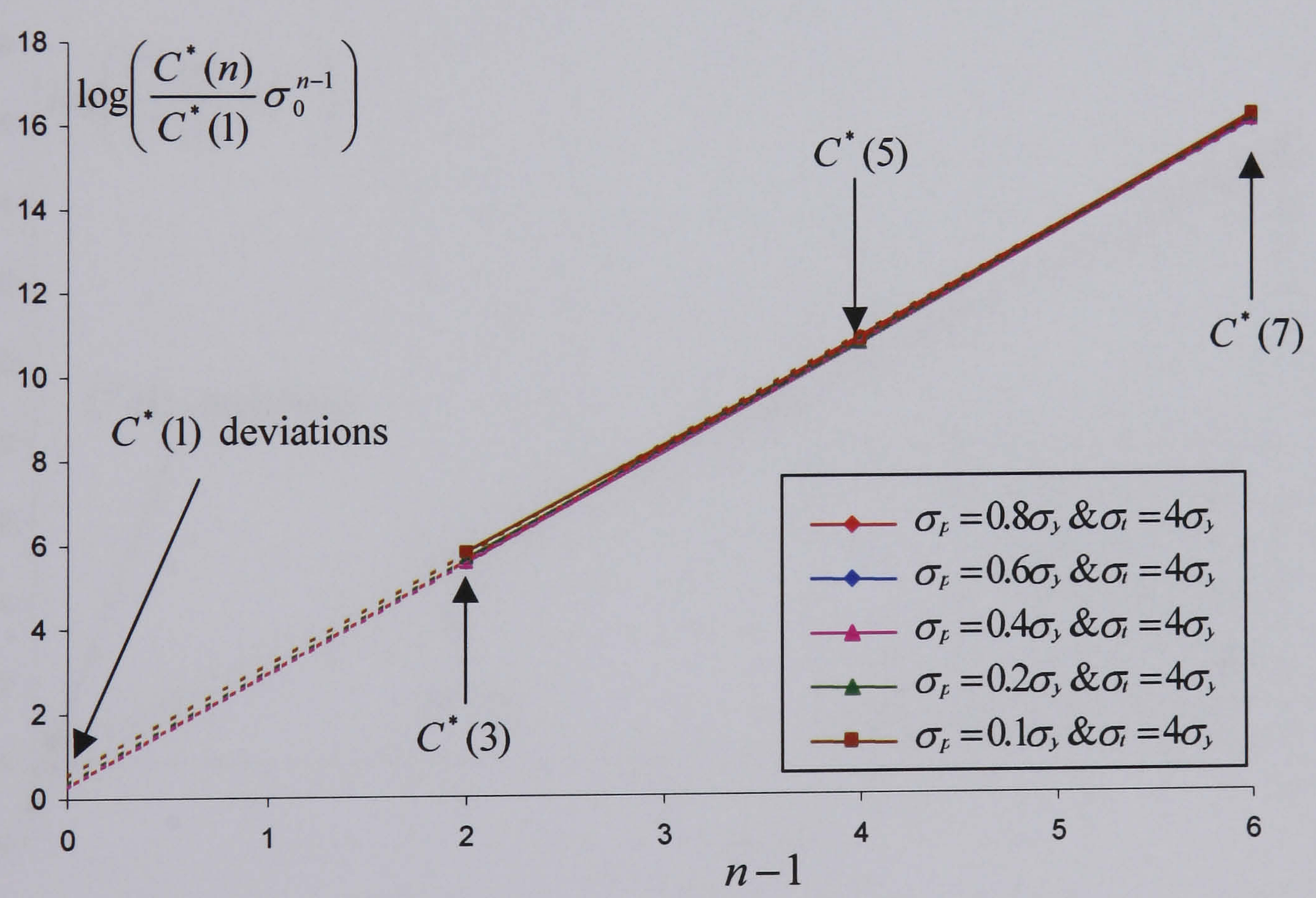

Figure 5.5: Plots of $\log\sigma_{ref}$ for Norton's law.

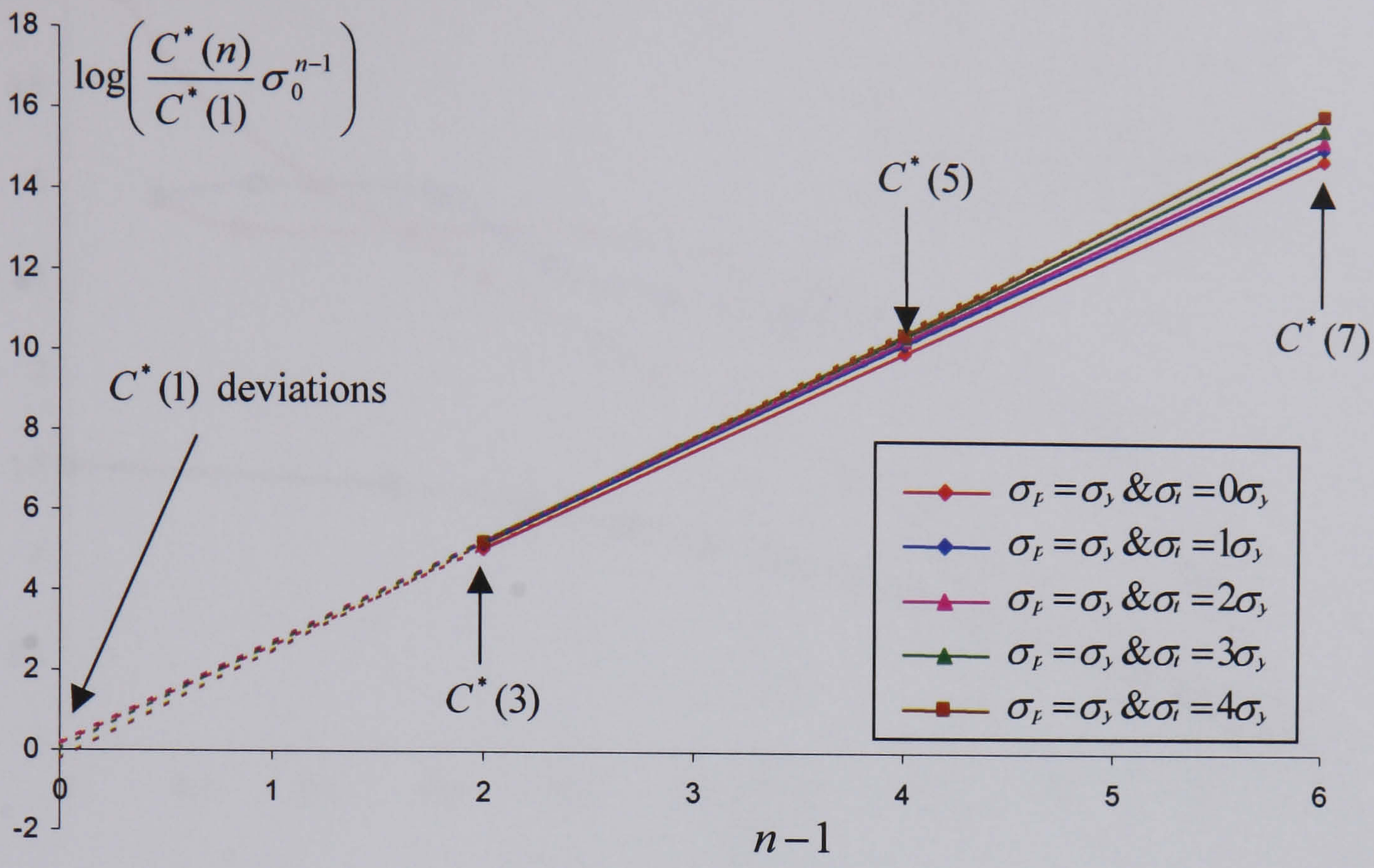

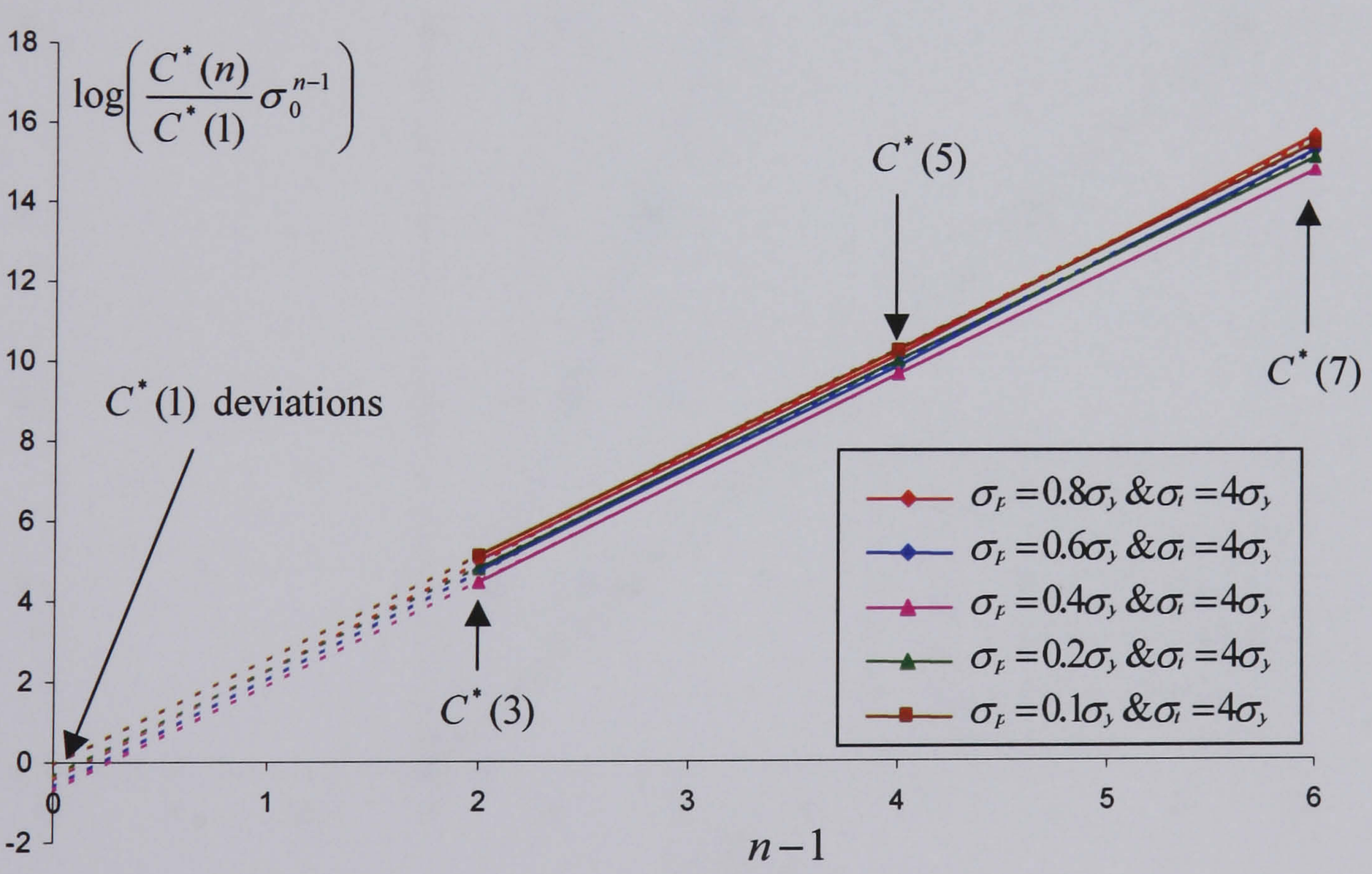

Figure 5.6: Plots of $\log \sigma_{ref}$ for the Bailey-Orowan model.

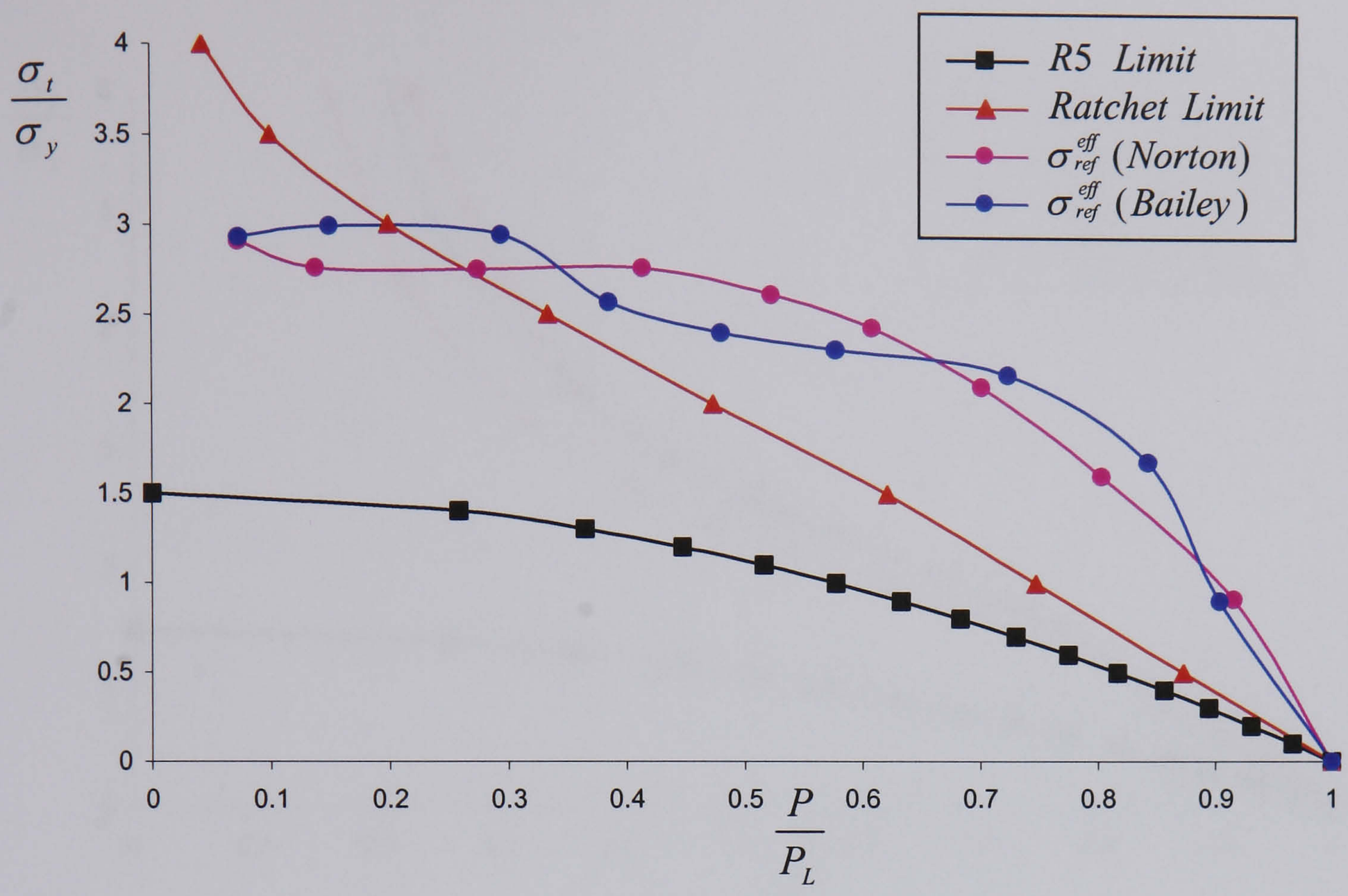

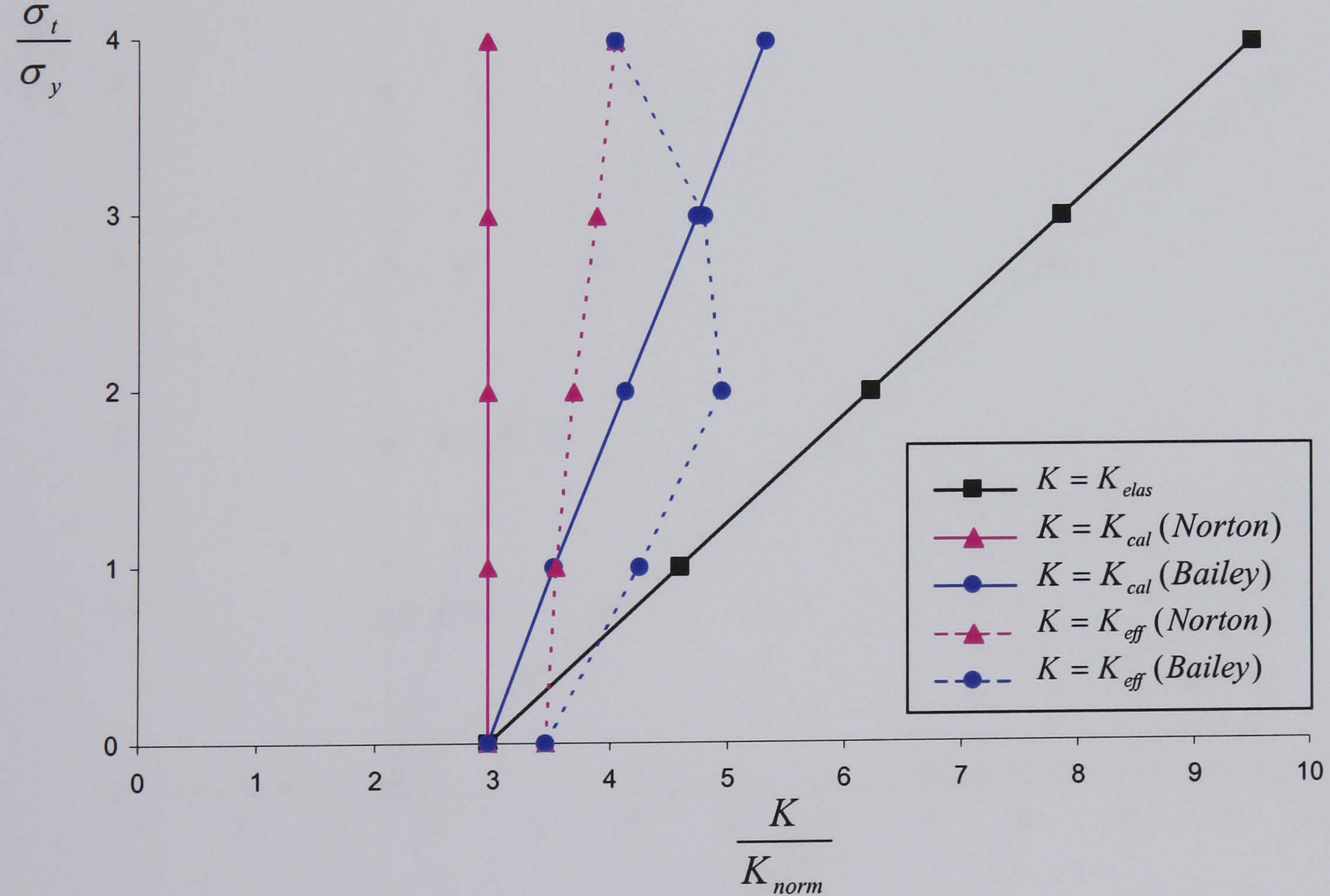

Figure 5.7: Solutions for the cracked axisymmetric Bree problem at $\frac{a}{w} = 0.4$.

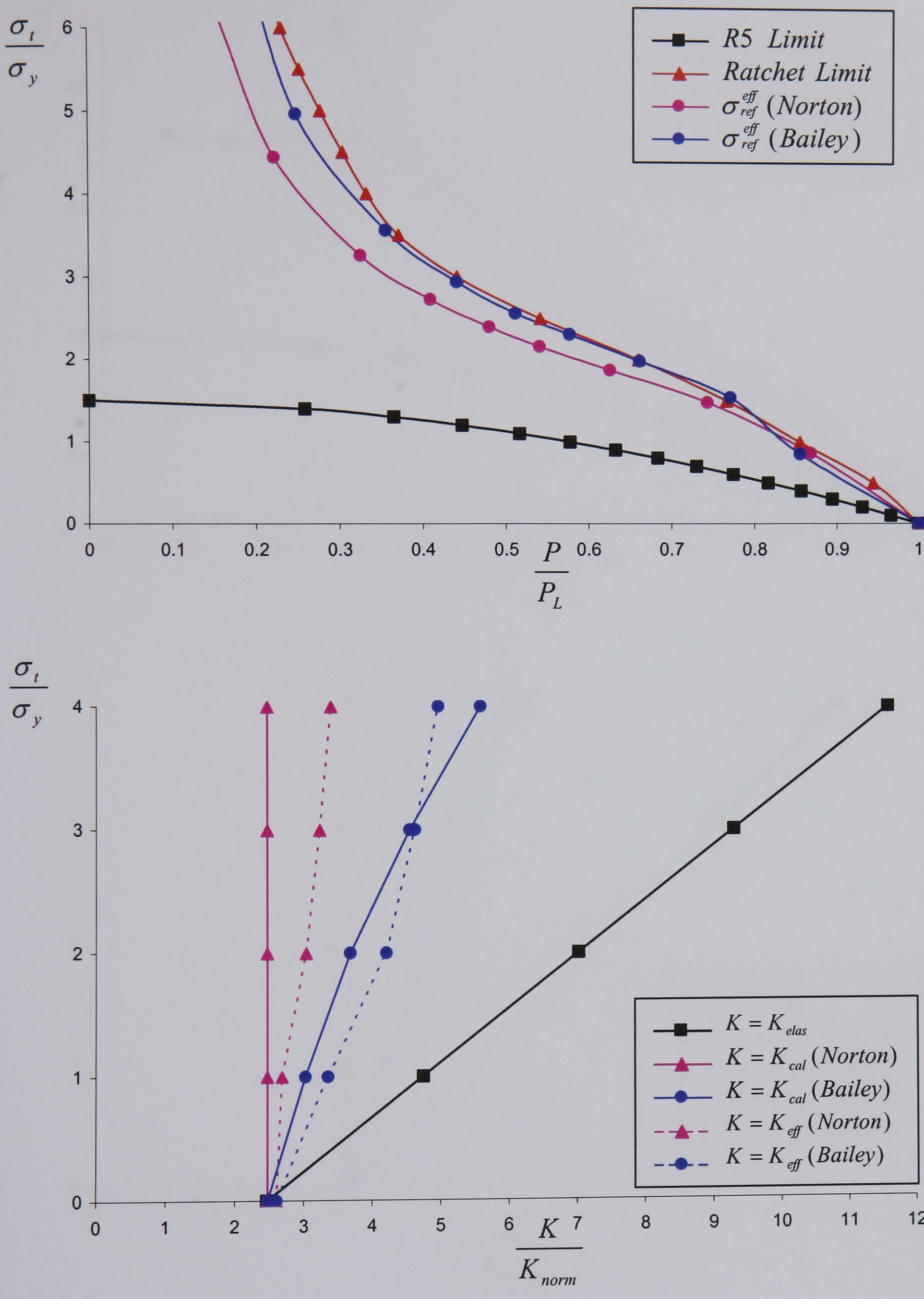

Figure 5.8: Solutions for the cracked axisymmetric Bree problem at $\frac{a}{w} = 0.04$.

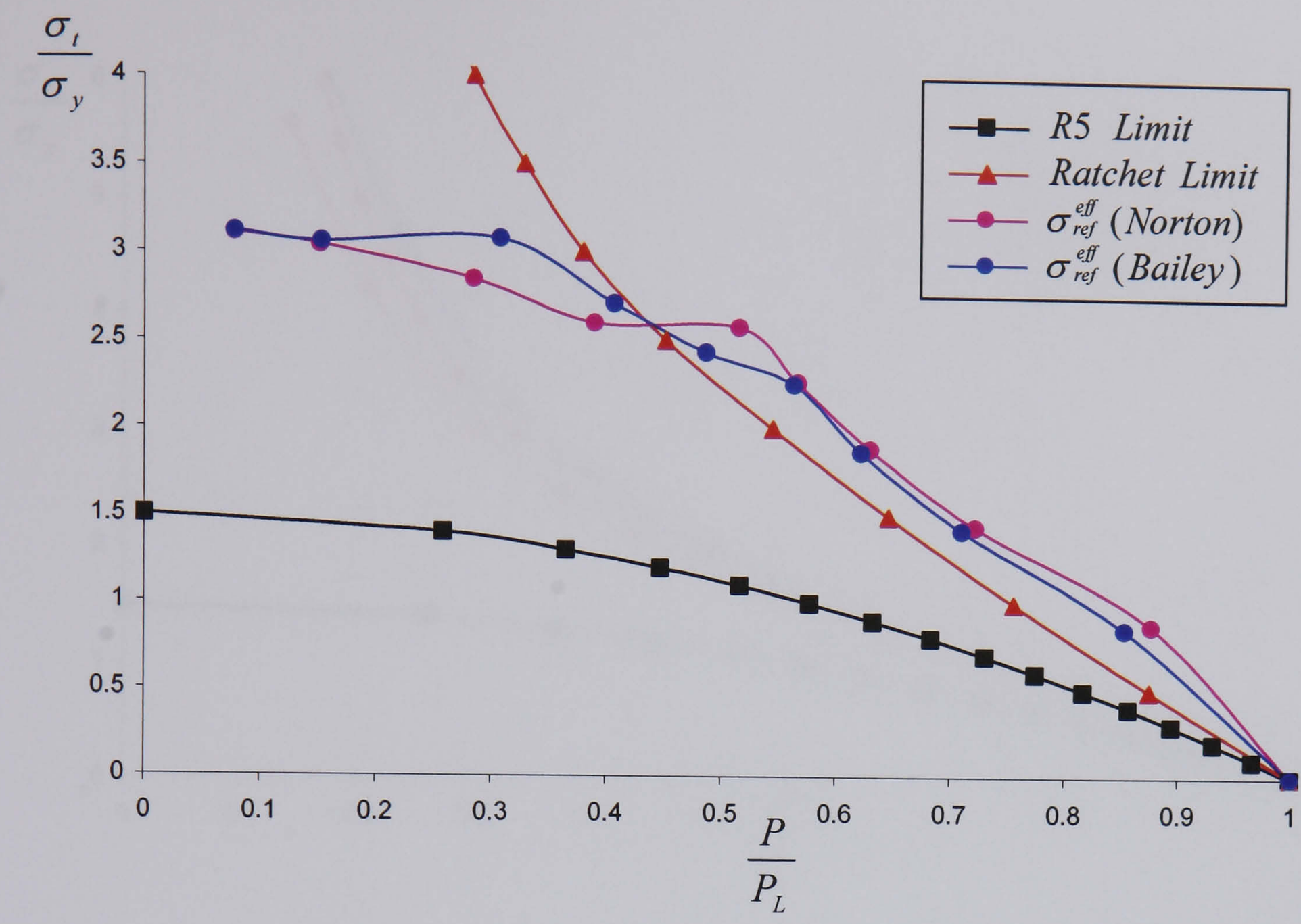

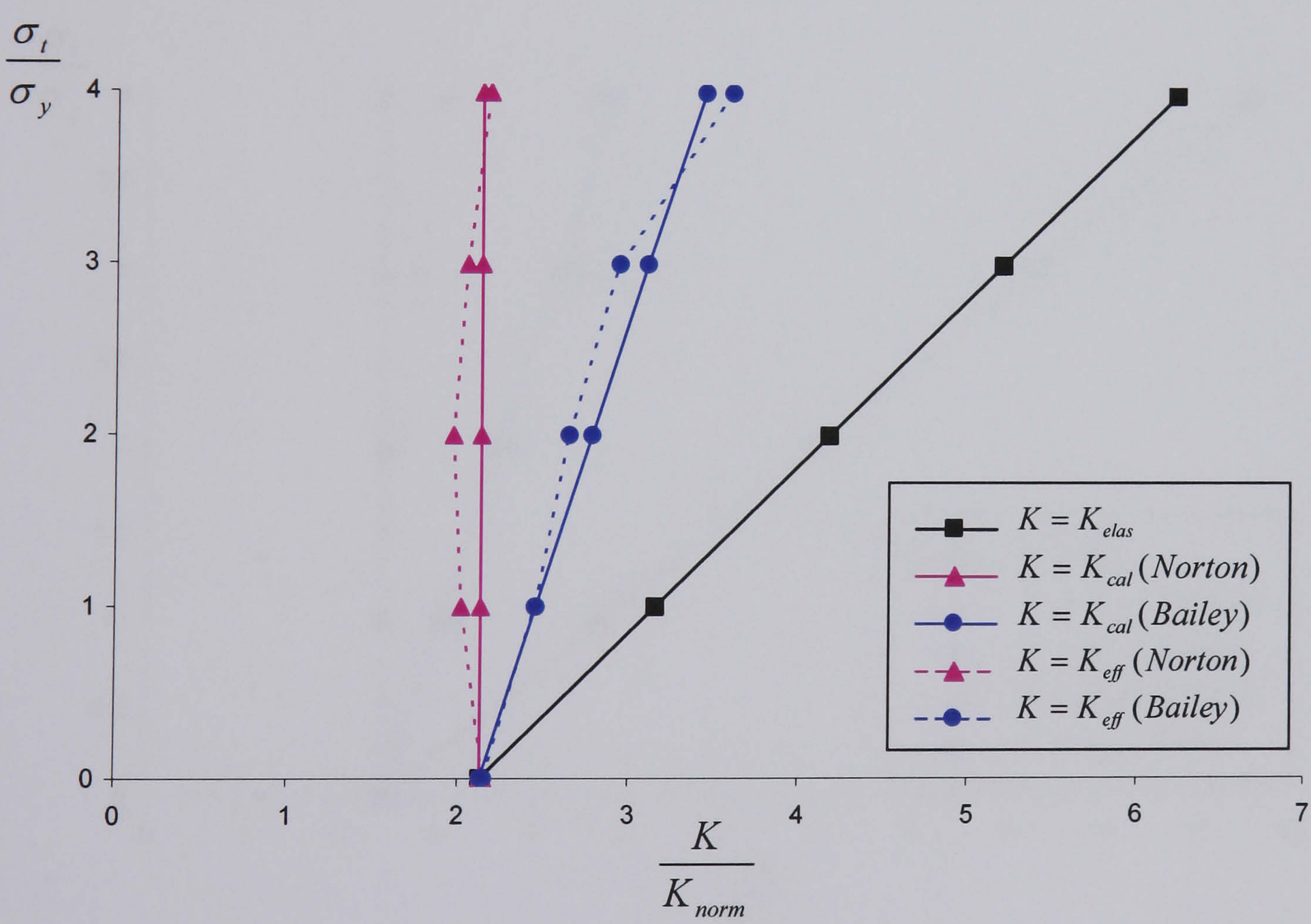

Figure 5.9: Solutions for the cracked plane stress Bree problem at $\frac{a}{w} = 0.4$.

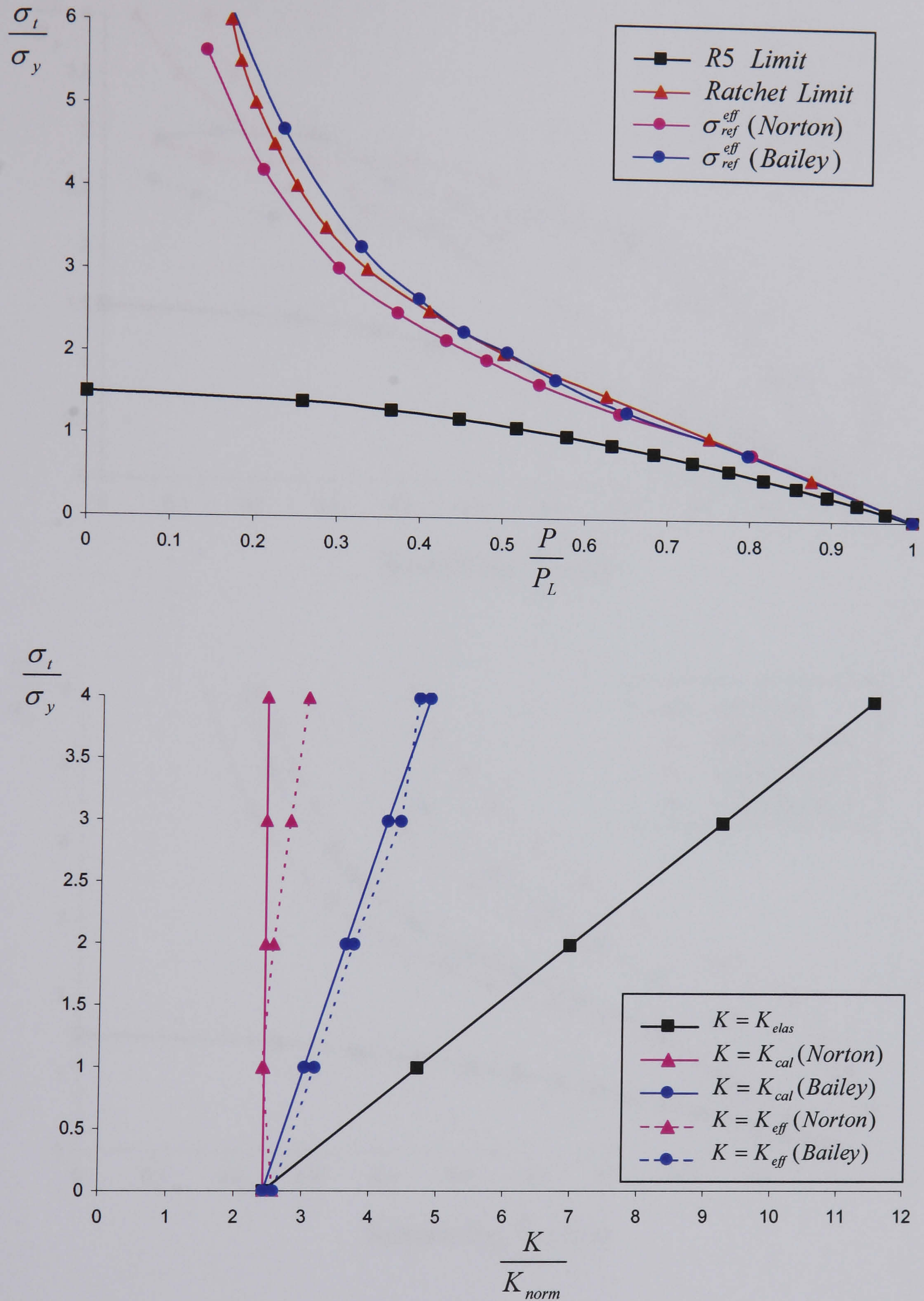

Figure 5.10: Solutions for the cracked plane stress Bree problem at $\frac{a}{w} = 0.04$.

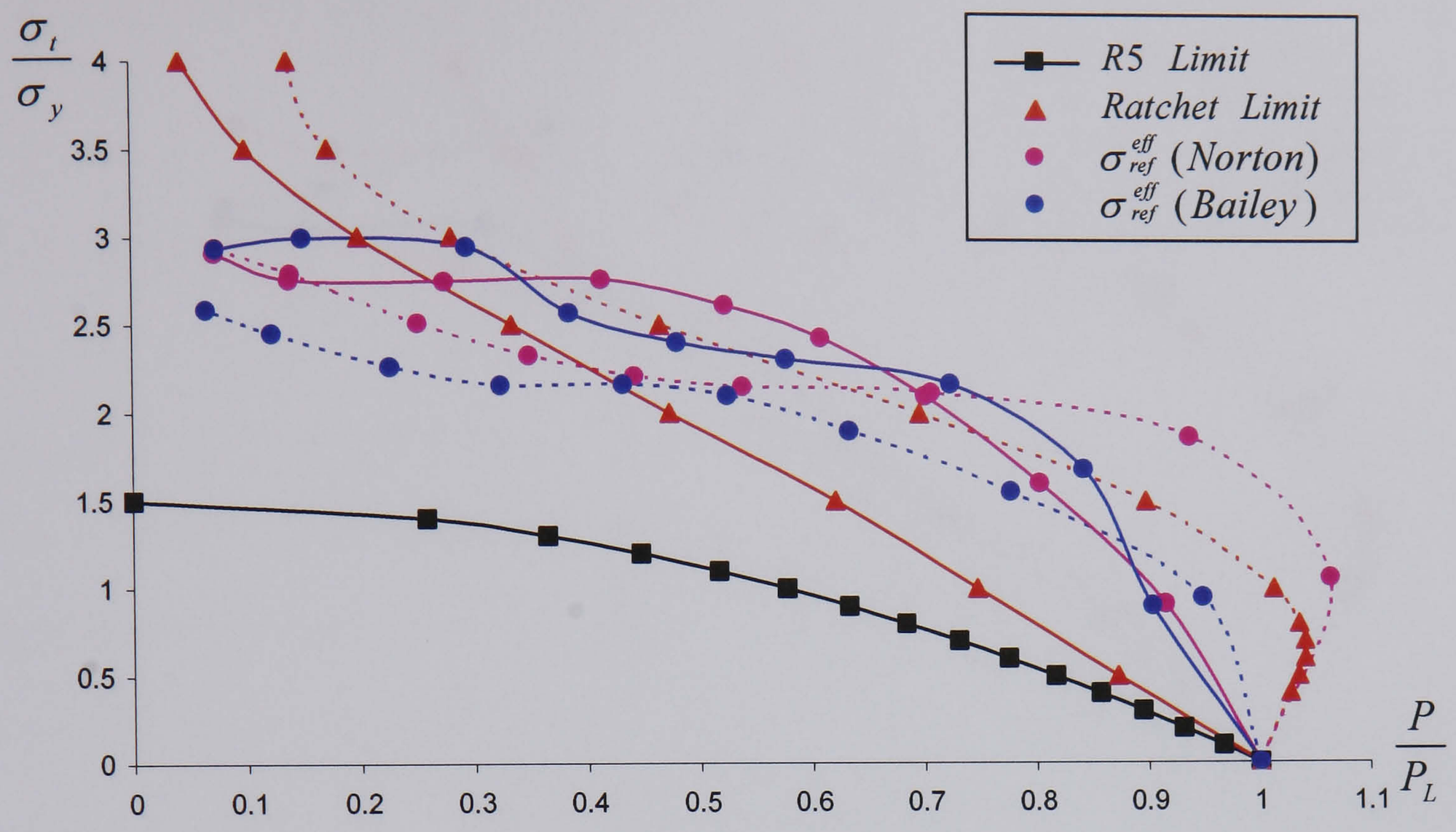

Results for $\frac{a}{w} = 0.4$

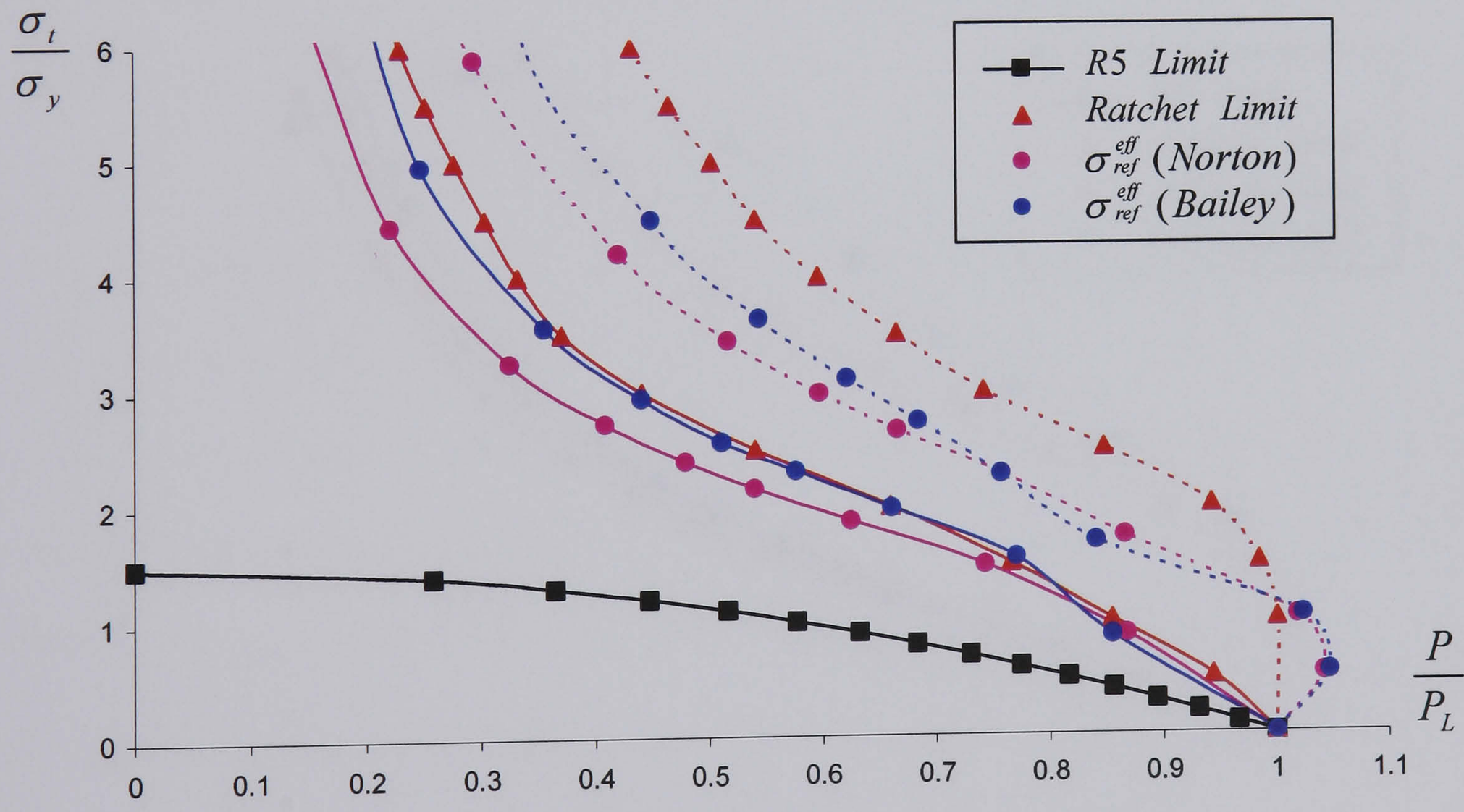

Results for $\frac{a}{w} = 0.04$

Figure 5.11: Comparisons between the cracked axisymmetric Bree problem.
(σ_p = constant(solid lines), σ_p = varying(dash lines))

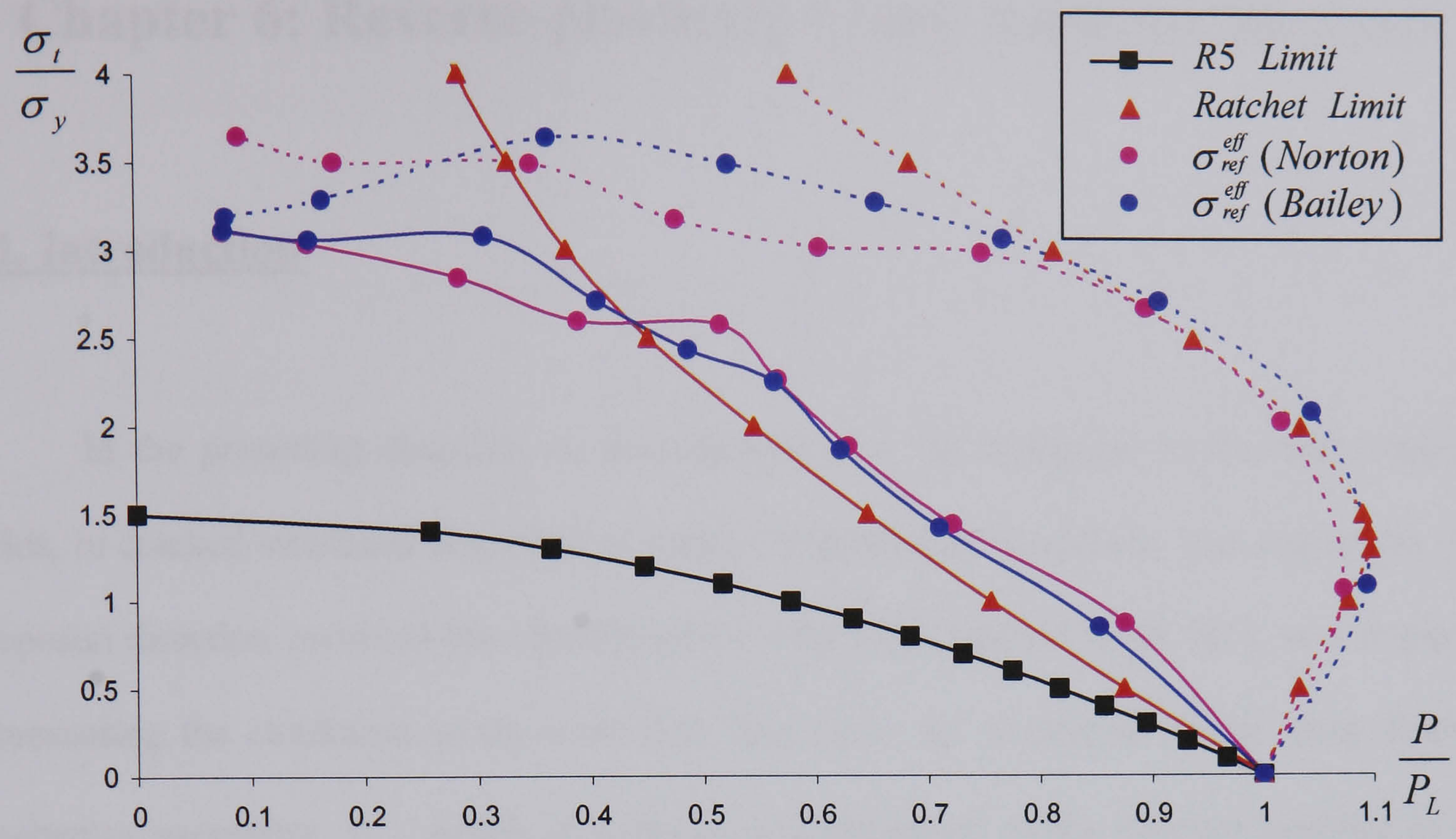

Results for $\frac{a}{w} = 0.4$

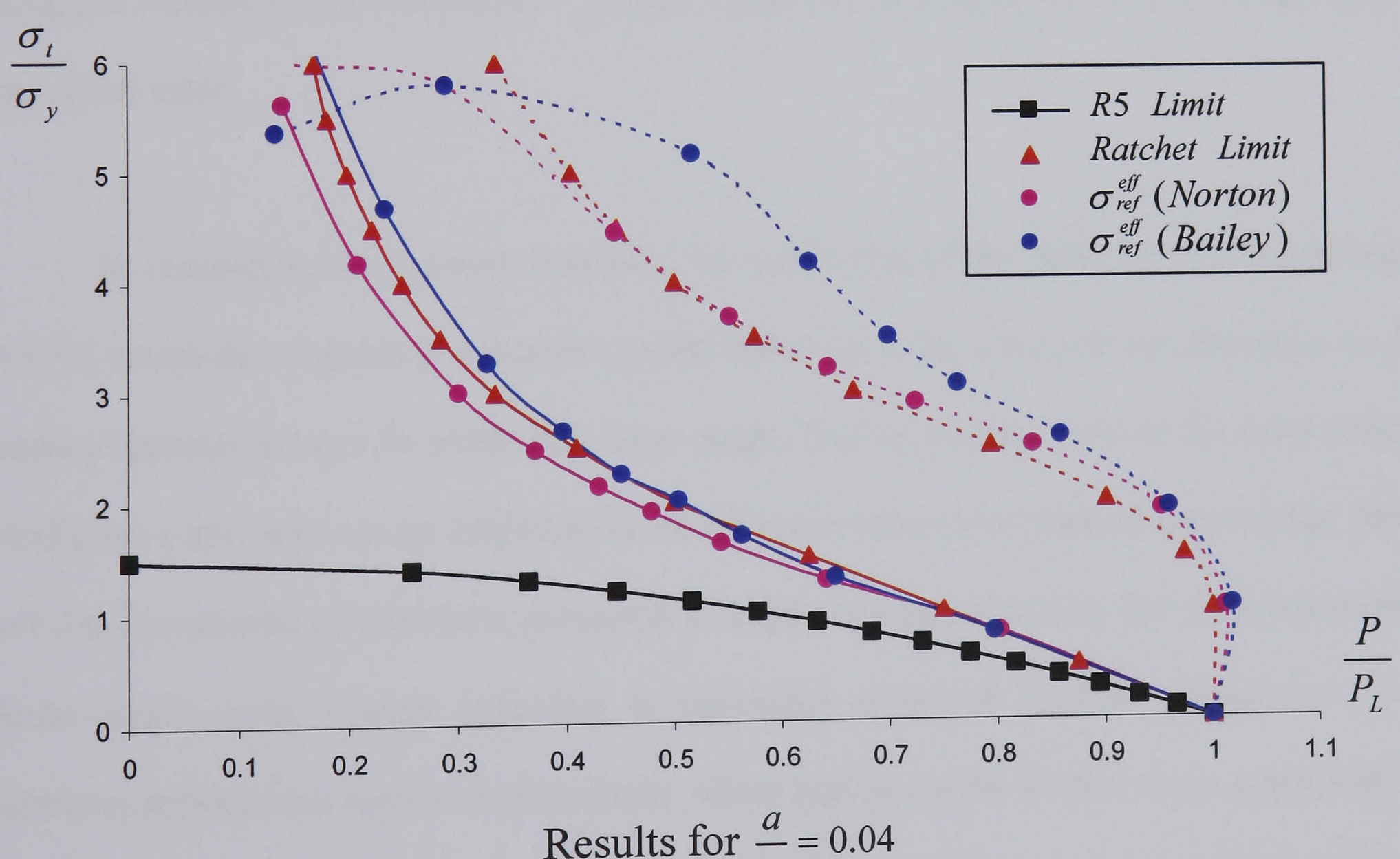

Results for $\frac{a}{w} = 0.04$

Figure 5.12: Comparisons between the cracked plane stress Bree problem.
(σ_p = constant(solid lines), σ_p = varying(dash lines))

Chapter 6: Reverse-plasticity/Creep Analysis Methods

6.1. Introduction

In the preceding chapters, an investigation into the behaviour of the near crack tip fields, in cracked structures subjected to cyclic creep loading conditions, was prescribed. The proposed direction involved the identification of the best-matched HRR field, as a means of representing the conditions at the crack tip. This led to the evaluation of the creep fracture mechanics parameter, C^*, which in essence, is a definition of the fracture criterion of the whole structure. The good correlations between these magnitudes of C^* and those computed using the reference stress method [1,19], provided the confidence that such an approach is sound and valid.

In conducting the previous analyses, the utilization of the rapid cycle creep solutions [69,70] meant the adoption of a material model based upon the elastic-creep behaviour, *i.e.* the loading histories always lie within the creep range. This is, perhaps, one of the most extreme conditions a structure can be subjected to. However, in many processes of engineering design and life assessment of structures subjected to cyclic loading histories, the occurrence of an elastic-plastic-creep material behaviour is commonly observed. This is witnessed in many industrial applications such as power plants; where typical cycles involve large stresses due to shutdown and start up, with intermittent periods when creep occurs at constant load and temperature. This implies the possibility of the loading histories operating within and outside the creep range. In this circumstance, the correct identification of the equivalent fracture

mechanics parameter, J, requires an equally accurate examination of the behaviour of the crack tip fields under such loading conditions.

The importance of undertaking such investigations was also outlined in the joint report by EPRI/CRIEPI/NE [33], for the liquid metal fast breeder reactor program. This report contains a study of fracture mechanics criteria within the UK, USA and Japan, and included both theoretical analyses and experimental data. The collaboration concluded that current flaw assessment procedures such as R5 [1], which is based upon the utilization of the small-scale yielding [34] and the reference stress formulations [1,19], is safe. Nonetheless, there are several remaining issues that were identified. One of those, examined in this chapter, is the treatment of the combined effects of variable loads and temperatures in cracked structures. This is, particularly, important in the current climate of operating structures at elevated temperatures. The conduction of such examinations, therefore, requires structural integrity methodologies, capable of examining the behaviour of these mechanically and thermally induced crack tip fields. This would then lead to the evaluation of ΔJ, the equivalent fracture mechanics parameter representing the crack tip conditions under variable loading conditions, to be identified.

In this chapter, an alternative approach for investigating the behaviour of cracked structures under reverse-plasticity and reverse-plasticity/creep loading conditions is described. Using the HRR field criterion [34,75,76] as the foundation, the examination of the near crack tip fields is then conducted using a methodology based upon the LMM, numerically implemented in a two-stage decoupled analysis process [9]. The behaviour of the near crack tip fields, under the two loading conditions, were then individually analysed, for cracked

structures under varying magnitudes of loads and temperatures. These analyses enabled relationships between the near crack tip fields and the cyclic loading histories to be identified, ultimately enabling judgement on the appropriateness of current design and life assessment procedures [1] to be assessed. (Note: The bulk of the results discussed, in this chapter, are concentrated on the behaviour of the crack tip fields under reverse-plasticity conditions. Although the numerical procedures associated with the reverse-plasticity/creep conditions are presented, only initial results from these investigations are included.)

6.2. Numerical Procedures

The numerical procedures utilized in this analysis are an extension of the methodology described in Chapter 3, for the identification of ratchet limits in excess of shakedown. Then, the applied loading histories were always assumed to lie below the creep range, with the amplitude of the plastic strain providing information concerning low cycle fatigue and the additional constant load indicating its proximity to a ratchet limit. Associated closely with such analysis is the varying plastic strain magnitude, $\Delta\varepsilon^p$, and the varying residual stress field, $\Delta\rho^p$. This purely reverse-plasticity mechanism is shown schematically in Figure 6.1(a).

If the loading histories were now allowed to exceed the creep range in some instances, a reverse-plasticity/creep mechanism may be observed in the body instead of a purely reverse-plasticity mechanism. In analysing such problems, a two-stage numerical procedure has been adopted [9]. The first stage involves the application of the above-mentioned conventional reverse-plasticity methodology. This is then followed by the second stage, whereby a reverse-plasticity/creep analysis is performed, with the initial elastic stress field, $\Delta\hat{\sigma}$, augmented by

the varying residual stress field, $\Delta\rho^p$, associated with the reverse-plasticity mechanism. The evaluation of the accumulated creep strain, $\Delta\varepsilon^c$, and the corresponding residual stress, $\Delta\rho^c$, due to creep relaxation dependent upon the creep dwell time, in this stage of the procedure, enabled the total strain over the cycle, $\Delta\varepsilon^{cp}$, to be determined. This is the sum of the varying plastic strain, $\Delta\varepsilon^p$, and the accumulated creep strain, $\Delta\varepsilon^c$, as shown schematically in Figure 6.1(b). The application of these procedures have been described for a three-dimensional tube plate problem [87], discussed in the design and life assessment procedures of R5 [1]. Their ability to compute, among others, the elastic follow-up factor, Z, and the total damage due to fatigue and creep within finite time, is potentially useful in the ensuing investigations of cracked bodies under cyclic loading histories.

In the following, the numerical procedures for the reverse-plasticity and the reverse-plasticity/creep solution methods are individually discussed. A problem with only two distinct extremes in the loading conditions is considered, *i.e.* the elastic stress solution varies proportionally between two extreme values, $\hat{\sigma}_{ij}^{\Delta}(t_1)$ and $\hat{\sigma}_{ij}^{\Delta}(t_2)$, in the stress space. As before, the utilization of the von-Mises yield condition is still assumed.

6.2.1. Numerical procedure for the reverse-plasticity solution method

For the reverse-plasticity solution method, the numerical procedure employed is the one previously described in Section 3.4.2 of this thesis. Essentially, the methodology involves identifying, for a prescribed loading history, a varying residual stress field, $\Delta\rho^p$, which keeps the elastic stress history, $\Delta\hat{\sigma}$, within the yield condition. Implemented within an iterative

process using the finite element analysis code, ABAQUS, the repeated application of the algorithms presented [6,7], enabled the identification of the associated plastic strain range, $\Delta\varepsilon^p$. At the absolute minimum of the functional, a converged solution is yielded, with the magnitudes of $\Delta\rho^p$ and $\Delta\varepsilon^p$ stored in files to be accessed later in subsequent (second stage) analysis.

6.2.2. Numerical procedure for the reverse-plasticity/creep solution method

For the reverse-plasticity/creep solution method, the numerical procedures are, by and large, identical to those described above, with the exception of some modifications. These are presented below for the case whereby the material creeps at instant t_1 of the loading history, leading to the appearance of the residual stress field, $\Delta\rho^c$, associated with stress relaxation and the accumulation of creep strain, $\Delta\varepsilon^c$, over the creep dwell time, Δt. At the other time instant t_2, no creep is assumed to occur but a reverse-plasticity mechanism still appears, with the total strain over the cycle equals to zero. In this circumstance, the condition of equations (3.20) & (3.22) yields,

$$\int_0^{t_1} \dot{\varepsilon}_{ij}^c dt = \Delta\varepsilon_{ij}^c \qquad \& \qquad \int_{t_1}^{t_2} \dot{\varepsilon}_{ij}^c dt = -\Delta\varepsilon_{ij}^c \tag{6.1}$$

and

$$\int_0^{t_1} \dot{\rho}_{ij}^c dt = \Delta\rho_{ij}^c \qquad \& \qquad \int_{t_1}^{t_2} \dot{\rho}_{ij}^c dt = -\Delta\rho_{ij}^c \tag{6.2}$$

Thus, by taking into consideration $\Delta\varepsilon_{ij}^{p}$, $\Delta\varepsilon_{ij}^{c}$, $\Delta\rho_{ij}^{p}$ and $\Delta\rho_{ij}^{c}$, the extremes of the reverse-plasticity/creep mechanism are identified, providing sufficient information for the reverse-plasticity/creep analysis.

The same minimisation process described in [6,7] is used. Based upon the linear matching method, it requires the solution of a sequence of linear problems. Thus, for an initial estimate of the strain increment, $\Delta\varepsilon_{ij}^{c} = \Delta\varepsilon_{ij}^{ci}$, a class of linear problems for a new estimate, $\Delta\varepsilon_{ij}^{c} = \Delta\varepsilon_{ij}^{cf}$, is then posed, such that the linear coefficient, $\overline{\mu}^{i}$, is related by,

$$\sigma_{y} + \sigma_{f}(\Delta t) = \left(\frac{3}{2}\right) 2\overline{\mu}^{i}\,\overline{\varepsilon}(\Delta\varepsilon_{ij}^{ci}) \tag{6.3}$$

where $\sigma_{f}(\Delta t)$ is the flow stress at the end of a particular creep dwell time. The new distribution of the strain increment, $\Delta\varepsilon_{ij}^{cf}$, is then defined as the solution to the following problem,

$$\Delta\varepsilon_{ij}^{cTf'} = \frac{1}{2\mu}\Delta\rho_{ij}^{f'} + \Delta\varepsilon_{ij}^{cf'}, \qquad \Delta\varepsilon_{kk}^{cTf} = \frac{1}{3K}\Delta\rho_{kk}^{f} \tag{6.4}$$

and

$$\Delta\varepsilon_{ij}^{cf'} = \left(\frac{1}{2\overline{\mu}^{i}}\right)\left(\Delta\hat{\sigma}_{ij}' + \Delta\rho_{ij}^{cf'}\right) \tag{6.5}$$

where $\Delta\varepsilon_{ij}^{cTf}$ and $\Delta\rho_{ij}^{f}$ satisfies the conditions of compatibility and equilibrium respectively, with

$$\Delta\hat{\sigma}_{ij} = \hat{\sigma}_{ij}^{\Delta}(t_1) - \hat{\sigma}_{ij}^{\Delta}(t_2) + \Delta\rho_{ij}^{p} \tag{6.6}$$

where $\Delta\rho_{ij}^{p}$ is the varying residual stress field calculated from the first stage (Section 6.2.1).

The repeated iterative application of these algorithms produces a sequence of solutions for $\Delta\varepsilon_{ij}^{ck}$, converging to the solution that minimises the functional I in equation (3.19). If two such consecutive iterations, k and $k+1$, are considered, then the relationship in (6.3) yields,

$$\overline{\mu}^{k+1} = \overline{\mu}^{k} \frac{\sigma_y + \sigma_f(\Delta t)}{\overline{\sigma}(\Delta\hat{\sigma}_{ij} + \Delta\rho_{ij}^{ck})} \tag{6.7}$$

The application of the above procedures requires an appropriate numerical technique for evaluating the flow stress, $\sigma_f(\Delta t)$. This is attempted below, for the power-law creep model, leading to the definition of the flow stress to be given by,

$$\sigma_f(\Delta t) = \sigma_0 \left(\frac{\dot{\varepsilon}^c(\Delta t)}{\dot{\varepsilon}_0} \right)^{\frac{1}{n}} \tag{6.8}$$

where σ_0, $\dot{\varepsilon}_0$ and n are material data for creep. The equation's dependency upon the creep dwell time is apparent. In the circumstance that Δt is short enough, then the creep strain rate, $\dot{\varepsilon}^c(\Delta t)$, can be approximated using,

$$\dot{\varepsilon}^c(\Delta t) \approx \frac{\Delta\varepsilon^c}{\Delta t} \tag{6.9}$$

where $\Delta\varepsilon^c$ is computed from (6.5). Thus, the substitution of equation (6.9) into (6.8) provides the necessary condition for the evaluation of the flow stress within the developed procedure.

However, in most situations, Δt is not sufficiently small for the approximation of (6.9) to be suitable. Their continued utilization would induce significant numerical errors in the computation of the creep strain rate, $\dot{\varepsilon}^c(\Delta t)$. In solving this problem, Chen & Ponter [87] derived a solution scheme, whereby equation (6.9) is amended by an improved theoretical formula. It is based upon the assumption that $\dot{\varepsilon}^c(\Delta t)$ is strictly equal to,

$$\dot{\varepsilon}^c(\Delta t) = \frac{\Delta\varepsilon^f}{\Delta t} \tag{6.10}$$

At this point, the calculation of the accumulated creep strain, $\Delta\varepsilon^c$, over the creep dwell time, Δt, is defined by,

$$\Delta\varepsilon^c = \frac{Z\Delta\rho^c}{\overline{E}} \tag{6.11}$$

where $\overline{E} = \frac{3E}{2(1+\nu)}$ and the elastic follow-up factor, Z, is assumed to remain constant during the relaxation over the creep dwell time. On the basis of such arguments, an improved theoretical formula, capable of representing the creep strain rate was developed,

$$\dot{\varepsilon}^c(\Delta t) = \frac{\Delta\varepsilon^c}{\Delta t} f(\sigma_f, \Delta\rho^c, n) = \frac{\Delta\varepsilon^c}{\Delta t}\frac{(\sigma_f)^n}{\Delta\rho^c}\frac{1}{n-1}\left\{\frac{1}{(\sigma_f)^{n-1}} - \frac{1}{(\sigma_f+\Delta\rho^c)^{n-1}}\right\} \tag{6.12}$$

In their applications [87], it was observed that equation (6.12) is an improved formula for estimating the creep strain rate, $\dot{\varepsilon}^c(\Delta t)$, at any creep dwell time, Δt. This acted as a replacement to equation (6.9), thus, justifying its exploitation in this thesis.

6.3. Reverse-plasticity Solutions

The purpose of this examination is to develop an understanding into the behaviour of cracked structures under cyclic loading histories, using the reverse-plasticity solution method described in Section 6.2.1. This involves an in-depth investigation into the near crack tip fields in the presence of variable loads, variable temperatures and their combinations. Although much work had been undertaken in this field [31,32], the emphases in most of these studies were only concerned with the performance of cracked bodies under variable mechanical loads. In the current environment of operating structures at elevated temperatures, however, an understanding into the behaviour of the crack tip fields in the presence of both variable loads and temperatures is indispensable. This would lead to the definition of the crack tip fracture criterion to be identified, which, in essence, is a representation of the safe operation of the whole structure. The ability of such analyses would also enable assessments on the appropriateness of current R5 [1] procedures, which is still based upon the replacement of thermal stresses as equivalent bending moments in the presence of the variable loads, to be made. The procedures also recommended, in cracked structures under cyclic hardening conditions, the utilization of the small-scale yielding [34] and the reference stress formulations [1,19]. (Note: The actual fully commented programs, for the ensuing numerical problems, are enclosed in the attached CD.)

6.3.1. HRR fields

The ensuing investigations are for the axisymmetric Bree problem [37], simulating the loading conditions typically observed in many structural components. As shown in Figure 6.2, it consists of a cracked axisymmetric tube of width, w, with circumferential cracks of width, a, assumed to occur at the centre of the line of symmetry. This enabled only half of the length to be modelled. In the following explorations, as before, the ratios of $\frac{a}{w} = 0.4$ and $\frac{a}{w} = 0.04$ are considered. The tube is also subjected to a varying axial stress, $\Delta\sigma_p$, and a linear temperature gradient arising from a temperature difference of $\Delta\theta$, which varies between zero and some maximum value. This is denoted by $\Delta\sigma_t$, the maximum varying thermo-elastic stress away from the crack, *i.e.* the value that would occur if the cracks were absent. In modelling the finite element problem, the same selective mesh refinement technique, used in Chapter 4 (Figure 4.3), is employed, with the exception of a much finer mesh at the crack tip this time round. This is done using the six-noded CAX6H triangular meshing elements.

In conducting such experiments, a postulation capable of describing the deformation fields at the crack tip is required. This is necessary, as it would provide a means of investigating the variations of the effective strain ranges, $\bar{\varepsilon}(\Delta\varepsilon_{ij}^{P})$, at the crack tip, associated with the applied stress ranges for the mechanical and thermal loads. Based upon the successful satisfaction of the HRR field criterion for the cracked cyclic creep solutions in Chapter 4, the same Hutchinson [75] and Rice and Rosengren [76] postulations are adopted here. Their findings revealed that in an isotropic, elastic-plastic material, satisfying the power-law hardening expression,

$$\bar{\varepsilon}(\varepsilon_{ij}^{p}) = \alpha\varepsilon_{y}\left(\frac{\bar{\sigma}(\sigma_{ij})}{\sigma_{y}}\right)^{N} \tag{6.13}$$

the near crack tip strain distributions varies in accordance with,

$$\bar{\varepsilon}(\varepsilon_{ij}^{p}) \rightarrow \left(\frac{1}{r}\right)^{\frac{N}{N+1}} \bar{f}(f_{ij}(\theta)) \tag{6.14}$$

where, as before, N is the power-law hardening exponent, σ_y, ε_y, α are material constants and r and θ are the radial and angular distances away from the crack tip respectively. Thus, the utilization of equation (6.14) allows the possibility of identifying an equivalent HRR field, for the perfectly plastic condition of $N = \infty$ considered here.

The behaviour of the mechanically and thermally induced crack tip fields was then examined at all locations away from the crack tip. In addition to cases where $\Delta\sigma_p$ and $\Delta\sigma_t$ each acted alone, the behaviour of the crack tip fields, for three differing combinations of $(\Delta\sigma_p, \Delta\sigma_t)$, were also investigated. A selection of plots of $\log\bar{\varepsilon}(\Delta\varepsilon_{ij}^{P})$ against $\log\frac{r}{w}$, are shown in Figures 6.3 and 6.4, for increasing individual magnitudes of $\Delta\sigma_p$ and $\Delta\sigma_t$. It was found that the satisfaction of the HRR field criterion was achieved at all locations, except in the first few elements, with the best-matched HRR field, as before, still occurring at $\theta = 70^0$. Similar investigations into the behaviour of the crack tip fields, under the combined actions of $(\Delta\sigma_p, \Delta\sigma_t)$, were also conducted. Although not included in this thesis, the satisfaction of the HRR field condition was still observed, with the best-matched HRR field still identified at the

aforementioned location. These characteristic behaviours were observed in both crack solutions.

In its identification, it is important to note that the best-matched HRR field, encompassed by six meshing elements in Figures 6.3 and 6.4, was identified within the plastic zone size, r_p. At low variable loads, it was observed that the sizes of the plastic zones were relatively close to the best-matched HRR field. However, as the loads were increased, the enlargement of the plastic zone sizes, in comparison with the location of the best-matched HRR field, which is very near the crack tip, indicates the appropriateness of choosing this field as a representation of the crack tip behaviour.

In the identification of the condition at the crack tip, the approach employed in this thesis involves the utilization of a sampling point within the so-called best-matched HRR field-satisfying gradient. For such a proposition to work, it was found that the employment of a fine finite element mesh at the crack tip is required. This is to ensure that the identified sampling point always lie within the plastic zone size, r_p, irrespective of the loading magnitudes, *i.e.* high or low loads. This is particularly important in the analysis into the behaviour of cracked structures at very low loads. In such situations, care must be taken to ensure that the chosen sampling point is still being identified within the plastic zone size. Therefore, as a precaution or warning to future researchers using this approach, the issue regarding the mesh fineness needs to be carefully deliberated before any numerical analysis is conducted. Else, the results obtained for very low loads would be unreliable, erroneous and inaccurate.

6.3.2. Elastic-plastic fracture mechanics parameter

In the field of fracture mechanics for structures subjected to monotonic and constant loadings, different quantities have been derived in defining the crack tip fracture criterion. In linear elastic fracture mechanics, the stress intensity factor, K, is the term normally used to describe the crack tip fields, while the equivalent in creep fracture mechanics is the parameter, C^*. In elastic-plastic fracture mechanics, the corresponding parameter is the integral, J. As discussed in Chapter 4, this term was proposed by Rice [34], who obtained the relationship between J and the crack tip fields, for materials satisfying the power-law hardening expression of (6.13), from the expression,

$$\bar{\varepsilon}(\varepsilon_{ij}^{p}) = \varepsilon_y \left(\frac{J}{I_N \sigma_y \varepsilon_y r} \right)^{\frac{N}{N+1}} \bar{\varepsilon}(\tilde{\varepsilon}(\theta, N)) \qquad (6.15)$$

where N, σ_y, ε_y are material constants, with I_N and $\bar{\varepsilon}(\tilde{\varepsilon}(\theta, N))$ being the dimensionless constant and functions of θ and N respectively, obtained from tables evaluated by Shih [82]. This allowed the magnitudes of J to be evaluated, by simply substituting the values of $\bar{\varepsilon}(\varepsilon_{ij}^{P})$, at a sampling point within the best-matched HRR field, into equation (6.15).

However, in the present investigations, it is the behaviour of cracked structures under variable, instead of monotonic, loading conditions, which were being investigated. This called for an alternative formulation capable of identifying ΔJ, the J equivalence in variable loads. In closing this gap, Rice *et al* [88] developed an argument, based upon the corresponding power-law hardening expression,

$$\bar{\varepsilon}(\Delta\varepsilon_{ij}^{p}) = \alpha\Delta\varepsilon_{y}\left(\frac{\bar{\sigma}(\Delta\sigma_{ij})}{\Delta\sigma_{y}}\right)^{N} \tag{6.16}$$

whereby he ascertained that ΔJ is analogous to J. This provided the necessary justification for the continued utilization of equation (6.15) in variable loading conditions, enabling ΔJ to be evaluated from the following comparable expression,

$$\bar{\varepsilon}(\Delta\varepsilon_{ij}^{P}) = \Delta\varepsilon_{y}\left(\frac{\Delta J}{I_{N}\Delta\sigma_{y}\Delta\varepsilon_{y}r}\right)^{\frac{N}{N+1}}\bar{\varepsilon}(\tilde{\varepsilon}(\theta,N)) \tag{6.17}$$

Thus, using the numerical values of $\bar{\varepsilon}(\Delta\varepsilon_{ij}^{P})$, at a sampling point within the best-matched HRR field, enabled the magnitudes of ΔJ to be evaluated, at the various combinations of variable loading conditions. It is important to note the values of ΔJ, evaluated in equation (6.17), was identified purely from the plastic strains, *i.e.* the effects of elastic strains is totally ignored in the computations. This conjecture holds true throughout the investigations conducted in this chapter.

At this juncture, if an objective magnitude of ΔJ, corresponding to a particular magnitude of $\Delta\sigma_{p}$ is chosen, then loading conditions associated with $\Delta\sigma_{t}$ and $(\Delta\sigma_{p},\Delta\sigma_{t})$ yielding this identical ΔJ, could then be identified. If this is then repeated for other magnitudes of ΔJ, corresponding to other magnitudes of $\Delta\sigma_{p}$, plots of contours of constant ΔJ are then obtained. These are shown in Figure 6.5, for the ratios of $\frac{a}{w} = 0.4$ and $\frac{a}{w} = 0.04$.

6.3.3. Explanation of results

For the plots of contours of constant ΔJ, presented in Figure 6.5, to be useful, explanations into the observed phenomenon were required. Various attempts were made in this respect, with the common behaviour observed along these contours being the identical plastic zone sizes, r_p. The best possible explanation was, however, achieved by classifying the plots into two distinct regions, represented by Region A1 and Region A2 respectively. In the following, the behaviour of these solutions, within these individual regions, is discussed; in relation to known properties of ΔJ within the available literature as well as for comparisons with the assumptions used within the current design and life assessment procedures of R5 [1].

In verifying the values of ΔJ obtained, step-by-step inelastic analysis calculations were performed. In conducting such analysis, it must be ensured that the solution reaches the steady cyclic state before the values of ΔJ were computed. Past investigations have revealed that the conduction of such solutions requires relatively long analysis times. However, a reasonable approximation to such solutions can be achieved by performing a monotonic loading calculation, but with σ_y replaced with $2\sigma_y$. This was examined by Chen *at al* [7] who discovered that in an uncracked body subjected to variable loading conditions, the variations between such monotonic loading solution with an equivalent cyclic solution, measured after a reasonable number of loading cycles, is relatively small. Using such an assumption, the step-by-step analysis values of ΔJ were then identified for the ratios of $\frac{a}{w} = 0.4$ and $\frac{a}{w} = 0.04$ under both variable loads and temperatures.

Parts of these solutions are shown in Figure 6.6, for the case where $\Delta\sigma_p$ are acting alone, in comparison with the previously generated LMM solutions. The plots clearly indicate that irrespective of the crack sizes considered, the two sets of ΔJ values lies within range of each other, *i.e.* the variations follows the same "shape". This provided the confidence on the magnitudes of ΔJ generated using the LMM-based methodology as well as validating the approach of identifying ΔJ using the HRR field criterion. The consistency of the results obtained was further evident in Figure 6.7; the corresponding plots for $\Delta\sigma_t$. Similar comparable behaviour between the two solutions was still observed in these plots. With regard to the differences observed between the two ΔJ solutions in certain loading conditions, the reasons behind such behaviour were not investigated here. This could be due to the differences in ΔJ solutions between the full step-by-step cyclic solution and the solutions obtained using the aforementioned monotonic assumptions.

At this juncture, an attempt was made in describing the observed behaviour with known available solutions. For low variable applied loads, such as those within **Region A1**, the current design and life assessment procedures of R5 [1] employ the small-scale yielding formulation [34]. For the cracked axisymmetric problem considered in the analysis, this is generally given by,

$$\Delta J = \left(\frac{1-\nu^2}{E}\right)\Delta K^2 \qquad (6.18)$$

with $\Delta K = \Delta K_{\Delta\sigma_p} + \Delta K_{\Delta\sigma_t}$

where $\Delta K_{\Delta\sigma_p}$ and $\Delta K_{\Delta\sigma_t}$ are the values of the stress intensity factors associated with the individual magnitudes of $\Delta\sigma_p$ and $\Delta\sigma_t$ respectively. In this thesis, the values of the stress intensity factors were evaluated from the computed linear elastic stress solutions, identified at a sampling point within the best-matched HRR field.

The argument behind the utilization of equation (6.18) is based upon the notion that in elastic materials, stresses tend to infinity as the crack tip is approached,

$$\sigma_{ij}(r,\theta) = \frac{K}{\sqrt{2\pi r}} f_{ij}(\theta) \tag{6.19}$$

i.e. as $r \to 0$, $\sigma_{ij}(r,\theta) \to \infty$. However, in the present investigations, whereby the behaviour of cracked bodies satisfying the elastic-plastic material behaviour was examined, yielding at the crack tip occurs to reduce these high stresses. In the case of small-scale yielding, it is assumed that plastic deformation is contained within a small plastic zone around the crack tip. In such situations, the theory [34] states that it is still possible to characterize the surrounding elastic region using the linear elastic stress fields of (6.19), provided the values of the stress intensity factors, ΔK, in equation (6.18), are increased to $\Delta K'$. This is necessary to balance the reduced stresses in the plastic zones with the higher elastic stresses away from the crack tip.

In this respect, an approximate estimation of $\Delta K'$ was provided by Irwin's theorem [31]. He argued that the occurrence of plasticity at the crack tip causes the crack to behave as if it was longer than its actual size, leading to larger displacements and lower material stiffness

than the purely elastic behaviour. In other words, the body behaves as if it contained a crack of somewhat larger size, defined by an a_{eff}, where $a_{eff} = (a + r_p)$ with a and r_p being the crack and plastic zone sizes respectively, identified from the numerical analysis solutions. In taking this into consideration, Irwin introduced correctional factors [32], designed to estimate the stress intensity factor, $\Delta K'$. This leads to equation (6.18) yielding the following comparable equation,

$$\Delta J = \left(\frac{1 - \nu^2}{E} \right) \Delta K'^2 \tag{6.20}$$

with $$\Delta K' = \Delta K'_{\Delta\sigma_p} + \Delta K'_{\Delta\sigma_t}$$

This enabled the corrected small-scale yielding magnitudes of ΔJ to be computed from equation (6.20), thus, allowing these values to be compared with the LMM solutions.

The results of these comparisons are shown in Figures 6.6 and 6.7, for loading conditions corresponding to individual magnitudes of mechanical and thermal loads respectively. The plots clearly indicate that equation (6.20) underestimates the values of ΔJ. This holds true irrespective of the crack sizes and loading conditions considered. This evidently shows the non-conservative nature of the small-scale yielding formulation, often utilized within the current design and life assessment procedure of R5 [1].

If the loading conditions were increased even further, then the structure is now operating in **Region A2**. This region is best described by the breaking down of the small-scale yielding of equation (6.20). For the perfectly plastic condition, a limit load or an equivalent

ratchet limit is approached. This implies that the sizes of the plastic zones are no longer restrained by the surrounding elastic stress fields. The continued operation of the loading conditions within this region, would thus, ultimately lead to structural failure either due to plastic collapse or the unlimited accumulation of plastic strains.

At this point, an alternative way of describing the behaviour observed in these two regions is presented. This is done using the Failure Assessment Diagram (FAD), employed within the current R6 procedures [89], in assessing the fitness of cracks in a material. Essentially, the diagram requires the evaluation of two parameters, namely ΔL_r and ΔK_r, identified from,

$$\Delta L_r = \frac{\Delta P}{\Delta P_L} \tag{6.21}$$

and

$$\Delta K_r = \left[\frac{\Delta J}{\Delta J_e}\right]^{-\frac{1}{2}} \tag{6.22}$$

where ΔJ_e are the values of ΔJ evaluated from equation (6.20) and ΔP_L is the limit load. Thus, by substituting the relevant quantities, used in the numerical calculations, into equations (6.21) and (6.22), enabled the failure assessment curves associated with both crack sizes to be identified.

Figure 6.8 shows the failure assessment curves corresponding to the two crack sizes considered, obtained from the LMM solutions. A limit to the value of ΔL_r, denoted by $\Delta L_r^{\max}$,

is also included in the diagram, to ensure that plastic collapse is avoided. In both diagrams, the non-conservativeness of the corrected small-scale yielding formulation is clearly apparent. It is also observed that the good correlation between the small-scale yielding and the LMM solutions is true for only low loads. Beyond which equation (6.20) breaks down. Furthermore, in comparison with the LMM solutions, the non-conservativeness of the current R6 procedures [89] FAD is also observed in both plots. This is particularly surprising as the results indicate the current procedures are unsafe. This could be due to the correlation between the small-scale yielding and the LMM solutions holding true for only low loads.

In its application, the utilization of the FAD involves identifying the loading point in the diagrams. If this point, represented by $\left(\Delta L_r^*, \Delta K_r^*\right)$ in Figure 6.8, lies within this curve, then fracture failure is avoided. On the other hand, if the loading point lies outside these curves, then the fracture criterion of equation (6.22) is exceeded and failure would occur. Another advantage of this diagram is that the position of this point relative to the failure assessment curves would provide an instant and visual appraisal of the margin to fracture. Compare LMM with FAD used in practise.

6.3.4. Further analysis

So far, an examination into the behaviour of cracked structures, in the presence of both variable mechanical and thermal loads, was prescribed. The approach requires the utilization of the effective strain ranges, $\bar{\varepsilon}(\Delta\varepsilon_{ij}^P)$, at the best-matched HRR field, as a means of evaluating the elastic-plastic fracture parameter. This enabled the subsequent identification of contours of constant ΔJ, with the observed phenomenon described by two distinct types of

behaviour occurring within two distinct regions. The encouraging results obtained, for the perfectly plastic condition, provided the confidence in pursuing a similar investigation for the cyclic hardening model. This involves the employment of an appropriate model, within the numerical procedures described in Section 6.2.1. In the ensuing analyses, the following model is adopted, whereby the total strain range, $\Delta\varepsilon_{ij}^{P}$, is now the sum of the initial elastic and cyclic plastic strains respectively, where,

$$\Delta\varepsilon_{ij}^{P} = \Delta\varepsilon_{ij}^{e} + \Delta\varepsilon_{ij}^{PP} \tag{6.23}$$

with $$\Delta\varepsilon_{kk}^{e} = \frac{1}{3K}\Delta\sigma_{kk}, \qquad \Delta\varepsilon_{ij}^{e'} = \frac{1}{2\mu}\Delta\sigma_{ij}^{'}$$

and $$\Delta\varepsilon_{ij}^{PP} = \frac{\Delta\varepsilon_0}{\Delta\sigma_0^{N}}\bar{\sigma}(\Delta\sigma_{ij})^{N}\frac{3}{2}\frac{\Delta\sigma_{ij}^{'}}{\bar{\sigma}(\Delta\sigma_{ij})}$$

The contributions of these individual strains towards the total strain range is, thus, greatly dependent upon the magnitudes of the applied loading conditions, $\Delta\sigma_{ij}$. In the numerical procedures, the material constants employed are extracted from the cyclic hardening plots of Figure 3.6.

In undertaking these additional investigations, the parallel fulfilment of the HRR field criterion of (6.14), needs to be realized, for the different values of N explored. In the following analyses, the behaviour of the cracked axisymmetric Bree problem was examined, for cyclic hardening exponents of $N = 3,5\,\&\,7$. These assessments are shown in Figures 6.9 and 6.10, as plots of $\log\bar{\varepsilon}(\Delta\varepsilon_{ij}^{P})$ against $\log\frac{r}{w}$, where $\bar{\varepsilon}(\Delta\varepsilon_{ij}^{P})$ are now the effective strains in (6.23). The satisfactions of the HRR field criterion were still observed, except in the first

few elements, with the best-matched HRR field still identified at the previous locations. Similar agreements, albeit not presented here, were also achieved, for corresponding $\Delta\sigma_p$ and $\Delta\sigma_t$ induced crack tip fields at $N=5$ and $N=7$. Unsurprisingly, these observations, under the combined actions of $(\Delta\sigma_p, \Delta\sigma_t)$, still hold true, for both crack sizes and the three cyclic hardening exponents considered.

The demonstration of the HRR fields, for the cyclic hardening model, is an essential pre-cursor in the evaluation of the equivalent elastic-plastic fracture parameter, ΔJ, in this circumstance. As before, this required the substitution of $\bar{\varepsilon}(\Delta\varepsilon_{ij}^{P})$, at a sampling point within the best-matched HRR field, into the equivalence of equation (6.17), given by,

$$\bar{\varepsilon}(\Delta\varepsilon_{ij}^{P}) = \Delta\varepsilon_0 \left(\frac{\Delta J}{I_N \Delta\sigma_0 \Delta\varepsilon_0 r} \right)^{\frac{N}{N+1}} \bar{\varepsilon}(\tilde{\varepsilon}(\theta, N)) \qquad (6.24)$$

where I_N & $\bar{\varepsilon}(\tilde{\varepsilon}(\theta, N))$ are values obtained from tables evaluated by Shih [64]. This, then, enabled the computations of the different magnitudes of ΔJ, corresponding to the loading conditions associated with $\Delta\sigma_p$ and $\Delta\sigma_t$. As a consequence, plots of contours of constant ΔJ were then identified, an example of which is shown in Figure 6.11.

Concurring with the perfectly plastic solutions, these additional contours still show two different modes of behaviour. In **Region A1**, the non-conservativeness of the small-scale yielding formulation of (6.20) in comparison with the LMM solutions was still evident. It was observed that this behaviour remains true, irrespective of the crack sizes and the cyclic

hardening exponents considered. This implies that the continued utilization of small-scale yielding formulation, beyond this region, would lead to non-conservative values of ΔJ.

If the loads were increased further, then the structure is now operating within **Region A2**. Unlike the earlier solutions for perfect plasticity, whereby the behaviour was described by the onset of plastic collapse or ratchetting, the cyclic hardening results clearly indicates otherwise. Within these solutions, the employment of the cyclic hardening model, represented by equation (6.23), enabled the total strain ranges, $\Delta\varepsilon_{ij}^{P}$, to be examined, far beyond the limit loads and the ratchet limits. In this respect, the investigations revealed that the continued intensification of the loading conditions would ultimately cause the elastic strain contributions towards $\Delta\varepsilon_{ij}^{P}$ to be negligible. This would then lead to the structural behaviour to be entirely described by the associated plastic strains, $\Delta\varepsilon_{ij}^{PP}$, *i.e.* the second term in (6.23). In such situations, the simplified reference stress method [1,19], used in Chapter 5 for estimating $C^{*}(n)$, may then be adopted, in approximating the magnitudes of $\Delta J(N)$. These can be evaluated from the following expressions, for the loading conditions where $\Delta\sigma_{p}$ is acting alone,

$$\Delta J_{ref}(N) = \left(\frac{\Delta\sigma_{ref}}{\Delta\sigma_{0}}\right)^{N+1} \Delta\sigma_{0}\Delta\varepsilon_{0}R' \qquad (6.25)$$

where $\Delta\sigma_{ref} = \Delta P\left(\frac{\sigma_{y}}{P_{L}}\right)$ & $R' = \left(\frac{\Delta K^{2}}{\Delta\sigma_{ref}^{2}}\right)$

with the terms having the same meanings as before.

Figure 6.12 shows the comparisons between the values of $\Delta J_{num}(N)$ and $\Delta J_{ref}(N)$, the numerical and reference stress estimates of $\Delta J(N)$ respectively. It distinctly shows the over-estimation of $\Delta J_{ref}(N)$, in some cases exceeding it by a factor of 5. This is not surprising as the simplified reference stress method was formulated with a great deal of conservativeness in mind [1,19]. Furthermore, the reproduction of such behaviour in Figure 6.13, the equivalent plot for short cracks, verified the consistency of the numerical solutions generated using the prescribed LMM-based methodology.

At this point, an effective definition of $\Delta J(N)$, designated by $\Delta J_{eff}(N)$, was proposed. This involves fitting equation (6.25) to the numerical values of $\Delta J(N)$. For such a proposition to work, however, it needs to be shown that $\Delta J_{num}(N)$ varies with $N+1$. The results in Figures 6.12 and 6.13 clearly show that this is the case. The fulfilment of this condition, thus, enabled the repositioning of the $N-$independent location of $\Delta J_{ref}(N)$, currently occurring at $\Delta\sigma_{ref} = \Delta\sigma_0$, to the corresponding $N-$independent location of $\Delta J_{eff}(N)$, which would occur at $\Delta\sigma_{ref}^{eff} = \Delta\sigma_0$. In achieving this "transfer", the analyses revealed the necessary re-definition of two quantities in (6.25), whereby,

$$\Delta\sigma_{ref}^{eff} = \Delta P\left(A\frac{\sigma_y}{P_L}\right) \quad \& \quad R'_{eff} = \left(B\frac{\Delta K^2}{\Delta\sigma_{ref}^2}\right) \tag{6.26}$$

where A and B are constants related to the downward shifting of $\Delta J_{ref}(N)$. In the solutions, these values were $(A = 0.85, B = 0.42)$ and $(A = 0.95, B = 0.25)$, for $\frac{a}{w} = 0.4$ and $\frac{a}{w} = 0.04$,

respectively. The substitutions of $\Delta\sigma_{ref}^{eff}$ and $R_{eff}^{'}$ into equation (6.25), in place of $\Delta\sigma_{ref}$ and $R^{'}$, thus, enabled the evaluation of $\Delta J_{eff}(N)$, as shown in Figures 6.12 and 6.13. (Note: It was observed that in the two crack problems considered, $\Delta\sigma_{ref}$ and $R^{'}$ was reduced by $85-95\%$ and $30-60\%$ respectively.)

In accounting for the effect of thermal loads, however, an equivalent definition for $\Delta\sigma_{ref}$ does not exist. Nonetheless, if it can be shown that $\Delta J_{num}(N)$, under the actions of $\Delta\sigma_t$, still varies with $N+1$, corresponding $N-$independent locations of $\Delta J_{eff}(N)$ can then be identified. Additional plots for individual thermal loads, shown in Figure 6.14, clearly prove that this is the case. It is clearly observed that the values of $\Delta J_{num}(N)$, associated with these loading conditions, were still found to vary in accordance with the prescribed condition. Similar conforming behaviours were also revealed, under the combined actions of $(\Delta\sigma_p, \Delta\sigma_t)$. At this juncture, if the mechanical and thermal loads, associated with these $N-$independent locations, were then identified, the yielding of contours of constant $\Delta\sigma_{ref}^{eff}$ would result. These are presented in Figure 6.15, with a comparison with the R5 [1] solution, identified using equation (5.5) of Chapter 5, the limit currently used in industry in assessing the behaviour of cracked structures. The contours, irrespective of the crack sizes, clearly indicates the appropriateness of the R5 limit, as the maximum differences between them were less than 10%. The behaviour of these solutions, thus, led to the conclusion that the employment of the R5 limit, within this region, is a reasonable representation of the behaviour of cracked structures subjected to loading conditions associated with mechanical and thermal loads.

6.3.5. Concluding remarks

So far, the investigations have successfully revealed the possibility of describing the behaviour of cracked structures, in the presence of both mechanical and thermal loads, in two separate regions. In Region A1, the behaviour was described by the small-scale yielding formulation of (6.18) and in Region A2, by the corresponding effective reference stress equation of (6.26), in conjunction with (6.25). For any judgment on the conservativeness or non-conservativeness of these solutions to be passed, however, it needs to be compared with solutions from current procedures [1], evaluated from the following expression,

$$\Delta J_{ref}^{Total} = \Delta J_e + \Delta J_{ref} \tag{6.27}$$

where ΔJ_e and ΔJ_{ref} are values obtained from equations (6.18) and (6.25) respectively. Also included is an additional solution, ΔJ_{eff}^{Total}, where the values of ΔJ_{ref} is now replaced by ΔJ_{eff}. These solutions are shown in Figure 6.16, for the two crack size problems considered. In both plots, the overestimation of the ΔJ_{ref}^{Total} solutions, especially in Region A2, is clearly observed. This is in agreement with the conclusion of the joint report by EPRI/CRIEPI/NE [33] on the conservativeness of the current solutions procedures [1]. This observation is particularly important in the context of the loading conditions applied in industry, which tends to operate within Region A2. In this regard, a slightly less conservative representation of the solutions can be obtained with the utilization of ΔJ_{eff}^{Total}.

6.4. Reverse-plasticity/Creep Solutions

The purpose of this examination is to develop an understanding into the behaviour of cracked structures under cyclic loading histories, where creep dwell times exists, using the reverse-plasticity/creep solution method described in Section 6.2.2. As before, this involves an in-depth investigation into the near crack tip fields, in the presence of both variable loads and variable temperatures. This would then enable the changes in the stresses and strains to be investigated over the dwell time, Δt. It was optimistic that the solutions generated from these analyses would provide the necessary information concerning the overall crack tip fracture behaviour. (Note: The actual fully commented programs are enclosed in the attached CD.)

6.4.1. HRR fields

As an initial investigation, the behaviour of the cracked Bree problem was considered, with only the mechanical loads applied. This allowed the near crack tip fields to be examined at all locations away from the crack tip, irrespective of the values of θ. An example is shown in Figure 6.17, the plot of $\log \bar{\varepsilon}(\Delta\varepsilon_{ij}^{cP})$ against $\log \frac{r}{w}$, where $\bar{\varepsilon}(\Delta\varepsilon_{ij}^{cp})$ is the total effective strains accumulated over the cycle. It was found that the satisfaction of the HRR field criterion was still achieved at all locations, except in the first few elements, with the best-matched HRR still observed at $\theta = 70^0$. An additional behaviour, indicating the solutions dependency upon Δt, was also observed. It was established that for small Δt, the crack tip fields were found to satisfy the HRR field criterion of $N = \infty$. As Δt was increased, however, the solutions were found to satisfy the HRR field criterion of $N = 3$ instead. Physically, the result indicates the

effect of creep at high dwell times, causing the plastic crack tip fields to be overcome by the dominating creep fields. At low times, however, the domination of the plastic fields was still observed at the crack tip. This behaviour was mirrored in the parallel investigation of short cracks, as shown in Figure 6.18. Although not included here, similar behaviours was observed at much higher loading conditions, in both crack conditions.

6.4.2. Some observations

In undertaking the investigations in this thesis, simplified solution procedures were adopted. It is no difference in the reverse-plasticity/creep analysis method prescribed here. However, in the initial explorations, it was found that the utilization of such procedures in creep conditions required much more thought. This was not anticipated and thus not pursued any further.

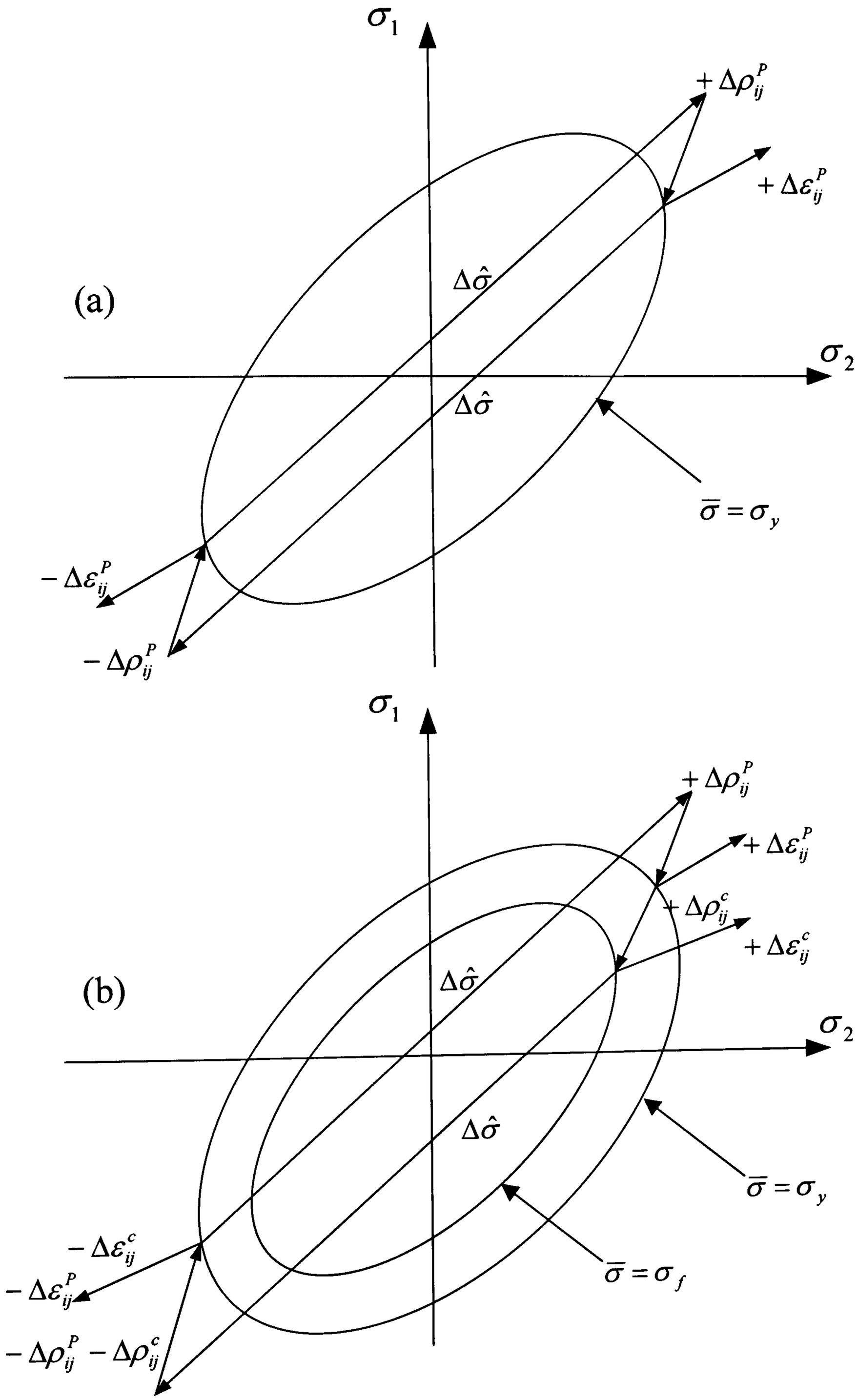

Figure 6.1: Schematic diagrams of the reverse-plasticity and reverse-plasticity/creep solution methods.

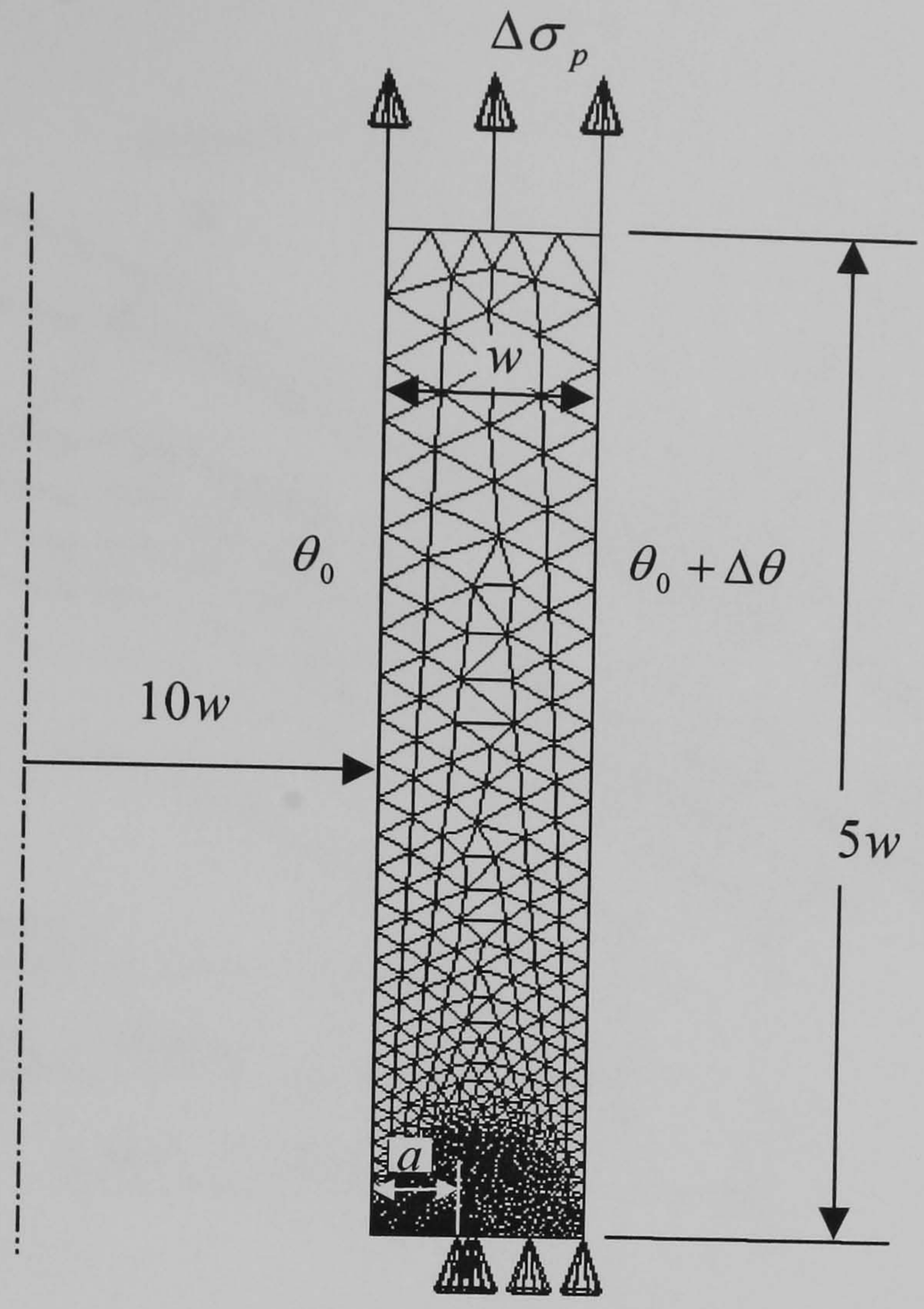

Finite element model

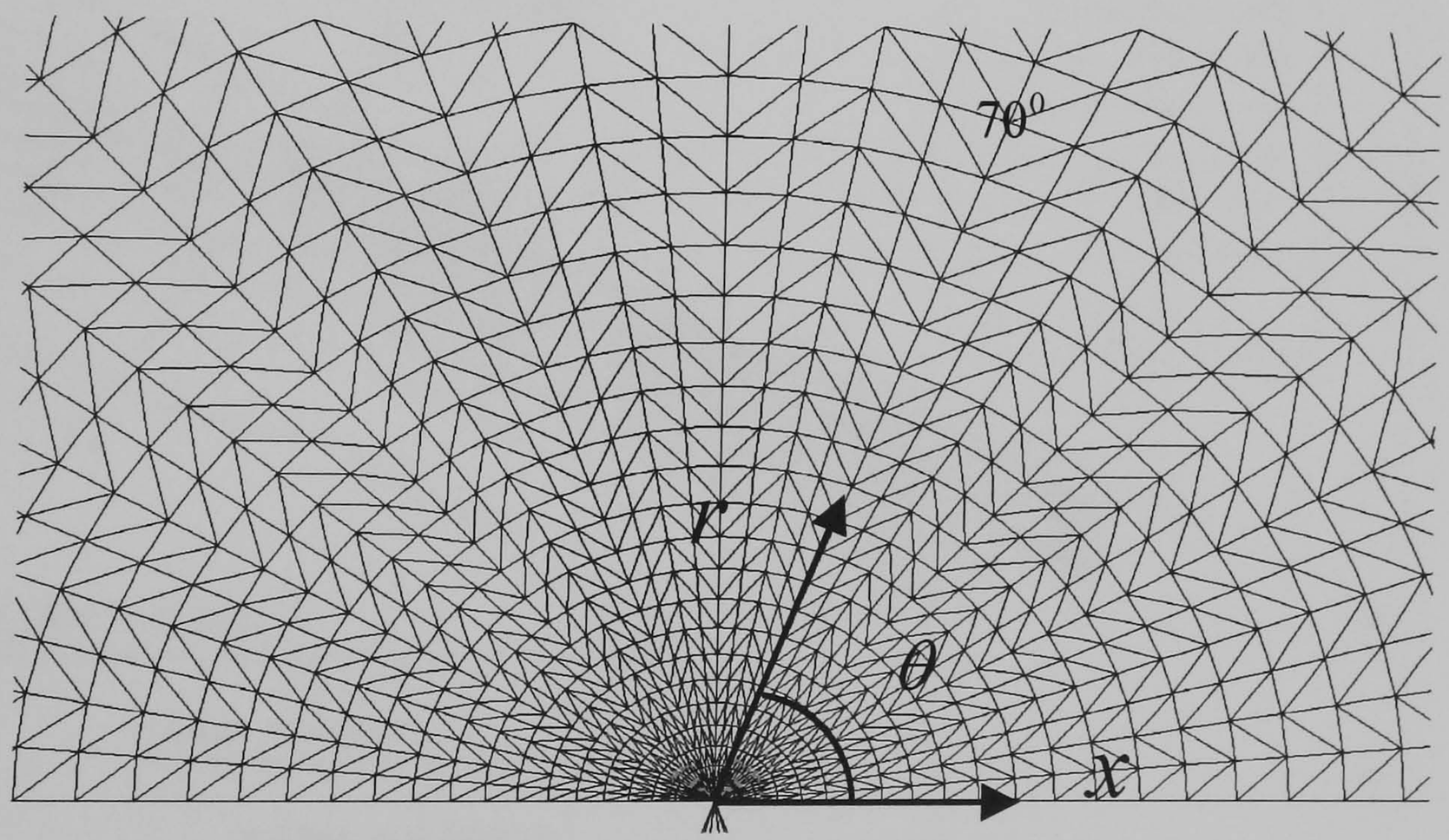

Mesh at the crack tip

Figure 6.2: The model of the cracked axisymmetric Bree problem considered in the reverse-plasticity and reverse-plasticity/creep analyses.

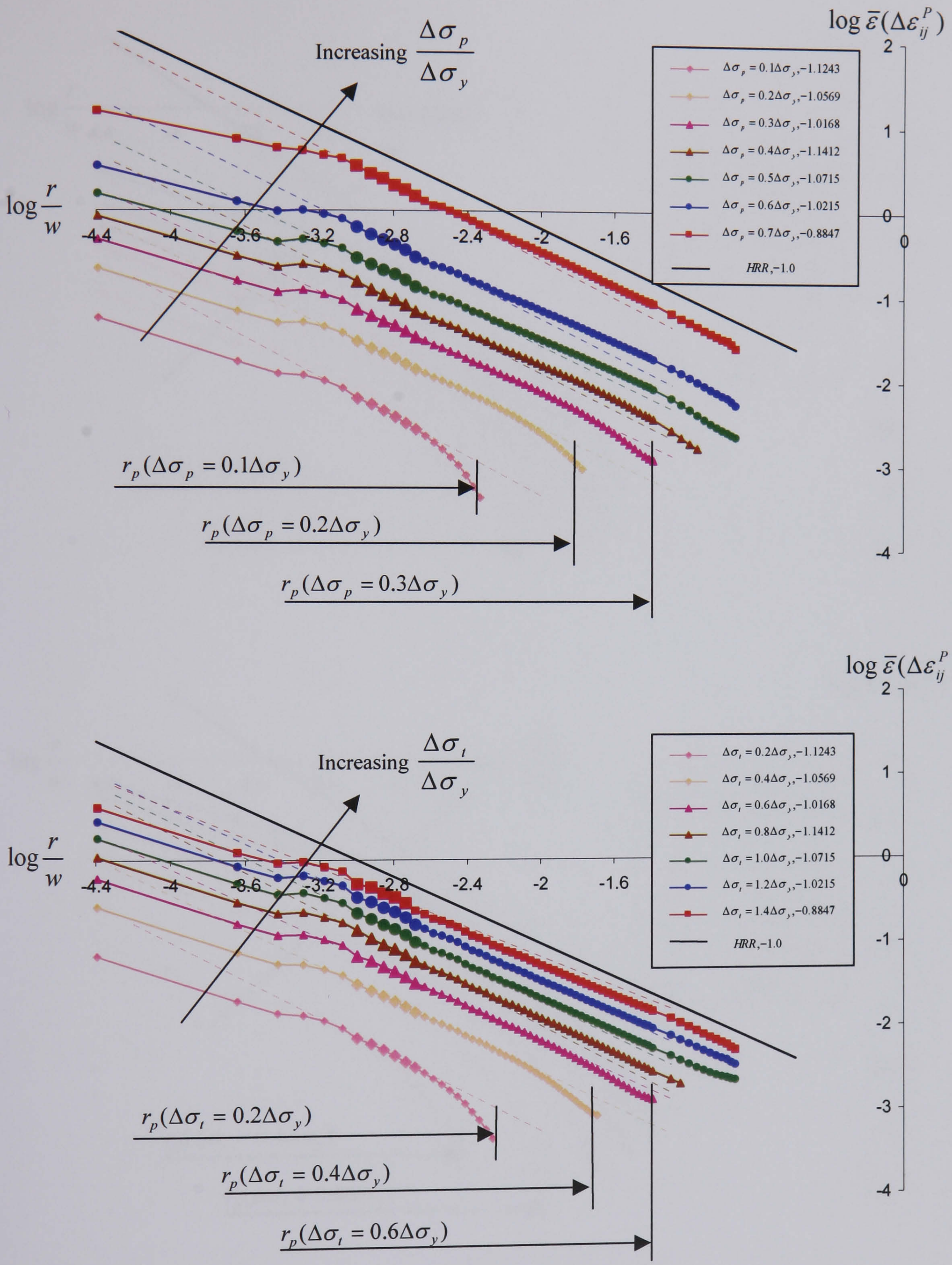

Figure 6.3: Crack tip solutions for increasing $\Delta\sigma_p$ & $\Delta\sigma_t$ at $\frac{a}{w} = 0.4$ and $\theta = 70^0$.

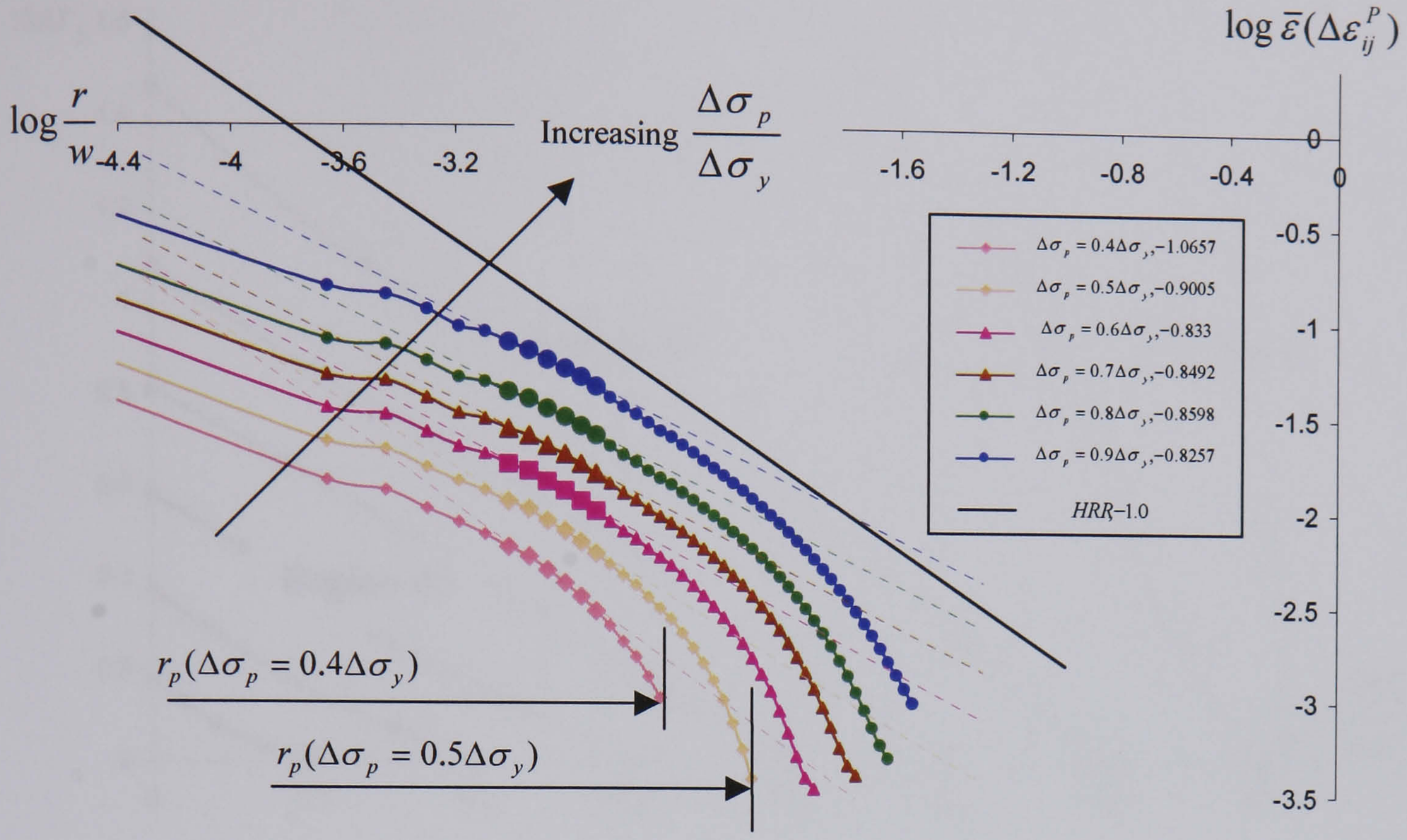

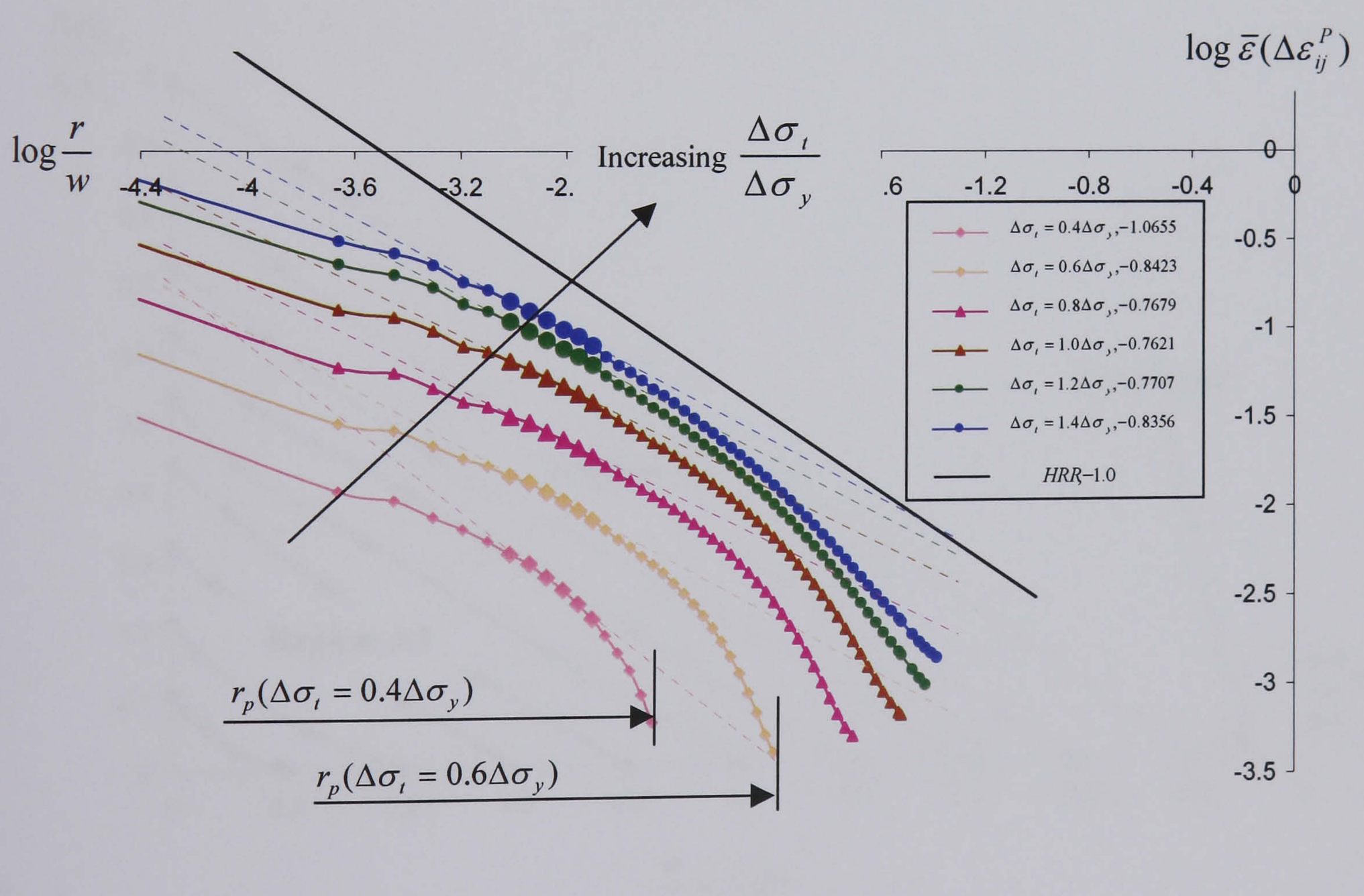

Figure 6.4: Crack tip solutions for increasing $\Delta\sigma_p$ & $\Delta\sigma_t$ at $\frac{a}{w} = 0.04$ and $\theta = 70^0$.

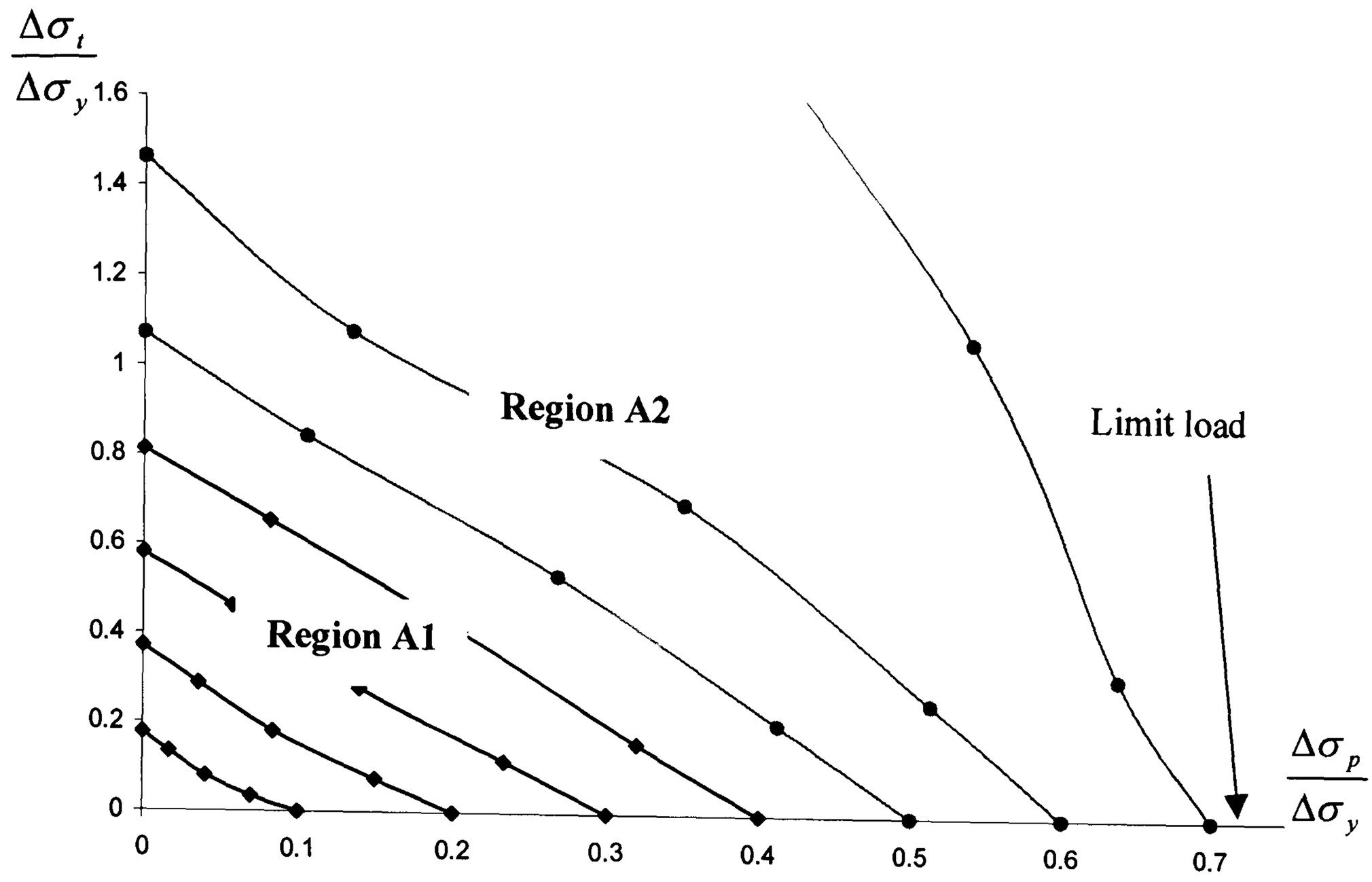

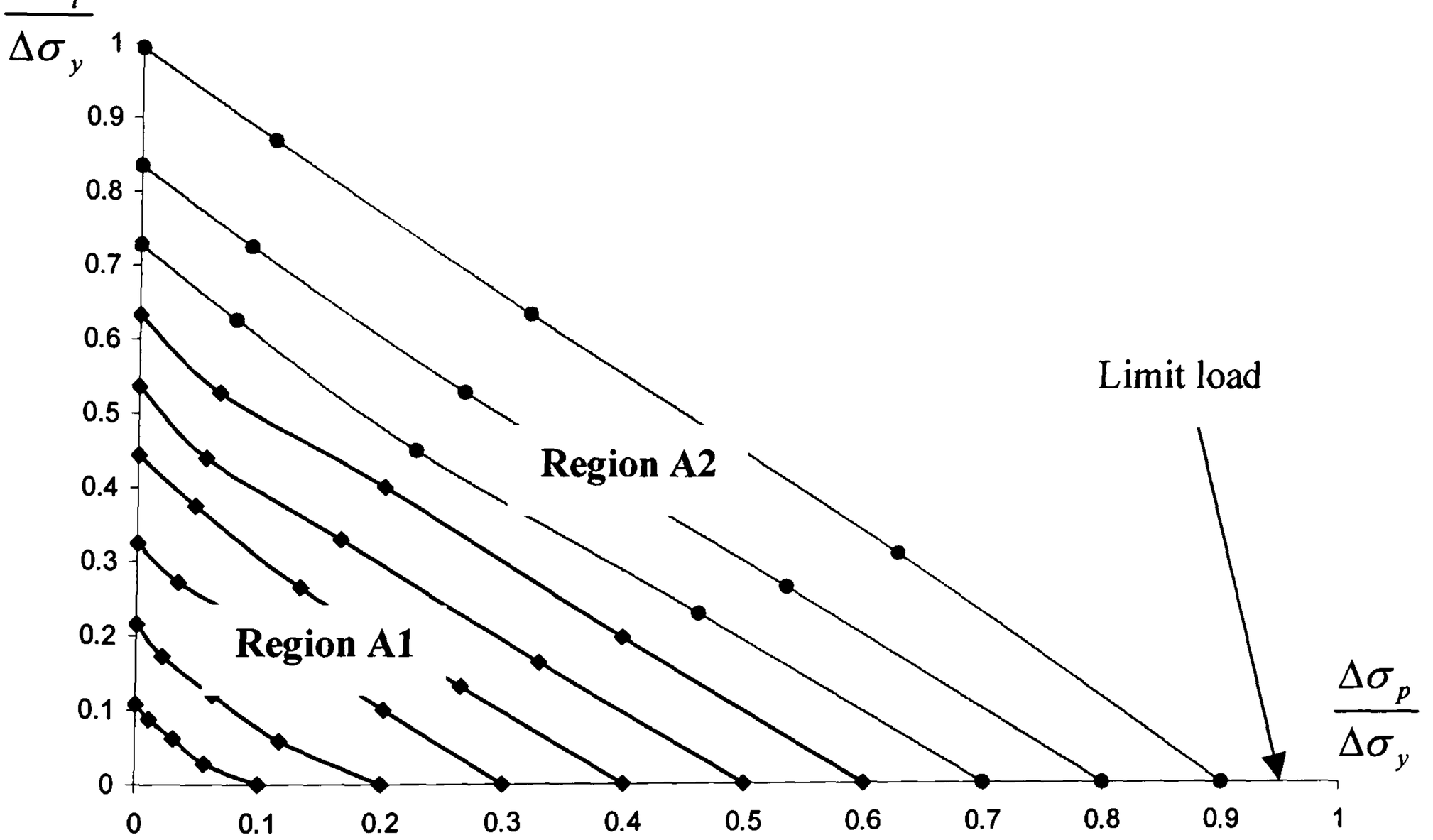

Figure 6.5: Contours of constant ΔJ.

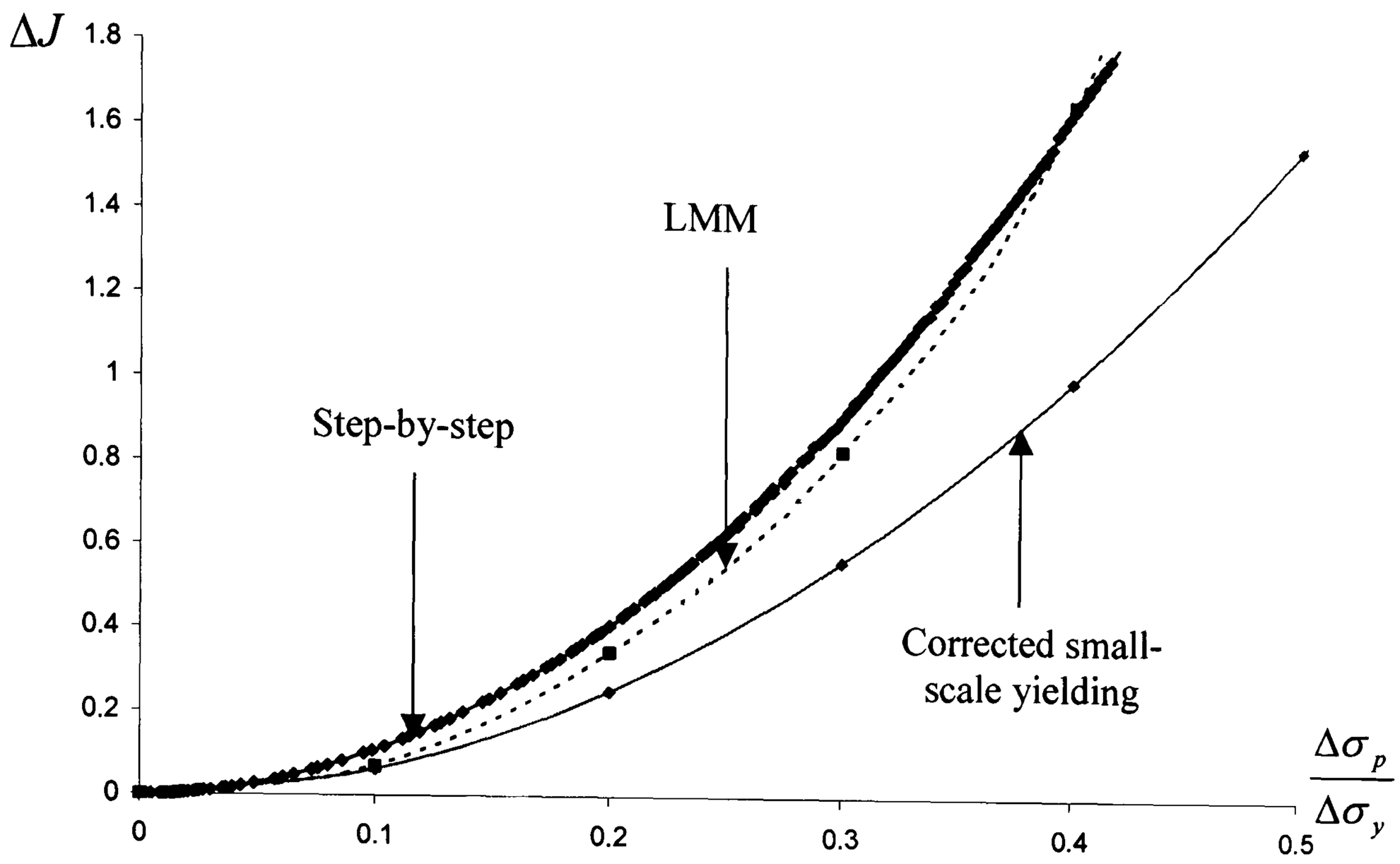

$\frac{a}{w} = 0.4$.

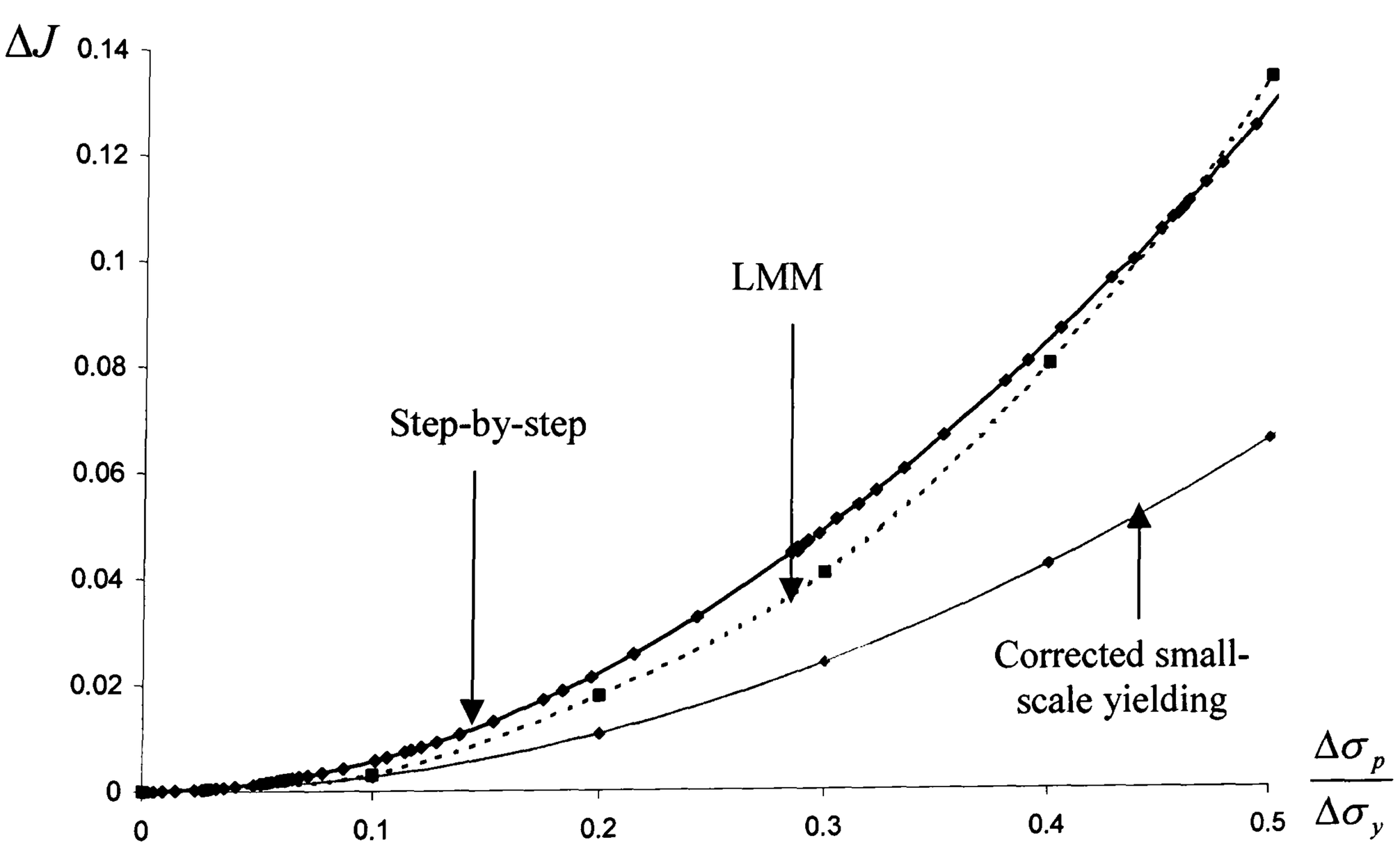

$\frac{a}{w} = 0.04$

Figure 6.6: Comparisons between the values of ΔJ for $\Delta\sigma_p$.

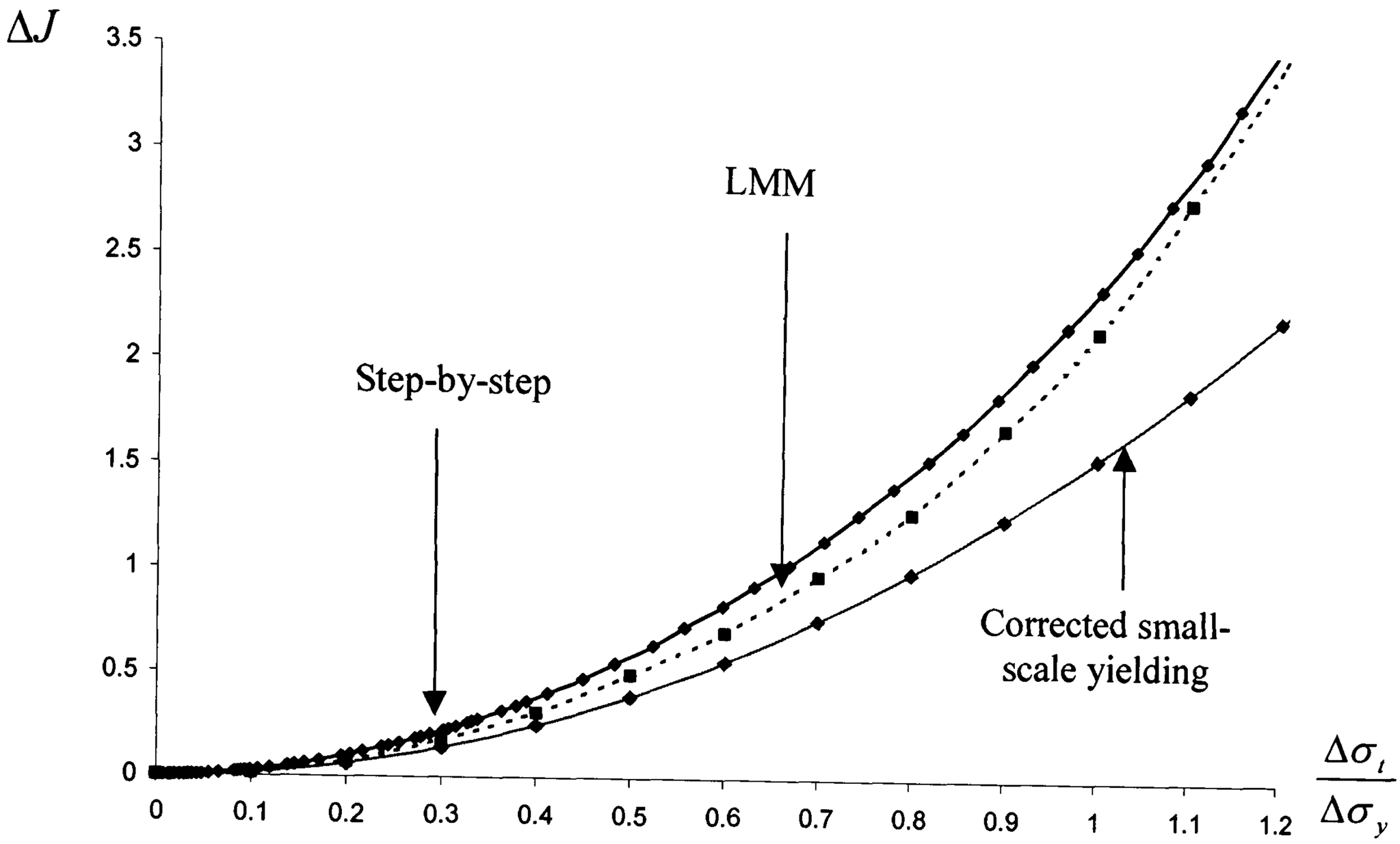

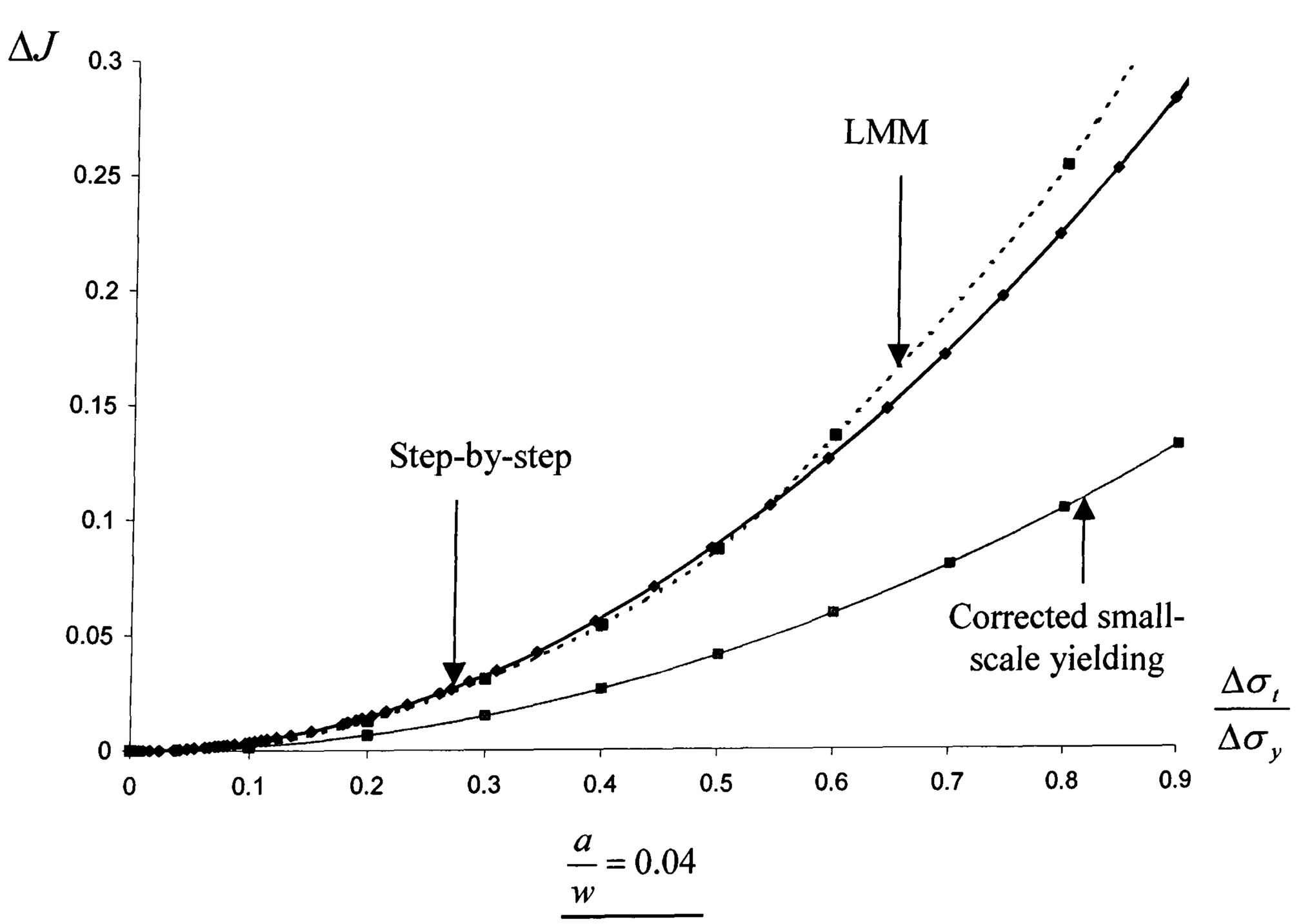

Figure 6.7: Comparisons between the values of ΔJ for $\Delta\sigma_t$.

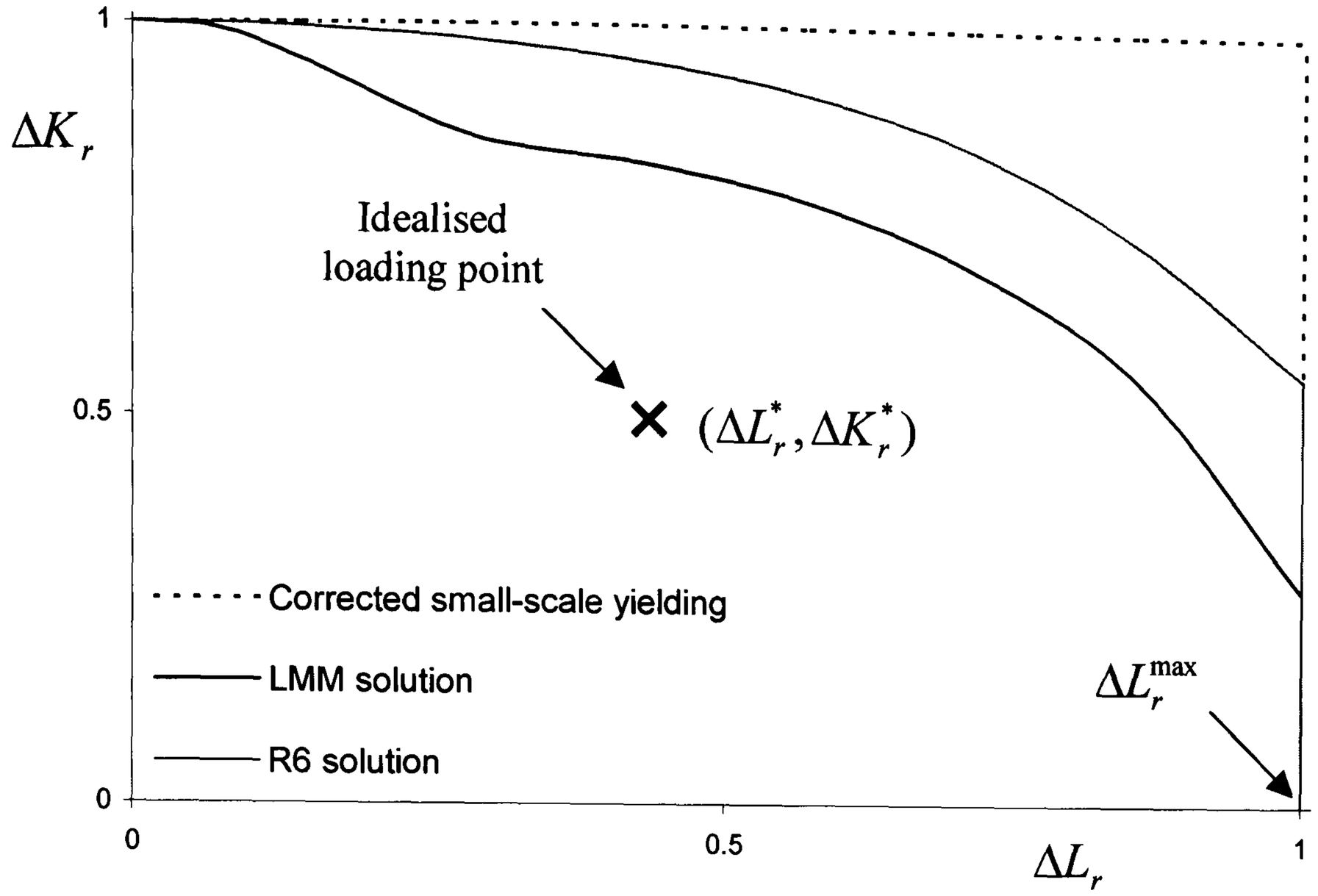

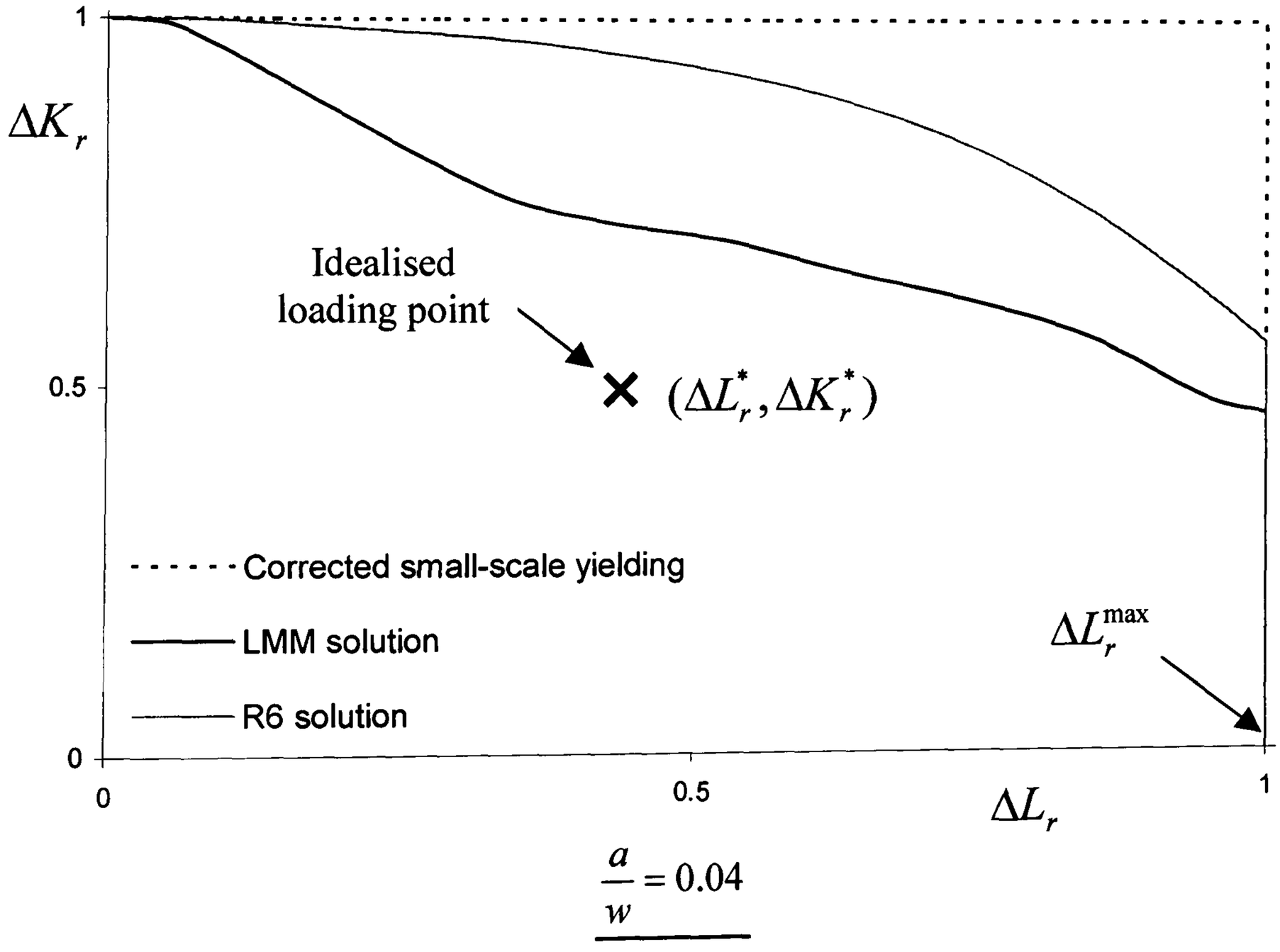

Figure 6.8: Failure assessment diagrams.

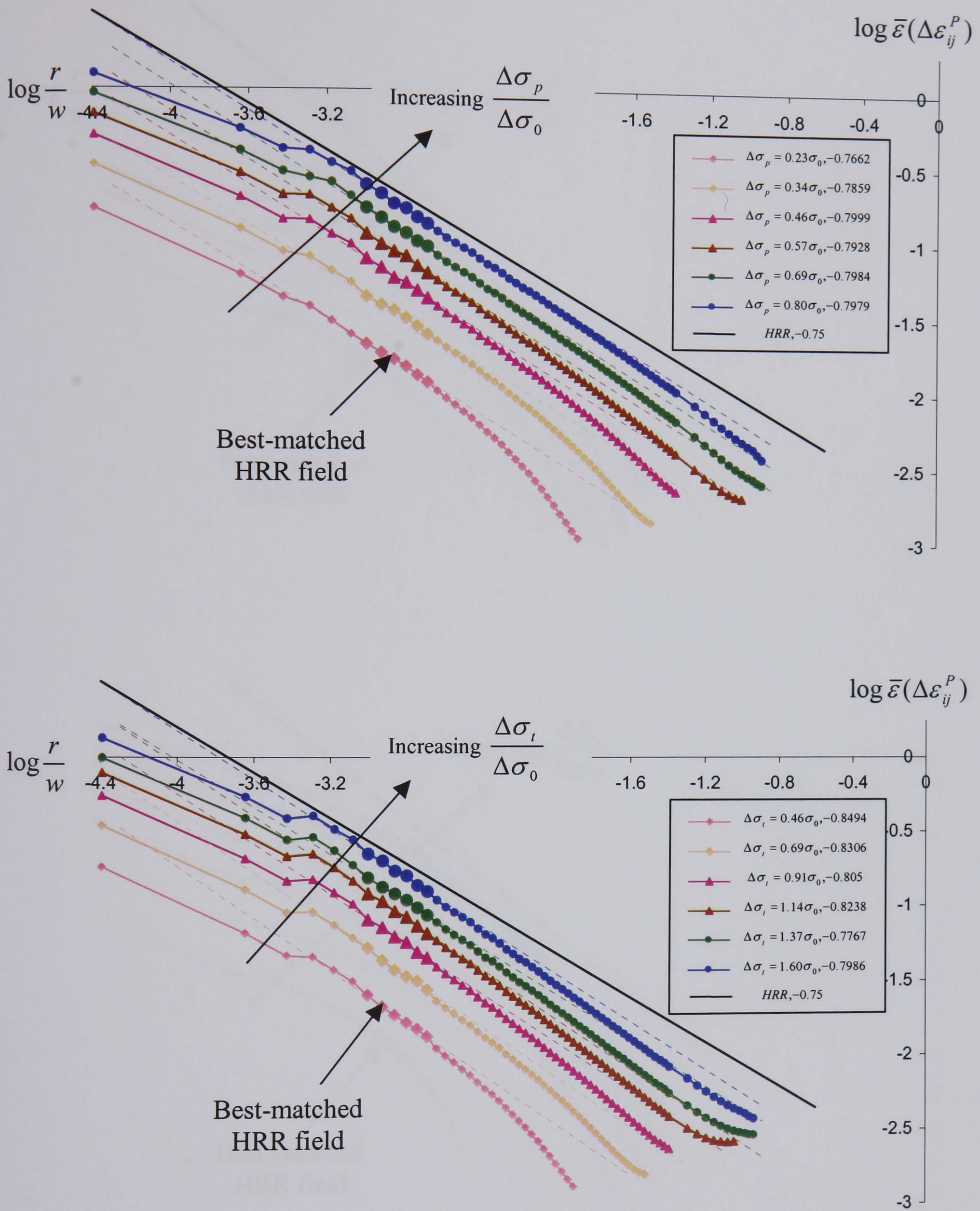

Figure 6.9: Crack tip solutions for increasing $\Delta\sigma_p$ & $\Delta\sigma_t$ at $N=3$ for $\frac{a}{w}=0.4$.

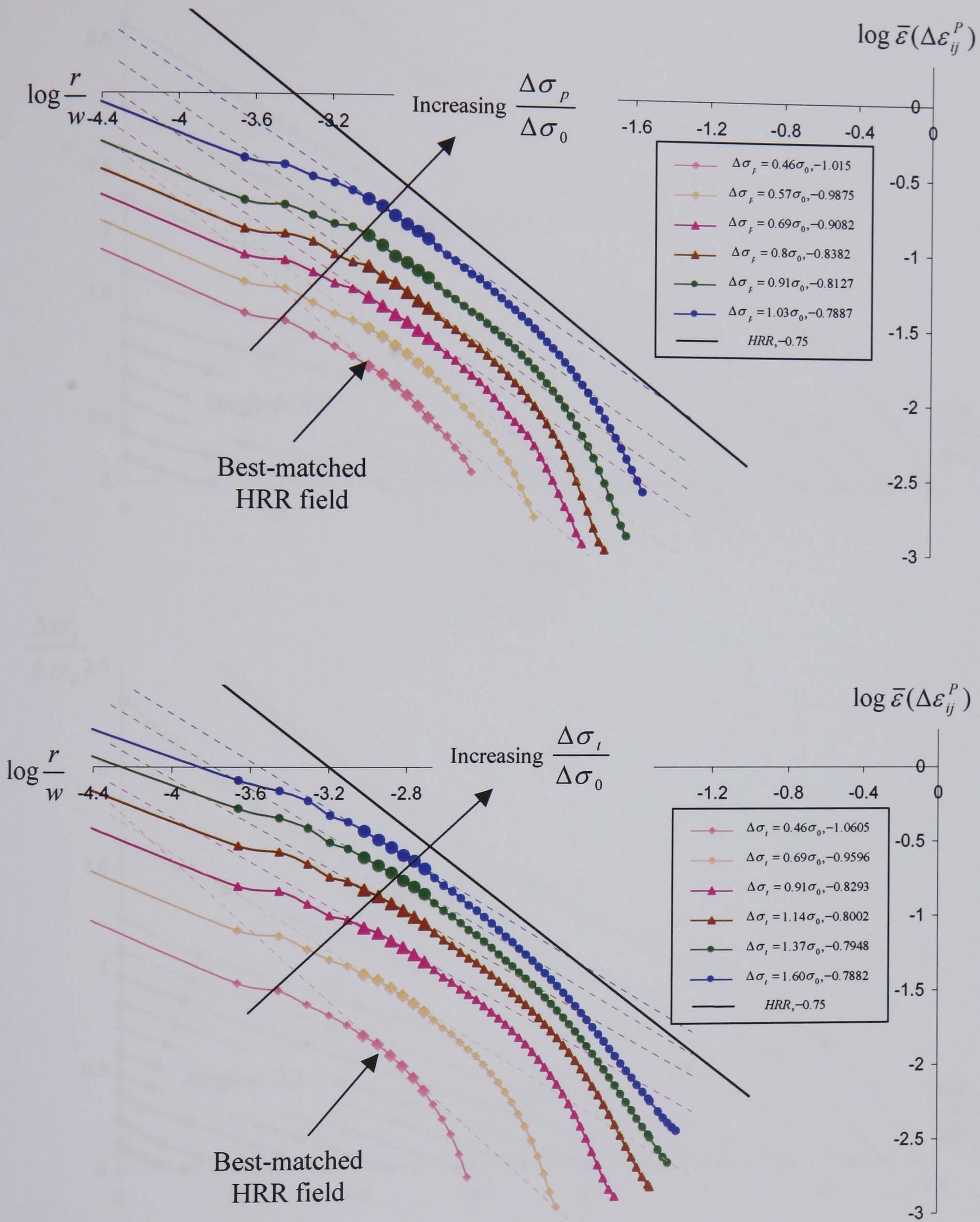

Figure 6.10: Crack tip solutions for increasing $\Delta\sigma_p$ & $\Delta\sigma_t$ at $N = 3$ for $\frac{a}{w} = 0.04$.

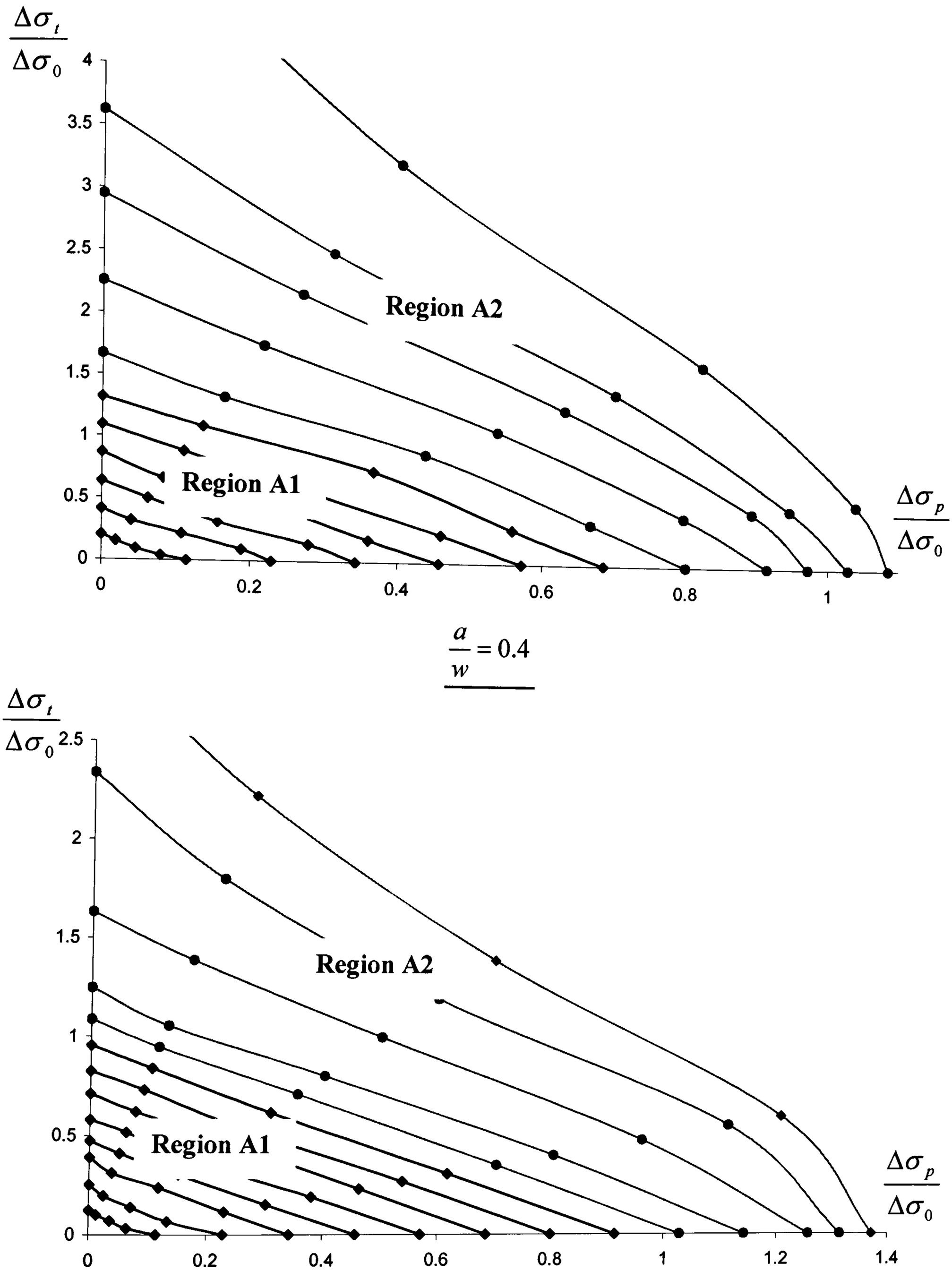

Figure 6.11: Contours of constant ΔJ for $N = 7$.

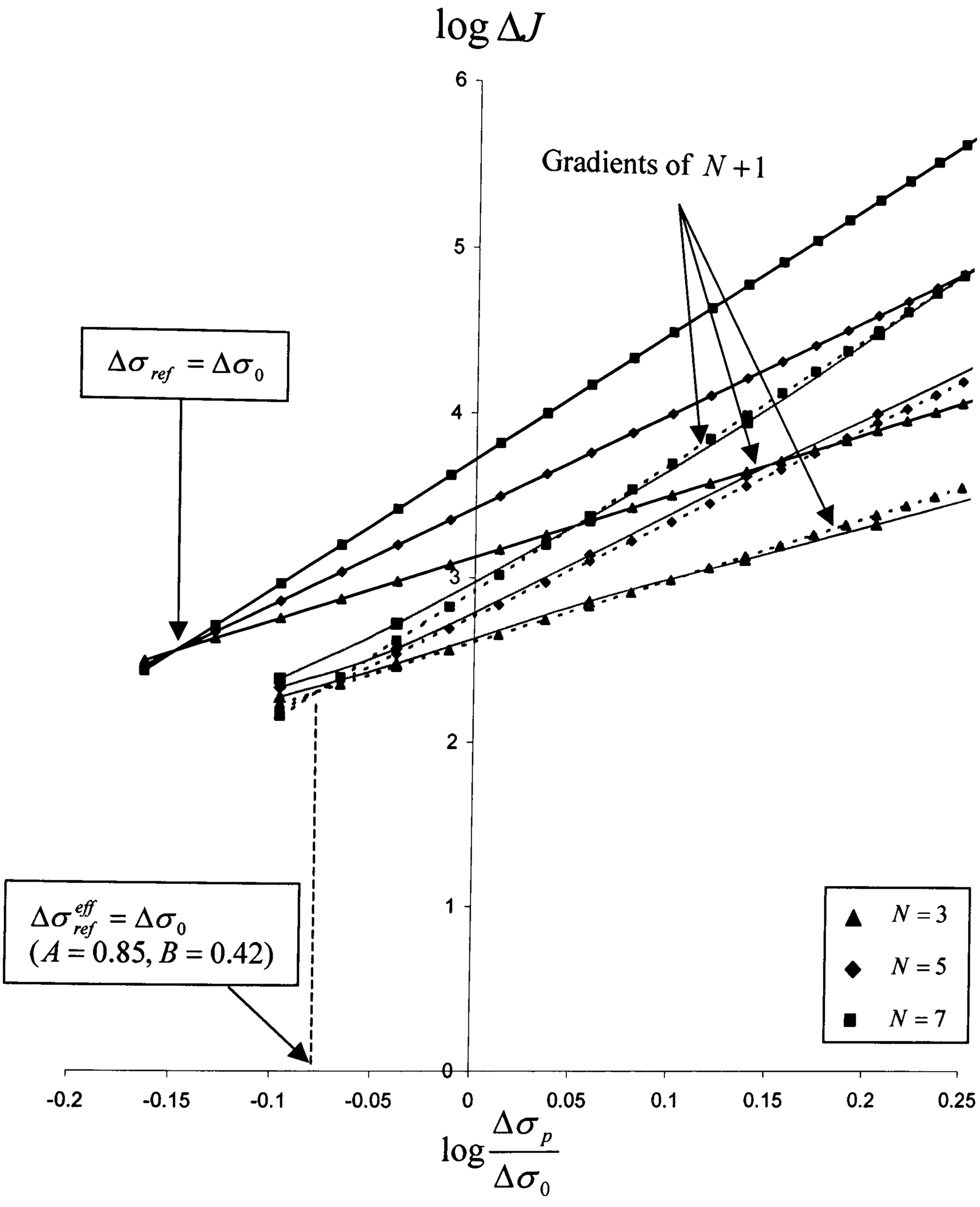

Figure 6.12: Comparison between the values of $\Delta J(N)$ for $\frac{a}{w} = 0.4$ in Region A2.

(—— $\Delta J_{num}(N)$ - Numerical values of $\Delta J(N)$,

—— $\Delta J_{ref}(N)$ - Reference stress,

····· $\Delta J_{eff}(N)$ - Effective reference stress)

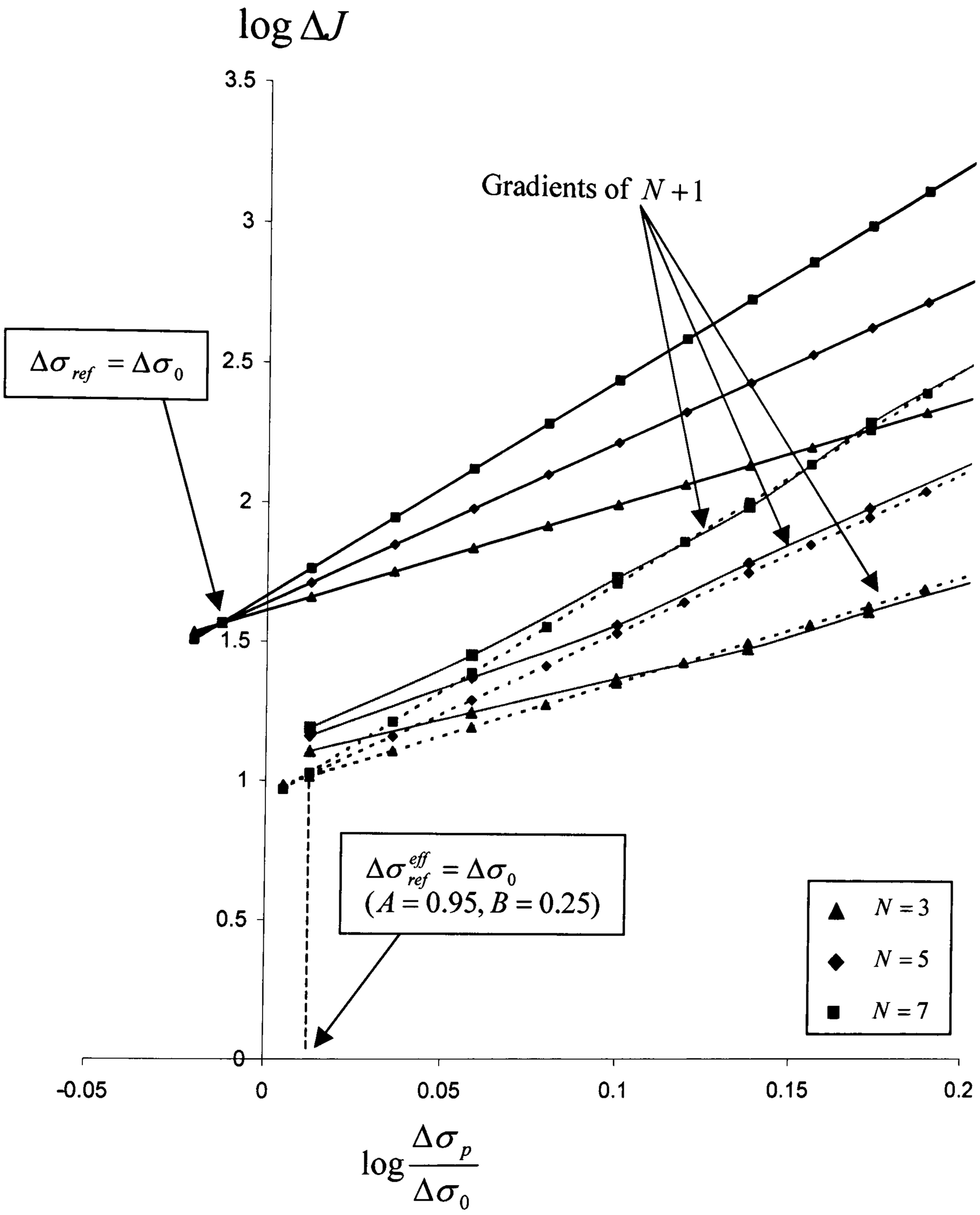

Figure 6.13: Comparison between the values of $\Delta J(N)$ for $\frac{a}{w} = 0.04$ in Region A2.

(—— $\Delta J_{num}(N)$ - Numerical values of $\Delta J(N)$,

—— $\Delta J_{ref}(N)$ - Reference stress,

····· $\Delta J_{eff}(N)$ - Effective reference stress)

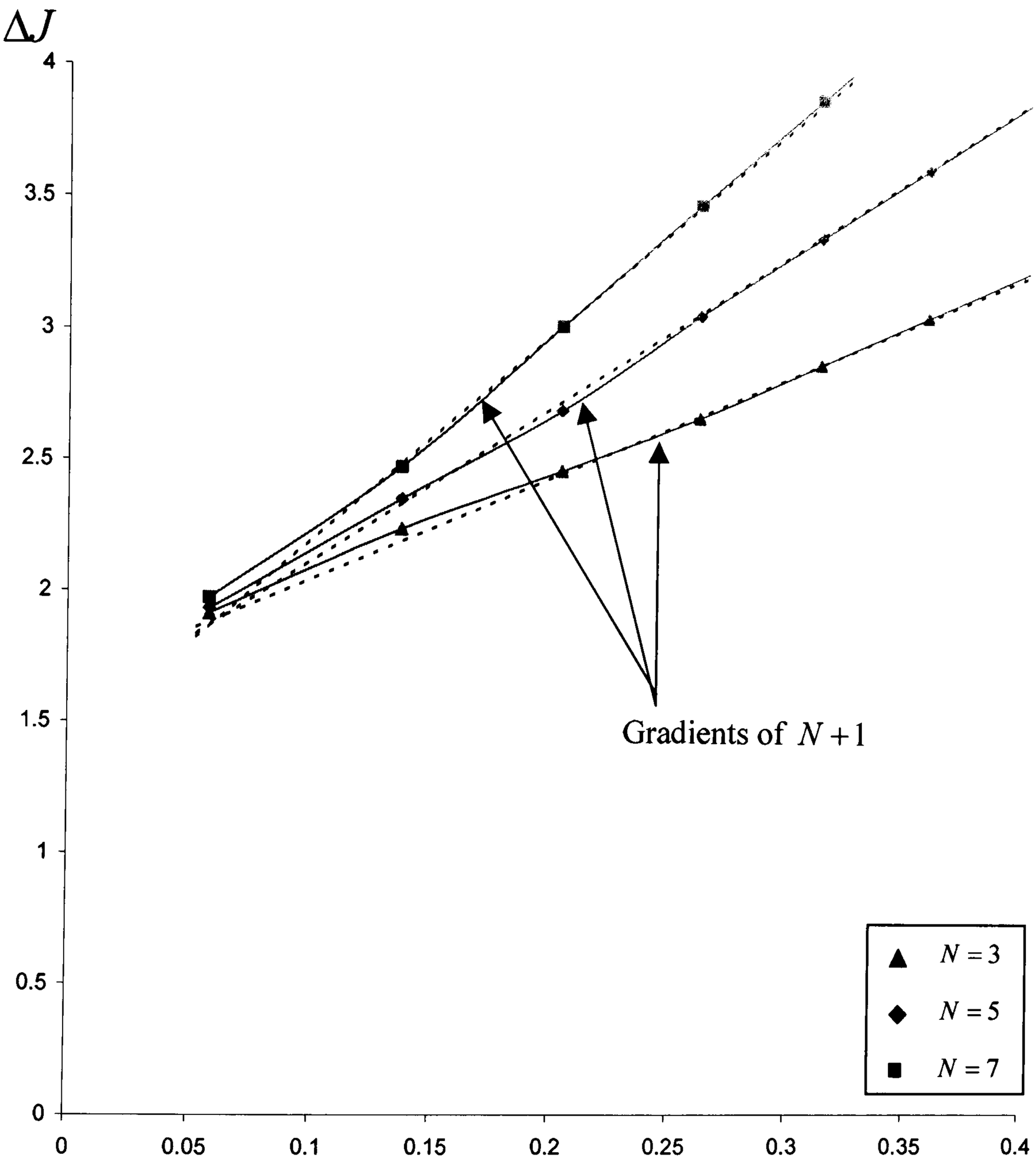

Figure 6.14: Comparison between the values of $\Delta J(N)$ for $\frac{a}{w} = 0.4$ in Region A2.

(—— $\Delta J_{num}(N)$ - Numerical values of $\Delta J(N)$,

····· $\Delta J_{eff}(N)$ - Effective reference stress)

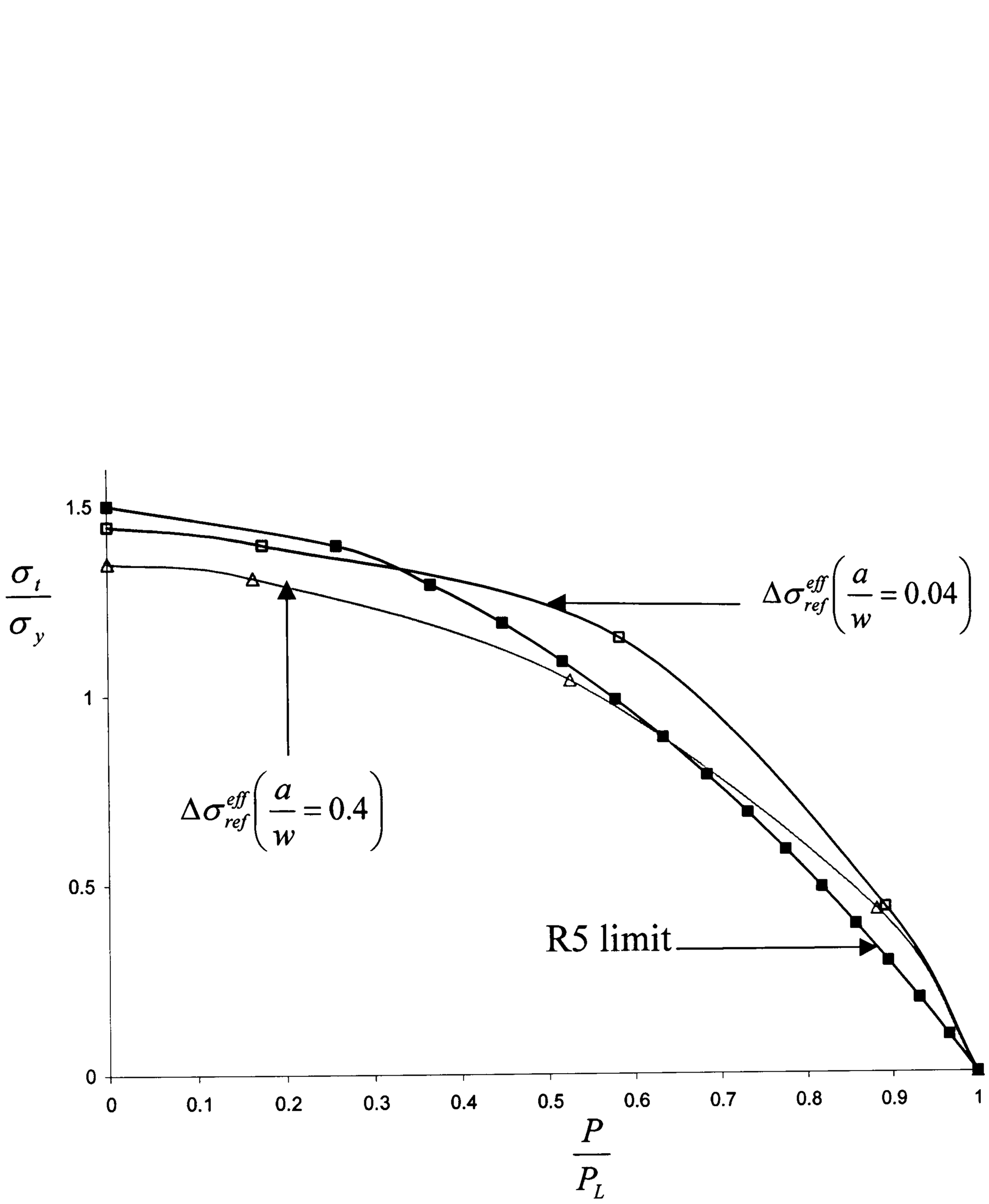

Figure 6.15: Plots of contours of constant crack tip conditions.

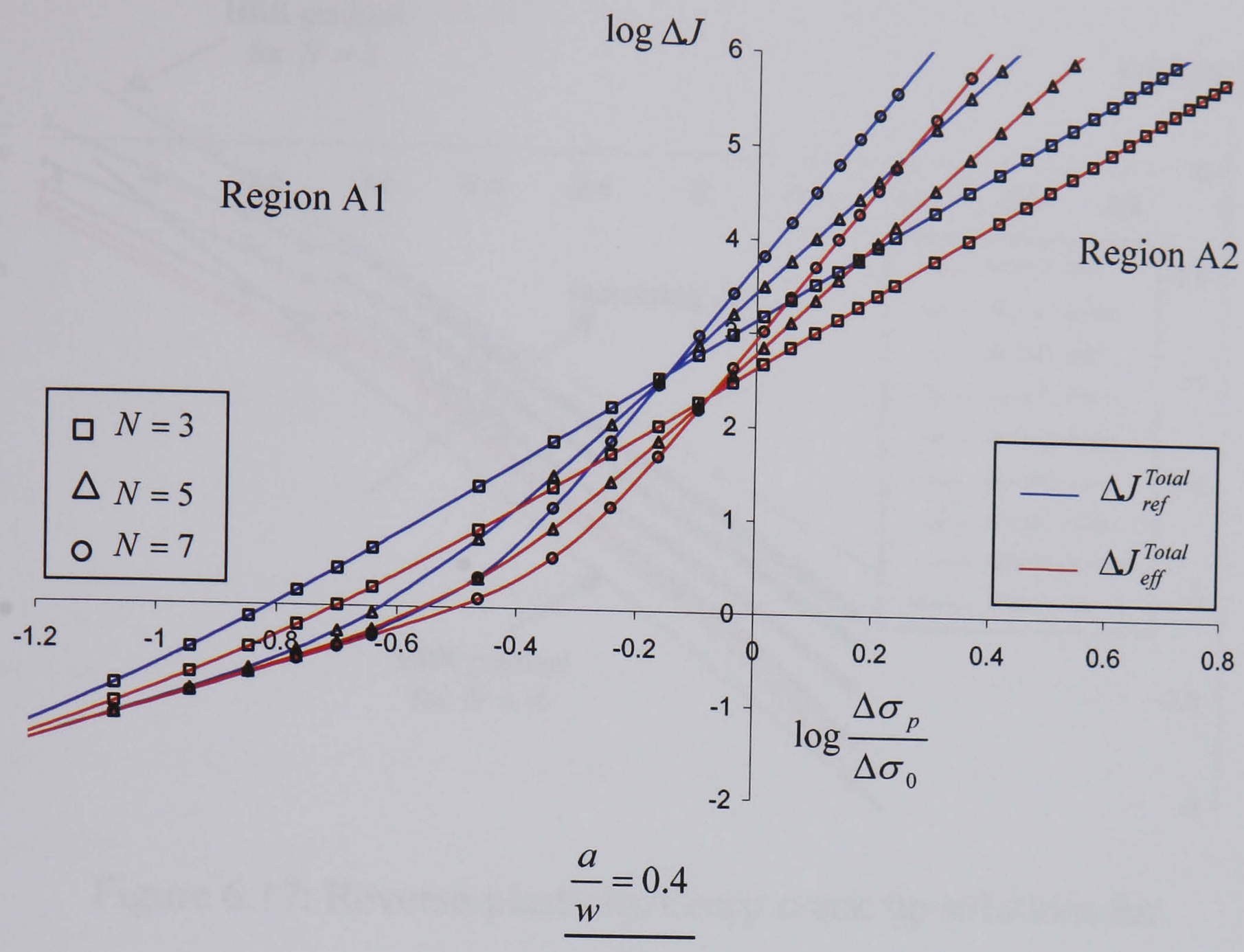

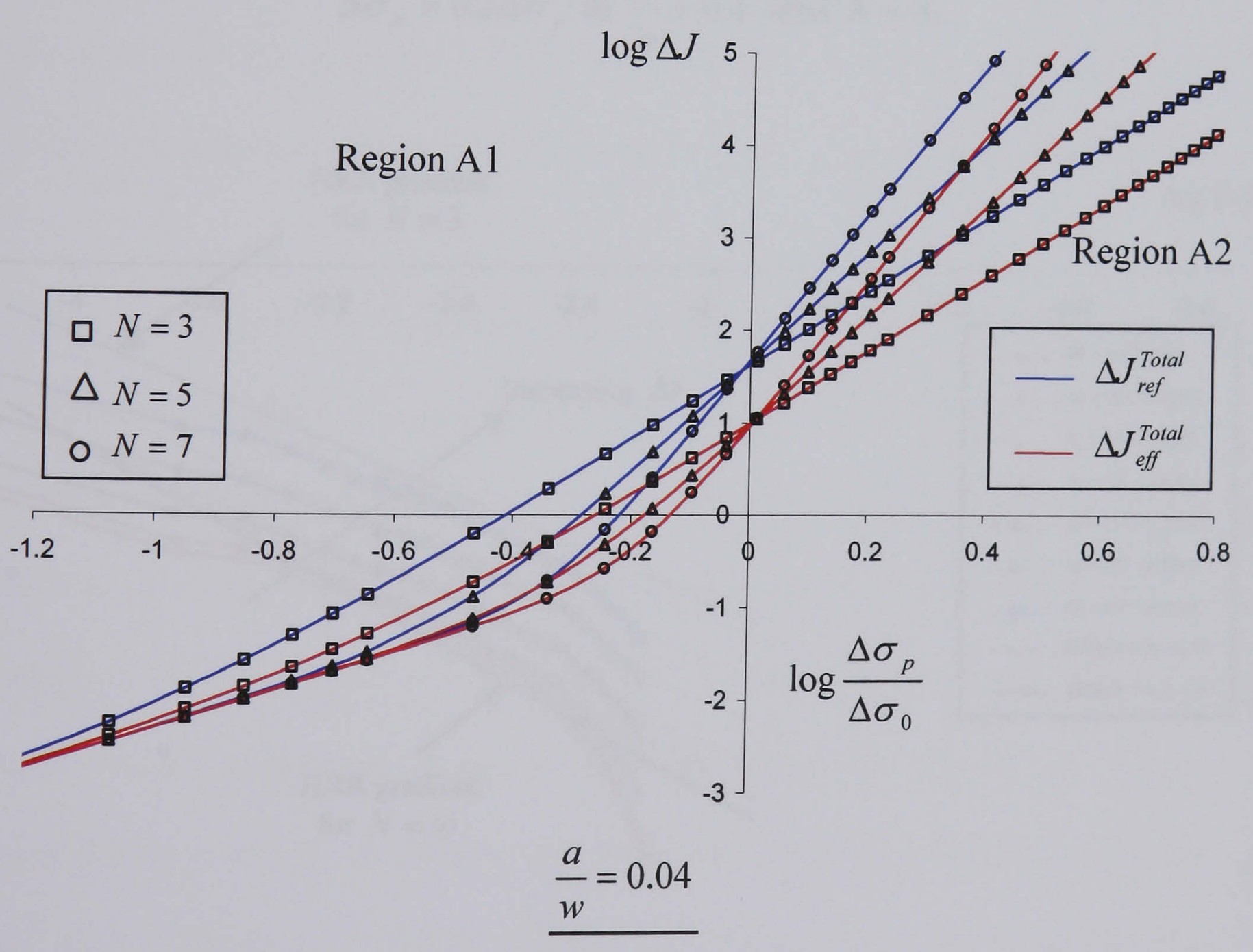

Figure 6.16: Overview of the solutions.

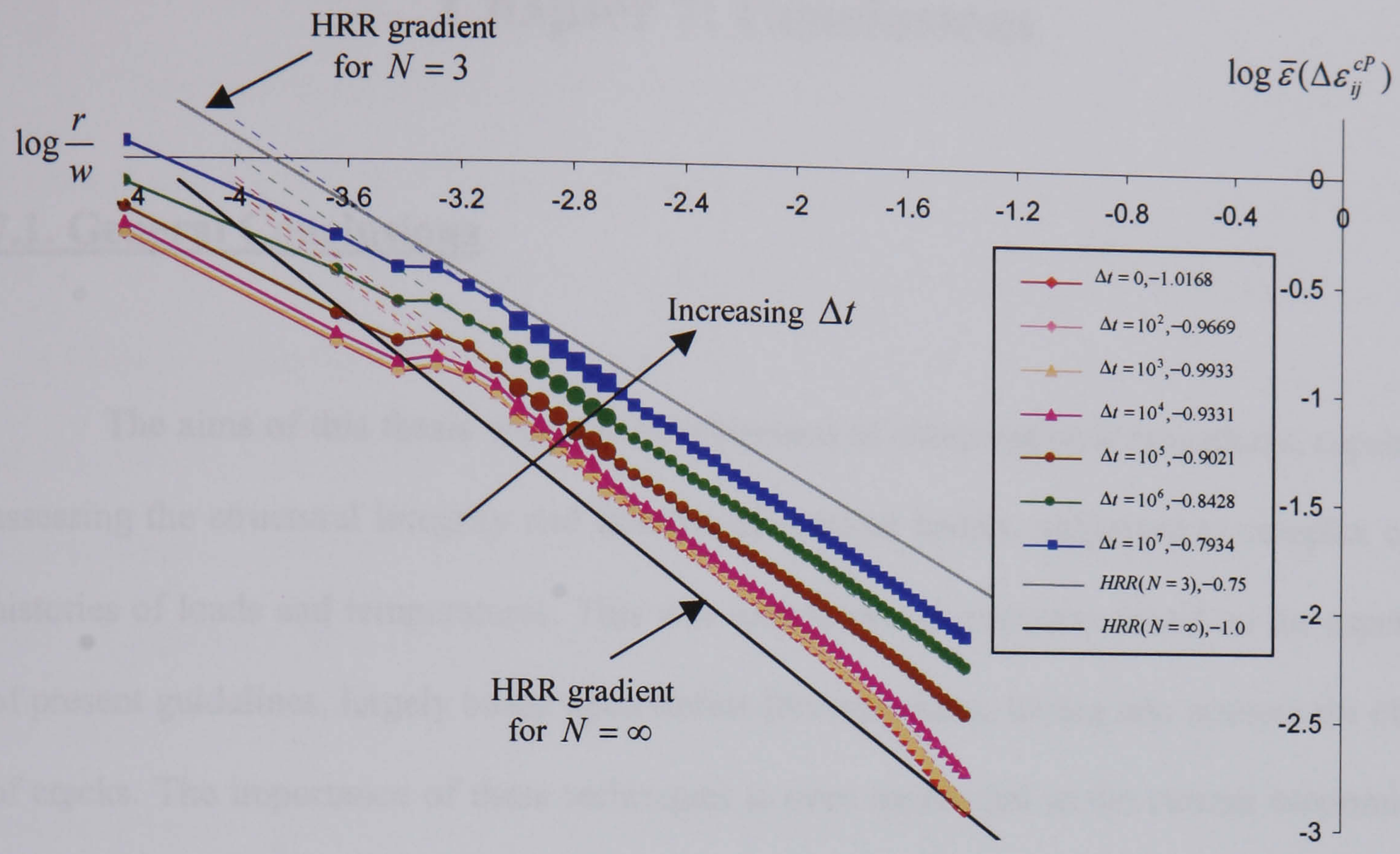

Figure 6.17: Reverse-plasticity/Creep crack tip solutions for $\Delta\sigma_p = 0.3\Delta\sigma_y$ at $\frac{a}{w} = 0.4$ and $N = 3$.

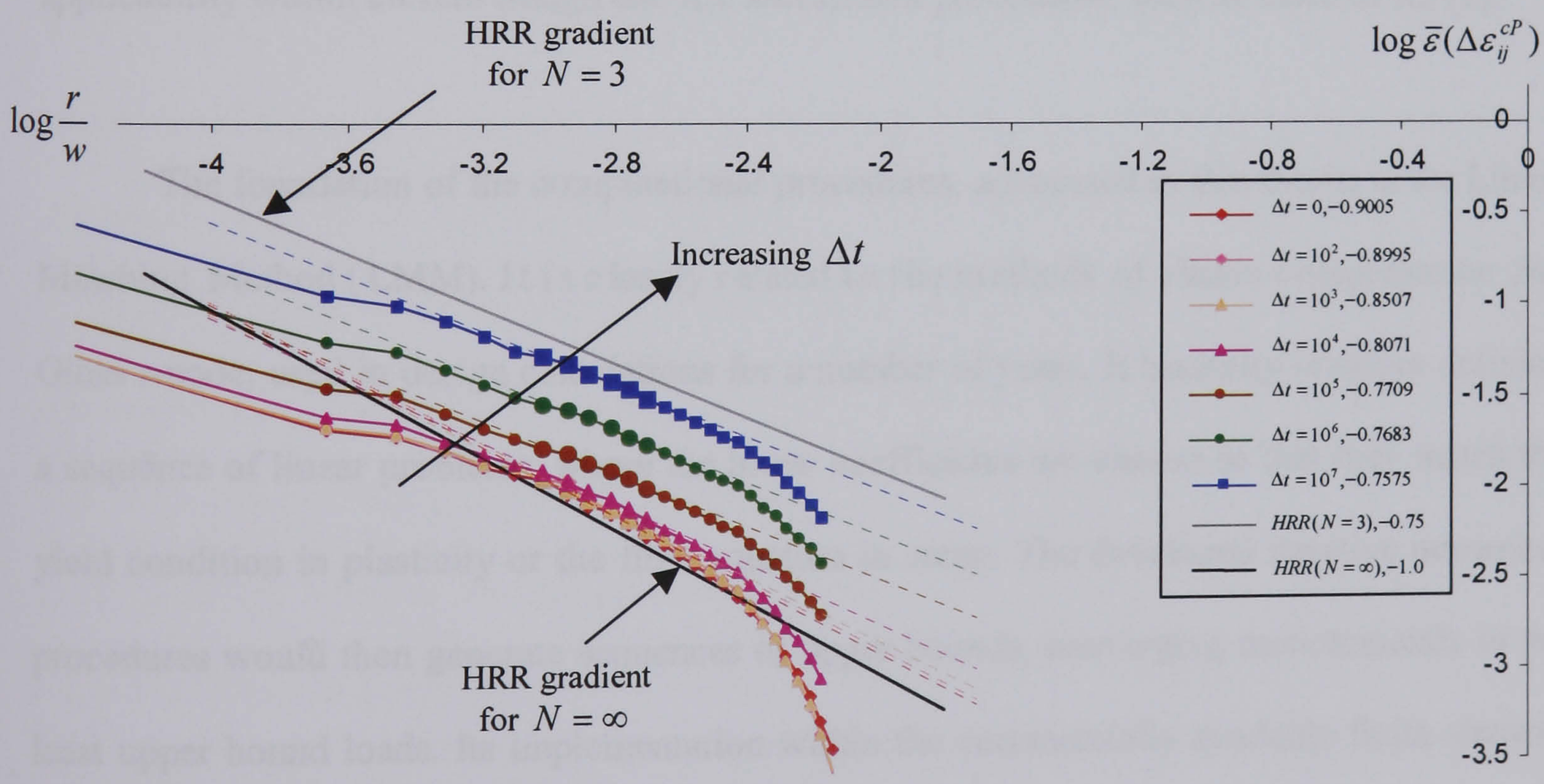

Figure 6.18: Reverse-plasticity/Creep crack tip solutions for $\Delta\sigma_p = 0.5\Delta\sigma_y$ at $\frac{a}{w} = 0.04$ and $N = 3$.

Chapter 7: Conclusions

1. General Conclusions

The aims of this thesis were the development of computational procedures, capable of sessing the structural integrity and lifetime of cracked bodies, subjected to complex cyclic stories of loads and temperatures. This was mainly due to concerns raised on the capability present guidelines, largely based upon defect-free structures, taking into account the effects cracks. The importance of these techniques is even more vital in the current economically iven environment, whereby structures are operating at much higher temperatures than eviously envisaged. Thus, the effectiveness and reliability of these procedures in assessing e safe operation of structures with such potential defects, ultimately enhances its pplicability within current design and life assessment procedures, such as those of R5 [1].

The foundation of the computational procedures, advocated in this thesis, is the Linear latching Method (LMM). It is closely related to the methods of elastic compensation and loss r-node, used in design calculations for a number of years. It basically involves defining sequence of linear problems, where the linear coefficients are chosen so that they match the ield condition in plasticity or the flow equation in creep. The developed iterative numerical rocedures would then generate sequences of upper bounds, converging monotonically to the ast upper bound loads. Its implementation within the commercially available finite element ftware, ABAQUS, as well as the existence of convergence proofs, delivering solutions ithin finite iterations, makes it the ideal choice.

The applications of the methodology, as an iterative upper limit analysis method, were scussed in Chapter 2. For the problems of cracked structures subjected to purely mechanical ads, two different implementation procedures for identifying limit loads were examined. ne involves operating the load directly on the body, while the other requires the application the loads through external linear elastic stress solutions. Numerically, the analyses revealed most identical solutions, with good converged upper bound limit loads achieved within the rst 20 iterations. The solutions were also found to be stable, insensitive to the meshing ements considered. The good correlation between the numerical and analytical limit load olutions further justifies the suitability of the adopted methodology.

In Chapter 3, the extension of the procedures for the identification of shakedown, everse-plasticity and ratchetting limits were presented. These were then investigated on the ree problem, in plane stress, plane strain and axisymmetric conditions. As before, the LMM-ased methodologies were still found to generate a monotonically reducing sequence of olutions, with good convergence attained at finite iterations. Also observed was the nsensitivity of the solutions towards cyclic hardening, as both perfectly plastic and complete yclic hardening ratchetting limits yielded almost identical results. Further examinations on a eal industrial problem justified the appropriateness of these procedures, as good correlations ere observed between the numerically generated and currently utilized shakedown limit olutions. The non-existence of the ratchetting limits was, however, overcame by the adopted umerical procedures, enhancing the prospect of the eventual applications of these omputational procedures to other structural-related problems.

The relationships between the cyclic loading histories and near crack tip fields, under clic creep conditions, were then examined in Chapter 4. The calculations demonstrated the ssibility of obtaining crack tip parameters, equivalent to $C^*(n)$, for problems involving riable loads and temperatures. This requires the identification of increments of strain over a cle of loading that vary radially from the crack tip, in the same manner as the HRR field. It as shown that under constant loading conditions, the adopted rapid cycle solutions for the o constitutive equations, Norton's law and Bailey-Orowan model, yielded the same steady ate creep behaviour. This led to the reproduction of the HRR field gradient in both cases. ince the rapid cycle solutions generate an upper bound to the effect of variable temperature, e computed values may be regarded as conservative for finite cycle times. Further vestigations into the behaviour of the cracked Bree problem, under variations in loading nditions, geometries and material properties, *etc*, provided the confidence on the capability f such procedures.

In Chapter 5, the calculated values of $C^*(n)$, in the previous chapter, were then terpreted in terms of a reference stress, independent of the creep index, n. To obtain a nsistent definition of a reference stress, it was found necessary to replace the computed alue of $C^*(n)$ at $n=1$, by an effective value, extrapolated from the values of $C^*(n)$ at $=3,5\,\&\,7$. With this modification, it was shown to be possible to define reference stress alues that are insensitive to n and the constitutive equations. Although, the effective values $^*(n)$ at $n=1$ shows some variation between the constitutive equations, these may be verestimated by a linear combination of the values for load and temperature, calculated parately. For the problem considered, a part through cracked cylinder subjected to axial load

ıd radial temperature gradient, the values of the effective stress calculated in this way dicate that, for thermal loading problems, the reference stress method described in R5 may ; conservative by a factor of about 2. This result also applies if the geometry is reinterpreted ; a plane stress problem.

Similar investigations into the relationships between the near crack tip fields and the yclic loading histories in plasticity conditions were then conducted in Chapter 6. It was stablished that the utilization of the HRR field criterion is still an appropriate representation f the behaviour at the crack tip. This was observed in the mechanically and thermally induced ack tip fields, in both perfect plasticity and an adaptation of the method for cyclic hardening. his enabled the equivalent crack tip fracture parameter, ΔJ , to be evaluated in all conditions, ith the observed phenomenon described by two distinct behaviours, strongly influenced by ıe effect of the stress intensity factors and the reference stress respectively. This enabled ıdgment on the aptness of current design and life assessment procedures to be demonstrated. n initial exploration into the behaviour of the near crack tip fields, under plasticity-creep ading conditions, was also examined. The solutions revealed the complexity of the analysis ınducted, which requires an in-depth understanding into the mechanics of the materials volved. Due to the time and resource constraints, these were not pursued any further.

So far, this thesis has shown the capabilities of utilizing such analysis methods in lving structural related problems associated with plasticity and creep. The ease and xibility in its implementation as well as its stability in analyzing cracked problems, makes e LMM the appropriate choice as an augmentation or alternative to current solution ocedures. Although in certain circumstances the analysis times for generating solutions

sing the LMM is much longer than the step-by-step analysis, the versatility of the LMM-ased methodology makes the time factor a non-issue. Finally, it is the author's opinion that e methodology adopted in this thesis is valuable tool in assessing the structural integrity of ructures, with the additional advantage of potentially being applied to answer other design nd life assessment problems.

.2. Remaining Issues

Although successful in addressing the issues raised in Chapter 1, there are still many reas, which need to be addressed. One particular area is the effect of thermal transients on the ehaviour of the solutions. The variations in the ratchetting limit for the cracked Bree roblem, considered in Chapter 3, needs to be investigated before an overall conclusion could e reached. Other circumstances which needs to be looked into includes the effect of thermal hocks, moving temperature fronts, non-linear variations in temperature through the thickness, *tc*. The change in the cyclic solutions for multiple instants of time in the cycle, instead of just vo, in the present study, is another subject interest.

Perhaps, the most important area that needs to be focussed on is the repeated pplications of the numerical procedures discussed in this thesis for other structural geometries nd/or loading conditions. This is necessary as the results from these additional investigations ould then enable general conclusions to be made on whether the phenomenon observed in is thesis is a specific one or witnessed in other cases as well.

Reference

1] Goodall, I. W., Goodman, A. M., Chell, G. C., Ainsworth, R. A., Williams, J. A., "*R5, Assessment procedures for the high temperature response of structures*", British Energy Generation Limited, Barnett Way, Barnwood, Gloucester, GL4 3RS.

2] Ponter, A. R. S., Carter, K. F., "*Limit state solutions, based upon linear elastic solutions with a spatially varying elastic modulus*", Computer Methods in Applied Mechanics and Engineering, Vol 140, pp 237-258, 1997.

3] Ponter, A. R. S., Carter, K. F., "*Shakedown state simulation techniques based on the linear elastic solutions*", Computer Methods in Applied Mechanics and Engineering, Vol 140, pp 259-279, 1997.

4] Ponter, A. R. S., Fuschi, P., Engelhardt, M., "*Limit analysis for a general class of yield conditions*", European Journal of Mechanics and Applied Solids, Vol 19, pp 401-421, 2000.

5] Ponter, A. R. S., Engelhardt, M., "*Shakedown limits for a general yield condition: Implementation and application for a von-Mises yield condition*", European Journal of Mechanics and Applied Solids, Vol 19, pp 423-445, 2000.

6] Ponter, A. R. S., Chen, H. F., "*A minimum theorem for cyclic load in excess of shakedown, with application to the evaluation of a ratchet limit",* European Journal of Mechanics and Applied Solids, Vol 20, pp 539-553, 2001.

7] Chen, H. F., Ponter, A. R. S., "*A method for the evaluation of a ratchet limit and the amplitude of plastic strain for bodies subjected to cyclic loading",* European Journal of Mechanics and Applied Solids, Vol 20, pp 555-571, 2001.

8] Chen, H. F., Ponter, A. R. S., "*Shakedown and limit analyses for 3-D structures using the linear matching method*", International Journal of Pressure Vessels and Piping, Vol 78, pp 443-451, 2001.

9] Chen, H. F., Ponter, A. R. S.,

"*Methods for the evaluation of creep relaxation and the amplitude of reverse-plastic strains for bodies subjected to cyclic loading*",
Pressure Vessels and Piping, Transaction of the ASME,
Cleveland, Ohio, July 2003.

[10] ANSYS Inc,
Southpointe, 275 Technology Drive,
Canonsburg, PA 15317, (www.ansys.com).

[11] Hibbit, Karlson and Sorensen Inc,
"*ABAQUS/Standard User's manual, Volumes 1, 2 & 3, Version 6.1*",
USA, 1997.

[12] ASME,
"*Boiler and pressure vessel code. Code case: Nuclear components, Case N-47-29, Class 1 components in elevated temperature service*",
Section II, Division 1, 1990.

[13] AFCEN,
"*Design and construction rules for mechanical components of FBR nuclear islands*",
RCC-MR, AFCEN, Paris, 1985.

[14] Mackenzie, D., Shi, J., Nadarajah, C., Boyle, J. T.,
"*An iterative elastic analysis procedure for establishing lower bound limit loads*",
In Proceedings of the ASME Pressure Vessels and Piping Conference, New Orleans, Louisiana, PVP-Vol 230, pp 129-134, 1992.

[15] Seshadri, R., Fernando, C. P. D.,
"*Limit loads of mechanical components and structures using the Gloss R-node method*",
In Proceedings of the ASME Pressure Vessels and Piping Conference, San Diego, California, PVP-Vol 210, pp 125-134, 1991.

[16] Maier, G.,
"*Mathematical programming methods for deformation analysis at plastic collapse*",
Computers and Structures,
Vol 7, pp 599-612, 1977.

[17] Corradi, L., Zavelani, A.,
"*A linear programming approach to shakedown analysis of structures*",
Computer Methods in Applied Mechanics and Engineering,
Vol 3, pp 37-53, 1974.

[18] Hachemi, A., Wiechert, A.,
"*Numerical shakedown analysis of damaged structures*",
Computer Methods in Applied Mechanics and Engineering,
Vol 160, pp 57-70, 1998.

[19] Webster, G. A., Ainsworth, R. A.,
"*High temperature component life assessment*",
Chapman & Hall, 1994.

[20] Miller, A. G.,
"*Review of limit loads of structures containing defects, 3rd edition*",
Central Electricity Generating Board (CEGB) internal report.

[21] Melan, E.,
"*Theorie Statisch Unbestimmter Systeme aus Ideal-Plastischem Bastoff*",
Sitzungsberichte der Akademie der Wissenschaft, Wien, Abt iia,
Vol 145, pp 195-218, 1936.

[22] Martin, J. B.,
"*Plasticity: Fundamentals and general results*",
M. I. T. Press, Boston, 1975.

[23] Ponter, A. R. S., Karadeniz, S.,
"*An extended shakedown theory for structures that suffer cyclic thermal loading*",
Part 1, Theory
Journal of Applied Mechanics, Transactions of the ASME,
Vol 52, pp 877-882, 1985.

[24] Ponter, A. R. S., Karadeniz, S.,
"*An extended shakedown theory for structures that suffer cyclic thermal loading*",
Part 2, Applications
Journal of Applied Mechanics, Transactions of the ASME,
Vol 52, pp 883-889, 1985.

[25] Koiter, W. T.,
"*General theorems for elastic-plastic structures*",
Progress in Solid Mechanics, Edited by Hill, R., and Sneddon, I., 2nd Edition,
North-Holland Publishing Company, Amsterdam, Vol 2, pp 167-219, 1964.

26] Huang, Y., Stein, E.,
"*Shakedown of a cracked body consisting of kinematic hardening material*",
Engineering Fracture Mechanics,
Vol 54, pp 107-112, 1996.

27] Feng, Xi-Qiao, Gross, D.,
"*A global/local shakedown analysis method of elastoplastic cracked structures*",
Engineering Fracture Mechanics,
Vol 63, pp 179-192, 1999.

28] Carpinteri, A.,
"*Energy dissipation in R.C.Beams under cyclic loadings*",
Engineering Fracture Mechanics,
Vol 39, pp 177-184, 1991.

[29] Le Mat-Hamata, N., Cocks, A. C. F., Li, S. X., Smith, D. J.,
"*High temperature crack tip fields in cyclically hardening engineering alloys*",
Proceeding 7th International Conference Creep and Fracture of Engineering Materials,
Earthman, J., Mohamed, F., 1997.

[30] Takeshi, I., Cocks, A. C. F., Smith, D. J., Nacera, L. M.,
"*Creep fatigue crack growth: Crack tip fields and growth mechanisms*",
Ahmed Benallal, Continuous Damage & Fracture,
Elsevier, pp 263-272, 2000.

[31] Broek, D.,
"*Elementary engineering fracture mechanics*",
Sitjhoff and Noordholf, Alphen aan den Rijn, 1978.

[32] Knott, J. F.,
"*Fundamentals of fracture mechanics*",
Butterworths, 1973.

[33] Ruggles, M. B., Takahashi, Y., Ainsworth, R. A.,
"*High-temperature flaw assessment procedure*",
Liquid Metal Breeder Reactor EPRI/CRIEPI/NE Joint Studies Report, 1991.

[34] Rice, J. R.,
"*A path independent integral and the approximate analysis of strain concentration by notches and cracks*",
Journal of Applied Mechanics, Transactions of the ASME,
Vol 35, pp 379-386, 1968.

[35] Clement, G., Roche, R.,
"*General review of available results of progressive tests of structures and structural components*", In: Ratchetting in the creep range by Ponter, A. R. S., Cocks, A. C. F., Clement, G., Roche, R., Corradi, L., & Franchi, A.,
Report EUR9876EN, Directorate-General, Science Research and Development Commission of the European Community, Brussels, 1985.

36] Cocks, A. C. F., Ponter, A. R. S.,
"*Computation of shakedown limits for structural components, Part II - The creep range (Brussels Diagram)*",
Internal Report, University of Leicester, 1992.

37] Bree, J.,
"*Elastic-plastic behaviour of thin tubes subjected to internal pressure and intermittent high-heat fluxes with application to fast-nuclear-reactor fuel elements*",
Journal of Strain Analysis,
Vol 2, No 3, pp 226-238, 1967.

38] O'Donnell, W. J., Porowski, J.,

"*Upper bounds for accumulated strains due to creep ratchetting*",
Journal of Pressure Vessel Technology, Transactions of the ASME,
Vol 96, pp 150-154, 1974.

[39] O'Donnell, W. J., Porowski, J.,
"*Design implications of recent advances in elevated temperature bounding technique*",
Report sponsored by the sub-committee on Elevated Temperature Design of the Pressure Vessel Research Committee of the Welding Research Council.

[40] Miller, D. R.,
"*Thermal-stress ratchet mechanism in pressure vessels*",
Journal of Basic Engineering, Transactions of the ASME, Series D,
Vol 81, pp 190-196, 1959.

[41] Parkes, E. W.,
"*Wings under repeated thermal stress*",
Aircraft Engineering,
Vol 26, pp 402-406, 1954.

[42] Gokfeld, D. A., Cherniavsky, O. F.,
"*Limit analysis of structures at thermal cycling*",
Sijthoff and Noorhoff, Alpen aan den Rijm,
The Netherlands, 1980.

[43] Ponter, A. R. S., Carter, K. F., Riou, B.,
"*Design rules for cylindrical shells subjected to axisymmetric temperature histories*",
Working Group on Codes and Standards, Activity Group 2,
Commission of the European Communities, Directorate General Environment, Nuclear Safety and Civil Protection,
Final Report, Study Contract RA1-0224-UK, 1996.

[44] Maier, G., Novati, G.,
"*Dynamic shakedown and bounding theory for a class of non-linear hardening discrete structural models*",
International Journal of Plasticity,
Vol 6, pp 551-572, 1990.

45] Polizzotto, C.,
"*A unified treatment of shakedown theory and related bounding techniques*",
Solid Mechanical Archive,
Vol 7, pp 19-75, 1982.

46] Ponter, A. R. S.,
"*Deformation, displacement and work bounds for structures in a state of creep and subjected to variable loading* ",
Journal of Applied Mechanics, Transactions of the ASME,
Vol 39, pp 953-959, 1972.

[47] Hamilton, R., Boyle, J. T., Shi, J., Mackenzie, D.,
"*A simple upper bound method for calculating approximate shakedown loads*",
Journal of Pressure Vessels Technology, Transactions of the ASME,
Vol 120, pp 195-199, 1996.

[48] Mackenzie, D., Shi, J., Boyle, J.T.
"*Finite element modeling for limit analysis by the Elastic Compensation Method*",
Computers and Structures,
Vol 51, pp 403-410, 1994.

[49] Engelhardt, M.,
"*Computational modelling of shakedown*",
University of Leicester, Thesis, 2000.

[50] Calladine, C. R.,
"*Engineering plasticity*",
Pergammon Press, 1969.

[51] Astley, R. J.,
"*Finite elements in solids and structures*",
Chapman & Hall, London, 1992.

[52] Marriott, D. L.,
"*Evaluation of deformation or load control of stresses under inelastic conditions using the elastic finite element stress analysis*",
In Proceedings of the ASME Pressure Vessels and Piping Conference, Pittsburgh, Pennsylvania, PVP-Vol 136, pp 3-9, 1988.

[53] Mackenzie, D., Boyle, J. T., Hamilton, R.,
"*The elastic compensation method for limit and shakedown analysis: a review*",
Journal of Strain Analysis for Engineering Design,
Vol 35, no 3, pp 171-188, 2000.

[54] Hill, R.,
"*The mathematical theory of plasticity*",
Oxford University Press, London, 1950.

[55] Sebastian, H.,
"*Finite element state solutions: Accuracy of an iterative method*",
University of Leicester, Internship Report, 1998.

[56] Gruning, M.,
"*Die Tragfahigkeit Statisch Unbestimmter Tragwerke aus Stahl bei Beliebig Haufig Weiderholter Belastung*",
Julius Springer, Berlin, 1926.

[57] Ponter, A. R. S., Carter, K. F., Riou, B.,

"*Design rules for cylindrical shells subjected to axisymmetric temperature histories*",
Working Group on Codes and Standards, Activity Group 2,
Commission of the European Communities, Directorate General Environment, Nuclear Safety and Civil Protection,
Final Report, Study Contract RA1-0224-UK, 1996.

[58] Ponter, A. R. S., Hearle, A. D., Johnson, K. L.,
"*Application of the kinematical theorem to rolling and sliding point contacts*",
Journal of Mechanical and Physical Solids,
Vol 33, pp 339-362, 1985.

[59] Boulbibane, M., Collins, I. F.,
"*Application of the kinematical theorem to pavement design*",
In Weichert, D., Maier, G. (Eds), Inelastic Analysis of Structures under variable loads, Theory and Applications,
Kluwer Academic Publishers, pp 365-380, 2000.

[60] Konig, J. A.,
"*Shakedown of elastic-plastic structures*",
PWN-Polish Scientific Publishers,
Warsaw, Elsevier, Amsterdam, 1987.

[61] Maier, G., Carvelli, V., Cocchetti, G.,
"*An introduction to direct methods for limit and shakedown analysis*",
In Weichert, D., Maier, G. (Eds), Inelastic Analysis of Structures under Variable Repeated Loading - Directly Analysis Methods,
International Centre for Mechanical Sciences Lecture Series,
No 432, Springer-Verlag, 2002.

[62] Ponter, A. R. S., Karadeniz, S., Carter, K. F.,
"*The computation of shakedown limits for structural components subjected to variable thermal loading-Brussels diagrams*",
University of Leicester,
Final Report, Contract RAP-054-UK, 1987.

[63] Ponter, A. R. S., Chen, H. F., Boulbibane, M., Habibullah, M.,
"*The linear matching method for the evaluation of limit loads, shakedown limits and related problems*",
Proceedings of the Fifth World Congress on Computational Mechanics (WCCM V), July 7-12, 2002, Vienna, Austria, Mang, H. A., Rammerstorfer, F. G., & Eberhadsteiner, J., Vienna University of Technology, Austria, ISBN 3-9501554-0-6.

[64] Ponter, A. R. S., Chen, H. F., Habibullah, M.,
"*Computation of ratchet limits for structures subjected to cyclic loading and temperature*",
In Computational Developments & Applications, Transactions of the ASME,
PVP, Vol 441, pp 143-152, New York, 2002.

[65] Ponter, A. R. S., Cocks, A. C. F.,
"*Computation of shakedown limits for structural components, Part II: The Creep Range*",
Directorate General for Science, Research and Development, Commission of the European Communities,
Report EUR 15682EN, Luxemburg, 1994.

[66] Lemaitre, J., Chaboche, J. L.,
"*Mechanics of solid materials*",
Cambridge University Press,
Cambridge, 1990.

[67] Kubo, S.,
"*Effect of creep recovery and hardening on stress and strain rate fields near a crack tip in creeping materials*",
Elastic-Plastic Fracture 2nd Symposium, Vol-1, Inelastic Crack Analysis,
ASTM STP 803, pp 594-614, 1983.

[68] Pugh, C. E., Robinson, D. N.,
"*Some trends in constitutive equation model development for high temperature behaviour of fast-reactor structural alloys*",
Vol 48, pp 269-276, 1978.

[69] Ponter, A. R. S.,
"*The analysis of cyclically loaded structures for short cycle times*",
International Journal of Solids and Structures,
Vol 12, pp 809-825, 1976.

[70] Ponter, A. R. S.,
"*Minimum theorems and iterative solutions methods for creep cyclic loading problems*",
Meccanica, Kluiver academic Publishers,
Vol 36, pp 37-47, 2001.

[71] Ponter, A. R. S.,
"*Deformation bounds for the Bailey Orowan theory of creep*",
Journal of Applied Mechanics, Transactions of the ASME,
Vol 42, pp 619-624, 1975.

[72] Ponter, A. R. S., Chen, H. F., Boulbibane, M., Habibullah, M.,
"*A direct method for the evaluation of properties of the cyclic behaviour of structures*",
2nd European Conference on Computational Mechanics,
Cracow, Poland, June 2001.

[73] Boulbibane, M., Ponter, A. R. S.,
"*A method for the evaluation of design limits for structural materials in a cyclic state of creep*",

European Journal of Mechanics of Applied Solids,
Vol 21, pp 899-914, 2002.

[74] Ponter, A. R. S., Boulbibane, M.,
"*Minimum theorems and the linear matching method for bodies in a cyclic state of creep*",
European Journal of Mechanics of Applied Solids,
Vol 21, pp 915-925, 2002.

[75] Hutchinson, J. W.,
"*Singular behaviour at the end of a tensile crack in a hardening material*",
Journal of Mechanics and Physical Solids,
Vol 16, pp 13-31, 1968.

[76] Rice, J. R., Rosengren, G. F.,
"*Plane strain deformation near a crack tip in a power law hardening material*",
Journal of Mechanics and Physical Solids,
Vol 16, pp 1-12, 1968.

[77] Yang, C. H., Soh, A. K.,
"*Modelling of voids/cracks and their interactions*",
Theoretical and Applied Fracture Mechanics,
Vol 38, pp 81-101, 2002.

[78] Barsoum, R. S.,
"*On the use of isoparametric finite elements in linear fracture mechanics*",
International Journal for Numerical Methods in Engineering,
Vol 10, pp 25-37, 1976.

[79] Yang, Z. J., Chen, J. F., Holt, G. D.,
"*Efficient evaluation of stress intensity factors using virtual crack extension technique*",
Computers and Structures,
Vol 79, pp 2705-2715, 2001.

[80] Henshell, R. D., Shaw, K. G.,
"*Crack tip finite elements are unnecessary*",
International Journal for Numerical Methods in Engineering,
Vol 9, pp 495-507, 1975.

[81] Nagtegaal, J. C., Parks, D. M., Rice, J. R.,
"*On numerically accurate finite element solutions in the fully plastic range*",
Computer Methods in Applied Mechanics and Engineering,
Vol 4, pp 153-177, 1974.

[82] Shih, C. F.,
"*Tables of Hutchinson-Rice-Rosengren singular field quantities*",
Brown University Report,

MRL E-147, Providence, RI, 1983.

[83] Penny, R. K., Marriott, D. L.,
"*Design for creep*",
McGraw-Hill, 1971.

[84] Bill, I. M., Mackenzie, A. C.,
"*Reference stress for redistribution time in creep of structures*",
International Journal of Mechanical Sciences,
Vol 11, 1969.

[85] Ainsworth, R. A.,
"*Approximate non-linear fracture mechanics calculations using reference stress techniques*",
CEGB Report RD/B/6074/R88, 1988.

[86] Goodall, I. W., Leckie, F. A., Ponter, A. R. S., Townley, C. H. A.,
"*The development of high temperature design methods based on reference stresses and bounding theorems*",
Journal of Engineering Materials and Technology, Transactions of the ASME,
Vol 101, pp 349-355, 1979.

[87] Chen, H. F., Ponter, A. R. S.,
"*Integrity assessment for 3D tube-plate using linear matching method, Report 2: Creep relaxation and reverse-plasticity* ",
University of Leicester, Internal Report, pp 1-18, 2002,

[88] Rice, J. R., Paris, P. C., Merkle, J. G.,
"*Some further results on J-integral analysis and estimates*",
Fracture Toughness,
ASTM STP 514, pp 40-69, 1972.

[89] Milne, I., Ainsworth, R. A., Dowling, A. R., Stewart, A. T.,
"*Assessment of the integrity of structures containing defects*",
International Journal of Pressure Vessels and Piping, Vol 32, pp 105-196, 1988.

Appendix A

The following are the Jacobians, *i.e.* the matrices containing the relationship between the stresses and strains, used in the programs.

Plane Stress

$$[J]=\frac{E^k}{(1-\nu^2)}\cdot\begin{bmatrix}1 & \nu & 0\\ \nu & 1 & 0\\ 0 & 0 & \frac{1}{2}(1-\nu)\end{bmatrix} \tag{A1}$$

Plane Strain

$$[J]=\frac{E^k}{(1+\nu)(1-2\nu)}\cdot\begin{bmatrix}(1-\nu) & \nu & \nu & 0\\ \nu & (1-\nu) & \nu & 0\\ \nu & \nu & (1-\nu) & 0\\ 0 & 0 & 0 & \frac{1}{2}(1-2\nu)\end{bmatrix} \tag{A2}$$

Axisymmetric

$$[J]=\frac{E^k}{(1+\nu)(1-2\nu)}\cdot\begin{bmatrix}(1-\nu) & \nu & \nu & 0\\ \nu & (1-\nu) & \nu & 0\\ \nu & \nu & (1-\nu) & 0\\ 0 & 0 & 0 & \frac{1}{2}(1-2\nu)\end{bmatrix} \tag{A3}$$

Appendix B

Double-edged Crack Plate (Plane Stress) using the LMM (Procedure A)

The following is the actual programming code used in the analysis. Although presented for the plane stress problem satisfying the Von–Mises yield condition, code listings are also available for three-dimensional and other two-dimensional situations (plane strain & axisymmetric). For each, the bulk of the method is the same except trivial changes made to the element type, Jacobian matrix and components of stress/strain tensor, *etc*.

```
C
CCCCCCCCCCCCCCCCCCCCCCCCCCCCCCCCCCCCCCCCCCCCCCCCCCCCCCCCCCCCCCCCCCCCCCCCCCC
C User subroutine UMAT allows the material behaviour, [J], of the model to be defined, at each material gauss
C point for each element. Using the incremental strains supplied by ABAQUS, this subroutine would then
C compute the stress fields, which would then be added up to obtain the total stress solution.
C
C The following standard block, from the user manual, acts as an interface between ABAQUS and UMAT.
CCCCCCCCCCCCCCCCCCCCCCCCCCCCCCCCCCCCCCCCCCCCCCCCCCCCCCCCCCCCCCCCCCCCCCCCCCC
C
      SUBROUTINE UMAT(STRESS, STATEV, DDSDDE, SSE, SPD, SCD,
     1 RPL, DDSDDT, DRPLDE, DRPLDT,
     2 STRAN, DSTRAN, TIME, DTIME, TEMP, DTEMP, PREDEF, DPRED, CMNAME,
     3 NDI, NSHR, NTENS, NSTATV, PROPS, NPROPS, COORDS, DROT, PNEWDT,
     4 CELENT, DFGRD0, DFGRD1, NOEL, NPT, LAYER, KSPT, KSTEP, KINC)
C
      INCLUDE 'ABA_PARAM.INC'
C
      CHARACTER*8 CMNAME
      DIMENSION STRESS(NTENS), STATEV(NSTATV),
     1 DDSDDE(NTENS, NTENS), DDSDDT(NTENS), DRPLDE(NTENS),
     2 STRAN(NTENS), DSTRAN(NTENS), TIME(2), PREDEF(1), DPRED(1),
     3 PROPS(NPROPS), COORDS(3), DROT(3,3), DFGRD0(3,3), DFGRD1(3,3)
C
CCCCCCCCCCCCCCCCCCCCCCCCCCCCCCCCCCCCCCCCCCCCCCCCCCCCCCCCCCCCCCCCCCCCCCCCCCC
C The PARAMETER option is used to declare the number of elements (NEL), number of integration points
C (NUPT), and number of stress and strain tensor components (NCO) used in the analysis.
CCCCCCCCCCCCCCCCCCCCCCCCCCCCCCCCCCCCCCCCCCCCCCCCCCCCCCCCCCCCCCCCCCCCCCCCCCC
C
      PARAMETER(NEL=30, NUPT=3, NCO=3)
C
CCCCCCCCCCCCCCCCCCCCCCCCCCCCCCCCCCCCCCCCCCCCCCCCCCCCCCCCCCCCCCCCCCCCCCCCCCC
C The following arrays are declared separately as they are specifically used only in this subroutine.
CCCCCCCCCCCCCCCCCCCCCCCCCCCCCCCCCCCCCCCCCCCCCCCCCCCCCCCCCCCCCCCCCCCCCCCCCCC
C
      DIMENSION DSTRESS(NCO), YMOD(NEL,NUPT), KMARK(NEL,NUPT), VMISTRESS(NEL,NUPT)
      SAVE
C
```

```
CCCCCCCCCCCCCCCCCCCCCCCCCCCCCCCCCCCCCCCCCCCCCCCCCCCCCCCCCCCCCCCCCCCCCCCCCCCC
C The COMMON block option is used to make the necessary variables available to other subroutines.
CCCCCCCCCCCCCCCCCCCCCCCCCCCCCCCCCCCCCCCCCCCCCCCCCCCCCCCCCCCCCCCCCCCCCCCCCCCC
C
      COMMON/KSTUFF1/A,B,C,E,S,DW,DF,P
      C = PROPS(2)
C
CCCCCCCCCCCCCCCCCCCCCCCCCCCCCCCCCCCCCCCCCCCCCCCCCCCCCCCCCCCCCCCCCCCCCCCCCCCC
C These files are opened and results written in them as the analysis continues.
CCCCCCCCCCCCCCCCCCCCCCCCCCCCCCCCCCCCCCCCCCCCCCCCCCCCCCCCCCCCCCCCCCCCCCCCCCCC
C
      OPEN(UNIT=18,FILE='/TEMP/msmh1/dplateps1.dat')
      OPEN(UNIT=17,FILE='/TEMP/msmh2/dplateps2.dat')
      OPEN(UNIT=15,FILE='/TEMP/msmh3/dplateps3.dat')
C
CCCCCCCCCCCCCCCCCCCCCCCCCCCCCCCCCCCCCCCCCCCCCCCCCCCCCCCCCCCCCCCCCCCCCCCCCCCC
C As ABAQUS is programmed to access the subroutines at least twice per increment, the array KMARK is used
C to ensure that any iteration is carried out only once. In the first increment, once an integration point is dealt
C with, KMARK is set to one. This would then ensure that particular integration point would not be considered
C until the start of the next iteration.
CCCCCCCCCCCCCCCCCCCCCCCCCCCCCCCCCCCCCCCCCCCCCCCCCCCCCCCCCCCCCCCCCCCCCCCCCCCC
C
      IF(KINC.NE.KINI) THEN
       KINI=KINC
       DO I1=1, NEL
         DO J1=1, NUPT
           KMARK(I1,J1)=0
         END DO
       END DO
      END IF
C
CCCCCCCCCCCCCCCCCCCCCCCCCCCCCCCCCCCCCCCCCCCCCCCCCCCCCCCCCCCCCCCCCCCCCCCCCCCC
C The stress increments, DSTRESS, is initialized to zero, ensuring a set of individual elastic solutions in each
C iteration.
CCCCCCCCCCCCCCCCCCCCCCCCCCCCCCCCCCCCCCCCCCCCCCCCCCCCCCCCCCCCCCCCCCCCCCCCCCCC
C
      DO K1=1, NTENS
        DSTRESS(K1)=0
      END DO
C
CCCCCCCCCCCCCCCCCCCCCCCCCCCCCCCCCCCCCCCCCCCCCCCCCCCCCCCCCCCCCCCCCCCCCCCCCCCC
C The elastic modulus, YMOD, is initialised to an arbitrary value in the first increment at each material gauss
C point. In subsequent iterations, it is updated using the relationship given in Equation (2.6). A limit is also set to
C YMOD to ensure numerical stability. The variables, PROPS(2) is the yield stress and VMISTRESS is the von-
C Mises effective stress.
CCCCCCCCCCCCCCCCCCCCCCCCCCCCCCCCCCCCCCCCCCCCCCCCCCCCCCCCCCCCCCCCCCCCCCCCCCCC
C
      IF(KINC.EQ.1) YMOD(NOEL,NPT)=1.0
      IF(KINC.EQ.1) GO TO 100
      IF(KMARK(NOEL,NPT).EQ.1) GO TO 100
C
```

```
      YMOD(NOEL,NPT)=(YMOD(NOEL,NPT)*PROPS(2))/VMISTRESS(NOEL,NPT)
      IF (YMOD(NOEL,NPT).GT.1.0E+08) THEN
        YMOD(NOEL,NPT)=1.0E+08
      END IF
C
 100  CONTINUE
C
CCCCCCCCCCCCCCCCCCCCCCCCCCCCCCCCCCCCCCCCCCCCCCCCCCCCCCCCCCCCCCCCCCCCCCCCCCC
C Here the Jacobian matrix, DDSDDE, is defined and assembled using the Poisson's ratio, PROPS(1) and
C YMOD.
CCCCCCCCCCCCCCCCCCCCCCCCCCCCCCCCCCCCCCCCCCCCCCCCCCCCCCCCCCCCCCCCCCCCCCCCCCC
C
      TERM  = 1.-PROPS(1)**2.
      TERM1 = YMOD(NOEL,NPT)/TERM
      TERM2 = YMOD(NOEL,NPT)*PROPS(1)/TERM
      TERM3 = (YMOD(NOEL,NPT)/TERM)*((1.-PROPS(1))/2.0)
C
      DO K1=1,NDI
        DDSDDE(K1,K1)=TERM1
      END DO
      DO K1=2,NDI
        N2=K1-1
        DO K2=1,N2
          DDSDDE(K2,K1) = TERM2
          DDSDDE(K1,K2) = TERM2
        END DO
      END DO
      DDSDDE(NTENS,NTENS)=TERM3
C
CCCCCCCCCCCCCCCCCCCCCCCCCCCCCCCCCCCCCCCCCCCCCCCCCCCCCCCCCCCCCCCCCCCCCCCCCCC
C In the following block, the stress increments, DSTRESS, is computed using the Jacobian, DDSDDE, and the
C strain increments obtained from ABAQUS, DSTRAN. These are then added up to STRESS, total stress, to
C trick ABAQUS into "thinking" it is solving a non-linear problem.
CCCCCCCCCCCCCCCCCCCCCCCCCCCCCCCCCCCCCCCCCCCCCCCCCCCCCCCCCCCCCCCCCCCCCCCCCCC
C
      DO K=1,NTENS
        DO I=1,NTENS
          DSTRESS(K) = DSTRESS(K)+DDSDDE(K,I)*DSTRAN(I)
        END DO
      END DO
C
      DO K=1, NTENS
        STRESS(K) = STRESS(K)+DSTRESS(K)
      END DO
C
CCCCCCCCCCCCCCCCCCCCCCCCCCCCCCCCCCCCCCCCCCCCCCCCCCCCCCCCCCCCCCCCCCCCCCCCCCC
C The actual Von-mises effective stress and the associated effective strain is calculated in the following block.
CCCCCCCCCCCCCCCCCCCCCCCCCCCCCCCCCCCCCCCCCCCCCCCCCCCCCCCCCCCCCCCCCCCCCCCCCCC
C
      HP=(DSTRESS(1)+DSTRESS(2))/3.0
      ST=1.5*((DSTRESS(1)-HP)**2.0+(DSTRESS(2)-HP)**2.0+(-1*HP)**2.0
```

```
     1    +2.0*(DSTRESS(3)**2.0))
      VMISTRESS(NOEL,NPT)=SQRT(ST)
C
      THSTRAN=(-PROPS(1)/YMOD(NOEL,NPT))*(DSTRESS(1)+DSTRESS(2))
      X = DSTRAN(1)**2.0+DSTRAN(2)**2.0+THSTRAN**2.0+0.5*DSTRAN(3)**2.0
      X = X*2.0/3.0
      ESTRAN = SQRT(X)
C
CCCCCCCCCCCCCCCCCCCCCCCCCCCCCCCCCCCCCCCCCCCCCCCCCCCCCCCCCCCCCCCCCCCCCCCCCC
C The following is the most important thing that comes out of the analysis. The internal solution-dependent state
C variable, SSE, is assigned to the value of the effective strain multiplied by the yield stress. This will then be
C utilized in the user subroutine, DLOAD, for the calculation of the upper bound limit loads.
CCCCCCCCCCCCCCCCCCCCCCCCCCCCCCCCCCCCCCCCCCCCCCCCCCCCCCCCCCCCCCCCCCCCCCCCCC
C
      SSE=ESTRAN*PROPS(2)
C
CCCCCCCCCCCCCCCCCCCCCCCCCCCCCCCCCCCCCCCCCCCCCCCCCCCCCCCCCCCCCCCCCCCCCCCCCC
C Here, local variables are assigned to STATEV(), where it is stored and accessible via ABAQUS/POST or
C user subroutine URDFIL.
CCCCCCCCCCCCCCCCCCCCCCCCCCCCCCCCCCCCCCCCCCCCCCCCCCCCCCCCCCCCCCCCCCCCCCCCCC
C
      STATEV(1) = VMISTRESS(NOEL,NPT)
      STATEV(2) = ESTRAN
      DO K=1,NTENS
        STATEV(K+2) = DSTRESS(K)
      END DO
C
      KMARK(NOEL,NPT)=1
C
  120 FORMAT('-----------------------------------------')
  130 FORMAT('UMAT---INCREMENT: ',I3)
  140 FORMAT('YOUNGS MODULUS:',E17.10)
  150 FORMAT('HYDROSTATIC PRESSURE: ',E17.10)
  160 FORMAT('VON MISES STRESS: ',E17.10)
  170 FORMAT('EFFECTIVE STRAIN: ',E17.10)
  180 FORMAT('STRESS INCREMENTS: ', I3)
  190 FORMAT(E17.10)
  200 FORMAT('JACOBIAN: ', I3, I3)
  210 FORMAT('STRESS COMP.',I3)
  220 FORMAT('INCREMENTS OF STRAIN ',I3)
  230 FORMAT('STRAINS: ', I3)
C
IF(NOEL.EQ.1.AND.NPT.EQ.1)THEN
  WRITE(18,120)
  WRITE(18,130)KINC
  WRITE(18,140)YMOD(NOEL,NPT)
  WRITE(18,150)HP
  WRITE(18,160)VMISTRESS(NOEL,NPT)
  WRITE(18,170)ESTRAN
  WRITE(18,*) 'JACOBIAN'
  DO I = 1, NTENS
```

```
      WRITE(18,*) (DDSDDE(I,J), J=1, NTENS)
    END DO
    WRITE(18,200) NTENS
    WRITE(18,190) (DSTRESS(I), I=1,NTENS)
    WRITE(18,210) NTENS
    WRITE(18,190) (STRESS(I), I=1,NTENS)
    WRITE(18,220) NTENS
    WRITE(18,190) (DSTRAN(I), I=1,NTENS)
    WRITE(18,230) NTENS
    WRITE(18,190) (STRAN(I), I=1,NTENS)
      END IF
C
      RETURN
      END
C
CCCCCCCCCCCCCCCCCCCCCCCCCCCCCCCCCCCCCCCCCCCCCCCCCCCCCCCCCCCCCCCCCCCCCCCCCCCCCC
C Subroutine DLOAD is used to define a non-uniform/uniform distributed load for each element at each load
C integration point. For the limit load analysis method, however, it is also used to calculate the upper bound limit
C loads, which is then applied to the model.
C
C As before, the following standard block, from the user's manual, acts as an interface between ABAQUS,
C UMAT and other subroutines.
CCCCCCCCCCCCCCCCCCCCCCCCCCCCCCCCCCCCCCCCCCCCCCCCCCCCCCCCCCCCCCCCCCCCCCCCCCCCCC
C
      SUBROUTINE DLOAD (F, KSTEP, KINC, TIME, NOEL, NPT, LAYER,
     1 KSPT, COORDS, JLTYP)
C
      INCLUDE 'ABA_PARAM.INC'
C
CCCCCCCCCCCCCCCCCCCCCCCCCCCCCCCCCCCCCCCCCCCCCCCCCCCCCCCCCCCCCCCCCCCCCCCCCCCCCC
C The PARAMETER option is used to declare the number of elements (NEL), number of integration points
C (NUPT), and number of stress and strain tensor components (NCO), which is done individually in each
C subroutine.
CCCCCCCCCCCCCCCCCCCCCCCCCCCCCCCCCCCCCCCCCCCCCCCCCCCCCCCCCCCCCCCCCCCCCCCCCCCCCC
C
     PARAMETER(NEL=30, NUPT=3, NCO=3)
C
CCCCCCCCCCCCCCCCCCCCCCCCCCCCCCCCCCCCCCCCCCCCCCCCCCCCCCCCCCCCCCCCCCCCCCCCCCCCCC
C The following arrays are declared separately as they are used only in this subroutine.
CCCCCCCCCCCCCCCCCCCCCCCCCCCCCCCCCCCCCCCCCCCCCCCCCCCCCCCCCCCCCCCCCCCCCCCCCCCCCC
C
      DIMENSION COORDS(3), TIME(2), KMARK(NEL,NUPT), TF(NEL,NUPT)
      SAVE
C
CCCCCCCCCCCCCCCCCCCCCCCCCCCCCCCCCCCCCCCCCCCCCCCCCCCCCCCCCCCCCCCCCCCCCCCCCCCCCC
C The COMMON block option is used to make the necessary variables available to other subroutines.
CCCCCCCCCCCCCCCCCCCCCCCCCCCCCCCCCCCCCCCCCCCCCCCCCCCCCCCCCCCCCCCCCCCCCCCCCCCCCC
C
      COMMON/KSTUFF1/A,B,C,E,S,DW,DF
      YSTRESS = C
      ENERGY = E
```

```
      HSTRESS = S
      KELE=A
      KINT=B
      DWORK=DW
C
CCCCCCCCCCCCCCCCCCCCCCCCCCCCCCCCCCCCCCCCCCCCCCCCCCCCCCCCCCCCCCCCCCCCCCCCCCC
C As before, the array, KMARK, is used to ensure that any iteration is carried out only once per increment
CCCCCCCCCCCCCCCCCCCCCCCCCCCCCCCCCCCCCCCCCCCCCCCCCCCCCCCCCCCCCCCCCCCCCCCCCCC
C
      IF(KINC.NE.KINI) THEN
       KINI=KINC
       DO I1=1, NEL
         DO J1=1, NUPT
           KMARK(I1,J1)=0
         END DO
       END DO
      END IF
C
CCCCCCCCCCCCCCCCCCCCCCCCCCCCCCCCCCCCCCCCCCCCCCCCCCCCCCCCCCCCCCCCCCCCCCCCCCC
C Here, the incremental displacement, DISPL, is calculated. It is done by using the incremental work done,
C DWORK, from URDFIL and the calculated total load, TF. In the first increment, however, TF is set to zero.
CCCCCCCCCCCCCCCCCCCCCCCCCCCCCCCCCCCCCCCCCCCCCCCCCCCCCCCCCCCCCCCCCCCCCCCCCCC
C
      IF (TF(NOEL,NPT).EQ.0) GO TO 5
      IF(KMARK(NOEL,NPT).EQ.1) GO TO 5
       DISPL=DWORK/TF(NOEL,NPT)
    5  CONTINUE
C
CCCCCCCCCCCCCCCCCCCCCCCCCCCCCCCCCCCCCCCCCCCCCCCCCCCCCCCCCCCCCCCCCCCCCCCCCCC
C In this block, the upper bound limit load, DF, is calculated using the effective strain integrated over the
C volume, ENERGY, and the displacement term, DISPL. This is then added to TF to obtain the total load,
C required to satisfy ABAQUS internal convergence criterion. In the first increment, however, this block is
C ignored and DF & TF is initialised to an arbitrary value.
CCCCCCCCCCCCCCCCCCCCCCCCCCCCCCCCCCCCCCCCCCCCCCCCCCCCCCCCCCCCCCCCCCCCCCCCCCC
C
      IF(KINC.EQ.1) GO TO 10
      IF(KMARK(NOEL,NPT).EQ.1) GO TO 20
       DF=ENERGY/DISPL
       TF(NOEL,NPT)=TF(NOEL,NPT)+DF
C
CCCCCCCCCCCCCCCCCCCCCCCCCCCCCCCCCCCCCCCCCCCCCCCCCCCCCCCCCCCCCCCCCCCCCCCCCCC
C In the first increment, the initial load applied to the model is defined. This is ignored in subsequent iterations.
CCCCCCCCCCCCCCCCCCCCCCCCCCCCCCCCCCCCCCCCCCCCCCCCCCCCCCCCCCCCCCCCCCCCCCCCCCC
C
      GO TO 20
   10  DF=-200
      TF(NOEL,NPT)=DF
   20  CONTINUE
      F=TF(NOEL,NPT)
C
      KMARK(NOEL,NPT)=1
```

```
C
 30   FORMAT('-----------------------------------')
 40   FORMAT('DLOAD---INCREMENT ',I3)
 50   FORMAT('TOTAL LOAD: ',E17.10)
 60   FORMAT('ENERGY: ',E17.10)
 70   FORMAT('INCREMENTAL WORK DONE: ',E17.10)
 80   FORMAT('DISPLACEMENT: ',E17.10)
 90   FORMAT('HIGHEST MISES STRESS: ',E12.5)
 100  FORMAT('ELEMENT: 'I6)
 110  FORMAT('INTEGRATION POINT: ',I3)
 240  FORMAT('TIME INCREMENT: ',E17.10)
 250  FORMAT('CURRENT VALUE OF TOTAL TIME: ',E17.10)
C
      IF(NOEL.EQ.24.AND.NPT.EQ.1)THEN
      WRITE(18,30)
      WRITE(18,40)KINC
      WRITE(18,50) F
      WRITE(18,60)ENERGY
      WRITE(18,70)DWORK
      WRITE(18,80)DISPL
      WRITE(18,90)HSTRESS
      WRITE(18,100)KELE
      WRITE(18,240)DTIME
      WRITE(18,250)TIME(2)
      END IF
C
      RETURN
      END
C
CCCCCCCCCCCCCCCCCCCCCCCCCCCCCCCCCCCCCCCCCCCCCCCCCCCCCCCCCCCCCCCCCCCCCCCCCCCC
C Subroutine URDFIL is called at the end of each increment and accesses the results file. It is, here, where all the
C necessary values of variables are extracted, updated and then made available to other subroutines via the
C common block option.
C
C As before, the following standard block, from the user's manual, acts as an interface between ABAQUS,
C UMAT and DLOAD subroutines.
CCCCCCCCCCCCCCCCCCCCCCCCCCCCCCCCCCCCCCCCCCCCCCCCCCCCCCCCCCCCCCCCCCCCCCCCCCCC
C
      SUBROUTINE URDFIL(LSTOP, LOVRWRT, KSTEP, KINC)
      INCLUDE 'ABA_PARAM.INC'
C
      DIMENSION ARRAY(513), JRRAY(NPRECD,513), ENERGIES(20)
      EQUIVALENCE (ARRAY(1), JRRAY(1,1))
C
CCCCCCCCCCCCCCCCCCCCCCCCCCCCCCCCCCCCCCCCCCCCCCCCCCCCCCCCCCCCCCCCCCCCCCCCCCCC
C The COMMON block option is used to make the necessary variables available to other subroutines.
CCCCCCCCCCCCCCCCCCCCCCCCCCCCCCCCCCCCCCCCCCCCCCCCCCCCCCCCCCCCCCCCCCCCCCCCCCCC
C
      COMMON/KSTUFF1/A,B,C,E,S,DW,DF
      SAVE
C
```

```
      TSTRESS=0.0
C
CCCCCCCCCCCCCCCCCCCCCCCCCCCCCCCCCCCCCCCCCCCCCCCCCCCCCCCCCCCCCCCCCCCCCCCCCCCCCCC
C The blocks, POSFIL & DBFILE, is specifically used to position URDFIL at the right location in the results
C file. Further explanation of its use is available in the ABAQUS/STANDARD manual.
CCCCCCCCCCCCCCCCCCCCCCCCCCCCCCCCCCCCCCCCCCCCCCCCCCCCCCCCCCCCCCCCCCCCCCCCCCCCCCC
C
      CALL POSFIL(KSTEP, KINC, ARRAY, JRCD)
      DO 1000 K=1,999999
        CALL DBFILE(0, ARRAY, JRCD)
        IF(JRCD.NE.0) GO TO 10
        KEY=JRRAY(1,2)
C
CCCCCCCCCCCCCCCCCCCCCCCCCCCCCCCCCCCCCCCCCCCCCCCCCCCCCCCCCCCCCCCCCCCCCCCCCCCCCCC
C ABAQUS stores the contents of the results file in different keys. The key, 1999, stores all the energy values.
C The array, ARRAY(3) has the integrated values of the yield stress multiplied by the effective strain in the
C model. This is stored as the variable, SSE, in UMAT ARRAY(4) stores the value of the work done. From this,
C the incremental work done is evaluated and used in subroutine DLOAD, to compute the incremental
C displacement.
CCCCCCCCCCCCCCCCCCCCCCCCCCCCCCCCCCCCCCCCCCCCCCCCCCCCCCCCCCCCCCCCCCCCCCCCCCCCCCC
C
        IF(KEY.EQ.1999) THEN
          ENERGY=ARRAY(4)
          WORK=ARRAY(5)
          E=ENERGY
          DWORK=WORK
          DWORK=DWORK-UW
          UW=UW+DWORK
          DW=DWORK
          DO L1=1,20
            ENERGIES(L1)=ARRAY(L1)
          END DO
C
        ELSE IF(KEY.EQ.1) THEN
          JEL=JRRAY(1,3)
          JPNT=JRRAY(1,4)
C
        ELSE IF(KEY.EQ.5) THEN
          IF (ARRAY(3).GT.TSTRESS) THEN
            TSTRESS=ARRAY(3)
            KELE=JEL
            KINT=JPNT
          END IF
        END IF
C
 1000 CONTINUE
 10   CONTINUE
C
CCCCCCCCCCCCCCCCCCCCCCCCCCCCCCCCCCCCCCCCCCCCCCCCCCCCCCCCCCCCCCCCCCCCCCCCCCCCCCC
C The convergence criterion, CONV, is specified here. As the termination of the program is controlled by the
C user subroutine, how and when the analysis stops can be accurately prescribed.
```

```
CCCCCCCCCCCCCCCCCCCCCCCCCCCCCCCCCCCCCCCCCCCCCCCCCCCCCCCCCCCCCCCCCCCCCCCC
C
      CONV=(DFP/DF)-1.0
      DFP=DF
      IF(CONV.LE.0.001) THEN
       KTOL=KTOL+1
      ELSE
       KTOL=0
      END IF
C
      IF(KTOL.EQ.5) LSTOP=1
      S=TSTRESS
      A=KELE
      B=KINT
      DFUB=-1*DF
      PLB=-1*P
C
 260  FORMAT('--------------------------------')
 270  FORMAT('INCREMENT ',I3)
 280  FORMAT('UB  : ',E17.10)
 290  FORMAT('LB  : ',E17.10)
 300  FORMAT('URDFIL---INCREMENT ',I3)
 310  FORMAT('TSTRESS: ',E17.10)
 320  FORMAT('ELEMENT: ',I6)
 330  FORMAT('INTEGRATION POINT: ',I3)
C
      WRITE(15,270)KINC
      WRITE(17,280)DFUB
      WRITE(15,290)PLB
      WRITE(18,260)
      WRITE(18,300)KINC
      WRITE(18,310)TSTRESS
      WRITE(18,320)KELE
      WRITE(18,330)KINT
C
      RETURN
      END
```

Appendix C

Double-edged Crack Plate (Plane Stress) using the LMM (Procedure B)

The following is the actual programming codes used in the analysis. The first program involves evaluating the linear elastic stress solution for a structure under purely mechanical load. This is then stored in a file, at each integration point for each element. These are then accessed by the second program, whereby the upper bound limit load is computed. To ensure that all the elements and integration points are serviced in the same order, the same mesh is used in both programs.

C1: Linear Elastic Stress Solution

```
C
CCCCCCCCCCCCCCCCCCCCCCCCCCCCCCCCCCCCCCCCCCCCCCCCCCCCCCCCCCCCCCCCCCCCCCCCCC
C User subroutine UMAT allows the material behaviour, [J] of the model to be defined, at each material
C integration point for each element. Using the incremental strains supplied by ABAQUS, this subroutine would
C then compute the stress field, which would then be added up to obtain the total stress solution.
C
C The following standard block, from the user manual, acts as an interface between ABAQUS and UMAT.
CCCCCCCCCCCCCCCCCCCCCCCCCCCCCCCCCCCCCCCCCCCCCCCCCCCCCCCCCCCCCCCCCCCCCCCCCC
C
      SUBROUTINE UMAT(STRESS, STATEV, DDSDDE, SSE, SPD, SCD,
     1 RPL, DDSDDT, DRPLDE, DRPLDT,
     2 STRAN, DSTRAN, TIME, DTIME, TEMP, DTEMP, PREDEF, DPRED, CMNAME,
     3 NDI, NSHR, NTENS, NSTATV, PROPS, NPROPS, COORDS, DROT, PNEWDT,
     4 CELENT, DFGRD0, DFGRD1, NOEL, NPT, LAYER, KSPT, KSTEP, KINC)
C
      INCLUDE 'ABA_PARAM.INC'
C
      CHARACTER*8 CMNAME
      DIMENSION STRESS(NTENS), STATEV(NSTATV),
     1 DDSDDE(NTENS, NTENS), DDSDDT(NTENS), DRPLDE(NTENS),
     2 STRAN(NTENS), DSTRAN(NTENS), TIME(2), PREDEF(1), DPRED(1),
     3 PROPS(NPROPS), COORDS(3), DROT(3,3), DFGRD0(3,3), DFGRD1(3,3)
C
CCCCCCCCCCCCCCCCCCCCCCCCCCCCCCCCCCCCCCCCCCCCCCCCCCCCCCCCCCCCCCCCCCCCCCCCCC
C The PARAMETER option is used to declare the number of elements (NEL), number of integration points
C (NUPT), and number of stress and strain tensor components (NCO)
CCCCCCCCCCCCCCCCCCCCCCCCCCCCCCCCCCCCCCCCCCCCCCCCCCCCCCCCCCCCCCCCCCCCCCCCCC
C
      PARAMETER(NUEL=30, NUPT=3, NCO=3)
C
CCCCCCCCCCCCCCCCCCCCCCCCCCCCCCCCCCCCCCCCCCCCCCCCCCCCCCCCCCCCCCCCCCCCCCCCCC
C The following arrays are declared separately as they are used only in this subroutine.
CCCCCCCCCCCCCCCCCCCCCCCCCCCCCCCCCCCCCCCCCCCCCCCCCCCCCCCCCCCCCCCCCCCCCCCCCC
C
```

```
      DIMENSION DSTRESS(NCO), KMARK(NUEL,NUPT), IMARK(NUEL,NUPT)
      SAVE
C
CCCCCCCCCCCCCCCCCCCCCCCCCCCCCCCCCCCCCCCCCCCCCCCCCCCCCCCCCCCCCCCCCCCCCCCCCCC
C These files are opened and results written in them as the analysis continues.
CCCCCCCCCCCCCCCCCCCCCCCCCCCCCCCCCCCCCCCCCCCCCCCCCCCCCCCCCCCCCCCCCCCCCCCCCCC
C
      OPEN(18,FILE='/TEMP/msmh1/elastic11.dat')
      OPEN(UNIT=17,FILE='/TEMP/msmh2/elastic12.dat',STATUS='UNKNOWN',
     1   ACCESS='DIRECT',FORM='FORMATTED',RECL=17)
C
CCCCCCCCCCCCCCCCCCCCCCCCCCCCCCCCCCCCCCCCCCCCCCCCCCCCCCCCCCCCCCCCCCCCCCCCCCC
C As ABAQUS is programmed to access the subroutines at least twice per increment, the array, KMARK, is used
C to ensure that any iteration is carried out only once. In the first increment, once an integration point is dealt
C with, KMARK is set to one. This would then ensure that particular integration point would not be considered
C until the start of the next iteration.
CCCCCCCCCCCCCCCCCCCCCCCCCCCCCCCCCCCCCCCCCCCCCCCCCCCCCCCCCCCCCCCCCCCCCCCCCCC
C
      IF(KINC.NE.KINI) THEN
        KINI=KINC
        DO I1=1, NUEL
          DO J1=1, NUPT
            KMARK(I1,J1)=0
          END DO
        END DO
      END IF
C
CCCCCCCCCCCCCCCCCCCCCCCCCCCCCCCCCCCCCCCCCCCCCCCCCCCCCCCCCCCCCCCCCCCCCCCCCCC
C The stress increments, DSTRESS, is set to zero, ensuring a set of individual elastic solutions in each iteration.
CCCCCCCCCCCCCCCCCCCCCCCCCCCCCCCCCCCCCCCCCCCCCCCCCCCCCCCCCCCCCCCCCCCCCCCCCCC
C
      DO K1=1, NTENS
        DSTRESS(K1)=0
      END DO
C
CCCCCCCCCCCCCCCCCCCCCCCCCCCCCCCCCCCCCCCCCCCCCCCCCCCCCCCCCCCCCCCCCCCCCCCCCCC
C Here the Jacobian matrix, DDSDDE, is defined and assembled using the Poisson's ratio, PROPS(1), and the
C elastic modulus, PROPS(2), defined in the input file.
CCCCCCCCCCCCCCCCCCCCCCCCCCCCCCCCCCCCCCCCCCCCCCCCCCCCCCCCCCCCCCCCCCCCCCCCCCC
C
      TERM  = 1.0-PROPS(2)**2
      TERM1 = PROPS(1)/TERM
      TERM2 = PROPS(1)*PROPS(2)/TERM
      TERM3 = PROPS(1)*(1.0-PROPS(2))/2./TERM
C
      DO K1=1,NDI
        DDSDDE(K1,K1)=TERM1
      END DO
      DO K1=2,NDI
        N2=K1-1
        DO K2=1,N2
```

```
          DDSDDE(K2,K1) = TERM2
          DDSDDE(K1,K2) = TERM2
        END DO
      END DO
      DDSDDE(NTENS,NTENS)=TERM3
C
CCCCCCCCCCCCCCCCCCCCCCCCCCCCCCCCCCCCCCCCCCCCCCCCCCCCCCCCCCCCCCCCCCCCCCCCCCCCCC
C In the following block, the stress increments, DSTRESS, is computed using the Jacobian, DDSDDE, and
C the strain increments obtained from ABAQUS, DSTRAN. These are then added up to STRESS, total stress, to
C trick ABAQUS into "thinking" it is solving a non-linear problem.
CCCCCCCCCCCCCCCCCCCCCCCCCCCCCCCCCCCCCCCCCCCCCCCCCCCCCCCCCCCCCCCCCCCCCCCCCCCCCC
C
      DO K=1,NDI
        DO I=1,NDI
          DSTRESS(K) = DSTRESS(K)+(DDSDDE(K,I)*DSTRAN(I))
        END DO
      END DO
      DSTRESS(NTENS) = DDSDDE(NTENS,NTENS)*DSTRAN(NTENS)
C
    DO K=1, NTENS
      STRESS(K) = STRESS(K)+DSTRESS(K)
    END DO
C
CCCCCCCCCCCCCCCCCCCCCCCCCCCCCCCCCCCCCCCCCCCCCCCCCCCCCCCCCCCCCCCCCCCCCCCCCCCCCC
C Here, the stress values, which are essentially linear elastic stress solutions, is written to the file opened above.
C The way the stress tensor is recorded is governed by a counting system, which ensures that the correct values
C are extracted in the second program.
CCCCCCCCCCCCCCCCCCCCCCCCCCCCCCCCCCCCCCCCCCCCCCCCCCCCCCCCCCCCCCCCCCCCCCCCCCCCCC
C
    IF (KMARK(NOEL,NPT).EQ.0) GO TO 100
    IF (IMARK(NOEL,NPT).EQ.1) GO TO 100
      DO K=1,NTENS
      KCOUNT=KCOUNT+1
      WRITE(17,180,REC=KCOUNT) DSTRESS(K)
      END DO
      IMARK(NOEL,NPT)=1
 100  CONTINUE
C
CCCCCCCCCCCCCCCCCCCCCCCCCCCCCCCCCCCCCCCCCCCCCCCCCCCCCCCCCCCCCCCCCCCCCCCCCCCCCC
C The actual Von-mises effective stress and the associated effective strain is calculated in the following block.
CCCCCCCCCCCCCCCCCCCCCCCCCCCCCCCCCCCCCCCCCCCCCCCCCCCCCCCCCCCCCCCCCCCCCCCCCCCCCC
C
    HP=(DSTRESS(1)+DSTRESS(2))/3.0
    ST=1.5*((DSTRESS(1)-HP)**2.0+(DSTRESS(2)-HP)**2.0+(-1*HP)**2.0
   1   +2.0*(DSTRESS(3)**2.0))
    VMISTRESS(NOEL,NPT)=SQRT(ST)
C
    THSTRAN=(-PROPS(1)/YMOD(NOEL,NPT))*(DSTRESS(1)+DSTRESS(2))
    X = DSTRAN(1)**2.0+DSTRAN(2)**2.0+THSTRAN**2.0+0.5*DSTRAN(3)**2.0
    X = X*2.0/3.0
    ESTRAN = SQRT(X)
```

```
C
CCCCCCCCCCCCCCCCCCCCCCCCCCCCCCCCCCCCCCCCCCCCCCCCCCCCCCCCCCCCCCCCCCCCCCCCCCCC
C Here, local variables are assigned to STATEV(), where it is stored and could be accessed later by ABAQUS
C /POST or subroutine URDFIL.
CCCCCCCCCCCCCCCCCCCCCCCCCCCCCCCCCCCCCCCCCCCCCCCCCCCCCCCCCCCCCCCCCCCCCCCCCCCC
C
    DO K=1,NTENS
      STATEV(K)=DSTRESS(K)
    END DO
    STATEV(4)=HP
    STATEV(5)=VMSTRESS
C
    KMARK(NOEL,NPT)=1
C
 180  FORMAT(E17.10)
 200  FORMAT('-----------------------')
 210  FORMAT('ELEMENT ',I3,' POINT ',I1)
      IF (NOEL.EQ.NTENS.AND.NPT.EQ.1) THEN
        WRITE(18,200)
        WRITE(18,210)NOEL,NPT
        WRITE(18,*)'STRESS'
        WRITE(18,180)(DSTRESS(I), I=1,NTENS)
        WRITE(18,*)'EFFECTIVE STRESS'
        WRITE(18,180)VMSTRESS
      END IF
C
    RETURN
    END
C
CCCCCCCCCCCCCCCCCCCCCCCCCCCCCCCCCCCCCCCCCCCCCCCCCCCCCCCCCCCCCCCCCCCCCCCCCCCC
C Subroutine URDFIL is called at the end of each increment and accesses the results file. It is, here, where all the
C necessary values of variables are extracted, updated and then made available to other subroutines via the
C common block option.

C As before, the following standard block, from the user's manual, acts as an interface between ABAQUS,
C UMAT and DLOAD subroutines.
CCCCCCCCCCCCCCCCCCCCCCCCCCCCCCCCCCCCCCCCCCCCCCCCCCCCCCCCCCCCCCCCCCCCCCCCCCCC
C
    SUBROUTINE URDFIL(LSTOP, LOVRWRT, KSTEP, KINC)
C
    INCLUDE 'ABA_PARAM.INC'
C
    DIMENSION ARRAY(513), JRRAY(NPRECD,513), ENERGIES(20)
    EQUIVALENCE (ARRAY(1), JRRAY(1,1))
    TSTRESS=0.0
    XSTRESS=0.0
    YSTRESS=0.0
C
CCCCCCCCCCCCCCCCCCCCCCCCCCCCCCCCCCCCCCCCCCCCCCCCCCCCCCCCCCCCCCCCCCCCCCCCCCCC
C The blocks, POSFIL & DBFILE, is specifically used to position URDFIL at the right location in the results
C file. Further explanation of its use is available in the ABAQUS/STANDARD manual.
```

```
CCCCCCCCCCCCCCCCCCCCCCCCCCCCCCCCCCCCCCCCCCCCCCCCCCCCCCCCCCCCCCCCCCCC
C
   CALL POSFIL(KSTEP, KINC, ARRAY, JRCD)
   DO 1000 K=1,999999
     CALL DBFILE(0, ARRAY, JRCD)
     IF(JRCD.NE.0) GO TO 10
     KEY=JRRAY(1,2)
C
     IF(KEY.EQ.1) THEN
       JEL=JRRAY(1,3)
       JPNT=JRRAY(1,4)
C
     ELSE IF(KEY.EQ.11) THEN
       IF (ARRAY(3).GT.XSTRESS) THEN
         XSTRESS=ARRAY(3)
         IELE=JEL
         IINT=JPNT
       ELSE IF (ARRAY(4).GT.YSTRESS) THEN
         YSTRESS=ARRAY(4)
         JELE=JEL
         JINT=JPNT
       END IF
C
     ELSE IF(KEY.EQ.12) THEN
       IF (ARRAY(3).GT.TSTRESS) THEN
         TSTRESS=ARRAY(3)
         KELE=JEL
         KINT=JPNT
       END IF
     END IF
 1000 CONTINUE
 10   CONTINUE
C
120  FORMAT('ELEMENT: ',I3,' POINT: ',I3)
130  FORMAT('--------------------------------')
     WRITE(18,*)'URDFIL'
     WRITE(18,*)'HIGEST EFFECTIVE STRESS:'
     WRITE(18,*)TSTRESS
     WRITE(18,*)'LOCATED AT:'
     WRITE(18,120)KELE,KINT
     WRITE(18,130)
     WRITE(18,*)'HIGHEST STRESS IN X-DIRECTION:'
     WRITE(18,*)XSTRESS
     WRITE(18,*)'LOCATED AT:'
     WRITE(18,120)IELE,IINT
     WRITE(18,130)
     WRITE(18,*)'HIGHEST STRESS IN Y-DIRECTION:'
     WRITE(18,*)YSTRESS
     WRITE(18,*)'LOCATED AT:'
     WRITE(18,120)JELE,JINT
C
```

```
      RETURN
      END
```

C2: Limit Analysis Solution

```
C
CCCCCCCCCCCCCCCCCCCCCCCCCCCCCCCCCCCCCCCCCCCCCCCCCCCCCCCCCCCCCCCCCCCCCCC
C User subroutine UMAT allows the material behaviour, [J] of the model to be defined, at each material
C integration point for each element. Using the incremental strains from ABAQUS, this subroutine would then
C compute the stress field, which would then be added up to obtain the total stress solution.
C
C The following standard block, from the user manual, acts as an interface between ABAQUS and UMAT.
CCCCCCCCCCCCCCCCCCCCCCCCCCCCCCCCCCCCCCCCCCCCCCCCCCCCCCCCCCCCCCCCCCCCCCC
C
      SUBROUTINE UMAT(STRESS, STATEV, DDSDDE, SSE, SPD, SCD,
     1 RPL, DDSDDT, DRPLDE, DRPLDT,
     2 STRAN, DSTRAN, TIME, DTIME, TEMP, DTEMP, PREDEF, DPRED, CMNAME,
     3 NDI, NSHR, NTENS, NSTATV, PROPS, NPROPS, COORDS, DROT, PNEWDT,
     4 CELENT, DFGRD0, DFGRD1, NOEL, NPT, LAYER, KSPT, KSTEP, KINC)
C
      INCLUDE 'ABA_PARAM.INC'
C
      CHARACTER*8 CMNAME
      DIMENSION STRESS(NTENS), STATEV(NSTATV),
     1 DDSDDE(NTENS, NTENS), DDSDDT(NTENS), DRPLDE(NTENS),
     2 STRAN(NTENS), DSTRAN(NTENS), TIME(2), PREDEF(1), DPRED(1),
     3 PROPS(NPROPS), COORDS(3), DROT(3,3), DFGRD0(3,3), DFGRD1(3,3)
C
CCCCCCCCCCCCCCCCCCCCCCCCCCCCCCCCCCCCCCCCCCCCCCCCCCCCCCCCCCCCCCCCCCCCCCC
C The PARAMETER option is used to declare the number of elements (NEL), number of integration points
C (NUPT), and number of stress and strain tensor components (NCO)
CCCCCCCCCCCCCCCCCCCCCCCCCCCCCCCCCCCCCCCCCCCCCCCCCCCCCCCCCCCCCCCCCCCCCCC
C
      PARAMETER(NEL=30, NUPT=3, NSO=3, NCO=3)
C
CCCCCCCCCCCCCCCCCCCCCCCCCCCCCCCCCCCCCCCCCCCCCCCCCCCCCCCCCCCCCCCCCCCCCCC
C The following arrays are declared separately as they are used only in this subroutine.
CCCCCCCCCCCCCCCCCCCCCCCCCCCCCCCCCCCCCCCCCCCCCCCCCCCCCCCCCCCCCCCCCCCCCCC
C
      DIMENSION DSTRESS(NCO), KMARK(NEL,NUPT), ESTRAN(NEL,NUPT,NSO),
     1 STRESSIN(NCO), SM(NEL,NUPT,NSO), DEVA(NEL,NUPT,NCO),
     2 DEVB(NEL,NUPT,NCO), DEVC(NEL,NUPT,NCO), DEV(NSO,NCO), RO(NCO),
     3 SSTRAN(NSO,NCO), COMP(NSO,NCO,NCO), ELA(NEL,NUPT,NCO),
     4 ELB(NEL,NUPT,NCO),ELC(NEL,NUPT,NCO),THISTRAN(NSO)
C
CCCCCCCCCCCCCCCCCCCCCCCCCCCCCCCCCCCCCCCCCCCCCCCCCCCCCCCCCCCCCCCCCCCCCCC
C The COMMON block option is used to make the necessary variables available to other subroutines.
CCCCCCCCCCCCCCCCCCCCCCCCCCCCCCCCCCCCCCCCCCCCCCCCCCCCCCCCCCCCCCCCCCCCCCC
C
```

```
      COMMON/KSTUFF/SF,YLAMB
      SAVE
C
CCCCCCCCCCCCCCCCCCCCCCCCCCCCCCCCCCCCCCCCCCCCCCCCCCCCCCCCCCCCCCCCCCCCCCCCCCCCCCC
C These files are opened and results written in them as the analysis continues.
CCCCCCCCCCCCCCCCCCCCCCCCCCCCCCCCCCCCCCCCCCCCCCCCCCCCCCCCCCCCCCCCCCCCCCCCCCCCCCC
C
      OPEN(UNIT=18,FILE='/TEMP/msmh1/dplateps1.dat')
      OPEN(UNIT=15,FILE='/TEMP/msmh2/dplateps2.dat')
C
CCCCCCCCCCCCCCCCCCCCCCCCCCCCCCCCCCCCCCCCCCCCCCCCCCCCCCCCCCCCCCCCCCCCCCCCCCCCCCC
C Assigning solution-dependent state variables, STATEV(), to local variables to be analysed later.
CCCCCCCCCCCCCCCCCCCCCCCCCCCCCCCCCCCCCCCCCCCCCCCCCCCCCCCCCCCCCCCCCCCCCCCCCCCCCCC
C
      STATEV(1)=KINC
      STATEV(2)=YLAMB
      STATEV(3)=SF
C
CCCCCCCCCCCCCCCCCCCCCCCCCCCCCCCCCCCCCCCCCCCCCCCCCCCCCCCCCCCCCCCCCCCCCCCCCCCCCCC
C As ABAQUS is programmed to access the subroutines at least twice per increment, the array, KMARK, is used
C to ensure that any iteration is carried out only once. In the first increment, once an integration point is dealt
C with, KMARK is set to one. This would then ensure that particular integration point would not be considered
C until the start of the next iteration.
C
C A counter, KCOUNTA, is also initialised to ensure that the linear elastic solution is correctly read.
CCCCCCCCCCCCCCCCCCCCCCCCCCCCCCCCCCCCCCCCCCCCCCCCCCCCCCCCCCCCCCCCCCCCCCCCCCCCCCC
C
      IF(KINC.NE.KINI) THEN
       KINI=KINC
       KCOUNTA=1
       DO I1=1, NEL
         DO J1=1, NUPT
           KMARK(I1,J1)=0
         END DO
       END DO
      END IF
C
CCCCCCCCCCCCCCCCCCCCCCCCCCCCCCCCCCCCCCCCCCCCCCCCCCCCCCCCCCCCCCCCCCCCCCCCCCCCCCC
C In the following block, the file storing the linear elastic stress solution is opened and assigned to the variable,
C ELA(NOEL,NPT,NTENS), which in turn is assigned to the stress history, DEVC(NOEL,NPT,NTENS).
CCCCCCCCCCCCCCCCCCCCCCCCCCCCCCCCCCCCCCCCCCCCCCCCCCCCCCCCCCCCCCCCCCCCCCCCCCCCCCC
C
      IF (KINC.EQ.1.AND.KMARK(NOEL,NPT).EQ.0) THEN
       OPEN(UNIT=17,FILE='/TEMP/msmh2/elastic12.dat',
     1 STATUS='OLD',ACCESS='DIRECT',FORM='FORMATTED',RECL=17)
      DO K=1,NTENS
         READ(17,180,REC=KCOUNTA) ELA(NOEL,NPT,K)
         KCOUNTA=KCOUNTA+1
      END DO
      CLOSE(17)
C
```

```
      DO K=1,NTENS
        DEVC(NOEL,NPT,K)=ELA(NOEL,NPT,K)
      END DO
      END IF
C
CCCCCCCCCCCCCCCCCCCCCCCCCCCCCCCCCCCCCCCCCCCCCCCCCCCCCCCCCCCCCCCCCCCCCCCCCCCCCC
C A scaling factor, SF, is introduced. This is to scale down the stress history so as to prevent numerical errors
C which would otherwise occur due to stress values becoming too large.
CCCCCCCCCCCCCCCCCCCCCCCCCCCCCCCCCCCCCCCCCCCCCCCCCCCCCCCCCCCCCCCCCCCCCCCCCCCCC
C
      IF (KMARK(NOEL,NPT).EQ.1) GO TO 50
      IF (KINC.EQ.1) GO TO 50
      DO K=1,NTENS
        DEVC(NOEL,NPT,K)=DEVC(NOEL,NPT,K)*SF
      END DO
C
 50   CONTINUE
C
CCCCCCCCCCCCCCCCCCCCCCCCCCCCCCCCCCCCCCCCCCCCCCCCCCCCCCCCCCCCCCCCCCCCCCCCCCCCC
C In this block, the stress history is re-assigned to a two-dimensional array, which makes the data easier to handle
C during subsequent programming operations.
CCCCCCCCCCCCCCCCCCCCCCCCCCCCCCCCCCCCCCCCCCCCCCCCCCCCCCCCCCCCCCCCCCCCCCCCCCCCC
C
      DO K=1,NTENS
          DEV(3,K)=DEVC(NOEL,NPT,K)
      END DO
C
CCCCCCCCCCCCCCCCCCCCCCCCCCCCCCCCCCCCCCCCCCCCCCCCCCCCCCCCCCCCCCCCCCCCCCCCCCCCC
C Here, all arrays, stresses and strains, as well as variables used in the program are initialised.
CCCCCCCCCCCCCCCCCCCCCCCCCCCCCCCCCCCCCCCCCCCCCCCCCCCCCCCCCCCCCCCCCCCCCCCCCCCCC
C
      DO K1=1, NTENS
        DSTRESS(K1)=0.0
        STRESSIN(K1)=0.0
      END DO
      SMTOT=0.0
      THSTRAN=0.0
      SSE=0.0
      SPD=0.0
      DO I=1,NSO
        THISTRAN(I)=0.0
        DO K=1,NTENS
          SSTRAN(I,K)=0.0
        END DO
      END DO
C
CCCCCCCCCCCCCCCCCCCCCCCCCCCCCCCCCCCCCCCCCCCCCCCCCCCCCCCCCCCCCCCCCCCCCCCCCCCCC
C In the first increment, the linear moduli is initialised to an arbitrary value. It is important to note that the
C reciprocal values are used here instead. In subsequent iterations, these reciprocal linear moduli are updated
C using the relationship presented. A limit of the magnitude of these values is also set to prevent any numerical
C complications.
```

```
CCCCCCCCCCCCCCCCCCCCCCCCCCCCCCCCCCCCCCCCCCCCCCCCCCCCCCCCCCCCCCCCC
C
   IF (KINC.EQ.1) THEN
     DO I=1,NSO
       SM(NOEL,NPT,I)=1.0/2.0
     END DO
     GO TO 100
   END IF
C
   IF (KMARK(NOEL,NPT).EQ.1) GO TO 100
   DO I=1,NSO
     SM(NOEL,NPT,I)=ESTRAN(NOEL,NPT,I)/PROPS(1)
     IF (SM(NOEL,NPT,I).LT.1.0E-08) THEN
       SM(NOEL,NPT,I)=1.0E-08
     END IF
   END DO
C
 100 CONTINUE
C
CCCCCCCCCCCCCCCCCCCCCCCCCCCCCCCCCCCCCCCCCCCCCCCCCCCCCCCCCCCCCCCCC
C These linear moduli are then added up to give the average value, SMTOT. This is then followed by the
C determination of the initial stress, STRESSIN.
CCCCCCCCCCCCCCCCCCCCCCCCCCCCCCCCCCCCCCCCCCCCCCCCCCCCCCCCCCCCCCCCC
C
   DO I=1,NSO
     SMTOT=SMTOT+SM(NOEL,NPT,I)
   END DO
C
   DO I=1,NSO
     DO K=1,NTENS
       STRESSIN(K)=STRESSIN(K)+(SM(NOEL,NPT,I)*DEV(I,K))
     END DO
   END DO
   DO K=1,NTENS
     STRESSIN(K)=STRESSIN(K)/SMTOT
   END DO
C
CCCCCCCCCCCCCCCCCCCCCCCCCCCCCCCCCCCCCCCCCCCCCCCCCCCCCCCCCCCCCCCCC
C Here the Jacobian matrix, DDSDDE, is defined and assembled using the Poisson's ratio, PROPS(2), and the
C inverse of the average linear moduli, SMTOT.
CCCCCCCCCCCCCCCCCCCCCCCCCCCCCCCCCCCCCCCCCCCCCCCCCCCCCCCCCCCCCCCCC
C
   TERM  = 1.0-PROPS(2)**2
   TERM1 = 1.0/SMTOT/TERM
   TERM2 = 1.0/SMTOT*PROPS(2)/TERM
   TERM3 = TERM1*((1.0-PROPS(2))/2)
C
   DO K1=1,NDI
     DDSDDE(K1,K1)=TERM1
   END DO
   DO K1=2,NDI
```

```
      K2=K1-1
      DO K3=1,K2
        DDSDDE(K3,K1) = TERM2
        DDSDDE(K1,K3) = TERM2
      END DO
    END DO
    DDSDDE(NCO,NCO)=TERM3
C
CCCCCCCCCCCCCCCCCCCCCCCCCCCCCCCCCCCCCCCCCCCCCCCCCCCCCCCCCCCCCCCCCCCCCCCCCCC
C The material behaviour is defined, i.e the global stiffness matrix is assembled. This is then followed by the
C computation of the equilibrium stress field, which in this case is the residual stress field as no loads is applied.
C But since the initial stresses, STRESSIN, are fed in during the first increment, this effectively results in the
C application of the load history via linear elastic stresses.
CCCCCCCCCCCCCCCCCCCCCCCCCCCCCCCCCCCCCCCCCCCCCCCCCCCCCCCCCCCCCCCCCCCCCCCCCCC
C
    DO K=1,NDI
      DO I=1,NDI
        DSTRESS(K) = DSTRESS(K)+(DDSDDE(K,I)*DSTRAN(I))
      END DO
    END DO
    DSTRESS(NTENS) = TERM3*DSTRAN(NTENS)
    DO K1=1,NTENS
      DSTRESS(K1)=DSTRESS(K1)-STRESSIN(K1)
    END DO
C
CCCCCCCCCCCCCCCCCCCCCCCCCCCCCCCCCCCCCCCCCCCCCCCCCCCCCCCCCCCCCCCCCCCCCCCCCCC
C As this is a plane stress analysis, the through-thickness strain component needs to be calculated separately as it
C is not provided by ABAQUS in its strain tensor.
CCCCCCCCCCCCCCCCCCCCCCCCCCCCCCCCCCCCCCCCCCCCCCCCCCCCCCCCCCCCCCCCCCCCCCCCCCC
C
    THSTRAN=-PROPS(2)*(DSTRESS(1)+STRESSIN(1)+DSTRESS(2)+STRESSIN(2))*SMTOT
C
CCCCCCCCCCCCCCCCCCCCCCCCCCCCCCCCCCCCCCCCCCCCCCCCCCCCCCCCCCCCCCCCCCCCCCCCCCC
C In this block, the residual stress field, DSTRESS, is added up and written to STRESS. This is to trick
C ABAQUS into "thinking" it is solving a non-linear problem incrementally rather than a series of linear
C solutions.
CCCCCCCCCCCCCCCCCCCCCCCCCCCCCCCCCCCCCCCCCCCCCCCCCCCCCCCCCCCCCCCCCCCCCCCCCCC
C
    DO K=1, NTENS
      STRESS(K) = STRESS(K)+DSTRESS(K)
    END DO
C
CCCCCCCCCCCCCCCCCCCCCCCCCCCCCCCCCCCCCCCCCCCCCCCCCCCCCCCCCCCCCCCCCCCCCCCCCCC
C The compliance matrix is created in order to calculate the individual strains at each vertex. This is necessary in
C the evaluation of the volume integrals that will go towards the calculation of the upper bound limit load.
CCCCCCCCCCCCCCCCCCCCCCCCCCCCCCCCCCCCCCCCCCCCCCCCCCCCCCCCCCCCCCCCCCCCCCCCCCC
C
    DO I=1,NSO
      COM4 = SM(NOEL,NPT,I)
      COM1 = 1*COM4
      COM2 = -PROPS(2)*COM4
```

```
COM3 = 2.0*(1.0+PROPS(2))*COM4
DO K1=1,NDI
  COMP(I,K1,K1)=COM1
END DO
DO K1=2,NDI
  N2=K1-1
  DO K2=1,N2
    COMP(I,K2,K1) = COM2
    COMP(I,K1,K2) = COM2
  END DO
    END DO
    COMP(I,NCO,NCO)=COM3
C
    DO K=1,NDI
      DO K1=1,NDI
        SSTRAN(I,K)=SSTRAN(I,K)+(COMP(I,K,K1)*(DSTRESS(K1)+DEV(I,K1)))
      END DO
    END DO
  SSTRAN(I,NCO)=COMP(I,NCO,NCO)*(DSTRESS(NCO)+DEV(I,NCO))
  THISTRAN(I)=-PROPS(2)*(DSTRESS(1)+DSTRESS(2)+DEV(I,1)+DEV(I,2))*SM(NOEL,NPT,I)
  END DO
C
CCCCCCCCCCCCCCCCCCCCCCCCCCCCCCCCCCCCCCCCCCCCCCCCCCCCCCCCCCCCCCCCCCCCCCCCCCCCC
C The actual Von-mises effective strain is calculated in the following block.
CCCCCCCCCCCCCCCCCCCCCCCCCCCCCCCCCCCCCCCCCCCCCCCCCCCCCCCCCCCCCCCCCCCCCCCCCCCCC
C
    DO I=1,NSO
      X = SSTRAN(I,1)**2+SSTRAN(I,2)**2+THISTRAN(I)**2
      X = X + 0.5*SSTRAN(I,3)**2
      X = X*2.0/3.0
      ESTRAN(NOEL,NPT,I) = SQRT(X)
    END DO
C
CCCCCCCCCCCCCCCCCCCCCCCCCCCCCCCCCCCCCCCCCCCCCCCCCCCCCCCCCCCCCCCCCCCCCCCCCCCCC
C The internal variables, SSE and SPD, are both integrands, integrated over the volume of the body by
C ABAQUS. These would then be retrieved by the subroutine URDFIL in the calculation of the upper bound
C limit load.
CCCCCCCCCCCCCCCCCCCCCCCCCCCCCCCCCCCCCCCCCCCCCCCCCCCCCCCCCCCCCCCCCCCCCCCCCCCCC
C
      SSE = SSE+(PROPS(1)*ESTRAN(NOEL,NPT,I))
      DO K=1,NTENS
        SPD=SPD+(DEV(I,K)*SSTRAN(I,K))
      END DO
    END DO
C
    KMARK(NOEL,NPT)=1
C
 120  FORMAT('-----------------------------------------------')
 130  FORMAT('STEP  ' ,I, ' INCREMENT ',I)
 160  FORMAT('ELEMENT ',I3, ' INTEGRATION POINT ', I3,'KMARK',I3)
 170  FORMAT('COORDINATES:', E12.5)
```

```
180  FORMAT(E17.10)
210  FORMAT('JACOBIAN: ', I3, I3)
220  FORMAT('STRESS COMP.',I3)
240  FORMAT('STRESS INCREMENTS: ', I3)
260  FORMAT('STRAINS: ', I3)
270  FORMAT('INCREMENTS OF STRAIN ',I3)
290  FORMAT('NO. OF MAT. COST.:', I3)
300  FORMAT('KMARK ', I3)
310  FORMAT('INCREMENT ',I3)
320  FORMAT('VO: ',E17.10)
330  FORMAT('TSTRESS: ',E12.5)
340  FORMAT('ELEMENT  ' ,I, ' INT. POINT ',I)
350  FORMAT('COORDINATES:', E12.5)
360  FORMAT('ELEMENT ',I3, ' INTEGRATION POINT ', I3)
C
     IF(NOEL.EQ.NEL)THEN
       WRITE(18,120)
       WRITE(18,130)KSTEP,KINC
       WRITE(18,160)NOEL,NPT,KMARK(NOEL,NPT)
       WRITE(18,*)'UMAT'
       WRITE(18,*)'ELA'
       WRITE(18,180)(ELA(NOEL,NPT,K), K=1,NTENS)
       WRITE(18,*)'ELASTIC SOLUTION A'
       WRITE(18,180)(DEVA(NOEL,NPT,K), K=1,NTENS)
       WRITE(18,*)'DEV(NCO=3,NCO=3)'
DO I=1,NSO
    WRITE(18,180) (DEV(I,K), K=1,NTENS)
END DO
WRITE(18,*)'SHEAR MODULI'
WRITE(18,180)(SM(NOEL,NPT,I), I=1,NSO)
WRITE(18,*)'AVERAGE SHEAR MODULUS'
WRITE(18,180)SMTOT
WRITE(18,*)'INITIAL STRESS'
WRITE(18,180)(STRESSIN(K), K=1,NTENS)
WRITE(18,*) 'JACOBIAN'
DO I = 1, NTENS
  WRITE(18,*) (DDSDDE(I,J), J=1, NTENS)
END DO
WRITE(18,240) NTENS
WRITE(18,180) (DSTRESS(I), I=1,NTENS)
WRITE(18,220) NTENS
 WRITE(18,180) (STRESS(I), I=1,NTENS)
 WRITE(18,270) NTENS
 WRITE(18,180) (DSTRAN(I), I=1,NTENS)
 WRITE(18,260) NTENS
 WRITE(18,180) (STRAN(I), I=1,NTENS)
WRITE(18,*)'INDIVIDUAL STRAINS'
 DO I = 1,NSO
   DO K=1,NTENS
     WRITE(18,180) SSTRAN(I,K)
   END DO
```

```
      END DO
      WRITE(18,*)'EFFECTIVE STRAIN: '
      WRITE(18,180)(ESTRAN(NOEL,NPT,K), K=1,NSO)
      WRITE(18,*)'SSE'
      WRITE(18,180)SSE
      WRITE(18,*)'SPD'
      WRITE(18,180)SPD
    END IF
C
    RETURN
    END
C
CCCCCCCCCCCCCCCCCCCCCCCCCCCCCCCCCCCCCCCCCCCCCCCCCCCCCCCCCCCCCCCCCCCCCCCCCCC
C Subroutine URDFIL is called at the end of each increment and accesses the results file. It is, here, where all the
C necessary values of variables are extracted, updated and then made available to other subroutines via the
C common block option.
C
C The following standard block, from the user's manual, acts as an interface between ABAQUS and UMAT.
CCCCCCCCCCCCCCCCCCCCCCCCCCCCCCCCCCCCCCCCCCCCCCCCCCCCCCCCCCCCCCCCCCCCCCCCCCC
C
    SUBROUTINE URDFIL(LSTOP, LOVRWRT, KSTEP, KINC)
    INCLUDE 'ABA_PARAM.INC'
C
    DIMENSION ARRAY(513), JRRAY(NPRECD,513)
    EQUIVALENCE (ARRAY(1), JRRAY(1,1))
C
    COMMON/KSTUFF/SF,YLAMB
    SAVE
C
CCCCCCCCCCCCCCCCCCCCCCCCCCCCCCCCCCCCCCCCCCCCCCCCCCCCCCCCCCCCCCCCCCCCCCCCCCC
C The blocks, POSFIL & DBFILE, is specifically used to position URDFIL at the right location in the results
C file. Further explanation of its use is available in the ABAQUS/STANDARD manual.
CCCCCCCCCCCCCCCCCCCCCCCCCCCCCCCCCCCCCCCCCCCCCCCCCCCCCCCCCCCCCCCCCCCCCCCCCCC
C
    CALL POSFIL(KSTEP, KINC, ARRAY, JRCD)
    DO 1000 K=1,999999
      CALL DBFILE(0, ARRAY, JRCD)
      IF(JRCD.NE.0) GO TO 10
      KEY=JRRAY(1,2)
      IF(KEY.EQ.1999) THEN
        SNUM=ARRAY(4)
        SDEN=ARRAY(6)
      END IF
 1000 CONTINUE
 10   CONTINUE
C
CCCCCCCCCCCCCCCCCCCCCCCCCCCCCCCCCCCCCCCCCCCCCCCCCCCCCCCCCCCCCCCCCCCCCCCCCCC
C In the following block, the volume integrands are extracted and the upper bound limit load is calculated. The
C scaling factor, SF, is then sent back to UMAT, where it effectively scales down the linear elastic stress
C solutions. A convergence criterion, CONV, is also specified here. As the termination of the program is
C controlled by the user subroutine, how and when the analysis stops can be accurately prescribed.
```

```
CCCCCCCCCCCCCCCCCCCCCCCCCCCCCCCCCCCCCCCCCCCCCCCCCCCCCCCCCCCCCCCCCCCCCCCCCCCC
C
   SF=SNUM/SDEN
   CONV=1.0-SF
   IF(CONV.LE.1.0E-04) THEN
    KTOL=KTOL+1
   ELSE
    KTOL=0
   END IF
C
   IF (KTOL.EQ.5) LSTOP=1
   IF (KINC.EQ.1) YLAMB=1.0
   YLAMB=YLAMB*SF
C
 40  FORMAT('INCREMENT ',I3)
 50  FORMAT('LAMBDA: ',E17.10)
 60  FORMAT('--------------------------')
 70  FORMAT('SF    : ',E17.10)
 80  FORMAT('RATIO : ',E17.10)
 90  FORMAT('KTOL  : ',I1)
 100 FORMAT('LSTOP : ',I1)
C
    WRITE(15,40)KINC
    WRITE(15,50) YLAMB
    WRITE(18,60)
    WRITE(18,*)'URDFIL'
    WRITE(18,*)'INCREMENT:'
    WRITE(18,*)KINC
    WRITE(18,*)'NUMERATOR'
    WRITE(18,*)SNUM
    WRITE(18,*)'DENOMINATOR'
    WRITE(18,*)SDEN
    WRITE(18,50)YLAMB
    WRITE(7,60)
    WRITE(7,50)YLAMB
    WRITE(7,70)SF
    WRITE(7,80)RATIO
    WRITE(7,90)KTOL
    WRITE(7,100)LSTOP
    END IF
C
    RETURN
    END
```